Steady State Multiplicity
In
Gas-Liquid CSTRs

by

Aqil Jamal

A Thesis Presented to the

FACULTY OF THE COLLEGE OF GRADUATE STUDIES

KING FAHD UNIVERSITY OF PETROLEUM & MINERALS

DHAHRAN, SAUDI ARABIA

In Partial Fulfillment of the
Requirements for the Degree of

MASTER OF SCIENCE

In

CHEMICAL ENGINEERING

August, 1992

INFORMATION TO USERS

This manuscript has been reproduced from the microfilm master. UMI films the text directly from the original or copy submitted. Thus, some thesis and dissertation copies are in typewriter face, while others may be from any type of computer printer.

The quality of this reproduction is dependent upon the quality of the copy submitted. Broken or indistinct print, colored or poor quality illustrations and photographs, print bleedthrough, substandard margins, and improper alignment can adversely affect reproduction.

In the unlikely event that the author did not send UMI a complete manuscript and there are missing pages, these will be noted. Also, if unauthorized copyright material had to be removed, a note will indicate the deletion.

Oversize materials (e.g., maps, drawings, charts) are reproduced by sectioning the original, beginning at the upper left-hand corner and continuing from left to right in equal sections with small overlaps. Each original is also photographed in one exposure and is included in reduced form at the back of the book.

Photographs included in the original manuscript have been reproduced xerographically in this copy. Higher quality 6" x 9" black and white photographic prints are available for any photographs or illustrations appearing in this copy for an additional charge. Contact UMI directly to order.

U·M·I

University Microfilms International
A Bell & Howell Information Company
300 North Zeeb Road. Ann Arbor. MI 48106-1346 USA
313/761-4700 800/521-0600

Order Number 1354023

Steady state multiplicity in gas-liquid CSTRs

Jamal, Aqil, M.S.

King Fahd University of Petroleum and Minerals (Saudi Arabia), 1992

U·M·I
300 N. Zeeb Rd.
Ann Arbor, MI 48106

STEADY STATE MULTIPLICITY IN GAS-LIQUID CSTRs

BY

AQIL JAMAL

A Thesis Presented to the

FACULTY OF THE COLLEGE OF GRADUATE STUDIES

KING FAHD UNIVERSITY OF PETROLEUM & MINERALS

DHAHRAN, SAUDI ARABIA

In Partial Fulfillment of the
Requirements for the Degree of

MASTER OF SCIENCE

In

CHEMICAL ENGINEERING

AUGUST, 1992

KING FAHD UNIVERSITY OF PETROLEUM AND MINERALS
DHAHRAN 31261, SAUDI ARABIA

COLLEGE OF GRADUATE STUDIES

This thesis, written by

AQIL JAMAL

under the direction of his Thesis Advisor and approved by his Thesis Committee, has been presented to and accepted by the Dean of the College of Graduate Studies, in partial fulfillment of the requirements for the degree of

MASTER OF SCIENCE IN CHEMICAL ENGINEERING.

Thesis Committee

Dr. Abdulla A. Shaikh
(Chairman)

Dr. Mehmet A. Hastaoglu
(Member)

Dr. Mohammad A. Al-Naafa
(Member)

Dr. Mohammad A. Al-Naafa
(Department Chairman)

Dr. Ala H. Al-Rabeh
(Dean, College of Graduate Studies)

Date : ١٤١٢/٢/١٠

Dedicated to my parents for
instilling in me the belief
that what I set out to
accomplish, I can

ACKNOWLEDGEMENT

Praise and gratitude be to Allah the Almighty, with whose gracious help it was possible to accomplish this work.

My sincere appreciation and gratitude are extended to Dr. Abdulla A. Shaikh, my thesis committee chairman, for his encouragement and counsel throughout the course of this research. He was always kind and sympathetic to me, and his invaluable suggestions and comments made this task easy. Working with him was indeed a wonderful experience which I thoroughly enjoyed.

I am also thankful to the other members of the committee, Dr. Mehmet A. Hastaoglu and Dr. Mohammad A. Al-Naafa for their cooperation, help and invaluable suggestions during the course of my research work.

I would like to thank the Chemical Engineering Department faculty members for their cooperation and help during my research work. I am also very thankful to the Chemical Engineering Department secretaries, Mr. Riasat Ali Khan and Mr. Tasudduq Hussain, for their cooperation.

I would like to thank my friends Mr. Azam Baig and Mr. Asaf Maruf who were helpful in many aspects of this research and were always a source of encouragement and moral support all along my stay at KFUPM.

Last, but by no means the least, I wish to thank my family for their love, support, patience and understanding.

TABLE OF CONTENTS

Chapter *Page*

LIST OF TABLES ix

LIST OF FIGURES xi

ABSTRACT(Arabic) xvii

ABSTRACT(English) xviii

1. INTRODUCTION 1

1.1 Present Status of the Problem 7

1.2 Objectives 10

2. LITERATURE REVIEW 12

2.1 Mathematical Models for Gas-Liquid CSTRs 12

2.2 Review of Correlations for Hydrodynamic, Transport and Associated Parameters 20

2.2.1 General Background 20

2.2.2 Minimum Impeller Speed 34

2.2.3 Impeller Power Consumption 37

2.2.4 Bubble Diameter 50

2.2.5 Bubble Rise Velocity 52

2.2.6 Gas Hold-up 56

2.2.7 Interfacial Area 62
2.2.8 Liquid-Side Mass Transfer Coefficient 67
2.2.9 Gas-Side Mass Transfer Coefficient 68
2.2.10 Tank-Side Heat Transfer Coefficient 72
2.2.11 Jacket or Coil-Side Heat Transfer Coefficient 95

3. DEVELOPMENT OF THE REACTOR MODEL 103

3.1 Assumptions 104
3.2 Equations for Mass Balance, Energy Balance and Rate of Absorption .. 105
3.2.1 Mass Balances 108
3.2.2 Energy Balance 109
3.2.3 Rate of Absorption 109
3.3 Model Equations in Dimensional Form 110
3.4 Model Equations in Dimensionless Form 112
3.5 Equations for Reaction Factor 115
3.6 Correlations for Heat Transfer Coefficients 118
3.6.1 Tank-Side Heat Transfer Coefficient 118
3.6.2 Jacket or Coil-Side Heat Transfer Coefficient 119
3.6.3 Overall Heat Transfer Coefficient 120
3.7 Correlations for Mass Transfer Coefficients 121
3.7.1 Liquid-Side Mass Transfer Coefficient 121
3.7.2 Gas-Side Mass Transfer Coefficient 122
3.8 Correlations for Hydrodynamic Parameters 122
3.8.1 Gas Hold-Up, Interfacial Area and Bubble Diameter 122

3.8.2 Bubble Rise Velocity 123
3.9 Correlations for Power Input 124
3.9.1 Power Input Due to Mechanical Agitation 124
3.9.2 Power Input Due to Aeration 126
3.9.3 Total Power Input 126
3.10 Correlation for Minimum Effective Impeller Speed 127

4. REACTION FACTOR EXPRESSION 128

4.1 Introduction 128
4.2 Model Development 132
4.2.1 Dimensional Form of Film-Theory Model Equations 132
4.2.2 Dimensionless Form of Model Equations 133
4.3 Approximate Analytical Solution of Model Equations 136
4.4 New Reaction Factor Expression 137
4.5 Numerical Solution of Model Equations 138
4.5.1 Finite Difference Approximation 138
4.5.2 Numerical Procedure 139
4.6 Results and Discussion 140
4.6.1 Asymptotic Behavior of the New Reaction Factor Expression 140
4.6.2 Accuracy of the New Reaction Factor Expression 142
4.6.3 Effect of Sphericity on the Mass Transfer with Chemical Reaction 148

5. REACTOR SIMULATION RESULTS AND DISCUSSION 157

5.1 Introduction 157

5.2 Physico-Chemical Parameters Used in Numerical Simulation 159

5.3 Numerical Procedure 159

5.4 Parametric Study 169

5.4.1 Effect of Reactivity 169

5.4.2 Effect of Gas and Liquid Residence Times 169

5.4.3 Effect of Feed Gas Purity 189

5.4.4 Effect of Feed Gas Temperature 194

5.4.5 Effect of Impeller Speed 200

5.5 Model Discrimination: Old versus New Model 203

5.5.1 Variable Gas Residence Time 203

5.5.2 Variable Liquid Residence Time 225

6. CONCLUSIONS AND RECOMMENDATIONS 244

NOMENCLATURE 249

REFERENCES 256

APPENDIX A : DETAILED DERIVATIONS 273

A1 Derivation of Reactor Model 273

A2 Derivation of Reaction Factor Expression 280

APPENDIX B : COMPUTER SIMULATION CODES **292**

B1 Computer Code for Solving Reactor Model Equations 292

B2 Computer Code for Solving Film Theory Model Equations 327

LIST OF TABLES

Table		Page
1.1	Industrial Reactions Carried Out in Gas-Liquid CSTRs ...	2
1.2	Relative Usage of Various Gas-Liquid Reactors ...	3
2.1	Summary of Published Work on Steady State Multiplicity in Gas-liquid CSTRs ...	13
2.2	Principal Variables Involved in the Correlations for Hydrodynamic and Transport Parameters ...	32
2.3	Dimensionless Numbers Involved in the Correlations for drodynamic and Transport Parameters ...	33
2.4	Correlations for Minimum Impeller Speed for Rushton Turbine Impeller ...	35
2.5	Correlations for Gassed Power Consumption by a Rushton Turbine ...	45
2.6	Correlations for Gas Hold-Up ...	58
2.7	Correlations for Interfacial Area ...	64
2.8	Correlations for K_L and $K_L a$ ...	69
2.9	Correlations for Tank-Side Heat Transfer Coefficients in Gas-Liquid CSTRs ...	79
2.10	Correlations for Jacket or Coil-Side Heat Transfer Coefficients ...	98
4.1	Comparison of Analytical and Numerical Values of Reaction Factor ($E_i = 500\ \alpha' = 100, \xi = 5.0$) ...	144
4.2	Comparison of Analytical and Numerical Values of Reaction Factor ($E_i = 50\ \alpha' = 200, \xi = 5.0$) ...	145
4.3	Comparison of Analytical and Numerical Values of Reaction Factor ($E_i = 50, \alpha' = 200, \xi = 0.1$) ...	146

4.4	Comparison of Analytical and Numerical Values of Reaction Factor ($E_i = 50, \alpha' = 200, \xi = 0.001$)	...	147
5.1	Temperature Dependent Physico-Chemical Parameters	...	160
5.2	Reference Data Set for the Reactor Simulation Using New Model	...	161
5.3	Reference Data Set for the Reactor Simulation Using Old Model	...	162
5.4	Comparison of Ignition and Extinction Points at Different Gas Flow Rates	...	176

LIST OF FIGURES

Figure		Page
1.1	Schematic Diagram of a Non-Isothermal CSTR ...	5
1.2	Basic Elements Involved in Modeling of Gas-Liquid CSTRs ...	8
2.1	Various Types of Impellers ...	22
2.2	Schematic Diagram of a Standard Gas-Liquid CSTR ...	24
2.3	Vortices Behind a Rushton Turbine Blade ...	27
2.4	Change in Cavity Structure at Increasing Gassing Rates for a Rushton Turbine ...	28
2.5	Gas Dispersion Regimes in a Stirred Tank Reactor ...	30
2.6	Power Curves for Flat Blade Disk Turbine Agitator with Various Baffle Widths ...	39
2.7	Different Type of Cavities and their Growth in Relation to the Gassed Power Curve ...	41
2.8	Effect of Number of Disk Blades on Gassed Power Ratio ...	42
2.9	Effect of stirrer Speed on Gassed Power Behavior ...	43
2.10	Gassed Power Curves for a 0.44 m Vessel (a) Measured (b) Calculated ...	51
2.11	Free Rise of Single Bubbles ...	54
2.12	Generalized Bubble Rise Velocity Correlation ...	57
2.13	Jacketed Stirred Tank Reactor ...	73
2.14	a. Stirred Tank Reactor with Internal Coils b. Stirred Tank Reactor with Vertical Baffles ...	74
2.15	a. Mechanism of Heat Transfer b. Transient Heat Conduction Eddies ...	88
2.16	Heat Transfer in a Stirred Tank Equipped with Disc Turbine ...	89

2.17	Influence of Aeration Intensity on Heat Transfer	...	90
2.18	Influence of Total Power Input Per Unit Volume on Heat Transfer in Gas-Liquid Systems	...	92
2.19	Common Arrangements of Heat Transfer Jackets and Internal Coils	...	96
3.1	Material and Energy Flow Diagram	...	106
4.1	Concentration Profile for Physical Mass Transfer Through a Spherical Surface	...	130
4.2	Flow Chart of the Computer Program GLRXN	...	141
4.3	Asymptotic Behavior of the New Reaction Factor	...	143
4.4	Effect of Sphericity on Concentration Profiles of Gaseous and Liquid Reactants ($E_i = 10, M = 2, \alpha' = 200, \xi = 0.001$)	...	149
4.5	Effect of Sphericity on Concentration Profiles of Gaseous and Liquid Reactants ($E_i = 10, M = 0.1, \alpha' = 200, \xi = 0.001$)	...	150
4.6a	Effect of Sphericity on the Reaction Factor ($E_i = 50, \alpha' = 200, \xi = 0.001$)	...	152
4.6b	Effect of Sphericity on the Reaction Factor ($E_i = 50, \alpha' = 200, \xi = 0.001$)	...	153
4.7a	Effect of Sphericity on the Reaction Factor ($E_i = 50, \alpha' = 200, \xi = 0.5$)	...	154
4.7b	Effect of Sphericity on the Reaction Factor ($E_i = 50, \alpha' = 200, \xi = 0.5$)	...	155
5.1	Flow Chart for the Reactor Simulation Program	...	164
5.2	Effect of Reactivity on the Regions and Patterns of Multiplicity Corresponding to Variable τ_G	...	170
5.3	Effect of Reactivity on the Regions and Patterns of Multiplicity Corresponding to Variable τ_L	...	171
5.4	Effect of F_{gf} on Temperature	...	172

5.5	Effect of F_{gf} on Dimensionless Conversion of Liquid Reactant	...	174
5.6	Effect of F_{gf} on Dimensionless Conversion of Gaseous Reactant	...	175
5.7	Effect of F_{gf} on Reaction Factor	...	177
5.8	Effect of F_{gf} on Dimensionless Concentration of A in Liquid Bulk	...	178
5.9	Effect of F_{gf} on Power Input	...	180
5.10	Effect of F_{gf} on Interfacial Area	...	181
5.11	Effect of F_{gf} on Gas Hold-Up	...	182
5.12	Effect of F_{gf} on Bubble Diameter	...	183
5.13	Effect of F_{gf} on Liquid-Side Mass Transfer Coefficient	...	185
5.14	Effect of F_{gf} on Gas-Side Mass Transfer Coefficient	...	186
5.15	Effect of F_{gf} on Tank-Side Heat Transfer Coefficient	...	187
5.16	Effect of F_{gf} on Overall Heat Transfer Coefficient	...	188
5.17	Effect of Feed Gas Purity on Steady State Multiplicity	...	190
5.18	Effect of Feed Gas Purity on Steady State Multiplicity Using New Model	...	191
5.19	Effect of Feed Gas Purity on Steady State Multiplicity Using Old Model	...	192
5.20	Effect of Feed Gas Purity on SSM with Variable Liquid Residence Time Using New Model	...	193
5.21	Effect of Feed Gas Temperature on Steady State Multiplicity with Variable Liquid Residence Time	...	195
5.22	Effect of Feed Gas Temperature on SSM with Variable Gas Residence Time	...	196

5.23	Effect of Liquid Feed Temperature on Steady State Multiplicity with Variable Liquid Residence Time	...	198
5.24	Effect of Liquid Feed Temperature on SSM with Variable Gas Residence Time	...	199
5.25	Effect of Impeller Speed on Steady State Multiplicity with Variable Gas Residence Time	...	201
5.26	Effect of Impeller Speed on SSM with Variable Liquid Residence Time	...	202
5.27	Comparison of the Multiplicity Regions Predicted by New and Old Models	...	204
5.28	Comparison of Steady State Temperatures Predicted by New and Old Models	...	205
5.29	Comparison of Steady State Temperature Predicted by New and Old Models	...	206
5.30	Comparison of Steady State Temperatures Predicted by New and Old Models	...	207
5.31	Comparison of Steady State Temperatures Predicted by New and Old Models	...	208
5.32	Minimum Impeller Speed versus Gas Residence Time	...	210
5.33	Power Input versus Gas Residence Time	...	211
5.34	Interfacial Area versus Gas Residence Time	...	212
5.35	Gas Holdup versus Gas Residence Time	...	213
5.36	Liquid-Side Mass Transfer Coefficient versus Gas Residence Time	...	214
5.37	Tank-Side Heat Transfer Coefficient versus Gas Residence Time	...	215
5.38	Overall Heat Transfer Coefficient versus Gas Residence Time	...	216
5.39	Gas-Side Mass Transfer Coefficient versus Gas Residence Time	...	218

5.40	Bubble Diameter versus Gas Residence Time	...	219
5.41	Comparison of Steady State Conversions of Gaseous Reactant Predicted by Old and New Models	...	220
5.42	Comparison of Steady State Conversions of Liquid Reactant Predicted by Old and New Models	...	221
5.43	Hatta Number versus Gas Residence Time: Predictions of Old and New Models	...	222
5.44	Reaction Factor versus Gas Residence Time: Predictions of Old and New Models	...	223
5.45	Dimensionless Concentration of A in Liquid Bulk versus Gas Residence Time: Predictions by Old and New Models	...	224
5.46	Comparison of the Multiplicity Regions Predicted by New and Old Models	...	226
5.47	Comparison of Steady State Temperatures Predicted by New and Old Models	...	227
5.48	Comparison of Steady State Temperature Predicted by New and Old Models	...	228
5.49	Comparison of Steady State Temperatures Predicted by New and Old Models	...	229
5.50	Steady State Reactor Temperature versus Liquid Residence Time: Predictions of Old and New Models	...	230
5.51	Conversion of Gaseous Reactant versus Liquid Residence Time: Predictions of Old and New Models	...	231
5.52	Conversion of Liquid Reactant versus Liquid Residence Time: Predictions of Old and New Models	...	232
5.53	Hatta Number versus Liquid Residence Time: Predictions of Old and New Models	...	233
5.54	Reaction Factor versus Liquid Residence Time: Predictions of Old and New Models	...	234
5.55	Dimensionless Concentration of A in Liquid Bulk versus Liquid Residence Time: Predictions of Old and New Models	...	235

5.56	Interfacial Area versus Liquid Residence Time	...	236
5.57	Gas-Holdup Liquid Residence Time	...	237
5.58	Bubble Diameter versus Liquid Residence Time	...	238
5.59	Liquid-Side Mass Transfer Coefficient versus Liquid Residence Time	...	239
5.60	Gas-Side Mass Transfer Coefficient versus Liquid Residence Time	...	240
5.61	Tank-Side Heat Transfer Coefficient versus Liquid Residence Time	...	241
5.62	Overall Heat Transfer Coefficient versus Liquid Residence Time	...	242
5.63	Power Input versus Liquid Residence Time	...	243

خلاصة الرسالة

اسم الطالب : عاقل جمال .

عنوان الدراسة : " تضاعفية الحالة الثابتة في مفاعلات الغازات والسوائل مستمرة الخلط "

التخصص : الهندسة الكيميائية .

تاريخ الشهادة : أغسطس ١٩٩٢م .

لقد تم في هذا البحث تطوير نموذج رياضي لدراسة خواص تضاعفية الحالة الثابتة في مفاعلات الغازات والسوائل مستمرة الخلط في ظروف التشغيل غير ثابتة الحرارة وذات التبادل الحراري . إن هذا النموذج النظري يأخذ في الأعتبار نوعية وسرعة التفاعل ، إنتقال المادة بين الطورين ، طريقة الإتصال الطبيعي ، وكذلك لأول مرة الشكل الهندسي للمفاعل وأداة الخلط . كما أن هذا النموذج الجديد يأخذ في الأعتبار لأول مرة إمكانية تغير قيم معالم الهيدرودينامكية ومعالم الأنتقال ، بأستخدام علاقات تجريبية في النموذج الرياضي . نقدم كذلك في هذا البحث مراجعة كاملة للبحوث المنشورة عن تلك العلاقات التجريبية وعن علاقات أخرى مرتبطة بها . كما أخذ في الأعتبار حين تطوير النموذج المذكور تأثير التفاعل الكيميائي على أمتصاص الغاز باستخدام معامل تفاعل تقريبي ، مشتق على أساس تفاعلات الدرجة الثانية العامة ودائرية فقاعة الغاز . لقد أتضح لنا من دراسة هذا المعامل أن دائرية الفقاعة قد تزيد أو تنقص قيمة معامل التفاعل حسب حجم الفقاعة بالمقارنة لطبقة التركيز المحاذية لها .

لقد أجريت في هذا البحث دراسة تحليلية مستفيضة لتمثيل المفاعلات المستمرة الخلط بهدف إيضاح تأثير التفاعلية ، طبيعة لقيم الغاز ، درجة حرارة لقيم الغاز ولقيم السائل ، سرعة جريان اللقيمين المذكورين عند دخولهما المفاعل ، بالإضافة إلى درجة الخلط . كما تمت مقارنة تمثيل المفاعلات هذه بأخرى تعتمد على إستخدام نماذج مبسطة سبق نشرها . لقد بينت هذه المقارنة بأن ظروف حدوث التضاعفية تختلف بصورة كبيرة ، على الرغم من أن أشكال التضاعفية والعدد الأقصى للحالات الثابتة لم يحدث بهما تغيير في كلا النموذجين ، أي النموذج الجديد المطور في هذا البحث وذلك المبسط .

إن نتائج البحث الحالي تبين بأن قيم المعالم الهيدرودينامكية ومعالم الإنتقال تتأثر بصورة واضحة مع تغير ظروف تشغيل المفاعل ، وهذا ما تم تجاهله في الأبحاث المنشورة سابقاً حين ثُبتت قيم هذه المتغيرات . ونتيجة لذلك يمكن الحكم بأن النتائج المنشورة سابقاً عن تضاعفية الحالة الثابتة تعتبر متحفظة .

درجة الماجستير في العلوم

جامعة الملك فهد للبترول والمعادن

الظهران ، المملكة العربية السعودية

أغسطس ١٩٩٢م

THESIS ABSTRACT

NAME OF STUDENT : *AQIL JAMAL*

TITLE OF STUDY : *Steady State Multiplicity in Gas-Liquid CSTRs*

MAJOR FIELD : *Chemical Engineering*

DATE OF DEGREE : *August, 1992*

A comprehensive model has been developed for the study of steady state multiplicity features of non-isothermal, non-adiabatic, gas-liquid continuous stirred tank reactors (CSTRs). The theoretical development takes into consideration the reaction kinetics, the interphase mass transfer, the mode of physical contact, and for the first time both reactor and impeller geometry. Possible variations in the hydrodynamic and transport parameters due to variable operating conditions also for the first time have been taken into account by incorporating empirical correlations in the model for these parameters. A comprehensive review of empirical correlations for various hydrodynamic, transport and associated parameters used in the model has also been presented. The influence of chemical reaction on gas absorption has been taken into consideration by using a new approximate reaction factor expression derived based on general second-order kinetics and spherical bubble geometry. A parametric study on the so-called local model shows that when the size of the gas bubble is comparable to the thickness of concentration boundary layer around it, the spherical effect depending on the system conditions may significantly increase or decrease the reaction factor values.

A detailed parametric study was carried out to show the individual effects of reactivity, nature of feed gas, gas and liquid feed temperatures and their flow rates, and degree of agitation. The results obtained by the rigorous model are compared with those predicted by simplified models reported in the literature. The analysis shows that although the proposed model predicts similar multiplicity patterns and maximum number of steady states, the conditions under which they occur are significantly different.

The hydrodynamic and transport parameters which have been assumed constant by the previous investigators have been shown to vary significantly with the operating conditions indicating that the predictions of multiplicity behavior based on previous simplified models are conservative.

MASTER OF SCIENCE DEGREE
KING FAHD UNIVERSITY OF PETROLEUM AND MINERALS
Dhahran , Saudi Arabia
August, 1992

CHAPTER 1

INTRODUCTION

Continuous stirred tank reactors (CSTRs) are used to carry out a variety of gas-liquid chemical reactions. Some of the industrially important reactions carried out in these reactors are listed in Table 1.1. Doraiswamy and Sharma [1] have given a comprehensive list of gas-liquid reactions along with the type of reactor normally used. Based on their list, the percent usage of various types of gas-liquid reactors is given in Table 1.2. It is clear from Table 1.2 that gas-liquid stirred reactors are used in the majority of industrial applications .

The wide spread use of CSTRs in the chemical process industries is due to the excellent heat and mass transfer characteristics of these reactors and the fact that they provide greater flexibility to independently change important operating conditions, such as mixing intensity and residence time. Because of mechanical agitation, interfacial areas as high as 2000 m^{-1} can be generated [3] which makes CSTRs suitable for slow reactions and reactions involving sparingly soluble gases. Furthermore, CSTRs are generally capable of effectively handling high liquid to gas flow rate ratios, viscous liquids and solid suspensions. The

Table 1.1 Industrial Reactions Carried Out in Gas-Liquid CSTRs [2]

Oxidations	of cyclohexane of mercaptans synthesis of lactic acid or of streptocomycine production of acetic, adipic and terephthalic acids production of phenol fermentations
Hydrogenations	of oleate into ethyl stearate of glucose into sorbitol
Chlorinations	of para-cresol of benzene and phenol
Nitrations	of toluene of aromatics
Sulfonations	productions of alpha-olefin sulfonates

Table 1.2 Relative Usage of Various Gas-Liquid Reactors

Type of Reactor	% Use
CSTR	42
BCR	31
Packed Column	19
Plate Column	6-8
Spray Column	0-2

drawbacks of CSTRs are considerable backmixing of both gas and liquid phases, presence of complex mechanical parts such as reduction gears, seals, bearings, and the requirement of relatively high power input per unit volume of liquid. These reactors are generally not suitable for high pressures and large scale operations [4]. Figure 1.1 shows a schematic diagram of a gas-liquid CSTR. The size of the reactor can be as small as few milliliters in the laboratory, or larger than 300 m^3 in industry. Both, standard and non-standard configurations are used in practice. Details of the standard configuration of a CSTR are given in Chapter 2.

An important feature of chemically reacting systems is the occurrence of more than one steady state under certain operating conditions. This interesting phenomenon, referred to as steady state multiplicity, has been observed experimentally in both single-phase and two-phase CSTRs and is known to occur particularly in highly exothermic reaction systems.

Multiplicity of steady states has many practical implications. The existence of steady state multiplicity may lead to a temperature hystersis of the reactor and may require sophisticated control techniques in order to maintain the system at a desired state. When multiplicity exists, dramatic changes in reactor performance, such as extinction and ignition, can be encountered which may cause unexpected problems in the control and operation of the reactor. Thus information regarding the conditions under which a reacting system exhibits steady state multiplicity, and parametric sensitivity of these steady states are essential for the rational design, operation and control of a reactor system. The

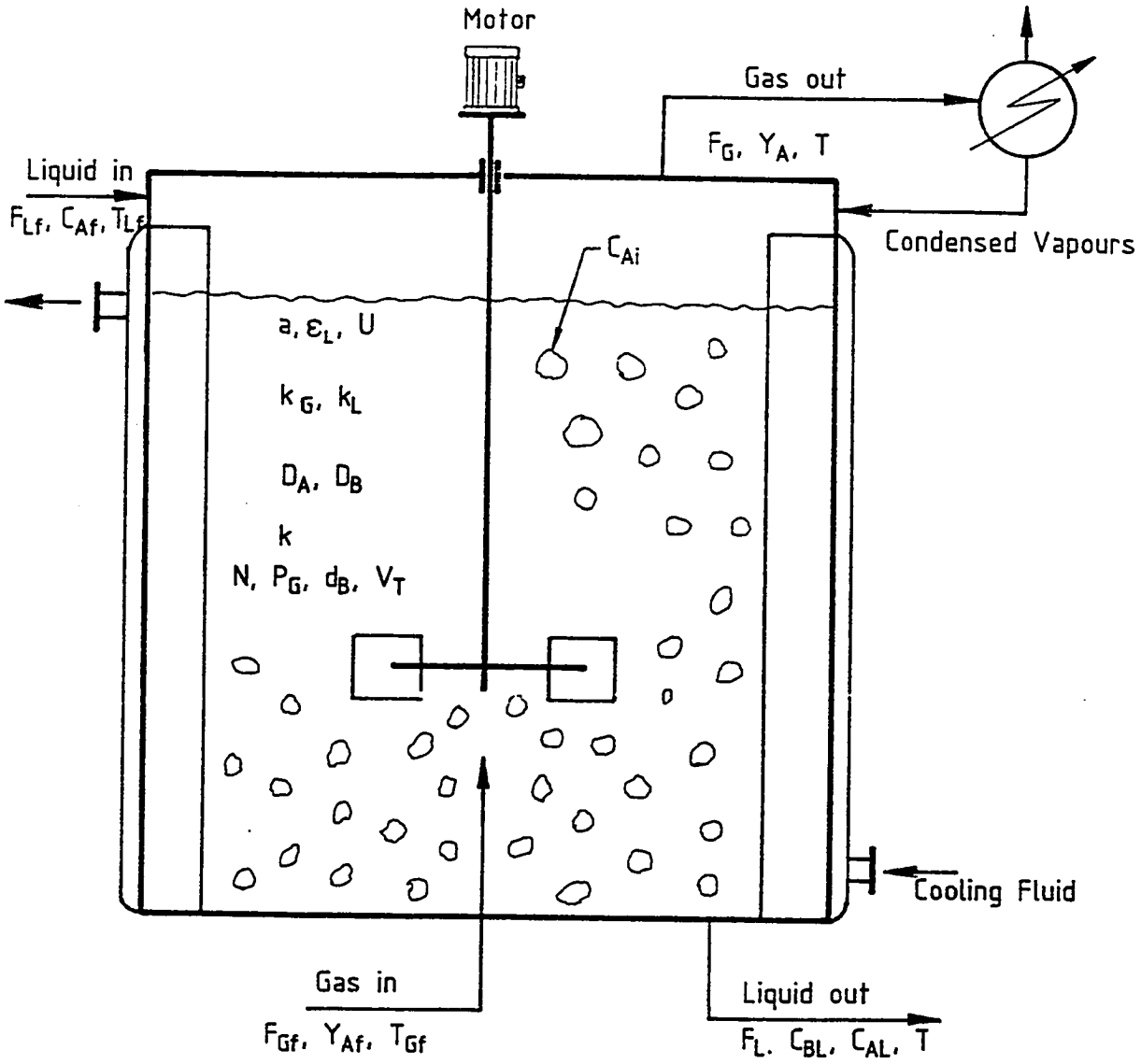

Figure 1.1 Schematic Diagram of a Non-Isothermal CSTR

multiplicity patterns are usually sensitive to the choice of the kinetic model and other parameters. It has been suggested by various investigators that this property can be used to discriminate among the rival kinetic models and for the estimation of kinetic parameters [5,6].

Many advances in our understanding of steady state multiplicity have occurred in recent years. A number of studies on the theoretical aspects of steady state multiplicity in two-phase CSTRs have been published. Experimental studies in this area, however, are scarce and to date only two studies [7,8] showing the existence of multiple steady states and chaotic or oscillatory behavior are reported. The scarcity of the literature on experimental work is mainly due to the operational difficulties in observing multiple steady states in a laboratory reactor.

In order to understand the steady state multiplicity features of a reacting system, it is essential to mathematically model the behavior of the reactor system. Modeling single-phase CSTRs with a single or complex reaction is relatively simple. Many investigators [9,10] have studied the steady state multiplicity of such reactors and criteria for uniqueness and multiplicity of steady states have been established. For example, it is well known that a single phase adiabatic CSTR in which a single irreversible reaction is carried out can have a maximum of three steady states.

When a gas-liquid reaction is carried out in a CSTR, modeling and analysis of the reactor is much more complex due to the interaction between the reaction rate and the transport of gaseous and liquid reactants and products. The heat

loss by liquid evaporation, influence of temperature and conversion on various physico-chemical parameters, and prevailing hydrodynamic and mixing conditions, if included, may further complicate the model. Various models describing the performance of a gas-liquid CSTR with very simple to fairly general kinetics have been developed. Numerical and theoretical simulation studies based on these models have shown the existence of multiple steady states and as many as seven steady states were reported [5]. Due to the complex nature of these models it is very difficult to establish analytic criteria for uniqueness and multiplicity of steady state. However, in some cases necessary and sufficient conditions have been derived analytically (see, e.g., [11]).

1.1 Present Status of the Problem

As stated before modeling of gas-liquid CSTRs is quite complex. In order to mathematically model the behavior of such reactors the interaction of chemical, physical and geometrical aspects of the reactor system, as illustrated in Figure 1.2, should be considered. Almost all of the previous studies on the modeling and simulation of gas-liquid CSTR have been based only on the interaction of chemical reaction and interphase mass transfer as shown in Figure 1.2.

Although these models provide good insight into the subject their scope is somewhat limited. The main point of weakness in most of the previous modeling studies of steady state multiplicity in gas-liquid CSTRs is that the strong interdependence of the hydrodynamic parameters and the operating conditions has not been taken into account. In all of the previous simulation

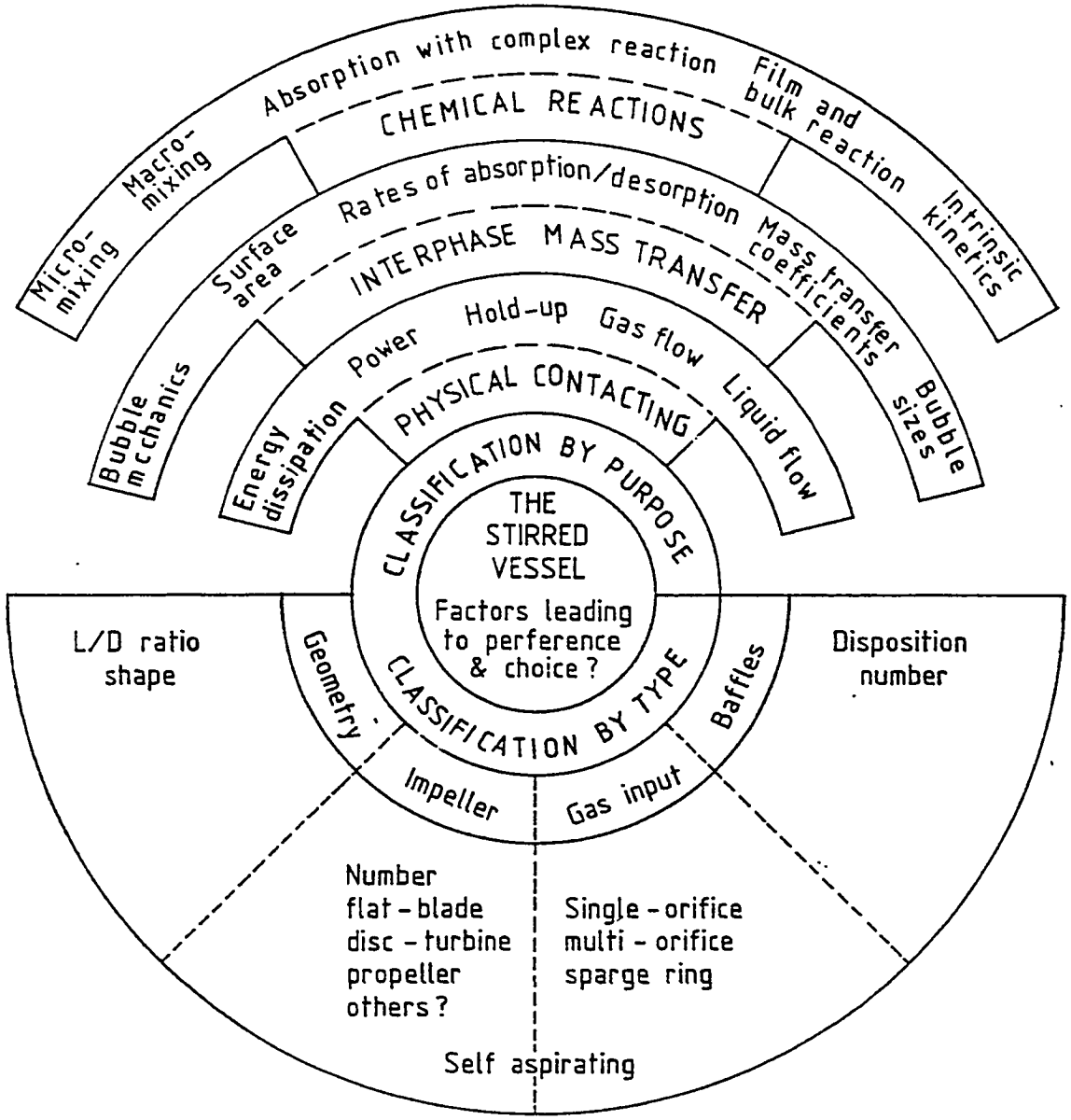

Figure 1.2 Basic Elements Involved in Modeling of Gas-Liquid CSTR$_S$ [4]

studies, when the influence of a certain parameter was investigated, values of the hydrodynamic parameters (i.e., phase hold-ups, interfacial area and transport coefficients) were kept constant. Though this has been done mainly to simplify the mathematics and numerical solution of resulting complex model equations, it is, however, not always realistic to fix these parameters while the operating conditions are changing, since they are the result of the combined action of physico-chemical properties of the reaction fluids, vessel geometry, and operating conditions as indicated by Figure 1.2. The main purpose of this thesis, therefore, is to develop a model which accounts for the variation of hydrodynamic and transport parameters with the operating conditions using empirical correlations available in the literature and to study the steady-state behavioral features of nonisothermal, nonadiabatic, gas-liquid CSTRs.

The model will be based on the common case of irreversible general second-order gas-liquid reactions. Therefore, the model will utilize the reaction factor expression derived originally by van Krevelen & Hoftijzer [12] and extended by Teramoto et al. [13] for the case of non-volatile liquid reactant and the expression developed by Zarook [14] in case of volatile liquid reactant, to account for the interaction of interfacial mass transfer and chemical reaction.

All of the previous reaction factor expressions have been developed based on the assumption that the liquid film thickness surrounding the gas bubble is very small compared to the bubble diameter. This has been done mainly to simplify the mathematics since the governing equations are coupled non-linear second-order differential equations and can not be solved analytically; although

approximate solutions have been obtained (see e.g. [12]). However, as will be shown in the present study, the gas bubble diameter needs to be be calculated, it would therefore be appropriate to account for the effect of change in bubble diameter, due to change in the operating conditions, on the reaction factor. Thus, a new reaction factor expression which will take into account the sphericity of the gas bubble will be developed and used in our CSTR model.

In order to account for the effect of changing operating conditions on hydrodynamic and transport parameters, various correlations for phase holdups, bubble size, interfacial area, mass and heat transfer coefficients will be reviewed and will be incorporated in the model. Due to the complex nature of these correlations and the reaction factors, the resulting reactor model equations will be complicated non-linear algebraic equations and will have to be solved numerically. Therefore, a numerical scheme will be devised to solve the model equations and examine the influence of various parameters on the occurrence of multiple steady states.

1.2 Objectives

The objectives of the present research are as follows :

1. To analyze in detail the reactor models used in previous studies.

2. To survey the literature for empirical correlations to evaluate all relevant hydrodynamic and transport parameters (i.e. phase holdups, interfacial area, mass transfer coefficients, heat transfer coefficients).

3. To develop a new mathematical model for nonisothermal, nonadiabatic, gas-

liquid CSTRs taking into account the variation of hydrodynamic and transport parameters with the operating conditions.

4. To develop a new reaction factor expression for a general second-order kinetics taking into account the sphericity of the gas bubble and compare the approximate analytical results so obtained with the numerical results.

5. To use the new model to simulate reactor behavior and study the possible occurrence of steady state multiplicity.

6. To discriminate among rival reactor models.

CHAPTER 2

LITERATURE REVIEW

2.1 Mathematical Models for Gas-Liquid CSTRs

Many advances in our understanding of steady state multiplicity have occurred in recent years. A number of theoretical studies of steady state multiplicity in gas-liquid CSTRs have been published. Various models describing the performance of a gas-liquid CSTR with very simple to fairly general kinetics have been developed. Published theoretical and experimental studies of steady state multiplicity in gas-liquid CSTRs are summarized in Table 2.1.

Early theoretical studies on steady state multiplicity and stability of gas-liquid CSTRs were published by Schmitz and Amundson [15]. In their models they assumed that chemical reaction and interfacial mass transfer are two independent and non-interacting processes, which is true only in the case of negligible mass transfer resistance. Moreover, these models do not take into account the enhancement of the gas absorption rate due to chemical reaction and fail to describe the behavior of gas-liquid CSTRs in case the reaction regime shifts from chemical to mass transfer control, a case usually encountered during

Table 2.1 Summary of Published Work on Steady State Multiplicity in Gas-Liquid CSTRs

Study	Reaction Regime	Theoretical	Numerical	Effect of Hydrodynamics
THEORETICAL				
1. Schmitz and Amundson (1963) [15]	Irreversible, fast, 1st-Order Reaction	Y	N	N
2. Hoffman et al. (1975) [16]	Irreversible, 2nd-Order Reaction	Y	N	N
3. Sharma et al. (1976) [5]	Consecutive, 2nd-Order Reaction	Y	N	N
4. Raghuram and Shah (1977) [17]	Pseudo-1st-Order and fast, 2nd-Order Reaction	Y	N	N
5. Raghuram at al. (1979) [18]	Pseudo-1st-Order Reaction	Y	Y	N
6. Huang and Varma (1981) [19]	Fast, Pseudo-1st-Order Reaction	Y	Y	N
7. Huang and Varma (1981) [6]	General 2nd-Order Reaction	Y	Y	N

Contd.

Table 2.1 contd.

8. Singh et al. (1982) [21]	Fast, Pseudo-1st-Order Reaction	Y	N	N
9. Shaikh and Varma (1984) [22]	Fast, Pseudo-1st-Order Reaction	Y	N	Y
10. Shaikh (1987) [11]	Fast, Pseudo-1st-Order Reaction	Y	N	Y
11. Shaikh et al. (1991) [26]	General, 2nd-Order Reaction	Y	Y	N
EXPERIMENTAL				
12. Ding et al. (1974) [7]	Chlorination of Liquid n-Decane.	N	N	N
13. Hancock and Kenny (1977) [8]	Methanol Vapour with Hydrogen Chloride to give Methyl Chloride & Water	N	N	N

Y = Yes
N = No

nonisothermal operation [16].

Hoffman et al. [16] developed a model for a single exothermic second-order gas-liquid reaction in an adiabatic CSTR and demonstrated that, under certain operating conditions, up to five steady states can exist. They also carried out parametric sensitivity studies of steady state multiplicity for this system and attributed the occurrence of five steady states to the interactions of chemical reaction rate, diffusional resistance and solubility. The unique feature of this model was that the authors utilized the concept of reaction factor to take into account the interaction between chemical reaction and mass transfer. As pointed out by Sharma et al. [5], this concept enables one to express the overall rate of gas-liquid reactions over a wide range of temperatures in which controlling resistances may shift from kinetic to mass transfer.

The occurrence of multiple steady states was demonstrated experimentally by Ding et al. [7] for the chlorination of n-decane. They reported that for a certain feed flow rate of chlorine two stable steady states with distinctly different levels of temperature, conversion and selectivity were possible. The authors also pointed out that steady state multiplicity and dynamic behavior of the reactor were strongly dependent on the presence of small amounts of impurities.

Another experimental study in this area which has not been referred to often in the literature is by Hancock and Kenny [8]. They studied the reaction of methanol and hydrogen chloride in a concentrated aqueous solution containing zinc chloride catalyst. Under certain operating conditions, oscillatory

behavior of the reactor in terms of production of methyl chloride was reported. The authors carried out theoretical analysis to explain the dynamic characteristic of this system.

Sharma et al. [5] carried out numerical simulation of the experimental results of Ding et al. [7] and demonstrated the possible existence of up to seven steady states based on a model for consecutive second-order gas-liquid reactions in an adiabatic CSTR. The authors pointed out that the key parameters which influence the multiplicity patterns and regions are the kinetic rate constants, the interfacial area, the heat of reactions, the heat loss from the reactor and the liquid heat capacity. They also suggested that steady state multiplicity can be used to discriminate among rival models and for estimation of kinetic parameters.

Raghuram and Shah [17] derived criteria for uniqueness and multiplicity for the cases of pseudo first-order and fast second-order reactions in an adiabatic CSTR. They presented various plots in different parameter spaces to determine the number of steady states and pointed out that occurrence of five steady states in gas-liquid CSTRs is due to the accumulation of gaseous reactant in the liquid phase. Raghuram et al. [18] extended this work and studied the effect of the heat transfer coefficient on the multiplicity region. The authors reported that chances of multiplicity are reduced in case of large values of the heat transfer coefficient and calculated the minimum value of the heat transfer coefficient required to guarantee uniqueness.

Huang and Varma [19] pointed out that the analytical criteria of Raghuram and Shah [17] are not *a priori* and trial-and-error computations are required to calculate the steady state temperature which is included in the criteria. They developed less conservative explicit necessary and sufficient conditions for steady state uniqueness and multiplicity in a non-adiabatic gas-liquid CSTR with a fast pseudo first-order reaction.

Huang and Varma [6] subsequently developed a model for a general second-order reaction in non-adiabatic CSTR and carried out numerical simulations to study the effect of various parameters on steady state multiplicity patterns. In the adiabatic case they showed the possible existence of an "isola" with five steady states and pointed out that any loss of heat through the heat exchange device could eliminate the possibility of the existence of five steady states. The numerical simulation results are shown to agree reasonably well with the experimental data of Ding et al. [7] despite the difference in reaction kinetics. Huang and Varma [20] also numerically analysed the multiplicity patterns of fast second-order, pseudo first-order, and fast pseudo first-order reactions and concluded that the pseudo first-order model could most closely produce the multiplicity region of the general second-order reaction model, though multiplicity patterns for these two reaction models may differ significantly. The authors suggested that for the prediction of the multiplicity region of the general second-order reaction case, the fast pseudo first-order reaction model is better as the criteria for uniqueness and multiplicity were derived analytically [19] and no trial-and-error computation is needed.

Singh et al. [21] studied the effect of gas feed temperature on steady state multiplicity of an adiabatic CSTR with a fast pseudo first-order reaction. They pointed out that, in case of high pressure gas-liquid reactions, heat carried by the gas is significant and may influence the region of multiplicity and derived an expression for the minimum feed gas temperature beyond which uniqueness is assured. Shaikh and Varma [22], on the other hand, proved that the effect of feed gas temperature on the uniqueness region depends on the nature of feed gas, a parameter not considered by Singh et al. [21]. Shaikh and Varma [22] also obtained criteria for the uniqueness and multiplicity for the case of fast pseudo first-order reactions in a gas-liquid CSTR using models which account for the nature of feed gas and variation of interfacial area with conversion and temperature, and concluded that the multiplicity region increases with the increase in purity of feed gas.

White and Johns [23] based their reactor model on an approach taking into account the interfacial temperature rise and identified conditions under which it is important. They divided the total reaction zone into five operating regions and reported that a maximum of five steady states is possible and that there can be at most one solution in each region. In a limiting case this model reduces to the earlier model developed by Hoffman et al. [15].

Shaikh [11] analysed the effect of gas-side mass transfer resistance on uniqueness and multiplicity in a non-adiabatic gas-liquid CSTR with a fast pseudo first-order reaction.The author showed that the likelihood of multiplicity decreases in the presence of such resistance and proved that the number of

possible steady states with gas-side resistance does not exceed that encountered without gas-side resistance which is in contrast to the earlier speculation of Westerterp and Crombeen [24,25]. The effect of liquid volatility on steady state multiplicity has been studied by Westerterp and Crombeen [25] and very recently by Shaikh et al. [26]. Other notable research papers and reviews on steady state multiplicity features are those of Balakotaiah and Luss [27,28], Uppal et al. [29], Leib and Luss [30] on single-phase CSTRs, and Luss [31] on gas-liquid CSTRs.

It is evident from the literature review on steady state multiplicity in gas-liquid CSTRs that none of the previous studies has attempted to account for the variation of hydrodynamic and transport parameters (i.e. phase holdups, interfacial area and heat and mass transfer coefficients) with the operating conditions in case of general second-order reactions. In the majority of these studies when the influence of a certain parameter on steady state multiplicity was investigated, the values of other hydrodynamic parameters were kept constant. Though this has been done mainly to simplify the mathematics and numerical solution of the resulting complex model equations, it is, however, not always realistic to fix these parameters while the operating conditions are changing, since they are the result of the combined action of physico-chemical properties of the reaction fluids, vessel geometry, and operating conditions. Thus, in the present work an attempt has been made to develop a rigorous model which accounts for the variation of hydrodynamic and transport parameters with the operating conditions using empirical correlations available in the literature. A review of published correlations for hydrodynamic and

transport parameters in a gas-liquid stirred tank reactor is given in the next section.

2.2 Review of Correlation for Hydrodynamic, Transport and Associated Parameters

Correlations published in the literature for the following hydrodynamic and transport parameters will be reviewed in this section:

- Minimum impeller speed for effective dispersion of gas.
- Specific power input with and without gas.
- Bubble diameter and rise velocity.
- Gas hold-up.
- Interfacial area.
- Liquid and gas-side mass transfer coefficients.
- Tank-side and jacket/coil-side heat transfer coefficients.

The correlations for minimum impeller speed, specific power input and bubble diameter are essential for the calculation of other parameters mentioned in the above list. In this review we will not discuss the measurement of various hydrodynamic parameters. An excellent review on the measurement techniques is given by Joshi et al. [32]. Other important review papers in this area are those of Oyevaar and Westerterp [33], Ridgway et al. [34] and Schugerl et al. [35].

2.2.1 General Background

A number of points which are of general importance are discussed in this section. They include the types of impellers, standard reactor configuration,

mechanism of gas dispersion by an agitator, and important dimensionless groups appearing in various correlations.

2.2.1.a Types of Impellers

The principal functions of an impeller in gas-liquid stirred tank reactors are to effectively disperse the gas into the liquid phase and to create interfacial area by breaking up the dispersed gas phase. A wide variety of impellers are used in practice. Some of the most common types of impellers are shown in Figure 2.1. Selection of an impeller is an important decision in case of multiphase systems since different impellers generate different gas and liquid flow patterns. The choice of a particular impeller depends on the mixing requirement of the process and the physical properties of the fluids to be handled.

High speed impellers such as propellers and disk turbines are used for substances of low viscosity and low speed impellers such as anchors are employed, generally, for highly viscous substances. Detailed discussions on various types of impellers are given in many references on mixing [37,38,39,40]. These references provide information on design and performance of different types of impellers. A good review on types and selection of impellers for gas-liquid systems from the heat transfer stand point is given by Steiff et al. [41].

The most widely used impeller for gas-liquid systems is the flat-blade disc turbine often referred to as Rushton turbine [42]. The widespread use of Rushton turbines is due to the fact that the disc in such impellers prevents short circuitting of the gas when a gas sparger is placed below the impeller. Also,

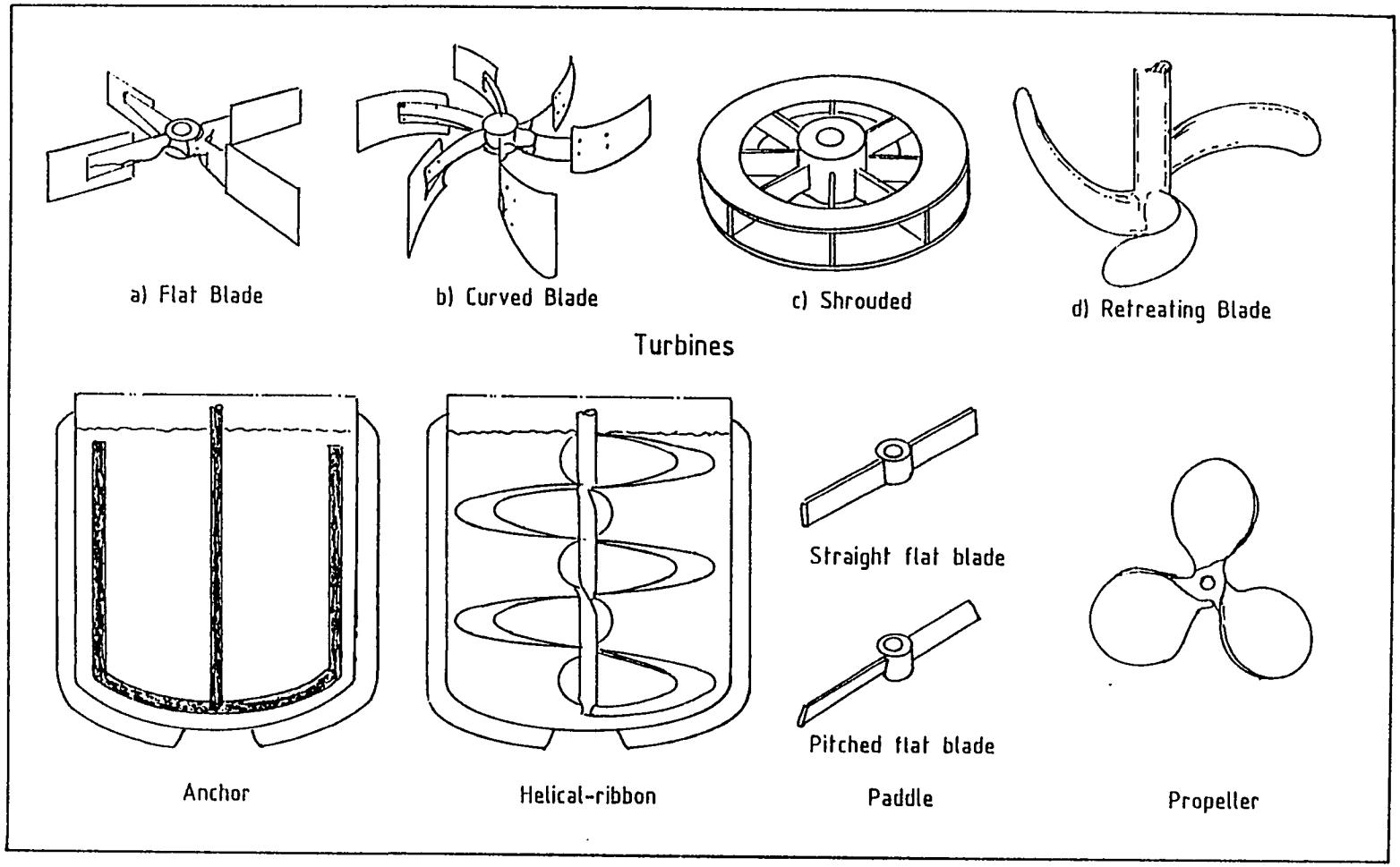

Figure 2.1 Various Types of Impellers [36]

these impellers have better gas handling capacity which can be further increased by incorporating more than six blades [4]. Flat-blade disc turbines are also used with the standard reactor configuration.

2.2.1.b Standard Reactor and Impeller Geometry

Most of the published experimental studies related to hydrodynamics and heat and mass transfer characteristics of gas-liquid stirred reactors have been performed using standard reactor and impeller configurations. A schematic diagram of a standard gas-liquid CSTR, originally proposed by Holland and Chapman [43], is shown in Figure 2.2. The standard configuration is comprised of a cylindrical tank with a flat bottom, liquid and gas feed and withdrawal arrangements, stirring device and a cooling or heating arrangement which could be either a jacket surrounding the tank or a helical coil inserted inside the reactor. In order to prevent swirling or vortex formation, the tank is often equipped with four baffles over its entire height. Power to a a six-blade disc turbine agitator is supplied through a rotating shaft and is used mainly to generate a suitable liquid and gas flow pattern and to create the interfacial area by breaking up the dispersed gas phase through the shearing action of the stirrer. The gas is generally introduced at the bottom of the reactor through a ring sparger placed just below the agitator [4]. The geometrical relationships of a standard gas-liquid CSTR are given as follows:

$$\text{Clear liquid height, } H_L = \text{Tank diameter, } D_T$$

$$\text{Impeller diameter, } D_I = \frac{D_T}{3}$$

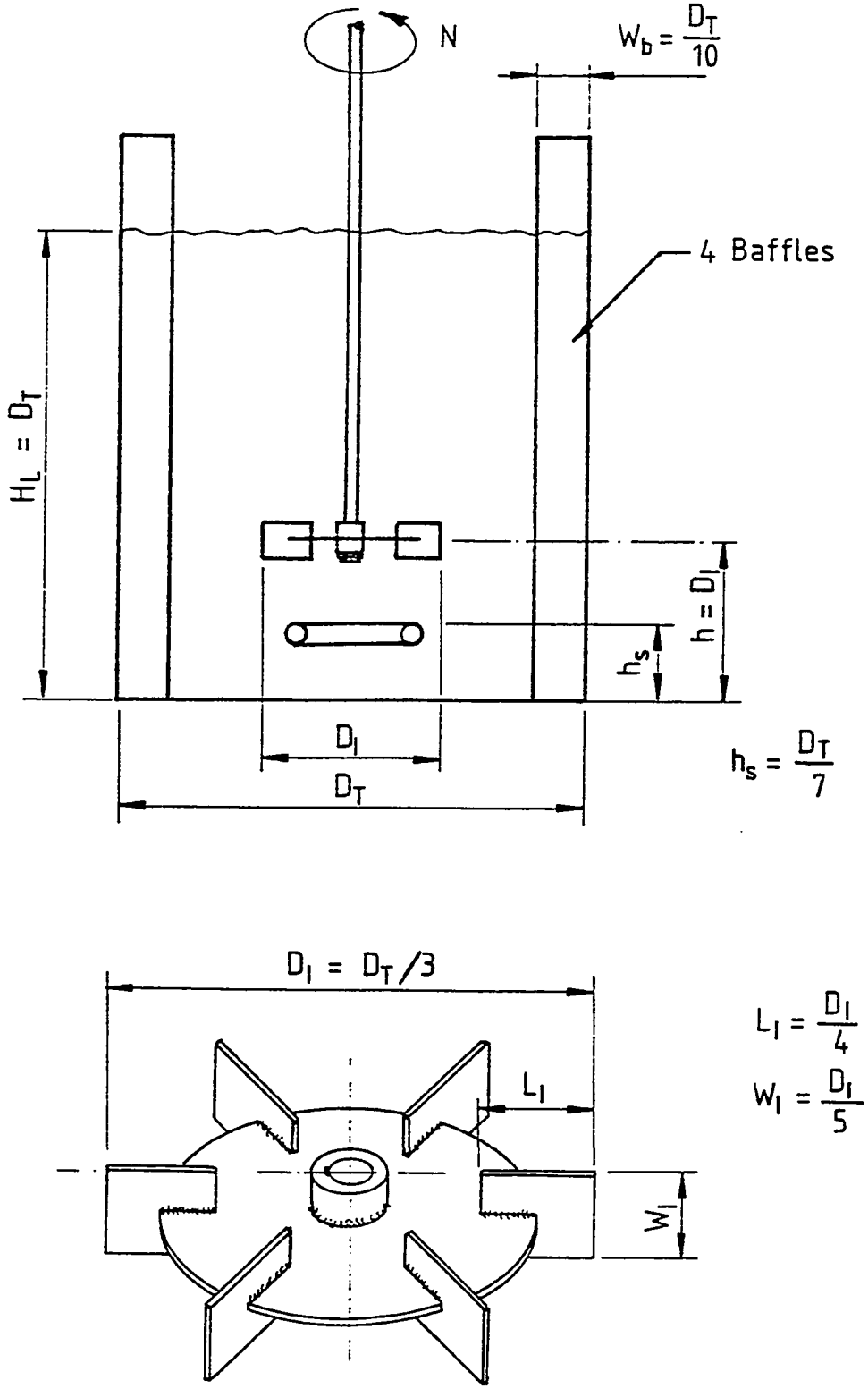

Figure 2.2 Schematic Diagram of a Standard Gas-Liquid CSTR [44]

Impeller position from the tank bottom, h = D_I

Impeller blade width, $W_I = \frac{D_I}{5}$

Impeller blade length $L_I = \frac{D_I}{4}$

Baffle width, $W_b = \frac{D_T}{10}$

Ring sparger diameter, $D_s = \frac{3D_I}{4}$

Sparger placement from tank bottom, $h_s = \frac{D_T}{7}$

Though, the standard configuration has been widely used in research, it is occasionally adopted in practice. A wide variation with regard to aspect ratio ($\frac{H_L}{D_T}$) and type of impeller exists in industry [40,45]. However, in order to develop a thorough understanding of the behavior of gas-liquid CSTRs and to be able to compare the results of different researchers, use of standard geometry is justified. For our numerical simulation study we will use standard reactor geometry.

2.2.1.c Mechanism of Gas Dispersion in a Standard Reactor Geometry

Adequate gas dispersion is essential for creating sufficient interfacial area and gas hold-up in a CSTR. Many authors [46,47,48,49] have explained the phenomenon of gas dispersion in a stirred tank reactor. According to these researchers under unaerated conditions, a pair of counter-rotating high speed

vortices, as shown in Figure 2.3, are formed behind each blade of a Rushton turbine. Due to large centrifugal forces in these vortices, low pressure regions are created. When a gas is sparged in such reactors, the low pressure regions of the vortices suck any gas bubble in the near vicinity of the impeller and form gas cavities behind the blades. Bubbles entering the impeller zone coalesce with the cavities and new bubbles are formed at the outer periphery of the cavities by turbulent forces [44].

The cavities play a very important role in gas-phase dispersion and reduce impeller power consumption by decreasing the drag coefficient of the blade. According to the shape and size, Bruijn et al. [50] classified the cavities into three categories: vortex cavity, clinging cavity and large cavity as shown in Figure 2.4. Warmoeskerken et al. [51], Ismail et al. [52], Nienow et al. [53] and recently Nienow et al. [54] have studied the sequence in which the cavities are formed in a Rushton turbine. According to these authors, at low gas feed rates, predominantly vortex cavities are formed. As the gas feed rate increases the cavity volume increases and six clinging cavities, one behind every blade, emerge. Further increase in the gas feed rate leads to the formation of three large and three clinging cavities with one large and one clinging cavity in alternate arrangement as shown in Figure 2.4c. At a very high gas feed rate, six large cavities of different sizes are formed. According to Warmoeskerken et al. [51], the most stable operating regime is that with three large and three clinging cavities. The large cavities are the most efficient from the gas dispersion point of view. Also, in case of large cavities the drag coefficient of the blade decreases significantly, leading to substantial decrease in power drawn at constant impeller

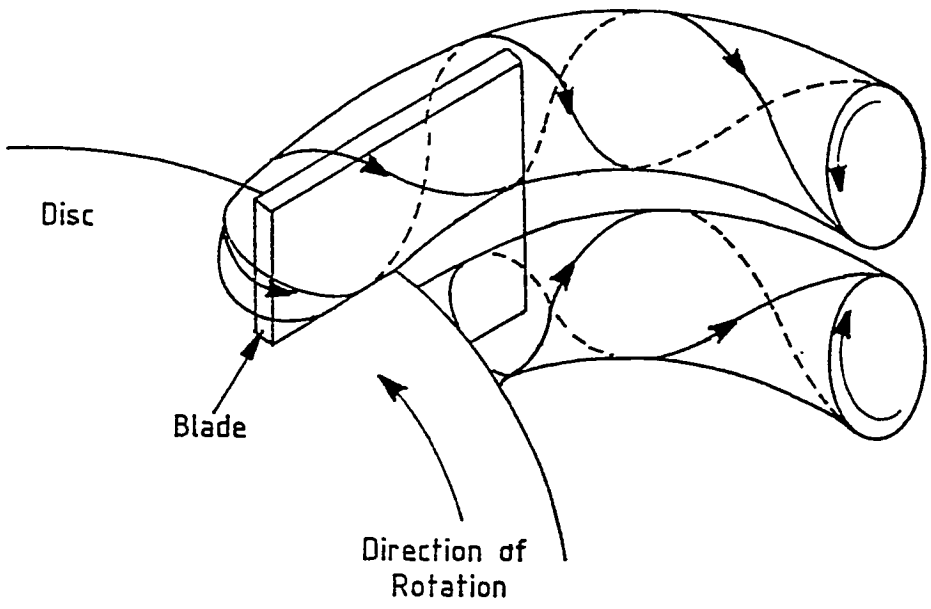

Figure 2.3 Vortices Behind a Rushton Turbine Blade [49]

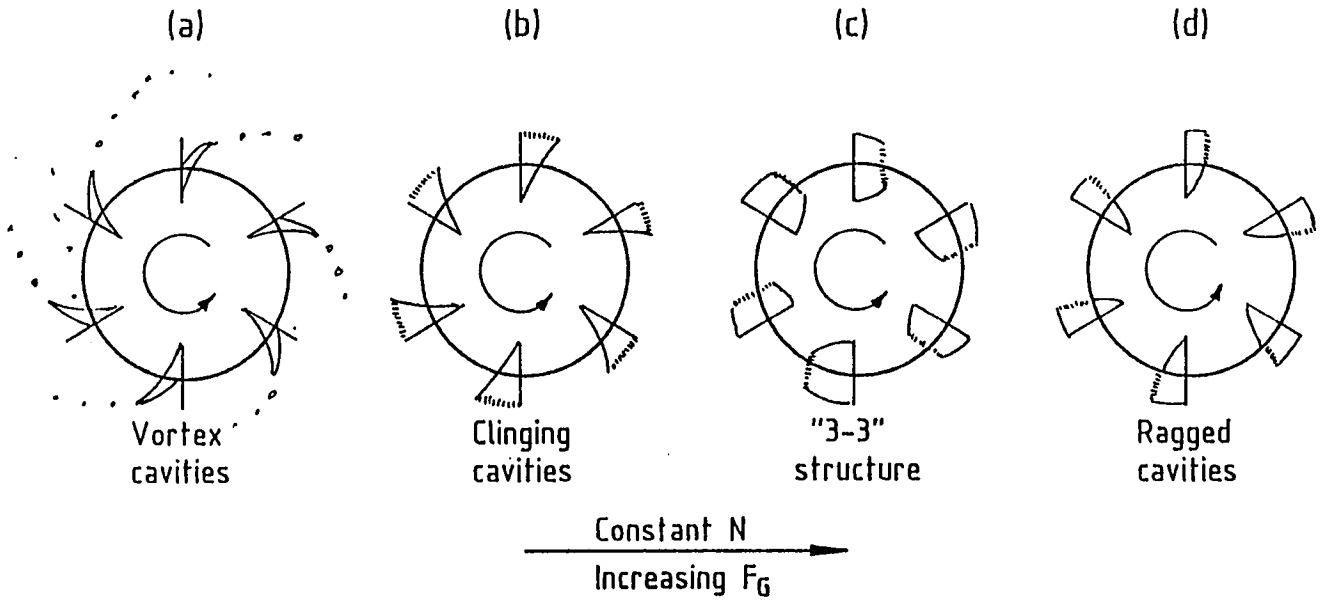

Figure 2.4 Change in Cavity Structure at Increasing Gassing Rates for a Rushton Turbine [54]

speed [55].

Nienow et al. [47] studied the dispersion of gas in a standard stirred tank reactor. They observed that at a constant gas feed rate, if impeller speed is increased several dispersion regimes are possible. These regimes are shown in Figure 2.5. At a very low impeller speed, the gas is not dispersed, it passes around the turbine and flows along the impeller shaft forming a partial bubble column as depicted in Figure 2.5a. This regime is called "flooding". By increasing the impeller speed the bubbles begin to disperse in the region above the impeller forming a full bubble column (see Figure 2.5b). A further increase in impeller speed initiates the circulation of gas below the impeller as shown in Figure 2.5c. Figure 2.5d shows a condition of complete dispersion. At this point the gas is just thoroughly dispersed and further increase in gas flow rate will be of no use since any additional gas will by-pass up the impeller shaft without being dispersed. At a very high impeller speed, secondary circulation of gas as shown in Figure 2.5e starts.

From the operational point of view the complete dispersion regime as shown in Figure 2.5d is *most desirable* and the regime of flooding as shown in Figure 2.5a is *most undesirable* and should be always avoided by operating the reactor at an impeller speed such that the condition of complete dispersion is achieved.

From the foregoing discussion it is clear that a complete gas dispersion regime can only be obtained if the reactor is operated beyond a *minimum impeller speed*. Also, the *impeller power consumption* is considerably reduced in case of complete gas dispersion. Therefore, for design and analysis of

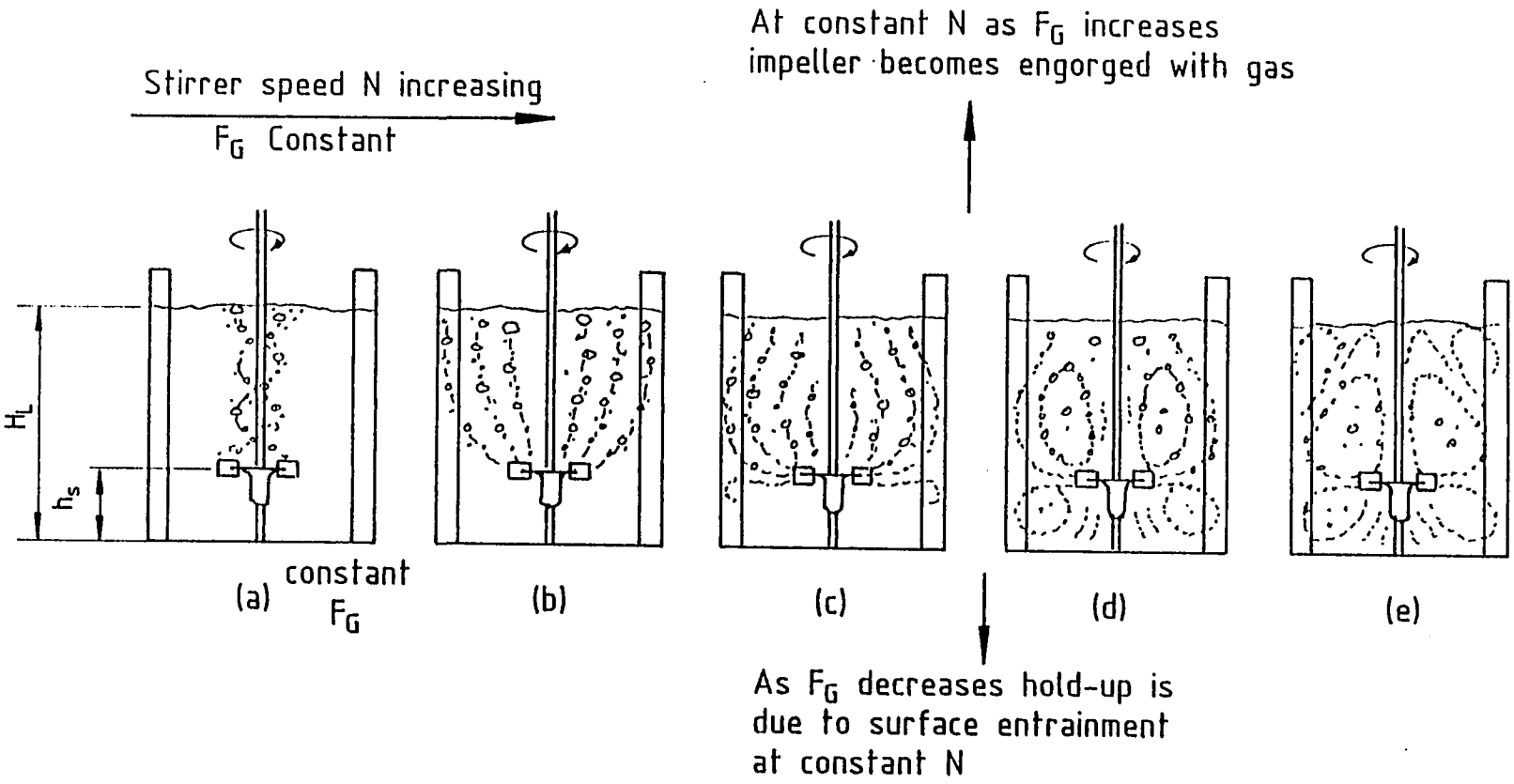

Figure 2.5 Gas Dispersion Regimes in a Stirred Tank Reactor [47]

such reactors prediction of these two quantities is important since they have significant influence on the other hydrodynamic parameters. Many correlations for predicting the minimum impeller speed and the power requirement in presence of gas have been proposed in the literature. A discussion of these correlations will be given in the next section. Further information concerning the dispersion of gas in stirred gas-liquid reactors can be obtained from many published reviews and research papers [4,53,54,55,56] on this subject.

The discussion so far is applicable only for low viscosity, newtonian liquids, in a standard geometry reactor equipped with a six blade Rushton turbine. Literature on viscous and non-newtonian liquids and other type of impellers will not be reviewed here. A recent paper of Nienow et al. [54] has covered gas dispersion performance of different types of impellers with non-newtonian liquids.

2.2.1.d Variables and Dimensionless Numbers Used in Correlations

Variables affecting the performance of gas-liquid CSTRs fall under three categories: physico-chemical variables, operating variables and geometrical variables. Some of the important *variables* involved in the correlations for hydrodynamic and transport parameters are summarized in Table 2.2. Important dimensionless *groups* appearing in various correlations to be discussed in the next sections are presented in Table 2.3.

Table 2.2 Principal Variables Involved in the Correlations for Hydrodynamic, Transport and Associated Parameters

Classification of Variable	Variable Name
Physical - Chemical	Liquid Viscosity (μ_L), Liquid Density (ρ_L), Interfacial Tension (σ), Partial Pressure of Reactive Gas Species (p_A), Diffusion Coefficient (D_A), Reaction Rate constant (K), Solubility of Gaseous Component (H_A, C_{Ai})
Operating	Speed of Rotation of the Impeller (N), Gas Flow Rate (F_G), Liquid Feed Rate and Volume (F_L, V_L)
Geometrical	Dimension and Geometric Ratios of the Tank (D_T, H_L, $\frac{D_I}{D_T}$), Type and Dimension of the Impeller (D_I,W,L), Type and Dimension of the Sparger (D_s)

Table 2.3 Dimensionless Numbers Involved in the Correlations of Hydrodynamic, Transport and Associated Parameters

Name	Definition	Physical Significance
Newton number, N_p	$\frac{P_o}{\rho_L N^3 D_I^5}$	$\frac{Power\ dissipated\ by\ the\ agitator}{Power\ dissipated\ by\ the\ inertial\ forces}$
Reynolds number (rotation), Re_n	$\frac{\rho_L N D_I^2}{\mu_L}$	$\frac{inertial\ force}{viscous\ force}$
Reynolds number (bubble), Re_b	$\frac{\rho_L V_T d_b}{\mu_L}$	$\frac{inertial\ force}{viscous\ force}$
Froude number (rotation), F_{rn}	$\frac{N^2 D_I}{g}$	$\frac{inertial\ force}{gravitational\ force}$
Aeration number, N_A	$\frac{F_G}{N D_I^3}$	$\frac{gas\ feed\ rate}{pumping\ rate}$
Weber number, W_{en}	$\frac{\rho_L N^2 D_I^3}{\sigma}$	$\frac{inertial\ force}{surface\ tension}$
Galileo number, G_a	$\frac{\rho_L^2 g D_I^3}{\mu_L^2}$	$\frac{inertial\ force \times gravity\ force}{viscous\ force^2}$
Schmidt number, *Sc*	$\frac{\nu_L}{D_A}$	$\frac{momentum\ diffusuvuty}{molecular\ diffusivity}$
Sherwood number, *Sh*	$\frac{K_L D_I}{D_A}$	$\frac{covectivity}{molecular\ diffusivity}$
Nusselt number, N_{uT}	$\frac{h_T D_T}{\lambda_L}$	$\frac{covectivity}{conductivity}$
Flow number, F_N	$\frac{g d_b^{8/3} \Delta\rho \rho_L^{2/3}}{\mu_L^{4/3} \sigma^{1/3}}$	Associated with the flow of the continuous phase due to motion of dispressed phase
Velocity number, V_N	$\frac{V_T d_b^{2/3} \rho_L^{2/3}}{\mu_L^{1/3} \sigma^{1/3}}$	Arised from the kinetic energy created in the continuous phase due to bubble motion

2.2.2 Minimum Impeller Speed

As stated in the previous section, flooding of impeller is undesirable from the operational view point. Under the condition of flooding, liquid circulation velocities are much reduced and the sparged gas is not well dispersed. As a result the gas hold-up and interfacial area are reduced to such an extent that they are not of any practical significance for gas-liquid reactions. Thus, to avoid impeller flooding and to create a condition of complete gas dispersion in the reactor, impeller speed should be kept beyond a certain minimum speed. An expression for the minimum impeller speed (N_m) can be obtained theoretically from simple bubble mechanics consideration, as first indicated by Westerterp et al. [57]. According to these authors, the speed of impeller should be such that the impeller tip velocity, $N_m D_I$, is always greater than the bubble rise velocity so that the bubbles are directed radially outward rather than escape axially upward.

Many authors have studied the flooding behavior of gas-liquid stirred reactors and have proposed correlations for predicting the minimum speed to avoid flooding. These correlations for Rushton turbines are summarized in Table 2.4. The correlations listed can be classified into two types: those that contain liquid physical properties as variables and those that do not contain the physical properties. Most of the recent correlations can be represented by the following dimensionless expression:

$$N_A = K (F_{rm})^a (\frac{D_I}{D_T})^b \qquad (2.1)$$

Table 2.4 Correlation for Minimum Impeller Speed for Rushton Turbine Impeller

Reference	Geometry	Correlation (Dimensionless)	Correlation (Explicit form)
Westerterp et al. (1963) [57]	$D_T(m) = 0.14 - 0.9$ $\frac{D_I}{D_T} = 0.2 - 0.7$	$\left(\frac{N_m D_I^2 \mu_L}{\sigma D_T}\right)\left(\frac{\sigma^3 \rho_L}{g\mu_L^4}\right)^{1/4} = 1.22\frac{D_I}{D_T} + 1.25$	$N_m \left(\frac{\sigma g}{\rho_L}\right)^{0.25} \frac{1}{D_I}\left[1.22 + 1.25\frac{D_T}{D_I}\right]$
Milkulcova et al. (1967) [58]	–	$\left(\frac{F_G}{N_m D_I^3}\right) = \frac{100}{6.11 \pm 1.24}\left(\frac{N_m^2 D_I}{g}\right)\left(\frac{D_I}{D_T}\right)^{+3.43}$	$N_m = \left(\frac{6.11 \pm 1.24}{100}\right)^{1/3}\left(\frac{F_G g}{D_I^4}\right)^{1/3}\left(\frac{D_T}{D_I}\right)^{1.143}$
Dierendonck et al. (1968) [59]	$D_T(m) = 0.15 - 0.92$ $\frac{D_I}{D_T} = 1/3$	Pure Liquid $\left(\frac{N_m D_I^2}{D_T}\right)(gD_T)^{-1/2} = 0.07, \quad D_T < 1.0\ m$ $D_T > 1.0\ m$ $\left(\frac{N_m D_I^2 H_L}{\sigma D_T}\right)\left(\frac{\rho_L \sigma^3}{g\mu_L^4}\right)^{1/4} = 2\left(\frac{\mu_L - h_s}{D_T}\right)^{1/2}$ Ionic Solution $\left(\frac{N_m D_I^2}{D_T}\right)\left(\frac{\rho_L}{g\sigma}\right)^{1/4} = 1$	Pure Liquids $N_m = 0.219 D_T^{1.5} D_I^{-2}$ for $D_T < 1.0\ m$ $N_m = 2(h_s D_T)^{1/2}(g\sigma/\rho_L)^{1/4} D_I^{-2}, D_T > 1.0m$ Ionic Solution $N_m = D_T D_I^{-2}(g\sigma/\rho_L)^{1/4}$
Smith et al. (1977) [60]	$D_T(m) = 0.44 - 1.83$ $\frac{D_I}{D_T} = 1/3 - 1/2$	$\left(\frac{N_m^2 D_I}{g}\right) = F_{rn} = 0.1 D_I^2$	$N_m = 0.99 D_I^{1/2}$
Nienow et al. (1977) [47]	$D_T(m) = 0.29$ $\frac{D_I}{D_T} = 1/3 - 2/3$	$\left(\frac{F_G}{N_m D_I^3}\right) = 0.196 F_{rn}^{0.5}\left(\frac{D_I}{D_T}\right)^{0.4} D_I^{0.1}$	$N_m = 4 F_G^{1/2} D_T^{1/4} D_I^{-2}$
Dickey (1979) [61]	–	$\left(\frac{F_G}{N_m D_I^3}\right) = 1.88\left(\frac{N_m^2 D_I}{g}\right)^{0.5}\left(\frac{D_I}{D_T}\right)^{1.5}$	$N_m = 0.73\left(\frac{F_G\sqrt{g}}{D_I^{3.5}}\right)^{1/2}\left(\frac{D_T}{D_I}\right)^{0.75}$
Wiedmann et al. (1980) [62]	$D_T(m) = 0.45$ $\frac{D_I}{D_T} = 1/3$	$\frac{F_G}{N_m D_I^3} = 0.539 F_{rn}^{1.265}$	$N_m = 2.694\ F_G^{0.283} D_I^{-1.207}$
Greaves and Kobbacy (1981) [55]	$D_T(m) = 0.203$ $\frac{D_I}{D_T} = 0.375 - 2/3$	$\left(\frac{F_G}{N_m D_I^3}\right) = 16.398 a^{-3.45} F_{rn}^{1.225}\left(\frac{D_I}{D_T}\right)^{0.689} D_I^{1.086}$ a = 1.52 for pure liquids a = 1.66 for ionic solution	$N_m = a F_G^{0.29} D_T^{0.2} D_I^{-1.74}$ a = 1.52, for pure liquids a = 1.66, for ionic solution.

Table 2.4 Continued

Reference	Geometry	Correlation (Dimensionless)	Correlation (Explicit form)
Ismail et al. (1984) [52]	$D_T(m) = 0.4$ $\frac{D_L}{D_T} = 1/3$	$\left(\frac{F_G}{N_m D_I^3}\right) = 13.4 F_{rn}^{0.873} \left(\frac{W n_b}{D_I}\right) \left(\frac{D_I^2 - d_I^2}{D_I^2}\right)$	$N_m = 0.39 \left(\frac{F_G g^{0.873}}{D_I^{3.873}}\right)^{0.364} \left(\frac{D_I}{W n_b}\right)^{0.364} \left(\frac{D_I^2}{D_I^2 - d_I^2}\right)^{0.364}$
Warmoeskerken and Smith (1985) [63]	$D_T(m) = 0.44 - 1.2m$ $\frac{D_L}{D_T} = 0.4$	$\left(\frac{F_G}{N_m D_I^3}\right) = 1.2\ F_{rn}$	$N_m = 0.941 \left(\frac{g F_G}{D_I^4}\right)^{1/3}$
Wong et al. (1986) [64]	$D_T(m) = 0.29$ $\frac{D_L}{D_T} = 1/3$	$\left(\frac{F_G}{N_m D_I^3}\right) = 37.45 F_{rn}^{1.167} D_I^{1.83}$	$N_m = 0.75 F_G^{0.3} D_I^{-1.8}$
Wiedmann et al. (1986) [63]	$D_T(m) = 0.2 - 1.5$ $\frac{D_L}{D_T} = 1/3$	$\left(\frac{F_G}{N_m D_I^3}\right) = 0.973 \left(-0.15 + M_r^{1/4} + 0.05 \ln\left(\frac{W_e}{F r_n}\right)\right) \times F_{rn}^a + 0.2\ Fr_n^{1.6}$ $a = 0.605 + 1/\ln\left(\frac{W_e}{F r_n}\right)$	$N_m = 5.544 \left(\frac{D_T}{T_I}\right)^{0.361} \left(\frac{F_G q^{1/3}}{D_I^{4.3}}\right)^{0.277} G_a^{-0.097}$
Lu and Chen (1986) [64]	$D_T(m) = 0.288$ $\frac{D_L}{D_T} = 0.33$	$\left(\frac{F_G}{N_m D_I^3}\right) = 111.93 (F_{rn})^{1.167} D_I^{1.83}$	$N_m = 0.54 Q_G^{0.3} D_I^{-1.8}$
Desplanches et al. (1988) [65]	$D_T(m) = 0.3 - 0.63$ $\frac{D_L}{D_T} = 0.33 - 0.5$	$\left(\frac{F_G}{N_m D_I^3}\right) = 0.0021 (F_{rn})^{1.3} \left(\frac{D_L}{D_T}\right)^{1.3} (Ga)^{0.35}$ valid for highly viscous liquids $(\mu_L = 100 - 1000\ cp)$	
Lu and Ju (1989) [66]	$D_T(m) = 0.238$ $\frac{D_L}{D_T} = 0.25 - 0.49$	$\left(\frac{F_G}{N_m D_I^3}\right) = \frac{F_{rn} (D_I/D_T)^{3.5}}{[A(4.07 + 1.21 n_b - 0.147 n_b^2)]^3}$	$N_m = A \left(\frac{D_T}{D_I}\right)^{3.5/3} \left(\frac{g F_G}{D_I^4}\right)^{1/3} (4.07 + 1.21 n_b - 0.147 n_b^2)$ $A = 0.072$ for the highest limit of impeller flooding. $A = 0.064$ for the lowest limit of gas dispersion.
Nienow et al. (1990) [54]	$D_T(m) = 0.29 - 1.2$ $\frac{D_L}{D_T} = 0.22 - 0.58$	$\left(\frac{F_G}{N_m D_I^3}\right) = 30 (F_{rn}) \left(\frac{D_L}{D_T}\right)^{3.5}$	$N_m = 0.322 \left(\frac{g F_G}{D_I^4}\right)^{1/3} \left(\frac{D_T}{D_I}\right)^{3.5/3}$

The exponents a and b in Equation (2.1) are always in the the following ranges:

$$a = 0.5 - 1.3$$

$$b = 0 - 3.5$$

The constant, K, however, varies very widely from 0.19 to 112. Equation (2.1) indicates that the impeller geometry and gas flow rate are the two important parameters which affect the flooding characteristics of the reactor.

2.2.3 Impeller Power Consumption

2.2.3.a Power Consumption in Unaerated Systems.

Power consumption of an impeller depends on the speed of rotation, number of phases, physical properties of the fluids and the type and geometry of the impeller. Since we will be using the standard reactor configuration in our simulation study, power characteristics of only Rushton turbines will be considered.

In order to calculate the power consumption by an impeller into a gas-liquid system, it is essential to know the relationship for the power consumption in an unaerated system, P_o, because most of the correlations for power uptake in presence of gas are based on P_o. This subject has been extensively studied and has been reviewed by Uhl and Gray [37], Nagata [38] and Holland and Chapman [43].

For a given geometry and arrangement of internals, the power consumption of an impeller in a single phase newtonian liquid is usually expressed as [43]:

$$P_o = N_p \rho_l N^3 D_I^5 \tag{2.2}$$

where, N_p is a dimensionless quantity called power number and depends on type of impeller and impeller Reynold number. Using dimensional analysis Rushton et al. [42] correlated the power data for Rushton turbines on the basis of the following relation:

$$N_p = K R_{en}^a F_{rn}^b \tag{2.3}$$

The Froude number is required to account for the vortex in swirling systems. The exponent b is usually zero in case of fully baffled reactors, which do not produce vortices. Some of the curves given by Rushton [42] are shown in Figure 2.6. The power number decreases linearly with R_{en} in the laminar regime ($R_{en} < 10$) and becomes constant in the turbulent regime ($R_{en} > 10^4$). These curves also show that in the turbulent regime the power consumption depends on the configuration of the turbine blades and the presence of baffles. Depending on the degree of baffling, Barona [69] has recommended the following values of power number for gas-liquid systems stirred with six flat blade disc turbine:

% Baffling :	17	10	4	0
N_p :	6.6	6.0	4.2	$2.2R_{en}^{-0.057}$

The power number can also be calculated from the dimensions of the impellers by using the equation of Calderbank and Moo-Young [70] which has the following form:

$$N_p = \frac{160 L_b W (D_I - L_b)}{D_I^3} \tag{2.4}$$

Once the power number corresponding to a given system is known, P_o can be

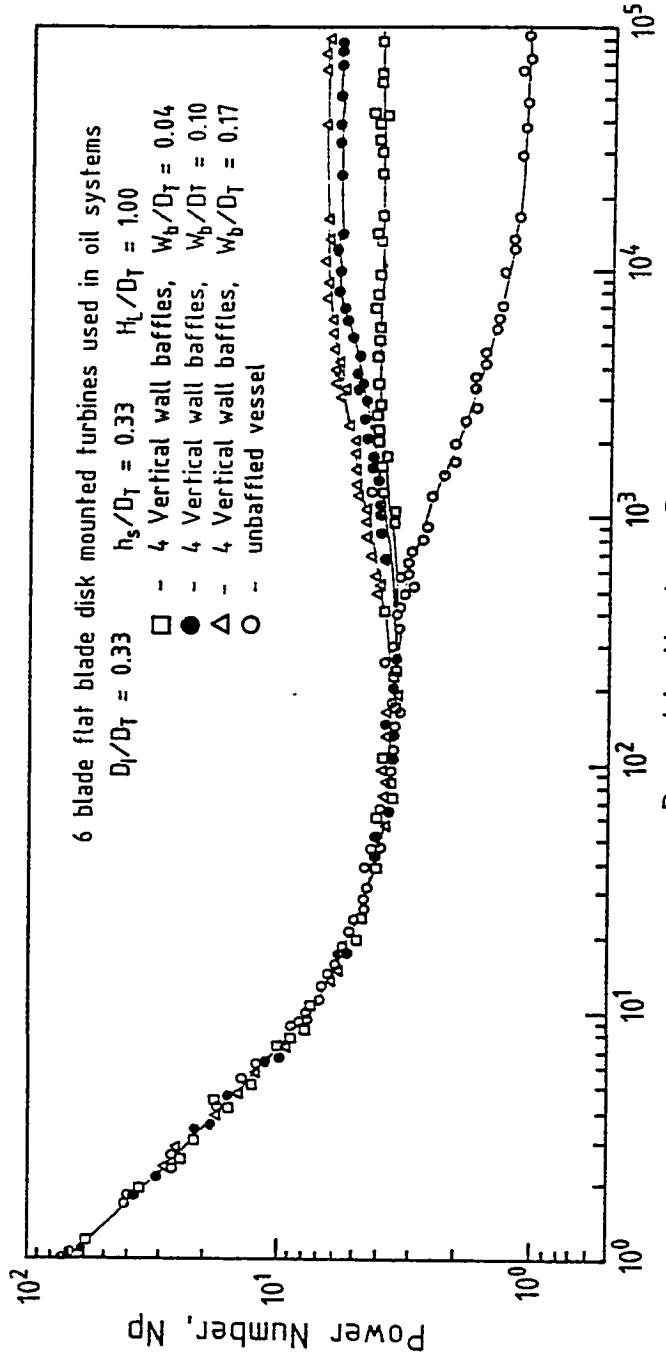

Figure 2.6 Power Curves for Flat Blade Disk Turbine Agitator with Various Baffle Widths [42]

calculated using Equation (2.2).

2.2.3.b Power Consumption in Presence of Gas

The presence of gas lowers the power uptake of the impeller significantly. The reduction in power is due to the formation of stable cavities at the rear of each impeller blade, which reduces the form drag and hence the power consumption [50]. Figure 2.7 shows the progressive drop in power drawn as the gas feed rate is increased [4]. Bruijn et al. [50] and Warmoeskerken and Smith [51] have shown that the reduction in power consumption in the presence of gas is greatly influenced by the number of blades and the impeller speed. Figure 2.8 shows that at any given gas rate, the power uptake is greater at higher number of blades. However, an increase in number of blades improves the gas handling capacity of the impeller due to the increased number of cavities. Figure 2.9 shows the effect of impeller speed on the gassed power behavior. It appears from Figure 2.9 that minimum value for P_G/P_o is about 0.27.

Extensive experimental work has been done on impeller power consumption in aerated vessels with or without baffles and an excellent review of this area is given by Midoux and Charpentier [2]. Mann [4] and Joshi et al. [71] have also reviewed the correlations for power consumption in presence of gas. Most of the investigators have correlated their gassed power data using the following form:

$$P_G = a\left[\frac{P_o^2 N D_I^3}{F_G^{0.56}}\right]^b \tag{2.5}$$

where a = 0.45 - 1.40 and b = 0.34 - 0.48

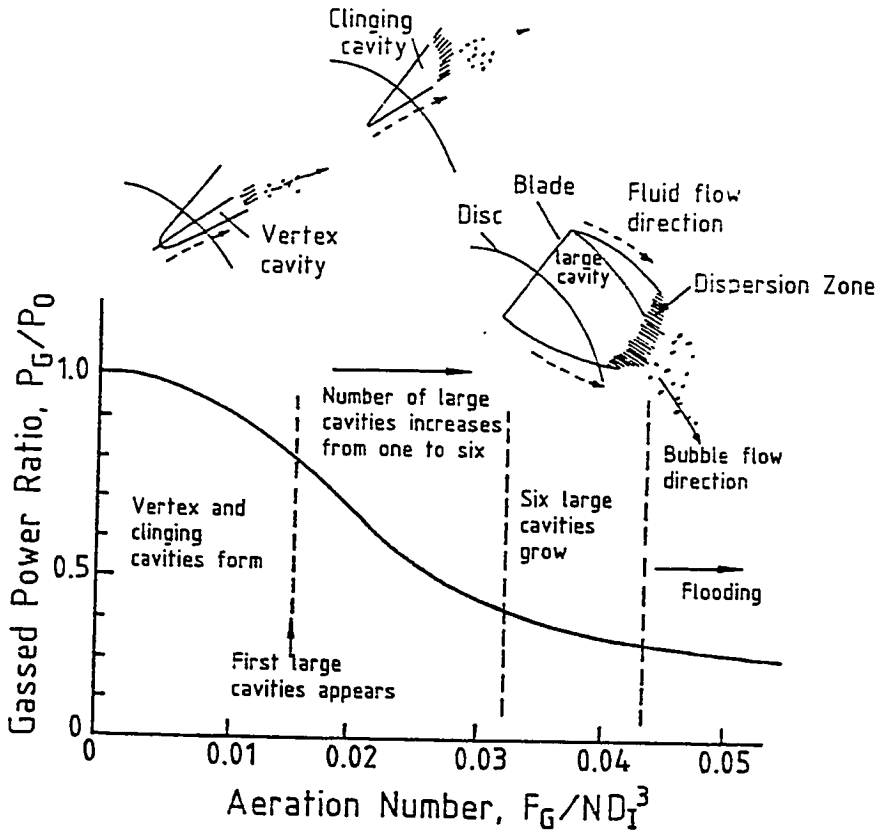

Figure 2.7 Different Type of Cavities and their Growth in Relation to the Gassed Power Curve [4]

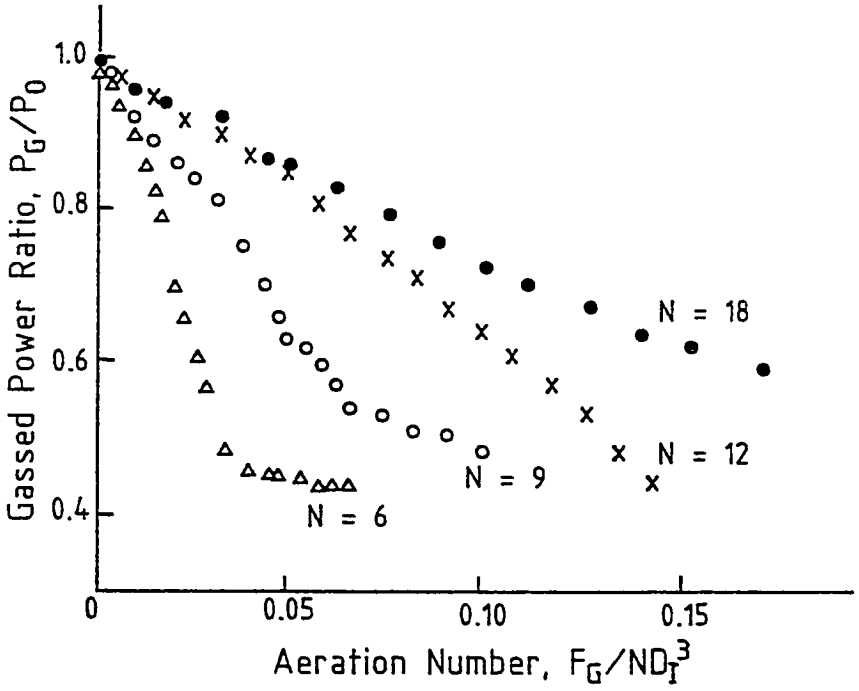

Figure 2.8 Effect of Number of Disk Blades on Gassed Power Ratio [50]

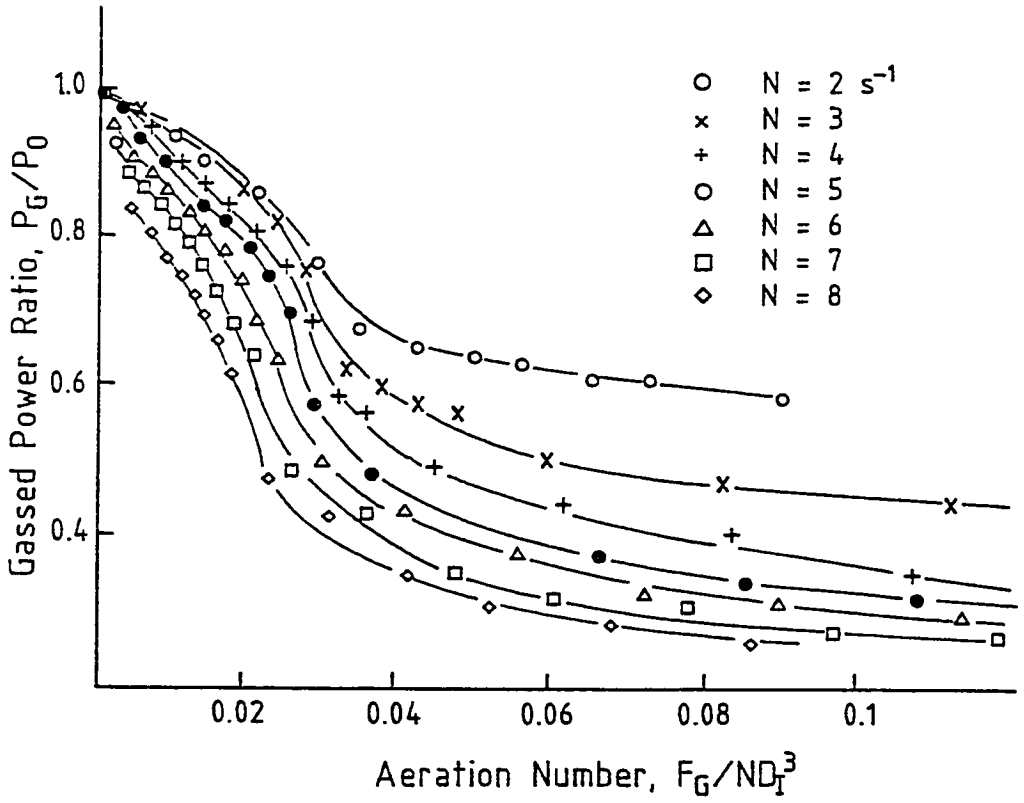

Figure 2.9 Effect of stirrer Speed on Gassed Power Behavior [51]

Equation (2.5) was first proposed by Michel and Miller [72] with a = 0.72 and b = 0.45. A comprehensive list of correlations of the above form along with the experimental details is given by Midoux and Charpentier [2]. Equation (2.5) is an empirical correlation and successfully correlates gassed power data over a wide range of system conditions [2]. Though Equation (2.5) is convenient to use, it fails at extreme values of gas feed rate. According to Mann [4], the usual good fit to the experimental data given by Equation (2.5) is due to the reason that P_G/P_o shows much less than one order of magnitude variation. Thus, P_G is expected to correlate well with $P_o^{0.9}$ as required by Equation (2.5).

Many other forms of correlations have also been proposed in the literature. The correlations other than the form shown by Equation (2.5) are summarized in Table 2.5. It is clear from Table 2.5 that the major correlating parameter in these correlations is the aeration number.

Correlations proposed by Calderbank [73] and Pharamond et al. [74] are similar in form. The main advantage of these correlations is that they are applicable as F_G approaches zero.

Nagata [38] proposed a different form of dimensionless correlation for a Rushton turbine. This correlation involves Raynold number for rotation, aeration number and the ratio of impeller to reactor diameter and is also applicable at $F_G=0$. Midoux and Charpentier [2] tested the correlation of Nagata [38] using the gassed power data of other researchers representing a wide range of liquid physical properties and found that Nagata's correlation

Table 2.5 Correlations for Gassed Power Consumption by a Rushton Turbine

Reference	Geometry	System	Correlation
Calderbank (1958) [73]	$D_T(m)$ = 0.5, 0.184 $\frac{D_I}{D_T}$ = 0.33 $\frac{H_L}{D_T}$ = 1	Air-Water	for $\frac{F_G}{ND_I^3} < 0.035$ $\frac{P_G}{P_o} = 1 - 1.26\left(\frac{F_G}{ND_I^3}\right)$ for $\frac{F_G}{ND_I^3} > 0.035$ $\frac{P_G}{P_o} = 0.62 - 1.85\left(\frac{F_G}{ND_I^3}\right)$
Pharamond et al. (1975) [74]	$D_T(m)$ = 0.29 – 1 $\frac{D_I}{D_T}$ = 0.33 $\frac{H_L}{D_T}$ = 1	Air-Water	$\frac{P_G}{P_o} = 1 - 1.6\left(\frac{F_G}{V_L}\right)D_I^{0.63}$
Nagata (1975) [38]	$D_T(m)$ = $\frac{D_I}{D_T}$ = $\frac{H_L}{D_T}$ =		$\frac{P_G}{P_o} = \exp\left[-442\left(\frac{D_I}{D_T}\right)^{4.38}\left(\frac{\rho_L N D_I^2}{\mu_L}\right)^{-0.115} \times \left(\frac{D_I N^2}{g}\right)^{1.96 D_I/D_T}\left(\frac{F_G}{ND_I^3}\right)\right]$
Hassan and Robinson (1977) [75]	$D_T(m)$ = 0.29 $\frac{D_I}{D_T}$ = 0.33 $\frac{H_L}{D_T}$ = 1	Air-Aqueous Solution	$\frac{P_G}{P_o} = C\left(\frac{\rho_L N^2 D_I^3}{\sigma}\right)^{-0.25}\left(\frac{F_G}{ND_I^3}\right)^{-0.38}$
Luong and Volesky (1979) [76]	$D_T(m)$ = 0.22 $\frac{D_I}{D_T}$ = 0.33 $\frac{H_L}{D_T}$ = 1	Air-Glycol Air-CMC Soln.	$\frac{P_G}{P_o} = 0.497\left(\frac{\rho_L N^2 D_I^3}{\sigma}\right)^{-0.18}\left(\frac{F_G}{ND_I^3}\right)^{-0.38}$

Contd.

Table 2.5 Continued.

Hughmark (1980) [77]			$\frac{P_G}{P_o} = 0.1\left(\frac{F_G}{NV_L}\right)^{-0.25}\left(\frac{N^2D_I^4}{gWV_L^{2/3}}\right)^{-0.2}$
Brown (1981) [78]	$D_T(m) = 3.05$ $\frac{D_I}{D_T} = 0.35,0.4,0.45$ $\frac{H_L}{D_T} = 1$	Air-Water	$\frac{P_G}{P_o} = \alpha\left(\frac{F_G}{ND_I^3}\right) EXP(-\beta F_G)$ for $\frac{D_I}{D_T} = 0.35$ $\alpha = 1.00, \beta = 3.41$ for $F_G < 0.170$ $\alpha = 0.65, \beta = 0.88$ for $F_G > 0.170$ for $\frac{D_I}{D_T} = 0.4$ $\alpha = 1.00, \beta = 2.86$ for $F_G < 0.195$ $\alpha = 0.68, \beta = 0.90$ for $F_G < 0.195$ for $\frac{D_I}{D_T} = 0.45$ $\alpha = 1.00, \beta = 1.68$ for $F_G < 0.275$ $\alpha = 0.79, \beta = 0.81$ for $F_G < 0.275$
Greaves and Kobbacy (1981) [55]	$D_T(m) = 0.203$ $\frac{D_I}{D_T} = 0.38,0.5,0.67$ $\frac{H_L}{D_T} = 1$	Air-Water	$P_G = 1007\left(\frac{N^{3.33}D_I^{6.33}}{(\eta F_G)^{0.404}}\right)$ for $N_f > N < N_R$ $\eta = 1$ for $N < N_f$ $\eta = \eta_f$ for $N > N_R$ $\eta = \eta_R$ where, $N_f = 1.52\left[\frac{D_T^{0.2}F_G^{0.29}}{D_I^{1.74}}\right]$ $N_R = 0.57\left[\frac{D_T^{0.97}F_G^{0.13}}{D_I^{2.34}}\right]$ $\eta_R = 4.13\left[\frac{N^{2.53}D_I^{5.93}}{D_T^{2.45}F_G^{0.33}}\right]$ $\eta_f = 0.4\Lambda$ for $\Lambda \leq 1$ $\eta_f = 0.25 + 0.26\Lambda$ for $\Lambda > 1$ $\Lambda = \left[\frac{N^{2.53}D_I^{4.4}}{D_T^{0.5}F_G^{0.73}}\right]$

Contd.

Table 2.5 Continued.

Warmoeskerken and Smith (1985) [63]	$D_T(m) = 0.44$ $\frac{D_I}{D_T} = 0.4$ $\frac{H_L}{D_T} = 1$	Air-Water	for $0 < N_A < (N_A)_{3\text{-}3}$ $\frac{P_G}{P_o} = 1 - 16.7\left(\frac{F_G}{ND_I^3}\right)\left(\frac{N^2 D_I}{g}\right)^{0.35}$ for $(N_A)_{3\text{-}3} < N_A < 0.1$ $\frac{P_G}{P_o} = B - 0.1\frac{A - B}{(N_A)_{3\text{-}3} - 0.1} + \frac{(A - B)\left(\frac{F_G}{ND_I^3}\right)}{(N_A)_{3\text{-}3} - 0.1}$ for $0.1 < N_A < 0.022F_{rm}^{-1}$ $\frac{P_G}{P_o} = 0.27 + 0.022\left(\frac{N^2 D_I}{g}\right)^{-1}$ Where, $(N_A)_{3\text{-}3} = 3.8 \times 10^{-3}\left(\frac{R_{en}^2}{F_{rm}}\right)^{0.07}\left(\frac{D_T}{D_I}\right)^{0.5}$ $(N_A)_f = 30\left(\frac{D_I}{D_T}\right)^{3.5}(F_{rm})_f$ $A = 1 - 17(N_A)_{3\text{-}3}(F_{rm})^{0.35}$ $B = 0.27 + \left(\frac{0.022}{F_{rm}}\right)$
Desplanches (1988) [67]	$D_T(m) = 0.3, 0.63$ $\frac{D_I}{D_T} = 0.33\text{-}0.5$ $\frac{H_L}{D_T} = 1$	Air-Glycerine $\mu_L = 100\text{-}1000cp$	$\frac{P_G}{P_o} = 0.34\left(\frac{F_G}{ND_I^3}\right)^{-0.15}\left(\frac{D_I}{D_T}\right)^{0.1}\left(\frac{\rho_L g D_I^5}{\mu_L}\right)^{0.1}$ *applicable* for $N > N_m$

overestimates the results. They proposed the constant of about -600 instead of -442 in the original correlation.

Correlations by Hassan and Robinson [75] and Luong and Volesky [76] are similar in form. These authors have used the Weber number, which includes surface tension, to correlate the power of agitation. Hughmark [77] performed a statistical analysis of many published gassed power data and found out that the effect of surface tension on the ratio P_G/P_o is not significant, which was also confirmed by Midoux and Charpentier [2]. Furthermore, Hughmark [77] proposed that most of the published gassed power data correlate well by using modified Froude number [$(N^2D^4)/(gWV_L^{2/3})$] and by defining the aeration number using liquid volume in place of D_I^3. Joshi et al [71] have recommended Hughmark's [77] correlations to calculate the impeller power requirement since it covers a very wide range of variables. However, this equation fails at extreme values of gas feed rates.

Most of the Michel and Miller type of correlations have been developed entirely based on an empirical approach. None of the previous authors have incorporated the nature of gas dispersion into gassed power prediction. Recently, after the pioneering work of van't Riet and Smith [46], Bruijn et al. [50] and Nienow et al.[47,53] an understanding of gas dispersion mechanism is emerging and many correlations have been proposed which take into account the prevailing gas dispersion regime.

Brown [78] studied the power consumption in presence of gas in an

industrial scale fermenter ($D_T = 3.05m$) using three impellers of different diameters. Brown's correlation involves two constants, α and β, which depend on the type of impeller and the gas flow rate. The α and β values for a standard impeller configuration are given in Table 2.5. Brown suggested that the power number for large scale unaerated system can be calculated by using Calderbank and Moo-Young [70] equation [see Equation (2.4)] with a constant value of 120 in place of 160 in the original equation. Brown's correlation is the only equation available for industrial scale reactors and is also valid at $F_G = 0$.

The first attempt to incorporate the nature of gas dispersion in predicting the gassed power was made by Greaves and Kobbacy [55]. They proposed a correlation for gassed power requirement which includes the gas dispersion efficiency of the impeller (η). The important features of this correlation are that it is applicable over an entire range of gas dispersion regime and is not based on the power consumption of unaerated system as it does not include P_o. The main drawbacks of this correlation are that it is based on experimental data obtained using very small vessel and the expressions for η, in different regimes were obtained based on qualitative features of gassed power curve with out confirming the correctness of the gas dispersion regime [4].

Warmoeskerken and Smith [63] have proposed a set of correlations to calculate the gassed power requirement in different gas dispersion regimes. This set of correlations has been experimentally verified by the authors using a 0.44 m diameter vessel at different impeller speeds and gas feed rates. A comparison of their predicted and experimental results with impeller diameter to tank

diameter ratio of 0.4 is shown in Figure 2.10. Nienow [54] in his recent paper has recommended the use of Warmoeskerken's equation to calculate the gassed power requirement for low viscosity system. However, this set of equation needs to be tested for large scale reactors.

Recently, Desplanches et al. [67] proposed a correlation for predicting gassed power consumption in a highly viscous gas-liquid system for complete dispersion regime. The Galileo number in their equation represents the effect of viscosity on the gassed power uptake. This correlation is applicable only for $N_A > (N_A)_{CD}$ (i.e. regime of complete dispersion).

2.2.4 Bubble Diameter

Liquid film controlled mass transfer in gas-liquid reactors depends on the bubble size, shape and motion. Thus, it is essential to predict the size of the bubbles and their rising velocity. The bubble diameter in CSTRs depends on the physico-chemical properties of the liquid, gas feed rate and the energy content of the liquid phase. Most industrial spargers for gas-liquid stirred reactors are designed to operate in the turbulent chain bubbling flow regime ($R_{eb} > 9$) [69]. In this regime the bubble size depends on volumetric gas flow rate through each sparger opening and is independent of orifice diameter.

Many correlations have been proposed to predict the mean bubble diameter in gas-liquid CSTRs. A comprehensive review of these correlations is given by Midoux and Charpentier [2]. The most widely

referred to correlations for bubble diameter in stirred reactors are those of

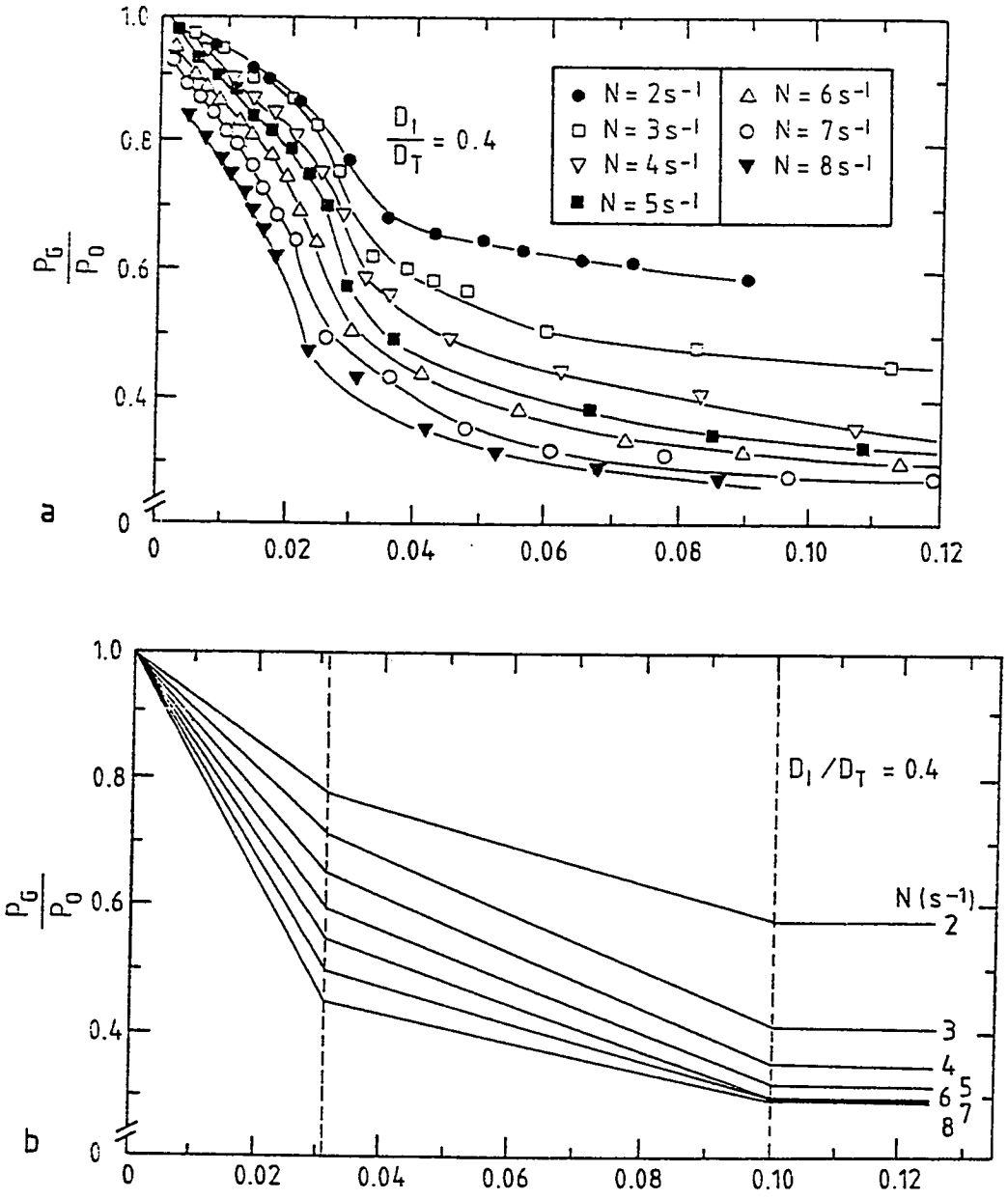

Figure 2.10 Gassed Power Curves for a 0.44 m Vessel
(a) Measured (b) Calculated [63]

Calderbank [73] and Miller [79].

According to Calderbank [73], the bubble size depends on a balance between forces due to surface tension and turbulence. The author proposed the following correlation:

$$d_b = 4.15\left[\frac{\sigma^{0.6}}{(\frac{P_G}{V_L})^{0.4}\rho_l^{0.2}}\right]\varepsilon_G^{0.5} + 0.0009 \qquad (2.6)$$

This correlation was experimentally verified by Calderbank [73] using air with water, ethanol and ethyl acetate. Calderbank's correlation was later modified by Miller [79] who used total effective power input in place of power input due to mechanical agitation used by Calderbank [73]. A discussion on the calculation of effective power input is given in section 2.2.7.

Hughmark [77] made statistical analysis of various published data and proposed following correlation for calculating the mean bubble diameter.

$$\frac{d_b^2 g\rho}{\sigma} = 5.5\frac{\varepsilon_G^{0.5}}{\left(\frac{N^2 D_I^3}{gWV_L^{2/3}(P_G/P_o)^{2/3}}\right)^{1.2}} \qquad (2.7)$$

An absolute average deviation of 10.6% was found between the calculated and experimental values of 39 data sets considered by the author.

2.2.5 Bubble Rise velocity

The characteristics of rising gas bubbles above the point of sparging have been studied extensively. The rise velocity of the gas bubbles depends primarily

on the size and shape of the bubbles. In stirred tanks, bubbles do not rise freely due to the formation of swarms or clouds . Thus, the motion of gas bubbles in stirred tanks can not be exactly described in terms of free rise of single bubbles. However, the knowledge of the flow behavior of a single bubble is important as it may provide an approximate estimation of the rise velocity of swarms. Grace [80] studied the motion of a single bubble and proposed correlations to predict the rising velocity and shape of a single bubble in different bubble flow regimes as shown in Figure 2.11.

Spherical Bubble Region ($R_{eb} < 0.2$):

In this region bubbles behave as solid spheres and their velocity of rise is consistent with Stoke's Law. Following equation applies in this region:

$$R_{eb} = \frac{\left(Eo^3/M\right)^{0.5}}{K} \tag{2.8}$$

where K = 18 for pure liquids, and K = 12 for liquids with surface active agents.

Ellipsoidal Bubble Region ($0.2 < R_{eb} < 100$):

In this region the bubbles are ellipsoidal in shape and the terminal velocity of the bubbles is best represented by Mendelson's equation [80].

$$R_{eb} = \left(\frac{4 + Eo}{2Eo}\right)^{0.5} \left(\frac{Eo^3}{M}\right)^{0.25} \tag{2.9}$$

Bubble Caps Region ($R_{eb} > 100$ and $Eo > 40$):

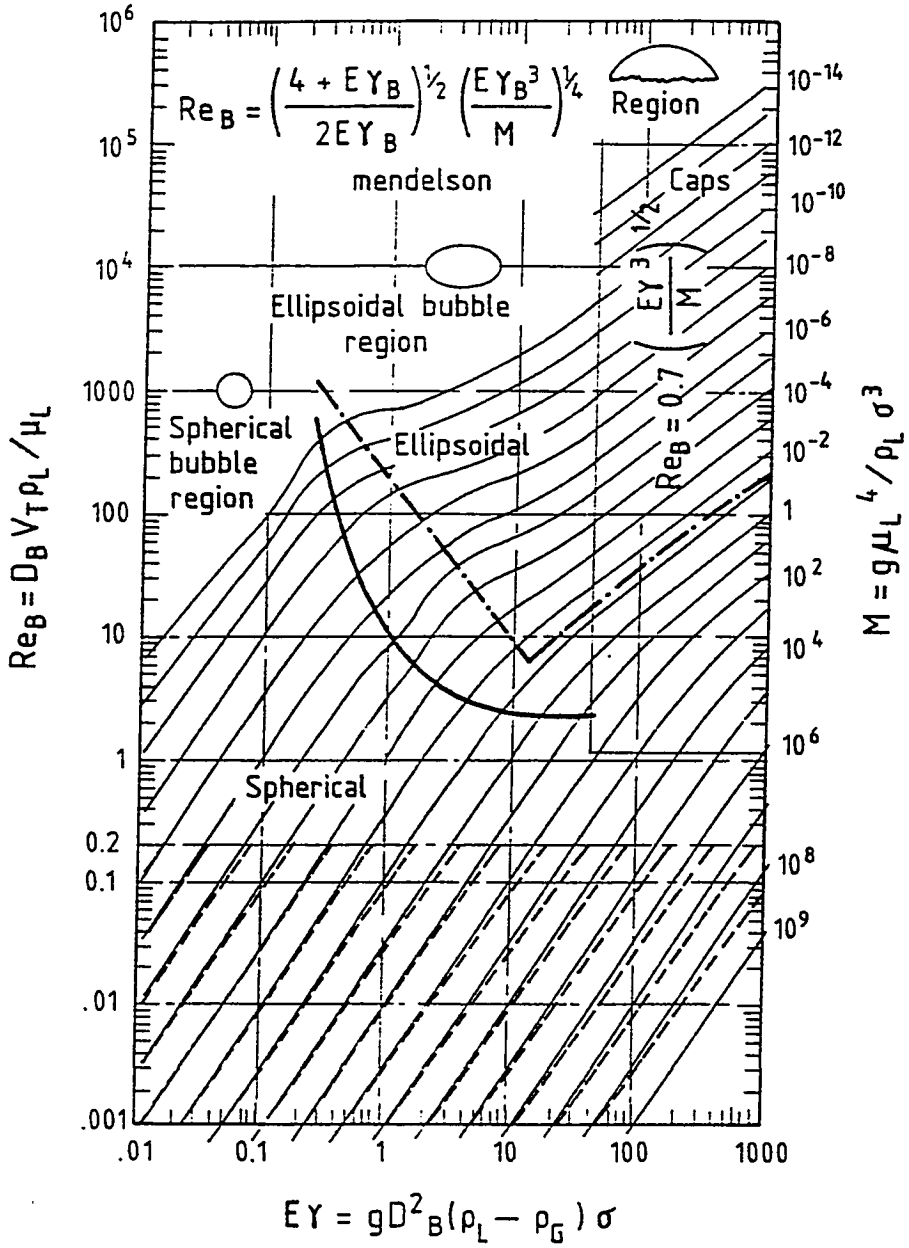

Figure 2.11 Free Rise of Single Bubbles [80]

In this region the bubbles assume a spherical cap shape and follow Devis and Taylor equation [80].

$$R_{eb} = 0.7\left(\frac{Eo^3}{M}\right)^{0.25} \tag{2.10}$$

Recently, Abu El-Hassan [81] developed a generalized correlation for the bubble rise velocity in newtonian liquids:

$$V_N = 0.75[(\log(F_N)]^2 \tag{2.11}$$

where

$$F_N = \left[\left(\frac{g d_b^{8/3}(\rho_l - \rho_g)\rho_l^{2/3}}{\mu_l^{4/3}\sigma^{1/3}}\right)\right]$$

$$V_N = \left[\left(\frac{V_T d_b^{2/3}\rho_l 2/3}{\mu_l^{1/3}\sigma^{1/3}}\right)\right]$$

Equation (2.11) is based on two new dimensionless groups, velocity number, V_N, and flow number, F_N, which contain various physico-chemical parameters influencing bubble rise velocity. Unlike Grace [80], this equation is independent of bubble flow regime and applicable under following conditions:

$$F_N = 1 - 10^6,\ V_N = 0.1 - 40,\ d_b = 1.2 - 15\ mm,\ C_D = 0.1 - 10^2$$

$$R_{eb} = 0.1 - 10^4,\ \sigma = 15 \times 10^{-3} - 72 \times 10^{-3}\ N/m$$

$$\mu_l = 0.23 \times 10^{-3} - 59 \times 10^{-3}\ Pa.s,\ \rho_l = 722.4 - 1196.6\ \frac{Kg}{m^3}$$

The author considered three types of bubble shapes: spherical, oblate spheroids, and mushroom with spherical cap. The bubble diameter was taken as the equivalent spherical diameter $d_b = 6/\pi(bubble\ volume)^{1/3}$. The correlation has

been shown to have good agreement with the various published data (see Figure 2.12).

2.2.6 Gas Hold-Up

In gas-liquid systems where the liquid phase is in batch mode and the gas phase is continuous, gas hold-up is related to superficial gas velocity and bubble terminal velocity by the following relation [79]:

$$\varepsilon_G = \frac{V_{gs}}{V_{gs} + V_T} \tag{2.12}$$

In agitated systems, the above equation is modified to account for the effect of turbulence created due to mechanical energy input to the system. Numerous investigators have studied gas hold-up with many different stirred systems, covering a wide range of liquid viscosity, surface tension, liquid density and vessel size. Most of the published correlations for gas hold-up have been reviewed by Midoux and Charpentier [2] and Mann [4].

The gas hold-up in stirred tank reactors is influenced by the type of impeller and the surface active agents present in the liquid phase. Also, since the ionic forces inhibit the coalescence of bubbles, the gas hold-up in such systems is different than in non-ionic liquids and, therefore, require special correlations. These effects have been discussed in detail in the reviews of Midoux and Charpentier [2] and Mann [4].

A summary of published correlations for predicting gas hold-up in stirred tank reactors is given in Table 2.6. These correlations fall into two categories:

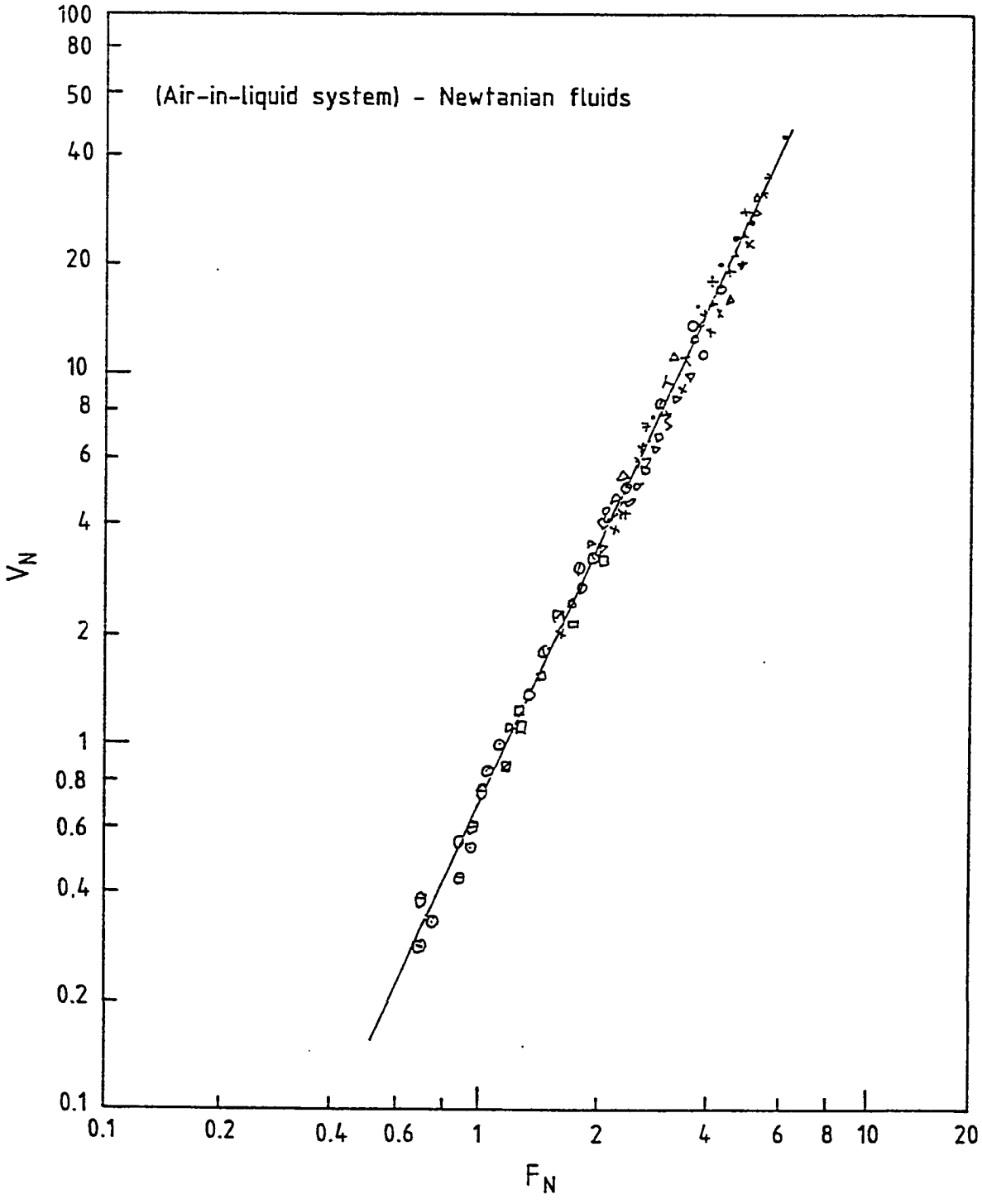

Figure 2.12 Generalized Bubble Rise Velocity Correlation [81]

Table 2.6 Correlations for Gas Hold-up

Reference	System	Geometry	Range of Variable Covered	Correlation
Calderbank (1958) [73]	air–water air–alcohol air-CCl_4 air– toluene air–nitrobenzene	$D_T(m) = 0.2 - 0.5$ $\frac{D_I}{D_T} = 0.33$	$V_{sg}(cm/sec) = 0.3 - 1.83$ $\epsilon_G = 0 - 8\%$ $\frac{P_G}{V}(W/m^3) = 263 - 5270$	$\epsilon_G = \left(\frac{V_{sg}\epsilon_G}{V_T}\right)^{0.5} + 2.16 \times 10^{-4}\left(\frac{(P_G/V_L)^{0.4}\rho_L^{0.2}}{\sigma^{0.6}}\right)\left(\frac{V_{sg}}{V_T}\right)^{0.5}$
Rushton and Bimbinet (1968) [82]	air–water air-corn syrup	$D_T(m) = 0.23 - 0.91$ $\frac{D_I}{D_T} = 0.177 - 0.53$	$V_{sg}(cm/sec) = 0 - 3$ $\epsilon_G = 0 - 35\%$ $\frac{P_G}{V}(W/m^3) = 200 - 6000$	$\frac{\epsilon_G}{1-\epsilon_G} = 0.31\left(\frac{P_{GT}}{V_L}\right)^{0.31}(V_{sg})^{0.6}$
Van Dierendonck (1968) [59]	Air, N_2, H_2 - Salt Solns. in Organic Liquids	$D_T(m) = 0.17 - 0.45$ $\frac{D_I}{D_T} = 0.31 - 0.55$	$V_{sg}(cm/sec) = 0.8 - 5$ $\epsilon_G = 0 - 35\%$ $\frac{P_G}{V_L}(W/m^3) = 2000 - 20,000$	$\epsilon_G = 0.31\left(\frac{\mu_L V_{sg}}{\sigma}\right)^{2.3}\left(\frac{\rho_L \sigma}{g\mu_L^4}\right)^{1/6} + 0.45\frac{(N-N_m)D_I^2}{D_T(gD_T)^{0.5}}$
Miller (1974) [79]	CO_2 - water	$D_T(m) = 0.15 - 0.68$ $\frac{D_I}{D_T} = 0.66$	$V_{sg}(cm/sec) = 0.76 - 15.0$ $\epsilon_G = 3 - 50\%$	$\epsilon_G = \left(\frac{V_{sg}\epsilon_G}{V_{sg}+V_T}\right)^{0.5} + 2.16 \times 10^{-4}\left(\frac{(P_{GT}/V_L)^{0.4}\rho_L^{0.2}}{\sigma^{0.6}}\right)\left(\frac{V_{sg}}{V_{sg}+V_T}\right)^{0.5}$
Hassan & Robinson (1977) [75]	air-water air-ethylene glycol solns. (8, 20%) air-glycerol soln. (40%)	$D_T(m) = 0.152,\ 0.29$ $\frac{D_I}{D_T} = 1/3, 2/3$	$V_{sg}(cm/sec) = 0.35 - 6.8$ $\epsilon_G = 2 - 50\%$ $\frac{P_G}{V_L}(W/m^3) = 30 - 16200$	$\epsilon_G = 0.113\left(\frac{P_G N^2}{\sigma}\right)^{0.57}$
Loiseau (1977) [85]	air-water + Lauric alcohol air-glycol air-ethanol (95%) air-sugar soln. (60%) air-sod. sulphate (1.2 M)	$D_T(m) = 0.22$ $\frac{D_I}{D_T} = 0.33$	$V_{sg}(cm/sec) = 0.74 - 1.98$ $\epsilon_G = 3.8 - 12.6\%$ $\frac{P_G}{V_L}(W/m^3) = 150 - 5800$	$\epsilon_G = 0.011\left(\frac{V_{sg}}{\sigma}\right)^{0.36}\left(\frac{P_{GT}}{V_L}\right)^{0.27}\frac{1}{\mu_L^{0.056}}$

Table 2.6 Continued

Reference	System	Geometry	Range of Variable Covered	Correlation
Figueiredo & Calderbank (1978) [83]	air-water air-water + hexanol	$D_T(m) = 0.91$ $\frac{D_L}{D_T} = 0.3$	$V_{sg}(cm/sec) = 0.63 - 1.27$ $\frac{P_G}{V_L}(W/m^3) = 300 - 5500$	$\epsilon_G = 0.23\left(\frac{P_G T}{V_L}\right)^{0.26}(V_{sg})^{0.68}$
Rouston (1978) [84]	air-water	$D_T(m) = 1.0$ $\frac{D_L}{D_T} = 0.4$	$V_{sg}(cm/sec) = 0.5 - 2.4$ $\epsilon_G = 2 - 16\%$	$\frac{\epsilon_G}{\epsilon_G - 1} = 4V_{sg} + 1.75 F_G^{0.6}\left(\frac{D_L}{D_T}\right)(N - N_R)$
Young et al (1979) [86]	air-wate air-ethyleneglycol Soln. (15, 30%) air-acetone (30%)	$D_T(m) = 0.4$ $\frac{D_L}{D_T} = 0.225 - 0.45$	$\epsilon_G = 1 - 20\%$	$\epsilon_G = 0.52\left(\frac{F_G}{N D_I^3}\right)^{0.5}\left(\frac{\rho_L N^2 D_I^3}{\sigma}\right)^{0.65}\left(\frac{D_L}{D_T}\right)^{1.4}$

correlations which are based on power input per unit volume and those which are based on impeller speed. The correlations based on power input per unit volume are not predictive since the power dissipated to the liquid depends on the gassing rate and should be estimated before calculating the gas hold-up. It is also evident from Table 2.6 that in most cases the gas hold is not affected by the liquid viscosity.

Calderbank [73] measured gas hold-ups for water, ethyl acetate and ethanol using standard geometries and proposed a correlation based on mechanical power input per unit volume in presence of gas. In Calderbank's work, the maximum value of V_{gs} was 0.018 m/s. Miller [79] conducted experiments using superficial gas velocity upto V_{gs} = 0.1524 m/s much higher than employed by Calderbank [73] and modified Calderbank's equation by using total effective power input in place of power input due to mechanical agitation used by Calderbank [73]. Calculation procedure for total specific power input, $\frac{P_{GT}}{V_L}$, is given in section 2.2.7. When P_{GT}/V_L or P_G/V_L approaches zero, Miller's and Calderbank's correlations reduce to Equation (2.12).

Correlations proposed by Rushton and Bimbinet [82], Figuereido and Calderbank [83] and Roustan et al. [84] are similar in form. These authors have used specific power input and the superficial gas velocity as the main correlating parameters. Figuereido and Calderbank [83], however, used total power input ($P_{GT} = P_G + P_{sG}$) in place of P_G used by Rushton and Bimbinet [82] and Roustan [84].

Loiseau et al. [85] measured the gas hold up using six different liquids of varying viscosity and surface tension. They proposed a correlation similar to previous authors [82,83,84]. The exponent on power input per unit volume in Loisesu's correlation is in close agreement with the other similar type of correlations, however, the exponent on superficial gas velocity differs significantly. The reason for a large difference in the exponent on V_{gs} in Loiseau's equation could be because Loiseau et al. conducted the experiment in a much smaller vessel ($D_T = 0.22m$) compared to Figuereido and Calderbank [83], Rushton and Bimbinet [82] and Rouston [84] who conducted experiments using large size stirred tanks ($D_T = 0.7\text{-}0.9m$).

Van Dierendonck et al. [59] and Roustan et al. [84] proposed conceptually similar correlations applicable in the regime of complete dispersion. The relationship for N^* and N_R can be obtained from the correlations for minimum impeller speed required for complete dispersion, discussed in section 2.2.2.

Correlations by Hassan and Robinson [75] and Young et al.[86] are based on dimensional analysis. These authors used gas flow rate instead of gas superficial velocity to correlate their data. Hughmark [77] performed statistical analysis of literature data and proposed the following correlation.

$$\varepsilon_G = 0.74\left(\frac{F_G}{NV_L}\right)^{0.5}\left(\frac{N^2D_I^4}{gWV^{2/3}}\right)^{1/2}\left(\frac{d_bN^2D_I^4}{\sigma V_L^{2/3}}\right) \qquad (2.13)$$

The author tested the above equation using 77 experimental data sets and found an average deviation of about 8%.

2.2.7 Interfacial Area

The interfacial area is the main variable for determining the capacity of an agitated gas liquid reactor. The literature concerning the interfacial area in gas-liquid agitated vessels is limited because it is difficult to measure. There are two main techniques to measure interfacial area. The first is chemical, and involves establishing the conditions for absorption and reaction such that the flux is directly proportional to the interfacial area. The second is physical, and generally involves the optical properties of the dispersion. Each method has its own advantages and disadvantages.

The major drawback of the chemical method is that, it is restricted to specific gas-liquid system and their particular physico-chemical properties and usually the results are not transposable to large reactors. Physical methods, on the other hand, allow one to easily determine local interfacial area in reactors of any size, which have to be integrated to obtain the overall value. The physical methods, however, suffer from the limitations on the maximum detectable interfacial area, geometrical limitations, maldistribution of the bubbles, bubble identification problems and an underestimation of the value of surface area for non spherical bubbles. Moreover, it is not clear whether the hydrodynamics of the dispersion are unaffected by the use of probes [33]. Compared to physical methods, the chemical method determines overall values of interfacial area, which represent only those surfaces across which mass transfer actually takes place. A comprehensive discussion on the measurement techniques of interfacial area is given in the recent review of Joshi et al. [32]. Other useful references are

those of Oyevaar and Westerterp [33] and Midoux and Charpentier [87].

A summary of the published correlations for interfacial area in agitated gas-liquid reactor is presented in Table 2.7. Various investigators have tried to relate interfacial area to the superficial velocity and the agitation power per unit volume, according to :

$$\underline{a} \propto \left[\frac{P_G}{V_L}\right]^{C_1} V_{sg}^{C_2} \tag{2.14}$$

or in terms of impeller speed,

$$\underline{a} \propto N^{C_3} V_{sg}^{C_4} \tag{2.15}$$

where, C_j's are constants. In general, there seems to be reasonable agreement, as far as exponents of the above equations are concerned. The exponent to agitator power is generally 0.4, which can also be theoretically predicted using the theory of isotropic turbulence [70].

Calderbank [73] was one of the first to correlate results obtained by optical methods in standard geometry, a function of specific agitator power input and superficial gas velocity. A correction factor was specified for high impeller Reynold numbers. In this equation, V_T has been assumed to remain constant at 0.265 m/s. Also, the experiments were conducted at superficial gas velocities less than 0.018 m/s.

Westerterp et al. [57] conducted a detailed study using different dimensions of tank, agitators and spargers proposed an interesting form of correlation which uses minimum impeller speed required for complete dispersion of gas (N_m).

Table 2.7 Correlations for Interfacial Area

Reference	System	Geometry	Method of Measurement	Correlation	Range of Variable Covered
Calderbank (1958) [73]	air-water air-alcohols air-CCl_4 air-toluene air-nitrobenzene	$D_T(m) = 0.2 - 0.5$ $\frac{D_L}{D_T} = 0.33$	Photographic	$a = \left[\frac{1.44\left(\frac{P_G}{V_L}\right)^{0.4}\rho_L^{0.2}}{\sigma^{0.6}}\right]\left(\frac{V_{gs}}{V_T}\right)^{0.5}$	$N(rsp) = 3 - 50$ $a \leq 120\ m^{-1}$ $\epsilon_G \leq 0.08$ $V_{gs}(\frac{cm}{sec}) = 0.3 - 1.8$ $P_G/V_L(W/m^3) = 300 - 5000$
Westerterp et al. (1963) [57]	O_2 - Sod. Sulfite Soln.	$D_T(m) = 0.14 - 0.91$ $\frac{D_L}{D_T} = 0.2 - 0.7$	Chemical	$a = \frac{(7.5\pm1.2)\times10^{-5}}{\sqrt{KD/\epsilon_L H_e}}(N - N_m)\left(\frac{D_L}{H_L}\right)\left(\frac{\rho_L D_T}{\sigma}\right)^{0.5}$	$N(rps) = 1.67 - 60$
Miller (1974) [79]	CO_2 - Water	$D_T(m) = 0.15,\ 0.31\ 0.67$ $\frac{D_L}{D_T} = 0.66$	Physical desorption	$a = 1.44\left[\frac{(P_{GT}/V_L)^{0.4}\rho_L^{0.2}}{\sigma^{0.6}}\right]\left[\frac{V_{sg}}{V_T+V_s}\right]^{0.5}$	$N(rps) = 0.42 - 7$ $V_{gs}(cm/sec) = 0.763 - 15.0$
Figueriredo and Calderbank (1979) [83]	air-water	$D_T(m) = 0.91$ $\frac{D_L}{D_T} = 0.3$	Light transmission	$a = 593\left(\frac{P_G}{V_L}\right)^{0.25}(V_{gs})^{0.75}$	$N(rps)\ 4.16 - 8.33$ $V_{gs}(cm/\sec) = 6.34 - 12.7$ $\frac{P_G}{V_L}(W/m^3) = 410 - 4800$
Sridhar & Potter (1980) [88]	O_2 - Cyclohexane	$D_T(m) = 0.13$ $\frac{D_L}{D_T} = 0.35$	Light transmission	$a = 1.44\left[\frac{\left(\frac{P_G}{V_L}\right)^{0.4}\rho_L^{0.2}}{\sigma^{0.6}}\right]\left(\frac{V_{gs}}{V_T}\right)^{0.5}\left(\frac{E_T}{P_G}\right)\left(\frac{\rho_G}{\rho_{air}}\right)^{0.16}$	$N(rsp) = 8 - -30$ $V_{gs}(cm/sec) = 1 - 5$ $\frac{P_G}{V_L}(W/m^3) = 376 - 2600$
Hughmark (1980) [77]		$D_T(m) = 0.1 - 1.0$ $\frac{D_L}{D_T} = 0.25 - 0.57$		$a = 1.38\left(\frac{g\rho_L}{\sigma}\right)^{0.5}\left(\frac{F_G}{NV_L}\right)^{1/3}\left(\frac{N^2D_I^4}{gWV_L^{2/3}}\right)^{0.592}\left(\frac{D_b N^2 D_I^4}{\sigma V_L^{2/3}}\right)^{0.187}$	$V_L(m^3) = 0.01 - 51$ $V_{gs}(,/sec) = 5.3\ cm/sec.$

According to this study, interfacial area is not affected by the impeller speed if it is below a minimum agitation speed, in this situation the interfacial area depends on the superficial gas velocity and the type of gas sparger. At impeller speed above N_m, interfacial area is linearly dependent on the agitation rate and independent of superficial gas velocity and sparger type.

The main drawback of Westerterp's correlation is that it underestimates the interfacial area by a factor of 10.0. Since these authors used the sulfite oxidation method and worked in the regime of slow reaction (M = 0.5), they overestimated the rate constant by a factor of 5 to 15 and at the same time underestimated the interfacial area [87].

Miller [79] conducted experiments using three different size vessels operated at higher gas velocities than employed by Calderbank [73] and correlated the results by modifying Calderbank's correlation. He proposed that the power input due to aeration should also be considered for calculating the specific power input to the reactor. To calculate $\frac{P_{GT}}{V_L}$, Miller [79] used the following equation:

$$P_{GT} = P_G + C_1(\eta P_K + P_{sG}) \tag{2.16}$$

where P_K represents jet energy developed at the sparger orifice and transmitted to the bulk liquid and P_{sG} is the energy required to move the gas through the static liquid head above the sparger. For well designed sparger first term in the parenthesis is often small and can be neglected [79]. Miller [79], however, used η = 0.06. The value of constant C_1 in Equation (2.16) has been established for

distributor-orifice diameter between 1.6 and 6.4 mm and tank volume between 2.5×10^{-3} and $0.25 m^3$. For a four flat blade agitator with $\frac{D_I}{D_T} = 2/3$, the constant C_1 can be calculated from the following relation [87].

$$C_1 = V_L^{-0.15}\left(1 - 1.4 D_o^{0.076}\right) \qquad (2.17)$$

It is clear from Equation (2.17) that the contribution of gas sparging in the total power input is more significant in case of small scale reactor. The gas phase energy input is generally an order of magnitude less than the agitation energy input [87].

Figueiredo and Calderbank [83] used light transmission technique to measure interfacial area in a relatively large vessel and correlated their results as a function of superficial gas velocity and specific power input due to agitation. This correlation, however, is applicable only to air-water system.

Sridhar and Potter [88] investigated gas-liquid contacting at higher reactor pressures and showed that by increasing the reactor pressure from 0.1 to 1.0 MPa, the interfacial area is increased by 75%. The increase in interfacial area was attributed to the increase in kinetic energy content of the inlet gas due to higher gas feed pressure. To correlate their results, these investigators modified Calderbank's correlation [73] by multiplying it by a factor of $(E_T/P_G)(\rho_G/\rho_{air})$. These authors used the correlation of Michel and Miller [72] to calculate the power input due to agitation. Recently, Oyevaar and Westerterp [89] investigated the effect of pressure on the interfacial area in gas-liquid stirred tank reactors and showed that an increase in reactor pressure increases the

interfacial area.

Hughmark [77] assembled a number of results from the literature and proposed a correlation for interfacial area applicable to reactor geometry closer to standard configuration.

2.2.8 Liquid-Side Mass Transfer Coefficient

In gas-liquid reactions, mass transfer between the gas and liquid phases often constitute the rate determining step for the overall reaction process. A knowledge of gas-liquid mass transfer coefficients is therefore needed. In the literature, liquid-side mass transfer coefficient, K_L, is generally expressed as a product of K_L and $\underline{a}$. This product is called as volumetric mass transfer coefficient. In gas-liquid stirred tank reactors, $K_L\underline{a}$ depends on the physical properties of the liquid, vessel and impeller geometry, specific power input, the mobility of the interface and the bubble coalescence rate. In most of the correlations, the specific power input and the gas superficial velocity are the two major correlating parameters. Correlations of the following type are frequently found in the literature:

$$K_L\underline{a} = K\left(\frac{P_G}{V_L}\right)^a V_{sg}^b \tag{2.18}$$

The constants a and b show a large variation in their values: $0.4 \le a \le 1.0$ and $0 \le b \le 0.7$. The values of K_L reported in the literature also show a great variation. For example, for the oxygen-water system, K_L reported at room temperature varies from 10^{-2} to $6 \times 10^{-6} ms^{-1}$ [90]. A summary of published

correlations for K_L and $K_L a$ is given in Table 2.8.

2.2.9 Gas-Side Mass Transfer Coefficient

Gas-side mass transfer coefficient for pure gas is infinity. Thus, for the instances where pure gas feed is used the gas film resistance can safely be neglected. This has also been experimentally verified by Calderbank [103] who measured both gas and liquid film resistances in a stirred gas-liquid system and found out that the gas film has much less resistance than the liquid film. The gas-side resistance becomes important only in case of dilute gases. In such cases correlation for gas-side mass transfer coefficient should be available so that proper estimation of mass transfer resistance can be made. Literature offers *very few* correlations for gas-side mass transfer coefficients in CSTRs.

Barona [69] has recommended the following correlation for calculating K_G:

$$K_G = 6.58\frac{D_A}{d_b RT}\left[\frac{P_T}{p_i}\right] \tag{2.19}$$

where P_T is the total pressure and p_i is the partial pressure of the inerts. Equation (2.19) was developed by Newman [104], who studied the diffusion of gaseous reactant A, across a stagnant inert film by using rigid sphere model. When the concentration of A in the feed gas is very low, p_i approaches P_T and K_G approaches $6.58D_A/d_bRT$. In case of pure gas, p_i approaches zero and K_G approaches infinity.

Rase [105] has recommended the correlation developed by Calderbank [103] which is a special case of Newman's equation for extremely dilute gases.

Table 2.8 Correlations for K_L and K_La

Reference	System	Geometry	Method	Correlation
Calderbank and Moo - Young (1961) [91]	Aq. glycerol Soln. - CO_2 Aq. glycol Soln. - CO_2 Water - CO_2 Brine - O_2 Polyacrylamide Soln. - CO_2 Wax - H_2		Physical Absorption and desorption	for $D_B < 2.5$ mm $K_L = 0.31 \left(\frac{g\mu_G}{\rho_e}\right)^{1/3} \left(\frac{\rho_L D_{AB}}{\mu_L}\right)^{2/3}$ for $D_B > 2.5$ mm $K_L = 0.42 \left(\frac{g\mu_L}{\rho_e}\right)^{1/3} \left(\frac{P_L D_{AB}}{\mu_L}\right)^{1/2}$
Prasher and Wills (1973) [92]	Dist. Water - CO_2 0.085 $NaOH$ Soln. - CO_2	$D_T(m) = 0.29$ $\frac{H_L}{D_T} = 1$ $\frac{D_I}{D_T} = 1/3$ Four baffles	Physical and chemical absorption	$K_L = 0.592(D_{AB})^{1/2} \left(\frac{P_G}{V_L \mu_L}\right)^{0.25}$
Yagi and Yoshida (1975) [93]	Aq. glycerol Soln. - O_2 Aq. miller jelly Soln. - O_2	$D_T(m) = 0.25$ $\frac{H_L}{D_T} = 1.0$ $\frac{D_I}{D_T} = 0.4$ Four baffles	Physical desorption	$\frac{K_L a D_I^2}{D_{AB}} = 0.06 \left(\frac{D_I^2 N \rho_L}{\mu_L}\right)^{1.5} \left(\frac{D_I N^2}{g}\right)^{0.19} \left(\frac{\mu_L}{\rho_L D_{AB}}\right)^{0.5} \left(\frac{\mu_L V_{sg}}{\sigma}\right)^{6.6} \left(\frac{N D_I}{V_{sg}}\right)^{0.32}$
Van't Riet (1979) [94]				For Pure Water $K_La = 2.6 \times 10^{-2} \left(\frac{P_G}{V_L}\right)^{0.4} V_{sg}^{0.5}$ Applicable $V_L =$ up to 2.6 m^3 $P_G/V_L = 500 - 10{,}000$ w/m^3 for ionic solutions $K_La = 2.010^{-3} \left(\frac{P_G}{V_L}\right)^{6.7} V_{sg}^{0.2}$ Applicable $V_L = 0.002 - 4.4$ m^3 $P_G/V_L = 500 - 10{,}000$ w/m^2

Table 2.8 Continued

Reference	System	Geometry	Method	Correlation
Barona (1979) [69]				$K_L = \left(\frac{P_G \mu_L}{V_L \rho_L^2}\right)^{0.25} \left(\frac{\rho_L D_{AB}}{\mu_L}\right)^{2/3}$
Lopes de Figueredo and Calderbank (1979) [95]	Water–air	$D_T(m) = 0.91$ $\frac{H_L}{D_T} = 1$ $\frac{D_I}{D_T} = 0.33$ Four baffles	Physical absorption	$K_L a = \frac{1 \times 10^{-3}}{V_L} P_G^{0.58} V_{sg}^{3/4} D_T$
Chandrashekharan (1981) [96]	Water-Air	$D_T(m) = 1.22$ $\frac{H_L}{D_T} = 1.0$ $\frac{D_I}{D_T} = 0.3$	Physical absorption	$K_L a = \frac{0.0248}{D_T^4} \cdot \left(\frac{P_G}{V_L}\right)^{0.55} (F_G)^{0.551/\sqrt{D_T}}$
Andrew, S.P.S. (1982) [97]	Water–CO_2 Water+foaming agent – CO_2 Aq. glycol Soln. – CO_2	$D_T(m) = 0.04$ $\frac{H_L}{D_T} = 0.95$ $\frac{D_I}{D_T} = 0.75$ Four metal gauge baffles	Physical absorption	$\frac{K_L a}{\epsilon_G} = 16 \left(\frac{P_G}{V_L}\right)^{0.8} \mu_L^{-0.5} (\sigma)^{-1}$
Judat, H. (1982) [98]	Coalescing systems	$D_T(m) = 0.15 - 1.8$ $\frac{H_L}{D_T} = 0.891 - 1$ $\frac{D_I}{D_T} = 0.2 - 0.5$		$K_L a* = \frac{9.8 \times 10^{-5} \left(\frac{P_G}{V_L}\right)^{*0.4}}{[B^{-0.6} + 0.81* 10^{-0.63/B}]}$ $K_L a^* = K_L a \left(\frac{\mu_L}{\rho_L g^2}\right)^{1/3}$ $K_L a* = K_L a \left(\frac{\mu_L}{\rho_L g^2}\right)^{1/3}$ $\left(\frac{P}{V}\right)^* = \left(\frac{P}{V}\right) \left[\rho_L \left(\frac{\mu_2 g^4}{\rho_L}\right)^{1/3}\right]^{-1}$ $B = \left(\frac{F_G}{D_T^2}\right) \left(\frac{\mu_L g}{\rho_L}\right)^{-1/3}$

Table 2.8 Continued

Reference	System	Geometry	Method	Correlation
Albal et al. (1983) [90]	Water - O_2 Aq. glycerin Soln. O_2 Aq. CMC Soln. - O_2 Aq. Triton CF-32 Soln. O_2	$D_T(m) = 0.101$ $\frac{H_L}{D_T} = 1.33 - 1.73$ $\frac{D_I}{D_T} = 0.33 - 0.57$ Four baffles	Physical absorption	$\frac{K_L a D_I^2}{D_{AB}} = 1.41 \times 10^{-3} \left(\frac{\mu_L}{\rho_L D_{AB}}\right)^{0.5} \left(\frac{D_I^2 N \rho_L}{\mu_L}\right)^{0.67} \left(\frac{\rho_L N D_I^3}{g}\right)^{1.29}$
Linek et al. (1987) [99]	Distilled water - O_2 Aq. Electrolyte Soln. - $O2$ Aq. CMC Soln. - O_2 Aq. glycerine Soln. - O_2	$D_T(m) = 0.29$ $\frac{H_L}{D_T} = 1.0$ $\frac{D_I}{D_T} = 1/3$ Four baffles	Physical and chemical absorption	For coalescing system: Water $K_L a = 4.95 \times 10^{-3} \left(\frac{P_a}{V_L}\right)^{0.593} (V_{sg})^{0.4}$ For non-coalescing system: Electrolyte Solns. $K_L a = 1.35 \times 10^{-3} \left(\frac{P_a}{V_L}\right)^{0.946} (V_{sg})^{0.4}$ For highly viscous media: Aq. Soln. of glycerine and CMC with electrolyte $K_L a = 0.355 W_N \left(\frac{P_a}{V_L}\right)^{0.896} (V_{sg})^{0.438}$ $W_N = \frac{\rho_L^{0.248} D_{AB}^{0.5}}{\mu_L^{1/6} \sigma^{0.6}}$
Schmitz et al. (1987) [100]	Na_2SO_4 Soln. - Air $Na_2SO_4 + CMC$ Soln. - Air	$D_T(m) = 0.2, 0.45, 1.5$ $\frac{H_L}{D_T} = 1.0$ $\frac{D_I}{D_T} = 1/3$ Four baffles	Sulphite oxidation	$K_L a = A_1 \left(\frac{P_a}{V_L}\right)^{a_1} (V_{gs})^{a_2} \left(\frac{\mu_2}{}\right)^{a_3}$ For $1.45 \times 10^{-3} \leq \mu_L(P_a s) = 20 \times 10^{-3}$ $A_1 = 5.97 \times 10^{-4}$ $a_1 = 0.78\ a_2 = 0.36\ a_3 = -0.27$ For $20 \times 10^{-3} \leq \mu_L(P_{as}) \leq 75 \times 10^{-3}$ $A_1 = 1.39 \times 10^{-4}$ $a_1 = 0.32\ a_2 = 0.33\ a_3 = -1.51$
Linek and Vacek (1988) [101]	1% CMC Soln. + 0.5 M $Na_2SO_4 - O_2$ $0.5\,M Na_2SO_4 - O_2$	$D_T(m) = 0.29$ $\frac{H_L}{D_T} = 1$ $\frac{D_I}{D_T} = 1/3$ Four baffles	Chemical oxidation	For 0.5 Na_2SO_4 + 1% CMC $K_L a = 1.07 \times 10^{-3} \left(\frac{P_a}{V_L}\right)^{0.944} (V_{sg})^{0.4}$ For 0.5 $M Na_2SO_4$ $K_L a = 1.35 \times 10^{-3} \left(\frac{P_a}{V_L}\right)^{0.946} (V_{sg})^{0.4}$
Hickman, A.D. (1988) [102]	Water - O_2 CMC Soln. - O_2	$D_T^{(m)} = 0.6 - 2.0\ m$ $H_L/D_T = 1.0$ $\frac{D_I}{D_T} = 1/3$ Four baffles	Generation of O_2 by decomposing H_2O_2	$K_L a = 0.046 \left(\frac{P_a}{V_L}\right)^{0.47} V_{sg}^{0.67}$

Trambouze et al. [3] have recommended the following correlation for K_G:

$$K_G = \frac{-d_b}{6t_G RT}\ln\left(\frac{6}{\pi^2}\right)\exp\left[\frac{-D_A\pi^2 t_G}{\left(\frac{d_b}{2}\right)^2}\right] \qquad (2.20)$$

Equation (2.20) was developed by Mashalkar and Sharma [106] for bubble column reactor. For the column height greater than 0.5 m, this equation also reduces to Newman's equation [104].

2.2.10 Tank-Side Heat Transfer Coefficient

In order to maintain the temperature, CSTRs usually have a provision for heat exchange. Depending on the type of reaction, heat is either removed from the reaction medium or supplied to it by installing a heat exchange surface inside the reactor. The heat transfer in a CSTR is usually carried out by providing an external jacket surrounding the tank as shown in Figure 2.13 or by immersing a coil inside the tank as shown in Figure 2.14a-b. Immersed coils are not always recommended because they present cleaning problem and modify mixing patterns. Jackets are usually preferred because of cheaper material of construction, less tendency to foul, easier cleaning and maintenance and fewer problems in circulating catalysts and viscous fluids. Coils should be considered only if jacketing alone will not provide sufficient heat transfer area, if jacket pressure will exceed 10 bar or if high temperature vacuum processing is required. Under the latter two conditions, a coil offers the advantage of a higher overall film coefficient, because of its thinner walls [36].

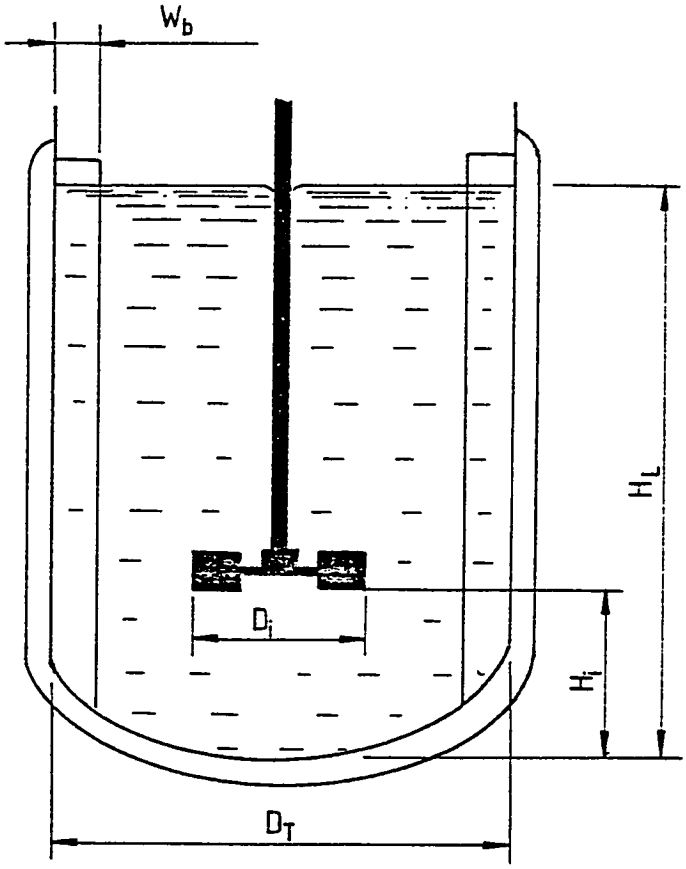

Figure 2.13 Jacketed Stirred Tank Reactor [43]

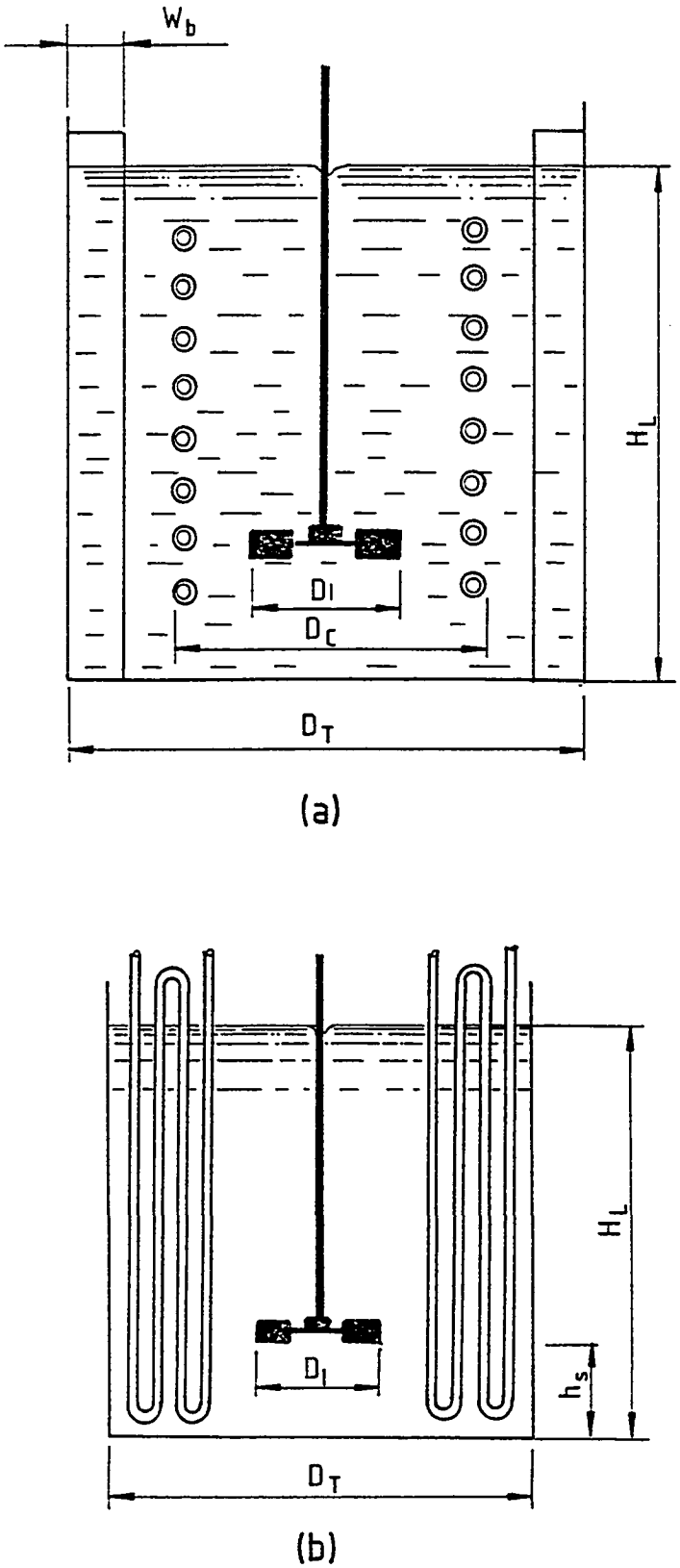

Figure 2.14 (a) Stirred Tank Reactor with Internal Coils
(b) Stirred Tank Reactor with Vertical Baffles [43]

A detailed understanding of heat exchange mechanism is essential for the design and analysis of gas-liquid CSTRs. The literature reports many correlations that can be used to calculate the the heat transfer coefficient corresponding to a given system. The form of these correlations, however, vary depending on the type of heat exchange surface, type of agitator, the geometry of the tank and number of phases, under consideration such as single phase or multiphase system. The correlations for heat transfer coefficients in a gas-liquid CSTR usually involve dimensionless numbers such as Nusselt number, Prandtl number, impeller and gas Reynold number, impeller and gas Froude number, Galileo number and Newton number. Physical significance and definitions of these numbers have been discussed in the previous section.

General Relationship:

Equation (2.21) represents a general relation to calculate the overall heat transfer coefficient, U, for a jacketed agitated tank reactor as shown in Figure 2.13

$$\frac{1}{U_i} = \frac{1}{h_T} + f_T + \frac{A_i l_{th}}{A_O \lambda_m} + f_J + \frac{A_i}{A_o h_j} \qquad (2.21)$$

Where U_i is the overall heat transfer coefficient based on the inside heat transfer surface area. When heat is transferred via internal coils or tubular baffles (see Figure 2.14a-b), the overall heat transfer coefficient is usually based on outer coil surface and is calculated by Equation (2.22).

$$\frac{1}{U_O} = \frac{1}{h_T} + f_T + \frac{T_{th} d_{co}}{\lambda_m d_{cm}} + f_c + \frac{d_{co}}{d_{ci} h_{ci}} \qquad (2.22)$$

Equations (2.21) and (2.22) indicate that the resistance to heat transfer has three main components : the resistance within the reaction mixture, within the wall and within the heat transfer medium. The wall resistance becomes significant only in case the reactor is constructed of glass or other low conductivity materials. Resistances within the reaction mixture and within the heat transfer medium is determined by agitated-side and jacket or coil-side heat transfer film coefficients represented as h_T, h_j *or* h_c respectively.

The heat transfer film coefficients, h_T, h_j or h_c, depend on the properties of the reaction and heat transfer fluids as well as on the hydrodynamic properties governed by the shape and size of the tank and impeller. These coefficients can be determined either experimentally or from the correlations published in the literature. In this section published correlations for tank-side heat transfer coefficient, h_T, are discussed.

Heat transfer characteristics of single phase CSTRs have been studied extensively and a large number of correlation are available in the literature. A critical review of the literature reveals that there is a general agreement about the final form of the correlating equation in this case. Tank side heat transfer coefficient in a single phase regime with forced convection have been generally related by the expression of following type [43]:

$$N_u = K R_{en}^{a} P_r^{b} V_i^{c} \qquad (2.23)$$

In most of the correlations, the exponents a, b, c in Equation (2.23) are always close to the following values:

$$a = 0.5 - 0.75\ (2/3)$$

$$b = 0.25 - 0.5\ (1/3)$$

$$c = -0.14 - -0.25\ (-0.14)$$

The values given in the parenthesis indicate the typical average values. The constant K is usually between 0.1 and 1. A comprehensive review of the published correlation for tank-side heat transfer film coefficient in case of single phase CSTR, for various types of agitator and vessel geometries, is given by Holland and Chapman [43]. Rase [105] has also given a list of recommended correlations and their range of applicability for a single phase CSTR.

Despite widespread use of gas-liquid CSTRs in chemical process industries and their favourable heat transfer properties, only few studies, on the heat transfer characteristics of such reactors, have been done. Rase [105] suggested that the correlations for single phase CSTRs along with appropriate correction factor can be used to calculate the tank-side heat transfer coefficient for gas-liquid CSTRs. For a baffled gas-liquid CSTR the author recommended the following equation:

$$h_T = h_L \left[\frac{P_G + P_{sG}}{P_o} \right]^{0.25} \qquad (2.24)$$

where h_L is the tank-side heat transfer coefficient for unaerated reactor operating under same conditions. P_G and P_o are the agitator power requirement with and without gas respectively. P_{sG} is the power input into the system from the gas when it is expanded adiabatically from the input pressure, P_{in}, to the

pressure above the liquid, P_{out}, which can be calculated from Equation (2.25).

$$P_{sG} = 1.013 \times 10^6 \frac{F_G P_{in} \gamma}{\gamma - 1} \left[1 - \left(\frac{P_{out}}{P_{in}} \right)^{\frac{\gamma - 1}{\gamma}} \right] \qquad (2.25)$$

For diatomic gas such as air, $\gamma = 1.31$

Equation (2.24) has not been experimentally verified. According to Equation (2.24) the presence of gas reduces the heat transfer coefficient which is contrary to the findings of many other investigators [107,108]. Moreover it does not truly represent the effect of prevailing complex hydrodynamic conditions on the tank-side heat transfer coefficient of a gas-liquid stirred tank reactor. This is because of the fact that the presence of gas alters the flow patterns significantly and influences the power transmitted to the liquid for a specified Reynold number, affecting both the average and local tank side heat transfer coefficients. Also the rising gas bubbles create circulatory currents in the liquid near the transfer surface in addition to those already created by the rotating impeller. Therefore, the correlations for single phase heat transfer in stirred tanks are not applicable for gas-liquid systems [109].

So far only few studies have been published dealing with the problem of heat transfer in mechanically agitated two phase gas -liquid systems. A brief review of the experimental studies carried out in gas-liquid agitated tank reactors is presented here. Almost all the published correlations for the tank-side heat transfer coefficient in a gas-liquid stirred tank reactor are summarized in Table 2.9, giving the ranges of variables covered, and stating any restricting condition. The most important process parameters which affect the heat

Table 2.9 Correlations for Tank Side Heat Transfer Coefficients in Gas-Liquid CSTRs

References	System	Vessel Geometry	Heat Transfer Surface	Agitator type	Aeration Arrangement	Dimensionless form of equation	Range of Variables Covered
Zlokarnik 1966 [110]	Air Sod. Sulphite Solution	$D_T(m) = 0.4$ $\frac{H_L}{D_T} = 1.0$ $\frac{D_T}{D_I} = 3.33$	Spiral shaped coil	Triangular hollow Stirrer	By suction through a hollow stirrer	Coil-Fluid: $N_u = 0.185 R_{eG}^{0.733} F_{rG}^{-0.267} P_{rL}^{0.466}$	$R_{eG} = 1680 - 10,000$ $R_{en} = 10^5 - 6 \times 10^5$ $F_{rG} = 7.2 \times 10^{-7} - 1.6 \times 10^{-4}$ $P_{rL} = 6.9$ $V_{gs}(m/s) = 0.0042 - 0.025$ $N(s^{-1}) = 8.3 - 25$
Rao & Murti (1973) [107]	Air-water Air-transformer oil Air-clavus oil	$D_T(m) = 0.23, 0.7$ $\frac{H_L}{D_T} = 1, 1.27$ $\frac{D_T}{D_I} = 3.0$ Dished bottom No baffles	Helical coil and jacket	Six flat blade disc turbine impeller	Ring sparger discharge downward.	Coil-fluid : $N_u = 0.87 (Re^*)^{0.64} (P_{rL})^{0.33} \left(\frac{\mu_w}{\mu_b}\right)^{-0.14} F_{rn}^{-0.1}$ Jacket-Fluid : $N_u = 1.35 (R_e^*)^{0.50} (P_{rL})^{0.3} \left(\frac{\mu_w}{\mu_b}\right)^{-0.14} (F_{rn})^{-0.1}$ where $R_e^* = R_{eG} + 4 R_{en}$	$R_e^* = 1 \times 10^3 - 5 \times 10^5$ $R_{eG} = 100 - 18900$ $R_{en} = 540 - 530,000$ $F_{rG} = 5.8 \times 10^{-7} - 3 \times 10^{-3}$ $P_{rL} = 2 - 266$ $V_{gs}(m/s) = 0.002 - 0.083$ $N(s^{-1}) = 0.7 - 8.33$ $\frac{\mu_w}{\mu_b} = 0.18 - 0.98$
Edney & Edwards 1976 [113]	Air-water Air-CMS solution Air-polyacrylamide	$D_T(m) = 1.22$ $\frac{H_L}{D_T} = 1.0$ $\frac{D_T}{D_I} = 4.0$ Flat bottom Baffled vessel $\frac{D_C}{D_T} = 0.458$ $\frac{D_C}{D_T} = 0.625$ $\frac{D_C}{D_T} = 0.792$	Three helical coils	Six flat blade disc turbine impeller	T-shaped sparge pipe	Coil-Fluid : $N_u = 0.036 R_{en}^{0.641} P_{rL}^{0.353} \left(\frac{D_C}{D_T}\right)^{-0.375} \left(\frac{\mu_w}{\mu_b}\right)^{-0.2}$ $N_u = \frac{h c d_{co}}{\lambda}$	$R_{en} = 4.01 \times 10^2 - 9.2 \times 10^5$ $P_{rL} = 4.34 - 1.9 \times 10^3$ $\mu(cp) = 0.65 - 283$ $N(s^{-1}) = 1.1 - 5.8$ $V_{gs}(m/s) = 0 - 0.02$
Nagata et al. 1976 [112]	Air-Water Air-glycerin solution Air-CMS solution	$D_T(m) = 0.3$ $\frac{H_L}{D_L} = 1.33$ $\frac{D_T}{D_I} = 2$ Flat Bottom Baffled Vessel	Helical coil and Jacket	Six flat blade disc turbine and three blade impeller with blade angle 60°	Ring sparger	Coil-Fluid : $N_{U_L} = 2.68 R_e^{0.56} P_r^{1/3} \left(\frac{\mu_w}{\mu_b}\right)^{-0.14} \left(\frac{D_I}{D_T}\right)^{-0.3} \left(\sum W I_i / D_T\right)^{0.35} (\mu_b)^{0.2} \left(\sum H R_i / i H_L\right)^{0.15} (\sin\theta)^{0.5} (H_L/D_T)^{-0.5}$ Jacket-Fluid : $N_u = 1.40 R_e'^{2/3} P_r^{1/3} \left(\frac{\mu_m}{\mu_b}\right)^{-0.14} \left(\frac{D_I}{D_T}\right)^{-0.3} \left(\sum b_i/D\right)^{0.43} \times (n_b)^{0.2} \left(\sum H_R i / I h_L\right)^{0.2} (\sin\theta)^{0.5} (H_L/D_T)^{-0.6}$ $R_e' = \left\{(P_g + P_a) g/e D_I^5 N_p\right\}^{1/3} \frac{D_I^2 e}{\mu}$	$V_{gs}(m/sec) = 0 - 027$ $N(s^{-1}) = 0 - 5.8$ $\mu_{cp} = 1 - 890$

Table 2.9 Continued

References	System	Vessel Geometry	Heat Coil Jacket	Agitator type	Aeration Arrangement	Dimensionless form of equation	Range of Variables Covered
Pollard and Topiwala (1976) [109]	Air-Water Air-0.19 MK_2SO_4 Solution	$D_T(m) = 0.513$ $\frac{H_L}{D_T} = 2.18$ $\frac{D_T}{D_I} = 3.0$ Four baffles	Helical coil	Six-Flat blade disc turbine impeller	Ring Sparger inward discharge	Coil-Fluid : $N_u = C_2 \left(\frac{P_{GT}}{V_L}\right)^{0.1} (\epsilon_G)^{0.35}$	$R_{en} = 1.4 - 3.5 \times 10^4$ $R_{eG} = 1268 - 3392$ $F_{rG} = 3.3 \times 10^{-5} - 2.3 \times 10^{-4}$ $V_{gs}(m/sec) = 7.42 \times 10^{-3} - 19.84 \times 10^{-2}$ $P_{rL} = 170$ $N(s^{-1}) = 5 - 11.7$
Maerteleire (1978) [111]	Air-water Air-water + surface Active agent Air-isopropyl alcohol Air-ethyleneglycol Air-BP Energol CS 100 Air-BP energol CS 200	$D_T(m) = 0.18$ $\frac{H_L}{D_T} = 1.13$ $\frac{D_T}{D_I} = 1.8$ Four baffles placed at right angle to the wall	Helical coil	Four bladed paddle impeller	Circular gas sparger made of porous sintered glass	Coil Fluid : $N_u = 0.318 (R_{en})^{0.627} (P_{rL})^{0.342} \left(\frac{\mu_w}{\mu_b}\right)^{-0.139} \times (W_e)^{0.053} (F_{rn})^{-0.156} \left(\frac{V_{gs}}{D_I N}\right)^{0.079}$	$R_{en} = 169 - 261000$ $F_{rG} = 0.0398 - 2.549$ $F_{rn} = 0.027 - 2.009$ $P_{rL} = 2.97 - 1270$ $V_{gs}(m/sec) = 0.1976 - 1.5814$ $N(s^{-1}) = 1.7 - 14.55$ $\frac{\mu_w}{\mu_b} = 0.243 - 0.904$ $W_e = 35 - 6263$
Steiff and Weinspach (1978) [108]	Air-water Air-baysilan M10 Air-Baysilon M100	$D_T(m) = 0.19 - 0.7$ $\frac{H_L}{D_T} = 1, 2, 3$ Four flat baffles at 90° intervals flat bottom	Helical coil and jacket with helical inserts	Six-flat blade disc turbine impeller	Sintered plate	Coil-Fluid : $St = 0.137 \left[(R_{eG} F_{rG} P_{rL}^2)^{1/3}\right]^{-(0.73+0.164 \times 10 R_{en})^{-5}} \times (R_{en} + 1000)^{0.047} \left(\frac{\mu_w}{\mu_b}\right)^{-0.42}$ Jacket-Fluid : $S_t = 0.054 \left[\left(R_{eG} F_{rG} P_{rL}^n\right)^{1/3}\right]^{(-0.79+0.186 \times 10^{-5} R_{en})} \times (R_{en} + 1,000)^{0.107} \left(\frac{\mu_w}{\mu_b}\right)^{-0.42}$	$R_{eG} = 0.5 - 16,000$ $R_{en} = 0 - 2.2 * 10^5$ $F_{rG} = 1.6 \times 10^{-9} - 4 \times 10^{-2}$ $P_{rL} = 4 - 825$ $V_{gs}(m/s) = 0.0003 - 0.1$ $N(s^{-1}) = 0 - 16.7$
Kurpiers et al. (1985) [114]	Air-Water Air-Ethylene glycol Air-Diethylene glycol Air-Glycerol at the rate of 80°C Air-Glycerol at the rate of 70°C Air-Glycerol at the rate of 62°C Air-liquid Glassbeads	$D_T(m) = 0.45$ $\frac{H_L}{D_T} = 1.35$ $\frac{D_T}{D_I} = 3.0, 1.93$ $\frac{H_B}{D_I} = 0.5$	Jacket	Six-Flat bladed disc turbine	Sintered plate	Jacket-fluid : $N_u = K \left[\xi \left(\frac{D_T}{D_I}\right) \left(\frac{D_T^3}{V_L}\right) N_e H_{en}^3 + G_a R_{eG} \left\{1 - 2 \left(\frac{D_I}{D_T}\right) \left(\frac{D_I}{H_L - e}\right)^{0.5} N_e F_{rn}\right\}\right]^{0.25} \times P_{rL}^{0.4} \left(\frac{\mu_w}{\mu_b}\right)^{-0.23}$ for single stage impeller system $K = 0.1$, $\xi = 0.2$ at $\frac{D_T}{D_I} = 3$ for $\frac{D_T}{D_I} = 1.98$ $K = 0.1$, $\xi = 0.37$	$R_{en} = 0 - 2 \times 10^6$ $R_{eG} = 0 - 8.9 \times 10^4$ $F_{rn} = 0 - 2.2$ $P_{rL} = 4.3 - 630$ $V_{gs}(m/s) = 0 - 043.3$ $\mu_{K_{(s)}} = 0.651 - 70.9$ $\rho_L = 992.3 - 1235 \left(\frac{Kg}{m^3}\right)$

Table 2.9 Continued

References	System	Vessel Geometry	Coil Jacket	Agitator type	Aeration Arrangement	Dimensionless form of equation	Range of Variables Covered
Kurpiers et al. (1985) [116]	Air-Water Air-NaCl Solution Air-Isopropanol Solution	$D_T = 0.45$ $\frac{H_L}{D_T} = 1.35$ $\frac{D_T}{D_I} = 3$ $\frac{H_R}{D_I} = 0.5$	Immersed Heating Probe	Six-flat blade Disc turbine	Sintered plate	Heating Probe-Fluid : Single-Stage Stirrer : $N_U = K\left[\xi\left(\frac{D_I^3}{V_L}\right)\left(\frac{d_A}{d_T}\right)^{3.25} N_e R_{en}^3 + \left(\frac{d_A}{D_T}\right)^4 G_a R_{eG}\right]^{8.25} P_{rL}^{0.4}\left(\frac{\mu_w}{\mu_b}\right)^{-0.23}$ $K \pm 0.15 \;\; \xi = 0.54$ Two-stage Stirrer : $N_{um} = 0.482\left[0.168\left(\frac{D_I^3}{V_K}\right)(frd_A D_I)^{3.25} N_{em} R_{enm}^3 + \left(\frac{d_A}{D_T}\right)^4 G_{am} R_{eGM}\right]^{0.211} P_{rLM}^{0.4}\left(\frac{\mu_i}{\mu_b}\right)^{0.23}$	$R_{en} = 7.2 \times 10^4 - 1.19 \times 10^6$ $R_{eG} = 2.95 \times 10^2 - 1.43 \times 10^5$ $P_{rL} = 4.36.70$ $N_u = 105 - 322$ $G_a = 8.05 \times 10^{11} - 3.66 \times 10^{13}$ $N_e = 0.666 - 4.02$ $V_{gs}(m/s) = 0 - 0.2$ $N(s^{-1}) = 3.36 - 11.7$ $N_{um} = 89 - 490$ $P_{rLM} = 4.1 - 7.6$ $G_{am} = 6.72 \times 10^{11} - 2.21 \times 10^{12}$
Kurpiers et al. (1986) [115]	Air-water Air-Ethylene glycol Air-Diethylene glycol Air-Glycerol at the rate of 80°C Air-Glycerol at the rate of 70°C Air-Glycerol at the rate of 62°C Air-liquid glass beads	$D_T(m) = 0.45$ $\frac{D_T}{D_I} = 3, 1.93$ $\frac{H_L}{D_T} = 1.35$ $\frac{H_{R1}}{D_I} = 0.5$ $\frac{H_{R2}}{D_I} = 2.58$	Jacket	Two-stage Six-flat Blade Disc turbine	Sintered Plate	Jacket-Fluid : $N_{um} = 0.1\left[11.58\left(\frac{D_T}{D_I}\right)\left(\frac{D_I^3}{V_L}\right) N_{em} R_{enm}^3 + G_{am} R_{eGM}\right]^{0.238} P_{rm}^{0.362}\left(\frac{\mu_w}{\mu_0}\right)_m^{-0.23}$	$205 \leq N_{um} \leq 6809$ $4.2 \leq P_{rm} \leq 632$ $0.033 \leq \left(\frac{\mu_b}{\mu_w}\right) \leq 3.021$ $2.69 \times 10^8 \leq G_{am} \leq 2.16 \times 10^{12}$ $1.94 \leq N_{em} \leq 10.17$ $6.51 \times 10^2 \leq R_{enm} \leq 4.05 \times 10^5$ $0.021 \leq F_{rn} \leq 2.15$ $0 \leq R_{eGm} \leq 7.067 \times 10^4$

transfer in aerated stirred tanks are gas flow rate, impeller speed, power input, physical properties of liquid and reactor and impeller geometry.

Most of the experiments were conducted using standard vessels equipped with a six-blade disc turbine and a sintered plate or a ring sparger. Notable exceptions are Zlokarnik [110] who used special type of gas inducing impeller and Maerteleire [111] who used four blade paddle impeller. A wide range of vessel sizes (D_T = 0.18 to 1.22 m) and testing fluids (μ = 0.65 to 70 cp) have been used by these investigators.

Zlokarnik [110] carried out experiments on heat transfer in a 0.4 m baffled agitated vessel using spiral cooling coil immersed in a newtonian liquid. Air was centrifugally distributed into the liquid by a fast moving gas inducing impeller. They observed that aeration has a little effect on the tank-side heat transfer coefficient and an increase of only 50 to 100% can be obtained by using such a type of an impeller.

First systematic experimental investigation of heat transfer in mechanically agitated gas-liquid system was carried out by Rao and Murti [107]. They conducted a series of experiments in unbaffled 0.226 m and 0.7 m diameter mechanically agitated vessels using flat blade turbine. Air-water, air-transformer oil and air-clavus oil were used as the two phase fluids. Effect of superficial gas velocity and impeller speed on the heat transfer coefficient was studied and it was noted that sparging of a gas into an agitated liquid improves the heat transfer coefficient at any impeller speed and for any liquid. However, the

influence of gas velocity was more pronounced at lower impeller speeds than at higher values. They argued that the increase in heat transfer coefficient was mainly due to the increase in turbulence near the heated wall caused by the gas bubbles. The experiments were conducted using both coil and jacket as the heat transfer surfaces and it was found that the coil heat transfer coefficient was slightly higher in magnitude than the jacket heat transfer coefficients in the air-water system and lower with the air-oil system. The authors observed that in all the cases studied the heat transfer coefficients for two phase gas-liquids systems were higher than the corresponding unaerated systems.

Nagata et al. [112] developed correlations for jacket and immersed cooling coil in a 0.3 m diameter aerated stirred tank using newtonian and non newtonian liquids. Stirring was done using two different types of impellers. The correlating equation is similar in form as those of non-aerated stirred vessel. The investigators used a modified Reynold number which takes into account the power required in mixing the vessel content in presence of gas and aeration power requirement. They noted that at low impeller speed heat transfer is controlled by aeration and effect of impeller becomes larger with increasing impeller speed. The dimensionless number, R_e', becomes smaller than impeller Reynolds number, R_{en}, when the increase in the power input due to aeration is smaller as compared to the reduction in agitation power requirement. In such a case heat transfer coefficient decreases by aeration.

According to Nagata et al. [112] tank side heat transfer coefficient for non-newtonian liquids with jacketed vessels is much higher than the vessels having

immersed coil. On the other hand, the tank-side heat transfer coefficient for newtonian liquids is 30-40 % higher in the vessel equipped with immersed coil than in the jacketed vessel regardless of the change of viscosity.

Edney and Edward [113] studied heat transfer in aerated stirred tank with immersed coil. They conducted experiments using both newtonian and non-newtonian liquids and proposed a correlation in which dimensionless parameters such as R_{en}, P_{rL} and V_i are defined using an average apparent viscosity based on power input to account for the non-newtonian behavior of the liquids. They noted that heat transfer does not vary significantly with the rate of aeration for both newtonian and non-newtonian liquids. According to Edney and Edwards [113], introduction of air in stirred tanks gives rise to two opposing effects. Aeration induces greater velocities in the region of heat transfer surfaces and hence leads to greater heat transfer coefficient. However, the presence of gas in the vicinity of the heat transfer surface tend to reduce heat transfer coefficient owing to its higher resistance than that of the liquid. Therefore, depending on the process conditions increase or decrease of heat transfer coefficient can be achieved with aeration.

Pollard and Topiwala [109] performed experiments in a pilot scale 0.3 m^3 conventional stirred tank fermenter using air-water and air - K_2SO_4 solution as the heat transfer media. They stated that previously published correlations for single phase heat transfer in stirred tanks are not applicable for gas-liquid systems. According to them for a given fluid and geometry, power input and gas hold up are the principal correlating parameters for the determination of tank

side heat transfer coefficients.

Maerteleire [111] conducted heat transfer experiments using 0.18 m diameter vessel equipped with four blade paddle impeller. They obtained heat transfer data using six different gas-liquid systems. The exponent of Reynolds number in Maerteleire's correlation agrees very closely with that of Rao and Murti [107] and Edney and Edward [73], despite of the fact that different impellers were used by these investigators. This indicates that the type of impeller has little or no influence on the value of the exponent on Reynolds number in gas-liquid systems when immersed coil is used as a heat transfer surface. The dimensionless number $V_{gs}/D_I N$ appearing in the Maerteleire's correlation accounts for the mutual influence of gas rate and impeller speed on the intensity of turbulence. Appearance of Froude number in Maerteleire's correlation and its close agreement with the results obtained by Rao and Murti [107] is not clear. As it is generally accepted that the Froude number is characteristic for surface waves and non level surface profiles due to vortex behavior which especially occurs in unbaffled tanks. Zlokarnik [110] also found a relationship between heat transfer coefficient and the Froude number in baffled tanks. A further comparison with the results of this investigator is limited because of the large differences in the dimensionless numbers defined and the exceptional use infrequently encountered gas inducing impeller.

Steiff and Weinspach [108] developed correlations for heat transfer coefficient in aerated liquids using both jacket and coil as the heat transfer surface. Experiments were performed using six different vessel geometries and

three test fluids with viscosity ranging from 0.65 to 88 cp. The proposed correlations reduce to the case of bubble columns when R_{cn} is set equal to zero. They observed that better heat transfer is obtained in the gas-liquid stirred tank reactors than in the bubble columns. Also, it was noted that the heat transfer coefficients in gas-liquid stirred tank were several times higher than that of single phase liquid pipe flow.

Steiff and Weinspach [108] demonstrated that there exists a maximum limit of impeller speed and gas superficial velocity beyond which any increase in these quantities does not lead to an improvement in heat transfer. This is in agreement with the conclusion drawn by Rao and Murti [107]. It was also noted that under comparable conditions, heat transfer at the coil is slightly higher than at the jacket. They explained that the higher heat transfer coefficient in case of immersed coil was due to the increased turbulence at the coil surface caused by the rising bubbles and impeller induced movements. The authors also compared their results with those of Rao and Murti [107] and Zlokarnik [110]. Despite partial geometric similarity of the systems used by these investigators a good agreement was shown to exist for air-water system. The comparison also reveals that aeration through sintered plate or the ring sparger across the whole of the reactor cross section produces better heat transfer than the central gas introduction system used by Zlokarnik [110].

The first attempt to theoretically derive the model for calculating heat transfer coefficient in jacketed gas-liquid stirred vessel was made by Kurpiers et al. [114]. They developed their model using the concept of Higbie's penetration

theory. The model is based on the assumption that in turbulent stirred system, liquid masses with momentary uniform velocity called "turbulent balls" with temperature T_L are driven through the viscous sublayer to the tank wall, remain there for some time and return to the main flow region, distant from the walls (see Figure 2.15). Also, it was assumed that about 20% of the total agitation energy is dissipated in the region where the heat transfer surface is arranged. They claim that this energy plays a predominant role in disturbing the viscous sublayer.

Equation of Kurpiers et al. [114] shows that the effective specific power input available in the region of heat transfer surface has a significant influence on heat transfer coefficient. Also, their equation is general in nature and can be used for bubble column reactors ($N_e = 0$) and single phase stirred reactors ($R_{eG} = 0$).

In order to check the accuracy of their equation, Kurpier et al. [114] performed heat transfer experiments in a 0.45 m diameter vessel using six different liquids. Experimental data were compared with the model predictions and a good agreement, with maximum deviation of ± 15%, was obtained.

It is interesting to note here that equation of Kurpiers et al. [114] gives lower heat transfer coefficient for aerated stirred vessels as compared to unaerated stirred vessels. As shown in Figure 2.16, higher heat transfer coefficients were obtained only at the beginning of the flooding. Figure 2.17 shows the effect of superficial gas velocity on heat transfer coefficient. It can be also be seen that

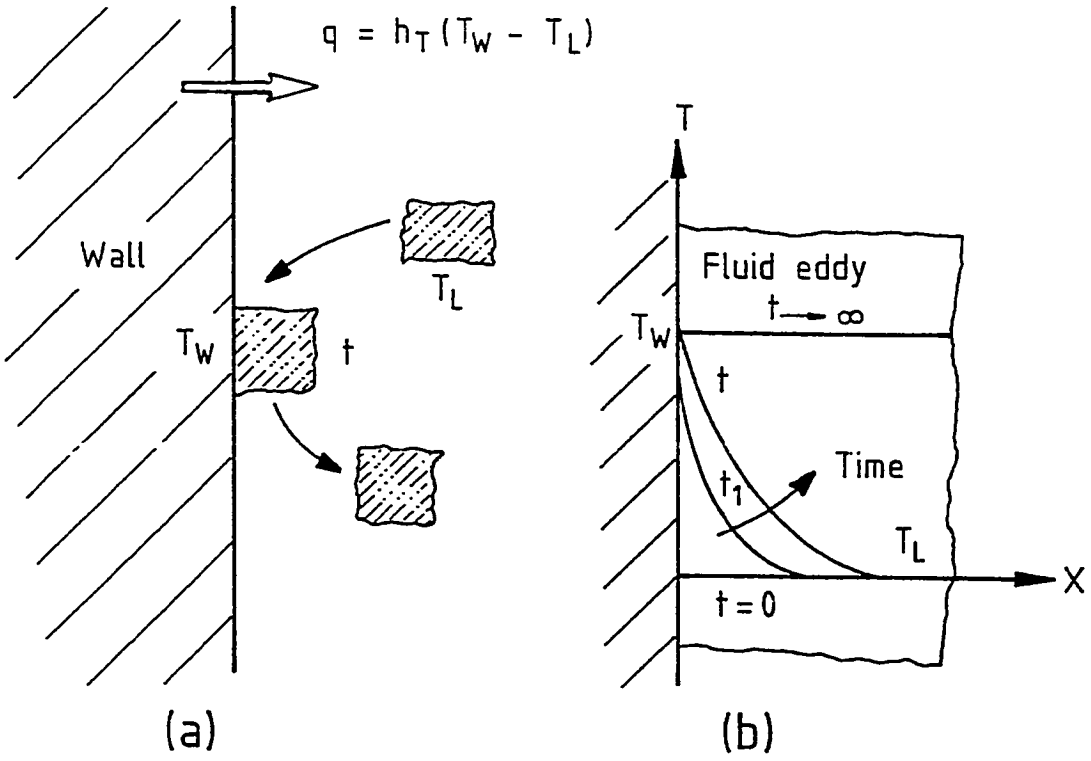

Figure 2.15 (a) Mechanism of Heat Transfer
(b) Transient Heat Conduction Eddies [114]

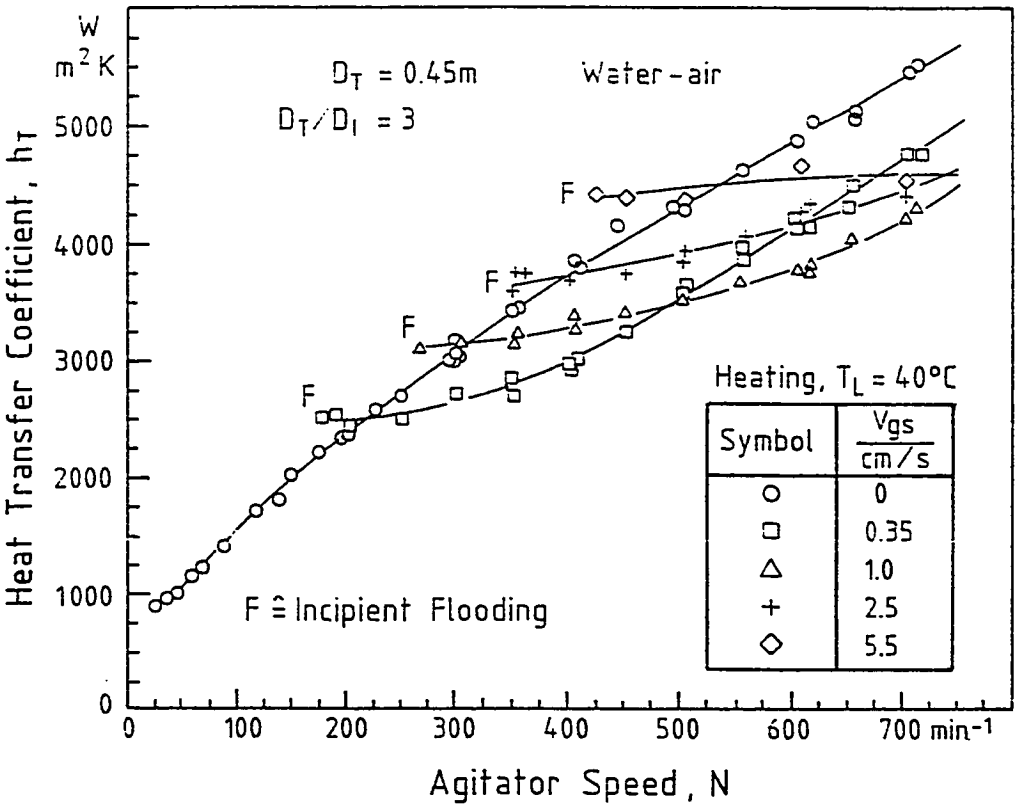

Figure 2.16 Heat Transfer in a Stirred Tank Equiped with Disc Turbine [114]

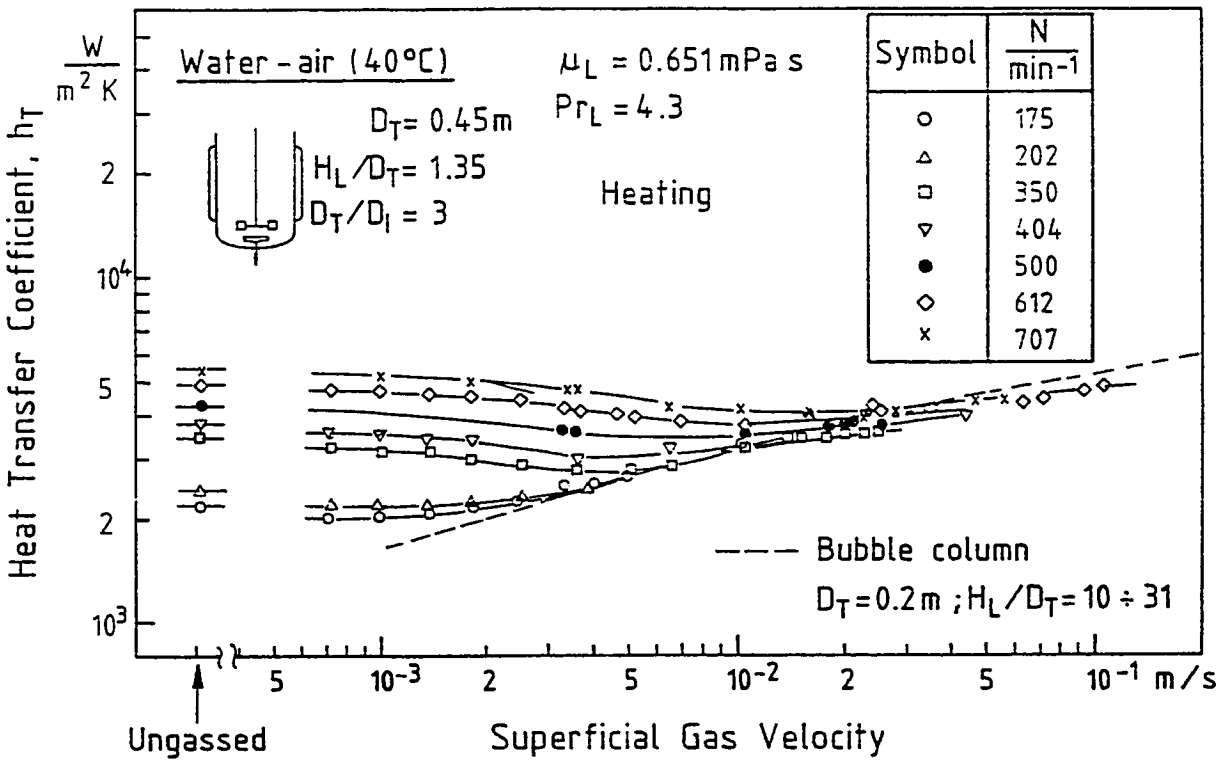

Figure 2.17 Influcnce of Acration Intensity on Heat Transfer [114]

the increase in superficial gas velocity has little or no effect on the value of heat transfer coefficient and mechanical agitation of gas-liquid system is advantageous for heat transfer only at low superficial gas velocities, which in this case are lower than 0.02 m/sec. Figure 2.17 also indicates that at high superficial gas velocities better heat transfer can be achieved in bubble columns than in stirred tanks.

Kurpiers et al. [114] explained that the decrease in heat transfer at low aeration rate is due to considerable reduction in power consumption of the stirrer in presence of air, thus, heat transfer deteriorates. At high gas flow rates the power requirement of the stirrer approaches a limiting value, in this case, any increase in the gas flow rate leads to an improvement in heat transfer. These researchers also conducted experiments using two stage impellers and observed that at the same power input per unit volume two-stage stirrer gives better heat transfer than a comparable one stage system, as shown in Figure 2.18

In a separate paper, Kurpier et al. [115] studied the influence of addition of solids in gas-liquid jacketed stirred reactor. They noted that addition of solids reduces heat transfer in both stirred liquid and gas-liquid systems. According to them heat transfer coefficient will always decrease at the suspension point due to an increase in solid concentration in the lower part of the vessel. The investigators concluded that the mechanism of heat transfer in suspensions is not significantly influenced by the presence of a dispersed gas phase. The authors pointed out that in three phase systems better heat transfer can be

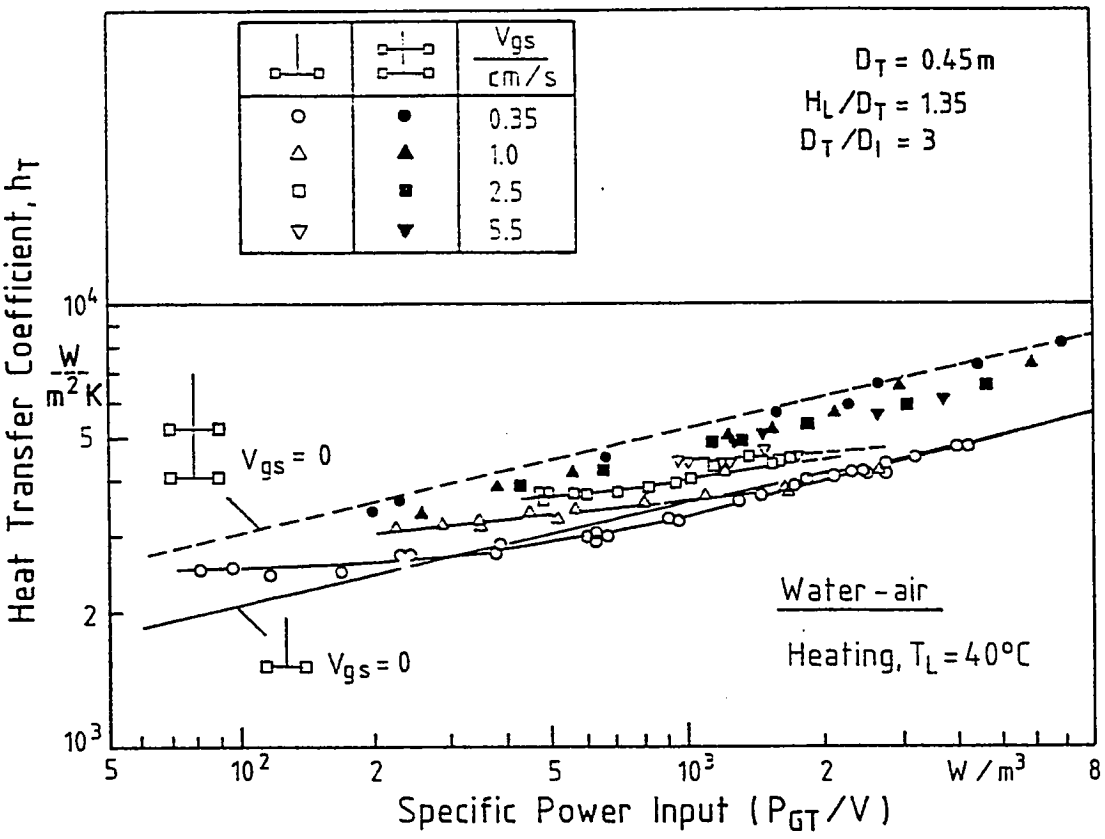

Figure 2.18 Influence of Total Power Input Per Unit Volume on Heat Transfer in Gas-Liquid Systems [114]

achieved by installing the second impeller on the same shaft and recommended that the distance between the two stirrer should be at least two times the stirrer diameter to ensure effective heat exchange.

Kurpiers et al. [116] studied the heat transfer characteristics of electrically heated probe using single and two stage disc turbine. They found out that heat transfer coefficients along the heating probe are considerably higher than those along the reactor jacket in both single stage and two stage stirring systems and gas hold up or the superficial gas velocity has no or very little effect on the heat transfer coefficient. On account of different flow conditions in one and two stage impeller arrangements, these researchers proposed separate correlations for the two situations.

Recently, Desplanches et al. [67] studied heat transfer in highly viscous, aerated stirred liquids using two different size tanks of standard geometry equipped with standard Rushton turbine. They proposed correlations for tank-side heat transfer coefficient in the complete gas dispersion regime, flooding regime and the transition regime. According to these correlations, the introduction of gas increases or decreases the tank-side heat transfer coefficient of a gas-liquid stirred reactor depending on the regime it is being operated. Correlation of Desplanches et al. [67] in complete dispersion regime is similar in the form as those of Zlokarnik[110] and Rao and Murti [107]. However, in their correlation Desplanches et al. [67] defined the Reynold number based on mean liquid circulation velocity in aerated condition rather than superficial gas velocity as in the cases of Zlokarnik [110] and Rao and Murti [107]. Edney and

Edwards [113] also studied the heat transfer in high viscosity gas-liquid systems, but their correlation, however, similar in form uses impeller Reynold number rather than circulation Reynold number used by Desplanches et al. [67].

It can be seen from Table 2.9 that although many experimental studies on the heat transfer characteristics of gas-liquid stirred reactor have been published, a general form correlation, as in the case of single phase system, has not emerged. Most researchers have used specific power input as a major correlating parameters. Moreover, except Kurpiers et al. [114], all previous correlations have been developed based on entirely empirical approach. empirical and have been developed based on dimensional analysis. Except Pollard and Topiwala [109], most of the authors have correlated their heat transfer data using either of the following two sets of dimensionless groups:

$$N_{uT} = f\left[R_{eG}, R_{en}, F_{rn}, P_{rL}, V_i\right] \tag{2.26}$$

$$N_{uT} = f\left[R_{en}, N_e or P_G, F_{rn}, \frac{D_T}{D_I}, P_{rL}, V_i\right] \tag{2.27}$$

The definition of Reynold number differs in certain cases. For example Rao and Murti [107] have used a modified Reynold number which involves both gas and impeller Reynold numbers and Desplanches et al. [67] used the Reynold number based on liquid circulation velocity under aerated conditions.

Except Rao and Murti [107], most of the investigators have shown that, depending on the gas dispersion regime, the presence of gas may increase or decrease the tank-side heat transfer coefficient. Rao and Murti [107], however, demonstrated that the presence of gas always increases the heat transfer

coefficient. This is because of the fact that these investigators conducted all their experiments under under a dispersion regime favourable to heat transfer.

With the exception of Kurpiers et al. [114], most of the correlations are entirely empirical and have been obtained using, mostly, laboratory scale data. Therefore, their applicability in case of large industrial scale reactors is questionable. Since the correlation of Kurpier et al. [114] is based on some theoretical understanding and also because it has been experimentally verefied, we will use Kurpier's correlation for calculating h_T for jacketed reactor. In case of immersed helical coil, correlation proposed by Rao and Murti [107] will be used.

2.2.11 Jacket or Coil-Side Heat Transfer Coefficient

Cooling Coils and jackets are used to remove or supply heat to stirred tank reactors. Some common types of coil and jacketing arrangement are shown in Figure 2.19. Knowledge of heat transfer coefficient inside the coil or a jacket (h_c or h_j) is essential for calculating the heat transfer surface area needed. The film coefficients h_c or h_j depend on the physical properties of the heat transfer medium, geometry of a jacket or coil arrangement and the flow characteristics of the heat transfer surfaces. As such very few experimental studies on the heat transfer characteristics of a coil or a jacket have been done. Heat transfer coefficients inside these transfer surfaces are usually calculated using already existing correlations for straight pipes by defining an equivalent diameter in place of pipe diameter and by using appropriate correction factors wherever

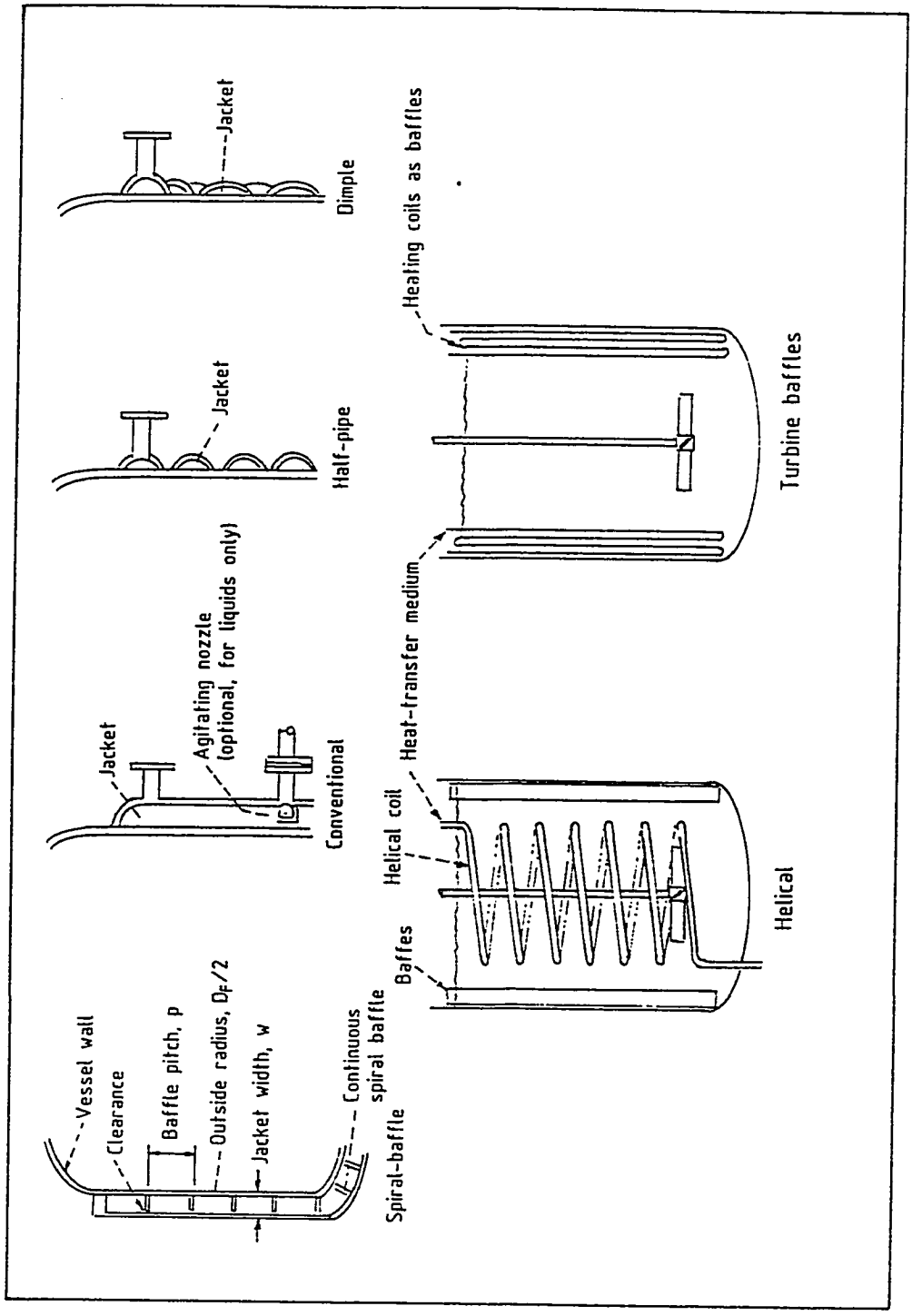

Figure 2.19 Common Arrangements of Heat Transfer Jackets and Internal Coils [36]

necessary.

Uhl and Gray [37] have given a very comprehensive review on various types of jacketing and cooling coil arrangement and have recommended correlations to calculate coil/jacket side heat transfer coefficient. Rase [105] and Rose [117] have also discussed the calculation of heat transfer coefficient inside a coil or a jacket and have provided a list of selected correlations along with the equivalent diameters for various geometries. Some most recent experimental studies as well as the proposed procedures for calculating coil or jacket side heat transfer coefficients are summarized in Table 2.10.

Lehrer [118] developed a correlation for heat transfer coefficient in simple jackets with radial and tangential inlet pipes using Prandtl analogy for smooth tubes. He conducted experiments using 0.676 m diameter jacketed, agitated tank and studied the effect of mode of injection of heat transfer medium into the jacket. The calculated and experimental results were shown to be in excellent agreement. Heat transfer coefficients for jacket with tangential inlet were reported to be much higher than those with the radial inlet owing to their higher characteristic velocity.

Bolliger [119] as well Bondy and Lippa [36] published methods of calculating heat transfer coefficient in different types of liquid carrier jackets and cooling coils based on the heat transfer in straight pipes. Recently, Stein and Schmidt [120] performed heat transfer experiments using laboratory scale (D_T = 90 mm) and large scale (D_T = 610 mm) stirred jacketed vessel and

Table 2.10 Correlation for Jacket or Coil Side Heat Transfer Coefficient

Reference	Type of Heat Transfer Surface	Dimensions	Formula for Calculating Equivalent Diameter	Dimensionless form of Working Equation	Range of Applicability
Lehrer (1970) [118]	Simple jacket with radial, or tangential inlet	$D_T(m) = 0.61$ $d_m(m) = 0.676$ $\ell m(m) = 0.597$ $b_m(m) = 0.025$	$D_g = (8/3)^{0.5} \cdot bm$	$N_{uj} = \frac{0.03R_{ec}^{0.75}P_{rc}}{1+\frac{1.74(P_{rc}-1)}{R_c^{-0.125}}}(\frac{\mu_{cb}}{\mu_{cw}})^{0.14}$ where $R_{ec} = \frac{D_g\{(V_{cm}V_{cs})^{0.5}+V_{cA}\}\rho_c}{\mu_c}$	$9000 < R_{ec} < 40,000$
Bolliger (1982) [119]	Simple jacket Jacket with agitation nozzle Spirally baffled jacket Dimple jackets Panel pipe coil jacket Partial pipe coil jacket	Jacket for Vessel volume upto 15 m^3 can be designed	$D_g = D_H = \frac{4\times \text{flow area}}{\text{wetted perimeter}}$	Simple Jacket $N_{uj} = \frac{h_j D_H}{\lambda_c} = 0.8K''(\frac{C_{pc}\mu_c}{\lambda_c})^{1/3}(\frac{D_H^3\rho_c^2 g\beta\Delta T_{LM}}{\mu_c^2})^{1/3}$ Other Jackets. for water: $h_j = 91(1+0.11T_c)V_{cs}^{0.8}/D_H^{0.2}$ for brine and organics: $\frac{h_j D_H}{\lambda_c} = 0.027(R_{ec})^{0.8}(P_{rc})^{1/3}$ $M_c^0(V_{cn}-V_{cs}) = \frac{4fL\rho_c}{D_H}(\frac{V_{cs}}{2})^2$	$V_c(m/s) = 0.03$ Panel type coils jacket $V_c(m/s) - 0.76 - 1.5$ Cooling fluid velocity Spirally baffled jackets $V_c = (m/s) - 0.3 - 1.2$ Dimple jacket $V_c(m/s) - 0.76 - 1.5$

Table 2.10 Continued

Reference	Type of Heat Transfer Surface	Dimensions	Formula for Calculating Equivalent Diameter	Dimensionless form of Working Equation	Range of Applicability
Bondy & Lippa (1983) [36]	Annular Jacket with Spiral baffles (AJSP) Annular jacket with no baffles (AJ) Half-pipe-coil jacket (HPCJ) Dimple jacket (DJ) Internal coils (IC)		AJSP: $Dg = 4b_m$ AJ $Dg = (\frac{D_{mo}^2 - D_{mi}^2}{D_{mi}})$ HPCJ $D_g = \frac{\pi}{2} dci$ (for 180°) $= 0.708\ dci$ (for 120°) DJ $D_g = 16.7\ mm$ IC $D_g = dci$	$R_{ec} > 10,000$ $\frac{h_j D_g}{\lambda_c} = N_{uj} = 0.027(R_{ec})^{0.8}(P_{rc})^{0.33}(\frac{\mu_{cb}}{\mu_{cw}})^{0.14} \times [1 + 3.5(\frac{Dg}{Dc})]$ $R_{ec} < 21,000$ $\frac{h_j D_g}{\lambda_c} = N_{uj} = 1.86(R_{ec} P_{rc} \frac{Dg}{\ell m})^{0.33}(\frac{\mu_{cb}}{\mu_{cw}})^{0.14}$	From laminar to turbulent flow conditions
Stein & Schmidt (1986) [120]	Coolng Jacket with radial pipe. Simple cooling jacket with gential pipes Cooling jacket consisting of semicircular pipe coil with tangential connection pipes		$Dg = \frac{\pi}{2} dci$	Gnielinski: $R_{ecr} = 2300[1 + 8.6(\frac{dci}{2dm})^{0.45}]$ $R_{ec} < R_{cr}$ $N_{ulam} = \frac{h_j Dg}{\lambda_c} = \{3.66 + 0.08[1 + 0.8(\frac{dci}{2du})^{0.9}] \times R_{ec}^a P_{erc}^{0.33}\}(\frac{\mu_{cb}}{\mu_{cw}})^{0.14}$	From laminar to turbulent flow conditions

Table 2.10 Continued

Reference	Type of Heat Transfer Surface	Dimensions	Formula for Calculating Equivalent Diameter	Dimensionless form of Working Equation	Range of Applicability
				$N_{uturb} = \frac{h_j D_e}{\lambda_c} = R_e \geq R_{etr}$	
				$= \frac{\frac{r_D}{8} R_{ec} P_{rc}}{1+12.7(\frac{r_D}{8})^{0.5}(Pr_C^{2/3}-1)} (\frac{\mu_{cb}}{\mu_{cw}})^{0.14}$	
				where	
				$r_D = \frac{0.3164}{R_{ec}^{0.25}} + 0.03(\frac{dci}{2dm})^{0.5}$	
				$R_{ecr} < R_e < R_{etr}$	
				$Nu = N_{uturb} - (N_{utur} - N_{ucr}) \frac{R_{etr} - Re}{R_{etr} - R_{ecr}}$	
				where	
				$N_{ucr} = N_{ulam}(R_{ecr})$	
				$N_{utr} = N_{uturb}(R_{etr})$	
				Bonding Lippa Method. $R_{ec} < 2300$	$0 < R_e < 10^6$
				$N_{ulam} = [(3.65)^3 + (1.61)^3 R_{ec} P_{rc} \frac{dm}{lm}$	$Pr = 0.7 - 7$
				$+(0.664)^3 R_{ec}^{1.5} P_{rc} (\frac{dm}{lm})^{1.5}]^{0.33} (\frac{\mu_{cb}}{\mu_{cw}})^{0.14}$	
				$R_{ec} > 2300$	
				$N_{uturb} = 0.0235 R_{ec}^{0.8} [1 - (\frac{2300}{R_{ec}})^{1.4}] \times$	
				$(1.8 p_{rc}^{0.3} - 0.8)[1 + \frac{d}{\rho})^{2/3}] (\frac{\mu_{cl}}{\mu_{cw}})^{0.14}$	
				$R_{ec} < 2300$:	
				$N_{uturb} = 0$	
				$N_u = [N_{ulam}^3 + N_{uturb}^3]^{1/3} (1 + 3.5 \frac{dc_i}{2dm})$	

compared their experimental results with those obtained by using methods proposed by other researchers [36,118,119]. These researchers used the methods proposed by Bolliger [119] and Bondy and Lippa [36] by incorporating recently published correlations which covers the entire range of laminar and turbulent flow in pipes. In most cases, heat transfer coefficients calculated using Bondy and Lippa [36] and Bolliger [119] methods were were either too high or too low compared to those of experimental values. However, they found that the Lehrer's correlation gives reasonably good fit to the experimental data obtained using large agitated tanks (D_T = 610 mm) equipped with simple jackets and radial or tangential inlet pipes. In general, the experimental results of Stein and Schmidt [120] obtained in laboratory scale vessels agree well with those obtained using large tanks.

Due to the lack of proper understanding of the flow behavior in different types of jackets and cooling coils, most of the methods for calculating jacket or coil side heat transfer coefficients are based on the correlations for straight pipes. Most of these equations, however, yield unsatisfactory results when applied to different geometries of transfer surfaces.

Experimental data on heat transfer inside a jacket or a cooling coil are scarce. To date only two experimental studies [118,120] on heat transfer inside jackets have been published. The experimental data for heat transfer inside cooling coils are non-existent. There is a need for more experimental work especially in case of jackets with complex configuration. In this work, for jacketed reactor Lehrer's [118] correlation will be used and for the cooling coils

correlation proposed by and Bondy and Lippa [36] will be used. This is because Lehrer's equation has been experimentally varified by Lehrer [118] and by Stein and Schmidt [120]. For the case of cooling coils correlation proposed by Bondy and Lippa [36] is the only one available in the literature.

CHAPTER 3

DEVELOPMENT OF THE REACTOR MODEL

In order to have a better understanding of the phenomena of steady state multiplicity in a reacting system, it is essential to mathematically model the behavior of the reactor under consideration. A mathematical model represents the physical and chemical processes occurring within the reactor by a set of equations. Solutions of these model equations enables one to carry out quantitative studies of the reactor system that could be used either to predict the full scale design of the reactor or to analyse the reactor behavior by studying the effect of various parameters on the performance of the reactor.

Modeling single-phase CSTRs with single or complex chemical reactions is relatively simple and both have been extensively studied [9,10]. However, modeling of gas-liquid reactions occurring in a CSTR is much more complex due to the interaction between the reaction rate and transport of gaseous and liquid reactants. The heat loss by liquid evaporation, influence of temperature and conversion on various physico-chemical properties and prevailing hydrodynamics conditions, if included, may further complicate the model.

The mathematical description of a process can be made as comprehensive as possible by taking into consideration each and every detail of the reacting system and by accurately describing the physical and chemical phenomena occurring in the reactor. However, the resulting model will be complex and difficult to solve and will contain too many parameters. In practice, therefore, a compromise is made by making some reasonable simplifying assumptions. Though, the present model will be developed by relaxing most of the crucial assumptions of the previous investigators [5,17,18], some of their assumptions will still be retained. The new model will be based on an irreversible second-order gas-liquid reaction taking place in a well mixed CSTR (see Figure 1.1). Effect of changing operating conditions on the reactor hydrodynamics will be incorporated by using empirical correlations for various hydrodynamic and transport parameters appearing in the model equations. To account for the effect of chemical reaction on inter-phase mass transfer, the reaction factor concept will be utilized. A detailed discussion on the appropriate reaction factor along with its derivation is provided in Chapter 4.

3.1 Assumptions

The model is developed based on the following assumptions:

1. The reactor contents are well mixed and it operates non-adiabatically under steady state condition.

2. Physical properties of gas and liquid, liquid phase mass transfer coefficient, the heat of solution and the heat of reaction are independent of conversion.

3. The liquid feed does not contain any dissolved gaseous reactant.

4. The gaseous feed is composed of species A and other inert species and the inerts are not absorbed in the liquid.

5. Effluent gas is saturated with the vapour of species B, and passes through an ideal condenser. The condensate is returned continuously to the reactor.

6. The total pressure inside the reactor is independent of position and of temperature.

7. Heat transfer resistance at the gas-liquid interface is negligible. and the gas and liquid are at the same temperature inside the reactor.

8. Phase equilibrium of the gaseous reactant follows Henry's Law :

$$p_{Ai} = \{H_A \exp(-\Delta Hs_i / RT)\} A_i$$

and that of the liquid reactant follows Raoult's law:

$$Log(p_{Bi}) = \{C_1 - C_2/(T + C_3)\} \frac{B_i}{\rho_l}$$

9. The ideal gas law applies and the temperature dependence of the rate constant is described by Arrhenius law.

3.2 Equations for Mass Balance, Energy Balance and Rate of Absorption

Figure 3.1 shows a material and energy flow diagram of a CSTR in which an irreversible exothermic second-order gas-liquid reaction:

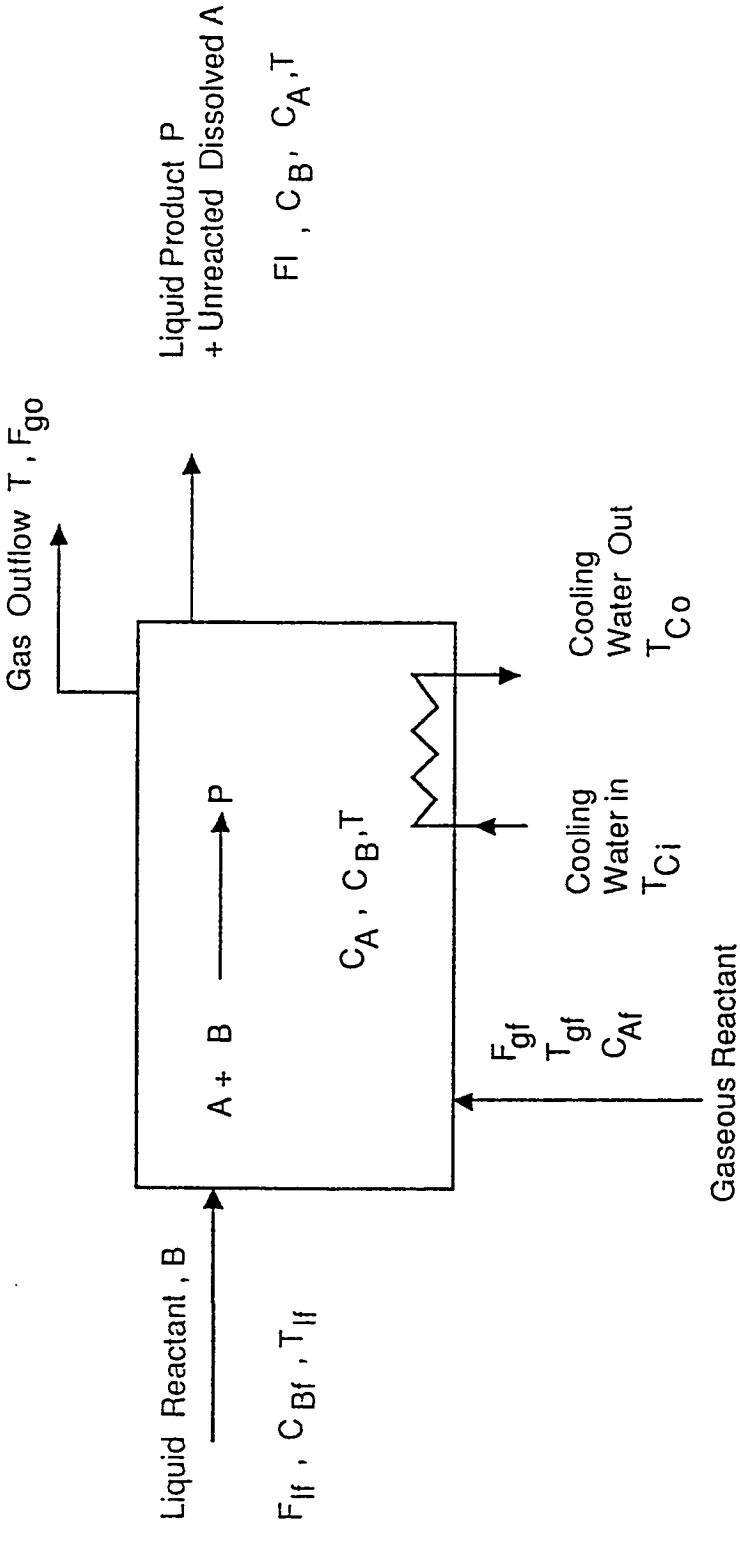

Figure 3.1 Material and Energy Flow Diagram

$$A_{(gas\text{-}liq)} + \nu B_{(liq)} = P_{(liq)} \tag{3.1}$$

is taking place according to general second-order kinetics as represented by Equation (3.2):

$$(-r_A) = KC_A C_B \tag{3.2}$$

The reactor is fed continuously with gas and liquid streams which contain reactants A and B, respectively. The gas stream also contains some quantity of insoluble inerts. The gaseous reactant A diffuses through the gas-liquid interface and subsequently reacts with a liquid phase reactant to give a liquid phase product P which flows out of the reactor with unreacted B and unreacted dissolved A.

The gas and liquid enter the reactor at different flow rates and temperatures. Since gas is absorbed into the liquid, outlet gas flow rate, F_{go} will be different from the inlet gas flow rate, F_{gf}. However, owing to no appreciable change in liquid volume due to reaction, outlet flow rate of liquid, F_l will remain approximately same as the liquid inlet flow rate. Furthermore, since both phases are assumed to be in perfectly mixed condition inside the reactor, at steady state both gas and liquid will leave the reactor at a composition and temperature as those existing inside the reactor in their respective phases.

The following sections will give the final form of the steady state mass and energy balance equations. Details of derivation of these equations are provided in Appendix A1.

3.2.1 Mass Balances

3.2.1.a Mass Balance for Gaseous reactant, A

A steady state mole balance for gaseous reactant A across the reactor gives:

Moles of A in Gas Feed − *Moles of A in Effluent Gas* = *Moles of A consumed in the Reaction* + *Moles of A in Effluent Liquid*

Substituting for each term in the above equation will give the mass balance equation for the gaseous reactant A.

$$N_{gf}Y_{Af} - N_{go}Y_{Ao} = R_A V_R + F_l A_l \tag{3.3}$$

3.2.1.b Mass Balance of Liquid Reactant, B

A steady state mole balance for liquid reactant B across the reactor gives:

Moles of B in Liquid Feed − *Moles of B in Liquid Effluent* = *Moles of B consumed in the Reaction* + *Moles of B in Effluent Gas*

Since it is assumed that the vaporised liquid is condensed and returned back to the reactor the last term can be set equal to zero. Substituting for the remaining terms yields the following relation:

$$F_l(B_{lf} - B_l) = \nu R_A V_R \tag{3.4}$$

3.2.1.c Mass Balance for Gaseous Inerts

A steady state mole balance for gaseous inerts across the reactor gives:

Moles of Inerts in Gas Feed = *Moles of Inerts in Effluent Gas* + *Moles of Inerts in Liquid Effluent*

Assuming that the inerts are not absorbed in the liquid, we get the following

equation:

$$N_{gf}(1 - Y_{Af}) = N_{go}(1 - Y_{Ao} - Y_{Bo}) \tag{3.5}$$

3.2.2 Energy Balance

The energy balance across the reactor involves the heat input and output due to the bulk flow of liquid and gas, heat generation due to exothermic reaction, absorption of gaseous reactant and agitation, and the heat loss due to liquid evaporation and external cooling. Thus, a steady state energy balance across the reactor can be represented as follows.

Heat Input + *Heat Generated* = *Heat Output* + *Heat Loss*
(*Liquid* + *Gas*) (*Reactn* + *Absptn* + *Agitn*) (*Liquid* + *Gas*) (*Cooling* + *Evaporation*)

$$F_l\rho_l C_{pl}(T_{lf} - T) + N_{gf}C_{pg}T_{gf} + [(-\Delta H_s) + (-\Delta H_R)]R_A V_R + (-\Delta H_s)F_l A_l$$
$$+ H_{ag} - N_{go}(1 - Y_{Bo})C_{pg}T - N_{go}Y_{Bo}(-\Delta H_v) - US(T - T_c) = 0 \tag{3.6}$$

where H_{ag} is the heat addition due to the agitation of reactor contents by the impeller as well as the sparged gas. This heat is is estimated based on the assumption that the total mechanical power dissipated to the system is converted into heat. It should be noted here that our work accounts for the heat addition due to mixing power for the first time, as is devoid of this effect in gas-liquid reactor modeling.

3.2.3 Rate of Absorption

To relate the mass and energy balance equations, developed in the previous sections, with the interphase mass transfer one should have relations for the rate

of absorption of gaseous reactant in terms of liquid and gas-side mass transfer coefficients. Rate of absorption of gaseous reactant A in terms of liquid-side mass transfer coefficient can be defined as:

$$N_A = \underline{a} K^{\circ}_L V_R A_i E^{\bullet}_A = (R_A V_R + F_l A_l) \tag{3.7}$$

The parameter $E^{\bullet}_A$, called reaction or enhancement factor, relates the chemical reaction with the interphase mass transfer. A detailed discussion on $E^{\bullet}_A$, is given in section 3.5 and Chapter 4.

Rate of absorption of gaseous reactant A in terms of gas-side mass transfer coefficient can be defined as:

$$N_A = \underline{a} K^{\circ}_G V_R (p_{Ab} - p_{Ai}) \tag{3.8}$$

Relations for p_{Ai} and p_{Ab} can be obtained by using Henry's law and ideal gas law, respectively (for details refer to Appendix A1).

3.3 Model Equations in Dimensional Form

Combining mass and energy balance equations with the equations of rate of absorption and using Henry's law and ideal gas law along with appropriate algebraic manipulations we obtain the following equations in dimensional form. Detailed derivation of dimensional model equations is given in Appendix A1.

Interfacial Concentration of Gaseous Reactant, A_i

$$A_i = \frac{N_{gf} Y_{Af}(1 - Y_{Bo})(1 - X_A) RT_{gf} \exp\left(\frac{\Delta H_s}{RT}\right)}{F_{gf}(1 - Y_{Af} X_A)\left[\exp\left(\frac{\Delta H_s}{RT}\right)\frac{K^{\circ}_L E^{\bullet}_A}{K^{\circ}_G} + H_A\right]} \qquad (3.9)$$

Conversion of Gaseous Reactant, X_A

$$X_A = \frac{(1 - X_A)(1 - Y_{Bo})}{(1 - Y_{Af} X_A)\left[\frac{F_{gf}}{\underline{a} V_R RT_{gf} K^{\circ}_G} + \frac{H_A F_{gf}}{\underline{a} K^{\circ}_L V_R E^{\bullet}_A RT_{gf}} \exp\left(\frac{-\Delta H_s}{RT}\right)\right]} \qquad (3.10)$$

Conversion of Liquid Reactant, X_B

$$X_B = \nu\left[\frac{F_{gf} A_{gf}}{F_l B_{lf}} X_A - \frac{A_l}{B_{lf}}\right] \qquad (3.11)$$

Steady State Temperature, T

$$F_l \rho_l C_{pl}(T_{lf} - T) + F_{gf} \rho_{gf} C_{pg} T_{gf}\left[1 - (1 - Y_{Af} X_A)\left(\frac{T}{T_{gf}}\right)\right] + [(-\Delta H_s) + (-\Delta H_r)] \times$$

$$\left[\frac{\underline{a} K^{\circ}_L V_R E^{\bullet}_A N_{gf} Y_{Af}(1 - X_A)(1 - Y_{Bo})}{F_{gf}(1 - Y_{af} X_A)} RT_{gf} K^{\circ}_G \left\{K^{\circ}_L E^{\bullet}_A + K^{\circ}_G H_A \exp\left(\frac{-\Delta H_s}{RT}\right)\right\}^{-1}\right]$$

$$- \frac{N_{gf}(1 - Y_{Af} X_A)(-\Delta H_v) Y_{Bo}}{(1 - Y_{Bo})} - (-\Delta H_R) F_l A_l - US(T - T_c) + H_{og} = 0 \qquad (3.12)$$

3.4 Model Equations in Dimensionless Form

In order to make the model equations dimensionless, the following dimensionless quantities are defined:

$$a_l = A_l/B_{lf} \qquad q = \frac{B_{lf}}{A_{gf}} \qquad Q = \frac{F_{gf}}{F_l}$$

$$p = \frac{(-\Delta H_R)F_l A_{gf}}{\rho_l C_{pl} T_{lf} F_{gf}} \qquad v = \frac{(-\Delta H_v)\rho_{gf}}{\rho_l C_{pl} T_{lf}} \qquad r = \frac{\rho_{gf} C_{pg}}{\rho_l C_{pl}}$$

$$\mathrm{B} = \frac{[(-\Delta H_s) + (-\Delta H_R)]A_{gf}}{\rho_l C_{pl} T_{lf}} \qquad D_{gf} = \frac{aK^{\circ}_L V_R H_o}{F_{gf}} \qquad H_o = \frac{RT_{gf}}{H_A}$$

$$\theta = \frac{T - T_{lf}}{T_{lf}} \qquad \theta_c = \frac{(T_c - T_{lf})}{T_{lf}} \qquad \theta_r = \frac{T_{gf}}{T_{lf}}$$

$$\alpha = \frac{1}{Q} + r \qquad \beta = \frac{US}{F_{gf}\rho_l C_{pl}} \qquad \delta = \frac{\Delta H_s}{RT_{lf}}$$

$$Y^{*}_{Bo} = \frac{Y_{Bo}}{(1 - Y_{Bo})} \qquad H_p = \frac{H_{ag}}{\rho_l C_{pl} T_{lf} F_{gf}} \qquad \Psi = \frac{K^{\circ}_L}{K^{\circ}_G H_A}$$

Introducing the above dimensionless quantities in Equations (3.9) to (3.12) and making necessary algebraic manipulation yield model equations in dimensionless form given as follows:

Interfacial Concentration of Gaseous Reactant, A_i

$$\frac{A_i}{A_{gf}} = \frac{(1 - Y_{Bo})(1 - X_A)H_o \exp\left(\frac{\delta}{1 + \theta}\right)}{(1 - Y_{Af}X_A)\left[\exp\left(\frac{\delta}{1 + \theta}\right)\Psi E^{*}_A + 1\right]} \tag{3.13}$$

Conversion of Gaseous Reactant, X_A

$$X_A = \frac{D_{gl}(1 - X_A)(1 - Y_{Bo})}{(1 - Y_{Af}X_A)}\left[\Psi + \left\{\frac{\exp\left(-\frac{\delta}{1 + \theta}\right)}{E^*_A}\right\}\right]^{-1} \tag{3.14}$$

or

$$X_A = \frac{(\alpha + \beta)\theta + pqa_l - \beta\theta_c - r(\theta_r - 1) + vY^*_{Bo} - H_p}{B + (1 + \theta)rY_{Af} + Y_{Af}vY^*_{Bo}} \tag{3.15}$$

Conversion of Liquid Reactant, X_B

$$X_B = v\left(\frac{Q}{q}X_A - a_l\right) \tag{3.16}$$

Steady State Temperature, θ

$$-\theta\left[\frac{1}{Q} + r - Y_{Af}X_A r\right] + r(\theta_r - 1) + rY_{Af}X_A - vY^*_{Bo}(1 - Y_{Af}X_A) - pqa_l - \beta(\theta - \theta_c)$$

$$+ H_p + B\left[\frac{D_{gl}(1 - X_A)(1 - Y_{Bo})}{(1 - Y_{AF}X_A)}\left\{\Psi + \frac{\exp\left(-\frac{\delta}{1 + \theta}\right)}{E^*_A}\right\}^{-1}\right] = 0 \tag{3.17}$$

or

$$\theta = \frac{\{B + Y_{Af}(r + vY^*_{Bo})\}X_A + \beta\theta_c + r(\theta_r - 1) - pqa_l - vY^*_{Bo} + H_p}{(\alpha + \beta - rY_{Af}X_A)} \tag{3.18}$$

Equation (3.18) can be used to obtain *a priori* temperature bounds which are necessary for numerical simulation study.

Upper Bound:

An upper bound for the temperature can be obtained by setting $X_A = 1$, $a_l = 0$ and $Y_{Bo} = 0$. Thus,

$$\theta_{ub} = \frac{B + rY_{Af} + \beta\theta_c + r(\theta_r - 1) + H_p}{\alpha + \beta - rY_{Af}} \tag{3.19}$$

Lower Bound:

A lower bound results when $X_A = a_l = 0$. Hence,

$$\theta_{lb} = \frac{\beta\theta_c + r(\theta_r - 1) - vY^*_{Bo} + H_p}{\alpha + \beta} \tag{3.20}$$

Note that an implicit relation for θ_{lb} can be obtained by substituting for Y^*_{Bo} in Equation (3.20) using Rault's law. Also, it can be observed from Equations (3.19) and (3.20) that θ_{ub} has a greater value in case of pure gas feed as compared to the dilute gas feed where as θ_{lb} is independent of feed gas purity [26].

The model Equations (3.13) to (3.18) are derived for volatile liquid case. However, these equations can be reduced to non-volatile liquid case by setting Y_{Bo} and/or v equal to zero. The dimensionless parameter Ψ in the model equations is a measure of gas-side resistance to mass transfer and its value approaches zero as the gas-side mass transfer coefficient K^o_G approaches infinity (e.g in case of pure gas feed).

In order to solve the model equations for temperature and conversions of liquid and gaseous reactants, expressions for the reaction factor, $E^{\bullet}_{A}$, and other transport, and hydrodynamic parameters such as U, K^{o}_{L}, K^{o}_{G}, $\underline{a}$ and ε_{G} will be required. Furthermore, relations for minimum stirrer speed, total power input, bubble rise velocity and bubble diameter will also be required since they will be needed for the evaluation of hydrodynamic and transport parameters mentioned as before. Based on the literature review, given in Chapter 2, selected correlations for aforementioned parameters are given in the following sections. These correlations along with the conversion and temperature equations and with the equations for reaction factor constitute the new reactor model which will be used for the numerical simulation discussed in Chapter 5.

3.5 Equations for Reaction Factor

The parameter $E^{\bullet}_{A}$, called reaction factor, is a measure of the effect of chemical reaction on the mass transfer of gaseous component A and is calculated by solving the "local" problem (i.e. by making the mass balance around a single gas bubble surrounded by a liquid film in which the said reaction is taking place). The resulting equations are coupled non-linear second-order ordinary differential equations which have to be solved either by using approximate analytical techniques or by numerical methods. For the purpose of numerical simulation of reactor behavior, it would be easier to have an analytical expression for $E^{\bullet}_{A}$. In the present work we can use the $E^{\bullet}_{A}$ expressions already developed by previous researchers [13,14]. It should, however, be noted

that all the previous expressions for E_A^* are based on rectangular consideration (i.e. the thickness of the film surrounding the gas bubble is very small compared to the bubble diameter). Since we will be calculating the gas bubble diameter in our simulation program, it will be appropriate to have an expression for E_A^* which will take into account the sphericity of the gas bubble and will relate to the bubble size. Thus, a new approximate analytical expression for E_A^* has been developed. Details of the development of the new reaction factor expression are given in Chapter 4.

Reaction Factor Expressions

Two reaction factor expressions have been used in this work. The first expression given by Equations 3.21a-c is for the spherical bubble geometry and has been developed in this thesis, as detailed in Chapter 4.

$$E_A^* = \frac{M_m\sqrt{b_i}\Omega}{(1+\Omega)}\left[\frac{M_m\sqrt{b_i}\tanh(M_m\sqrt{b_i})(1+\Omega)+\{M_1(1+\Omega)-1\}}{M_m\sqrt{b_i}(1+\Omega)+\{M_1(1+\Omega)-1\}\tanh(M_m\sqrt{b_i})}\right]+\frac{1}{1+\Omega} \qquad (3.21a)$$

where

$$M_1 = \left[M^2\left\{\alpha' - \left(\frac{1}{3}\left(\frac{1}{\Omega}\right)^2 + \left(\frac{1}{\Omega}\right) + 1\right)\right\} + \xi\right]$$

$$M = \frac{\sqrt{D_A K C_{BL}}}{K_L^\circ}$$

$$M_m = \frac{\sqrt{D_A K C_{BL}}}{K_L}\left(\frac{1+\Omega}{\Omega}\right)$$

$$\alpha' = \frac{\varepsilon_L K^{\circ}_L}{\underline{a} D_A}\left(\frac{\Omega}{1+\Omega}\right)$$

$$\xi = \frac{\varepsilon_l \Omega}{K^{\circ}_L \underline{a} \tau_L (1+\Omega)}$$

$$\Omega = \frac{K^{\circ}_L R - D_A}{D_A}$$

$$b_i = \frac{E_i - E^{*}_A - a_l}{E_i - 1} \tag{3.21b}$$

$$a_l = \frac{\Omega M_m \sqrt{b_i}}{M_m \sqrt{b_i}\cosh\left(M_m \sqrt{b_i}\right)(\Omega+1) + \{M_1(\Omega+1) - 1\}\sinh\left(M_m \sqrt{b_i}\right)} \tag{3.21c}$$

The second expression has been developed by Teramoto et al. [13] and is based on mass transfer through a plane surface. Note that in the limit our expression for E^{*}_A also reduces to the Teramoto's expression as will be shown in Chapter 4. This expression is given by Equations (3.22a-c):

$$E^{*}_A = M\sqrt{b_i}\left[\frac{M\sqrt{b_i}\tanh\left(M\sqrt{b_i}\right) + M_1}{M\sqrt{b_i} + M_1 \tanh\left(M\sqrt{b_i}\right)}\right] \tag{3.22a}$$

where

$$M_1 = M^2(\alpha' - 1) + \xi$$

$$M = \frac{\sqrt{D_A K C_{BL}}}{K^{\circ}_L}$$

$$\alpha' = \frac{\varepsilon_L K^{\circ}_L}{\underline{a} D_A}$$

$$\xi = \frac{\varepsilon_L}{K^{\circ}_L \underline{a} \tau_L}$$

$$b_i = \frac{E_i - E^*_A - a_I}{E_i - 1} \tag{3.22b}$$

$$a_I = \frac{M\sqrt{b_i}}{M\sqrt{b_i}\cosh(M\sqrt{b_i}) + M_1\sinh(M\sqrt{b_i})} \tag{3.22c}$$

3.6 Correlations for Heat Transfer Coefficients

3.6.1 Tank-Side Heat Transfer Coefficient

Jacket

Most of the correlations for tank-side heat transfer coefficients in jacketed CSTRs, with the exception of Kurpiers et al. [114], are entirely empirical and have been obtained using mostly laboratory scale data. For our model we have selected the correlation proposed by Kurpier et al. [114], because this correlation has been developed using semi-empirical approach and has also been verified experimentally for a wide range reactor sizes and operating conditions:

$$N_{uT} = K'\{\xi'(\frac{D_T}{D_I})(\frac{D_T^3}{V_L})N_e R^3_{en} + G_a R_{eG}[1 - 2(\frac{D_I}{D_T})(\frac{D_I}{H_o - e})N_e^{0.5}F_{rn}]\}^{0.25} P_{rL}^{0.4}(\frac{\mu_b}{\mu_w})_L^{0.23} \tag{3.23}$$

where

$$K' = 0.1, \quad \xi' = 0.2 \text{ for } \frac{D_T}{D_I} = 3 \text{ and } \xi' = 0.37 \text{ for } \frac{D_T}{D_I} = 1.93$$

$$N_{uT} = \frac{h_T D_T}{\lambda_L}, \; G_a = \frac{D_T^3 g}{\nu^2}, \; R_{en} = \frac{ND_I^2}{\nu}, \; N_e = \frac{P_o}{\rho_l N^3 D_I^5}, \; R_{eG} = \frac{V_{sg} D_T}{\nu}, \; F_{rn} = \frac{N^2 D_I}{g}$$

Internal Coils

To calculate tank-side heat transfer coefficient for internal coils correlation proposed by Rao and Murthy [107] has been selected. This correlation covers a wide range of reactor sizes and operating variables and agrees well with the experimental results of many other authors [110,111]:

$$N_{uT} = 0.87(\mathrm{Re}^{*})^{0.64}(P_{rL})^{0.33}\left(\frac{\mu_b}{\mu_w}\right)^{0.14}(F_{rn})^{-0.1} \tag{3.24}$$

where

$$N_{uT} = \frac{h_T D_T}{\lambda_L} \quad R_e^{*} = \frac{D_I}{\mu}(D_I N + 4\,V_{sg})\rho_l \quad F_{rn} = \frac{N^2 D_I}{g}$$

3.6.2 Jacket or Coil Side Heat Transfer Coefficient

Jacket

Many correlations to calculate the jacket-side heat transfer coefficient are given in the literature. However, except two [118,120], most of these correlations are based on the equations for straight pipes, where the diameter of the straight pipe is replaced by an equivalent jacket diameter as discussed in Chapter 2. For our model we have selected Lehrer's [118] correlation, because this correlation has been developed based on experimental data obtained in an actual jacketed reactor. Moreover, Lehrer's correlation was able to successfully reproduce the experimental results of Stein and Schmidt [120].

$$h_j = \frac{\lambda_c}{D_g}\left[\frac{0.03R_{ec}^{0.75}P_{rc}}{1 + \dfrac{1.74(P_{rc} - 1)}{R_{ec}^{0.25}}}\right]\left(\frac{\mu_c}{\mu_{c_w}}\right)^{0.14} \tag{3.25}$$

where

$$V_{in} = \frac{Q_c}{\frac{\pi}{4}D_{cp}^2} \qquad V_x = \frac{Q_c}{A_{lm}B_{lm}}$$

$$V_A = \left[gA_{lm}\left(-\frac{1}{\rho_c}\frac{d\rho_c}{dT} \right) \frac{T_{co} - T_{ci}}{2} \right]^{1/2}$$

$$V_c = (V_x V_{in})^{0.5} + V_A, \qquad R_{ec} = \frac{\Gamma_c D_g \rho_c}{\mu_c}, \qquad D_g = (\frac{8}{3})^{1/2} B_{lm}$$

Internal Coils

The correlation proposed by Bondy and Lippa [36] has been selected. Note that for cooling coils this is the only correlation available in th literature.

$$h_{ci} = \frac{0.027\lambda_c}{d_{ci}} R_{ec}^{0.8} P_{rc}^{0.33} (\frac{\mu_c}{\mu_{cw}})^{0.14} (1 + 3.5\frac{d_{ci}}{D_c}) \tag{3.26}$$

Where

$$R_{ec} = \frac{d_{ci} V_c \rho_c}{\mu_c}$$

3.6.3 Overall Heat Transfer Coefficient

Jacket

The overall heat transfer coefficient for a jacketed agitated tank reactor has been calculated from the following relationship:

$$\frac{1}{U_i} = \frac{1}{h_T} + f_T + \frac{A_i J_{th}}{A_O \lambda_m} + f_j + \frac{A_i}{A_c h_j} \tag{3.27}$$

where U_i is the overall heat transfer coefficient based on the inside heat transfer surface area.

Internal Coils

For internal coils following relationship has been used to compute overall heat transfer coefficient:

$$\frac{1}{U_O} = \frac{1}{h_T} + f_T + \frac{T_{th} d_{co}}{\lambda_m d_{cm}} + f_c + \frac{d_{co}}{d_{ci} h_{ci}} \tag{3.28}$$

where U_o is an over-all heat transfer coefficient based on outer coil surface.

3.7 Correlations for Mass Transfer Coefficients

3.7.1 Liquid-Side Mass Transfer Coefficient

Literature offers many correlations for evaluating liquid-side mass transfer coefficient. Most of these correlations, however, are given in the form of $K_L^o a$. For K_L^o alone there are only three correlations: Calderbank and Moo-Young [70], Barona [69], and Prasher and Wills [92]. The major drawback of the Calderbank and Moo-Young correlation is that it depends on the gas bubble diameter and does not give satisfactory values of K_L^o when $d_b \approx 2.5mm$. Barona's correlation was obtained by statistical analysis of literature data and has been recommended to be used for industrial scale reactors. Therefore, for our model we have selected the correlation proposed by Prasher and Wills [92]. This correlation, given below, was developed based on experimental data on a

laboratory scale reactor with standard configuration and has been shown to give satisfactory values of K_L^o over a wide range of operating conditions:

$$K_L^o = 0.592(D_A)^{1.2}\left(\frac{P_G}{V_L\mu_l}\right)^{0.25} \tag{3.29}$$

3.7.2 Gas-Side Mass Transfer Coefficient

For calculating gas-side mass transfer coefficient correlation proposed by Newman [104] has been selected. The only other correlation available in the literature is by Mashalkar and Sharma [106], which also in the limit reduces to Newman's correlation:

$$K_G^o = 6.58\frac{D_A}{d_b RT}\left(\frac{P_T}{p_i}\right) \tag{3.30}$$

3.8 Correlations for Hydrodynamic Parameters

3.8.1 Gas Hold-Up, Interfacial Area and Bubble Diameter

The most widely referred to correlations for estimating gas hold-up, interfacial area and the bubble diameter are those proposed by Miller [79]. These correlations reportedly give satisfactory predictions of the above parameters over a wide range of operating conditions. This is because of the fact that these correlations have been developed based on experimental data taken over three different size vessels and a wide variety of gas-liquid systems. Another important advantage in using these correlations is that they have been developed using the same experimental apparatus.

Gas Hold-Up

$$\varepsilon_G = \left[\frac{V_{sg}\varepsilon_G}{V_G + V_T}\right]^{0.5} + 2.16\times10^{-4}\left[\frac{(\frac{P_{GT}}{V_L})^{0.4}\rho_l^{0.2}}{\sigma^{0.6}}\right]\left[\frac{V_{sg}}{V_{sg} + V_T}\right]^{0.5} \tag{3.31}$$

Interfacial Area

$$\underline{a} = 1.44\left[\frac{(\frac{P_{GT}}{V_L})^{0.4}\rho_l^{0.2}}{\sigma^{0.6}}\right]\left[\frac{V_{sg}}{V_{sg} + V_T}\right]^{0.5} \tag{3.32}$$

Bubble Diameter

$$d_b = 4.15\left[\frac{\sigma^{0.6}}{(\frac{P_{GT}}{V_L})^{0.4}\rho_l^{0.2}}\right]\varepsilon_G^{0.5} + 0.0009 \tag{3.33}$$

3.8.2 Bubble Rise Velocity

For calculating the terminal velocity of rising gas bubble, correlation proposed by Abu El-Hassan [81] has been selected. The important characteristic of this correlation is that, unlike other correlations, it is independent of bubble flow regimes. This correlation has also been shown to accurately represent various published data for bubble rise velocity in stirred tank reactors.

$$V_N = 0.75(\log(F_N))^2 \tag{3.34}$$

where,

$$F_N = \left[\left(\frac{g d_b^{8/3}(\rho_l - \rho_g)\rho_l^{2/3}}{\mu_l^{4/3}\sigma^{1/3}}\right)\right]$$

$$V_N = \left[\left(\frac{V_T d_b^{2/3} \rho_l 2/3}{\mu_l^{1/3} \sigma^{1/3}}\right)\right]$$

3.9 Correlations for Power Input

The estimation of power input to the system is needed because of two reasons. Firstly, we need the total power input to evaluate the heat dissipated by the moving impeller and the sparged gas and secondly, most of the correlations for hydrodynamic and transport parameters are based on this parameter.

3.9.1 Power Input Due to Mechanical Agitation

There are many published correlations to predict power input by mechanical agitation. Most of these correlations, however, have been developed entirely on an empirical approach. Recently, after the pioneering work of Van-Riet and Smith [46], Nienow [47] and Bruijn et al [50] a better understanding of the mechanism of gas-dispersion in gas-liquid CSTRs has emerged, as a result few correlations which take into account the prevailing gas dispersion regime have been proposed. A widely recommended correlation of this nature is by Warmoeskerken and Smith [63]. These authors have proposed a set of correlations covering all the possible gas dispersion regimes and have experimentally verified them using a 0.44 m diameter vessel at different impeller speeds and gas feed rates. Another important characteristic of these correlations is that they are also applicable at $F_G = 0$. Thus, we have selected Warmoeskerken and Smith [63] correlations for our reactor modeling and simulation study. The correlations are given as follows:

For vortex and clinging cavities ($0 < N_A < (N_A)_{3\text{-}3}$):

$$\frac{P_G}{P_o} = 1 - 16.7(N_A)(F_{rn})^{0.35} \tag{3.35}$$

For small 3-3 cavities ($(N_A)_{3\text{-}3} < N_A < 0.1$):

$$\frac{P_G}{P_o} = B - 0.1\frac{A - B}{(N_A)_{3\text{-}3} - 0.1} + \frac{(A - B)(N_A)}{(N_A)_{3\text{-}3} - 0.1} \tag{3.36}$$

For large 3-3 cavities ($0.1 < N_A < (N_A)_F$):

$$\frac{P_G}{P_o} = 0.27 - 0.022(F_{rn})^{-1} \tag{3.37}$$

where

$$N_A = \frac{F_G}{ND_I^3}$$

$$(N_A)_{3\text{-}3} = 3.8 \times 10^{-3}\left(\frac{R_{en}^2}{F_{rn}}\right)^{0.07}\left(\frac{D_T}{D_I}\right)^{0.5}$$

$$(N_A)_F = 30\left(\frac{D_I}{D_T}\right)^{3.5}\left(F_{rn}\right)_F$$

$$A = 1 - 0.27(N_A)_{3\text{-}3}(F_{rn})^{0.35}$$

$$B = 0.27 + 0.022(F_{rn})^{-1}$$

The power consumption in the absence of gas (P_o) is calculated by the following equation:

$$P_o = N_P \rho_l N^3 D^5 \tag{3.38}$$

The Power number, N_p, can be calculated from impeller dimensions by using the

equation proposed by Calderbank and Moo-Young [70].

$$N_P = \frac{160 L_b W (D_I - L_b)}{D_I^3} \tag{3.39}$$

3.9.2 Power Input Due to Aeration

Power input due to aeration is obtained from the following relation [79]:

$$\frac{P_{sG}}{V_L} = \frac{F_G \rho_L}{V_L}\left[\frac{\eta V_c^2}{2} + \frac{RT}{Mw}\ln\left(\frac{P_{in}}{P}\right)\right] \tag{3.40}$$

In the above equation, the first term in bracket represents jet energy developed at sparger holes and transmitted to the bulk liquid. The second term is the energy required to move the gas through the static liquid head above the sparger. For a well designed sparger, the first term is often small and can be neglected [79]. Miller [79], however, used $\eta = 0.06$.

3.9.3 Total Power Input

According to Miller [79], although the two power inputs, P_G and P_{air}, can be predicted as a separate effect, their combination is not simply additive. The total power input is estimated by the following relation.

$$P_{GT} = P_G + C_1 P_{sG} \tag{3.41}$$

The constant C_1 in Equation (3.41) depends on sparger geometry, the size of the vessel and the bubble flow regime. For sparger-orifice diameter between 1.6 and 6.4 mm and tank volume between 2.5×10^{-3} and $0.25 m^3$, the constant C_1 can be calculated from the following relation [79]:

$$C_1 = V_L^{0.15}\left(1 - 1.4 D_o^{0.076}\right) \tag{3.42}$$

3.10 Correlation for Minimum Effective Impeller Speed

In order to create sufficient interfacial area and gas hold-up in a gas-liquid CSTR it is essential that the impeller speed should be such that the gas is fully dispersed and the condition of impeller flooding is avoided. Many correlations to predict minimum impeller speed to achieve complete gas dispersion have been proposed in the literature, a comprehensive review of these correlations is given in Chapter 2. For our model we have selected the correlation proposed by Nienow [54]. This is because Nienow's correlation, given below, is the most recent and has been shown to represent experimental data taken over a wide range of reactor sizes:

$$N_F = 0.322\left(\frac{gF_G}{D_I^4}\right)^{1/3}\left(\frac{D_T}{D_I}\right)^{3.5/3} \tag{3.43}$$

CHAPTER 4

REACTION FACTOR EXPRESSION

4.1 Introduction

Gas-liquid mass transfer in the presence of chemical reaction is an important area of Chemical Engineering. This is evident from the vast literature already available in this subject. Almost all published work in this area up to 1970 has been thoroughly reviewed by Dankwerts [121]. Other notable reviews in this field are those of Doraiswamy and Sharma [1] and Juvekar and Sharma [122]. Alper [123] has also given some useful research papers on gas-liquid mass transfer accompanied with chemical reaction.

In order to analyze the performance of gas-liquid reactors, it is essential to know the effect of chemical reaction on the the rate of gas absorption. When physical absorption of gas into a liquid is accompanied by simultaneous reaction in the liquid phase, an enhancement in the absorption rate occurs [124]. The enhancement in the rate of mass transfer is due to the fact that the chemical reaction causes the concentration gradient to steepen. The effect of chemical reaction on the rate of absorption is normally expressed in terms of reaction factor, $E_A^{\bullet}$, defined as the ratio of rate of absorption in presence of chemical

reaction to maximum rate of pure physical absorption. E_A^* plays an important role in the design and analysis of the performance of gas-liquid reactors, as we demonstrated in Chapter 3.

In order to investigate the influence of chemical reaction on the extent of gas absorption, it is necessary to know the concentration profile in the close vicinity of the gas-liquid interface. Several theories have been proposed to describe the condition in the close vicinity of the interface in case of physical absorption. Some of these important theories are two-film theory, penetration theory and surface renewal theory [121,124]. These theories have been applied in the case of mass transfer in the presence of chemical reaction also. However, the investigations were restricted to a plane surface (one dimensional case) only.

When the size of the gas bubble is of the same order of magnitude or smaller than the concentration boundary layer surrounding the bubble, then the mass transfer in such a case can not be considered the same as the mass-transfer through a plane surface. The so-called spherical effect increases with decreasing size of the bubble due to component diffusion in spherical space around the bubble [125]. This effect is shown schematically in Figure 4.1. Here, the concentration distribution in the boundary layer is not linear even in case of physical absorption. The concentration deformation increases with decreasing bubble size. Therefore, the mass transfer rate increases [125].

The mass transfer between a sphere and fluid accompanied by chemical reaction has been investigated by many authors [126,127] by means of boundary

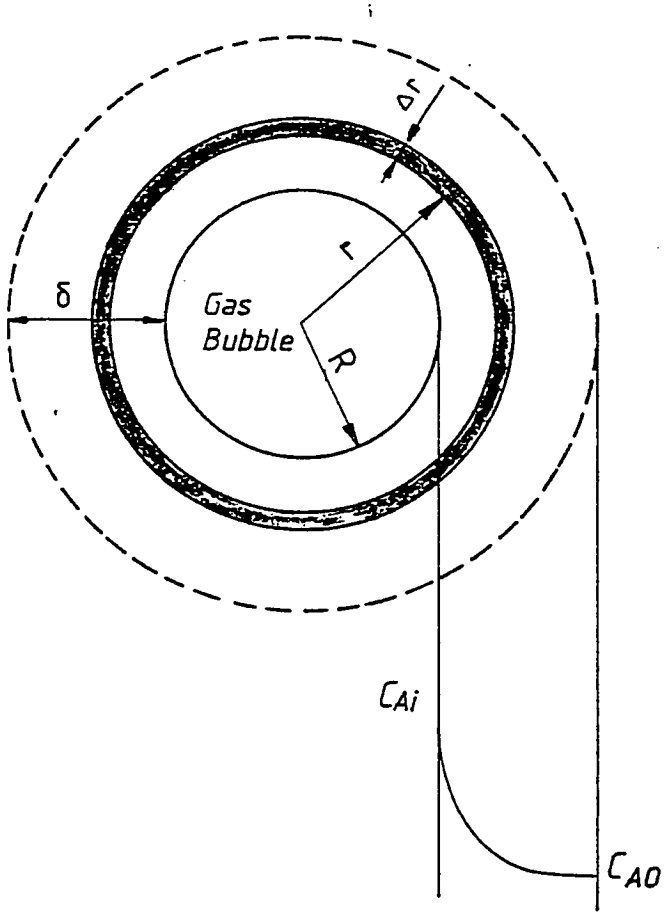

Figure 4.1 Concentration Profile for Physical Mass Transfer Through a Spherical Surface.

layer theory in the laminar flow regime. In all of these cases, the thickness of boundary layer was considered practically infinite. The effect of second order chemical reaction on the mass transfer was studied by Johnson and Akeheta [128] in stagnant liquid i.e. in the case of infinite thickness of boundary layer. Recently, Nagy et al. [125] studied the mass transfer through a spherical surface in presence of chemical reaction and concluded that the spherical effect, which increases with decreasing bubble size, diminishes the effect of chemical reaction on the mass transfer rate. The analysis of these authors, however, is incorrect, as they did not account for the spherical effect while evaluating the thickness of the concentration boundary layer. Thus, their results are questionable with regard to the effect of sphericity on mass transfer accompanied with chemical reaction.

The purpose of this Chapter is to develop an analytical expression for E_A^* to be used with the model equations developed in Chapter 3. The new expression for E_A^* will be based on the mass transfer through a stagnant liquid film surrounding a spherical gas bubble in which the following generic gas-liquid reaction is taking place:

$$A_{gas\text{-}liq} + \nu B_{liq} \rightarrow P_{liq} \tag{4.1}$$

where, A is a gaseous reactant and B is a nonvolatile liquid phase reactant which reacts with the dissolved A in the liquid film as well as in the liquid bulk. The kinetic rate expression for this reaction is assumed to be represented as follows:

$$(-r_A) = K C_A C_B \tag{4.2}$$

It is also assumed that the concentration of the gaseous reactant at the gas-liquid interface, C_{Ai}, is constant during the process. Therefore the only resistance to mass transfer is in the liquid film.

4.2 Model Development

4.2.1 Dimensional Form of Film Theory Model Equations

Mass balances around a differential element of fluid, of thickness Δr, located in the liquid film, of thickness δ, surrounding a spherical gas bubble, of radius R, as shown in Figure 4.1, yield the following equations:

Mass balance for reactant A:

$$D_A\left[\frac{d^2C_A}{dr^2} + \frac{2}{r}\frac{dC_A}{dr}\right] = KC_AC_B \tag{4.3}$$

Mass balance for reactant B:

$$D_B\left[\frac{d^2C_B}{dr^2} + \frac{2}{r}\frac{dC_B}{dr}\right] = \nu KC_AC_B \tag{4.4}$$

Boundary Conditions:

$r = R, \quad C_A = C_{Ai} \quad \text{and} \quad \frac{dC_B}{dr} = 0$

$r = R + \delta, \quad C_B = C_{BL}$

and

$$-D_A n4\pi(R + \delta)^2\frac{dC_A}{dr} = KC_AC_B\left[V_L - n\frac{4}{3}\pi\{(R + \delta)^3 - R^3\}\right] + F_lC_A$$

where n is the number of gas bubbles in the reactor.

4.2.2 Dimensionless Form of Model Equations

In order to make Equations (4.3) and (4.4) dimensionless, the following dimensionless variables are introduced:

$$a = \frac{C_A}{C_{Ai}}, \qquad b = \frac{C_B}{C_{BL}}$$

$$x = \frac{r - R}{\delta}, \qquad \gamma = \frac{D_B}{\nu D_A}, \qquad q' = \frac{C_{BL}}{C_{Ai}}$$

Substituting the above dimensionless quantities in Equation (4.3), we get:

$$\frac{d^2a}{dx^2} + \frac{2}{(x + R/\delta)}\frac{da}{dx} = \frac{\delta^2 K C_{Bl} ab}{D_A} \tag{4.5}$$

The term δ in Equation (4.5) is not known and is obtained by making a mass balance around a differential element of thickness Δr located in the spherical liquid film of thickness δ, surrounding a gas bubble of radius R, in the absence of chemical reaction in a manner similar to that used in conventional plane surface case. The governing equation in such a case is:

$$D_A\left[\frac{d^2C_A}{dr^2} + \frac{2}{r}\frac{dC_A}{dr}\right] = 0 \tag{4.6a}$$

Above equation can also be written in the following form:

$$\frac{d}{dr}\left(r^2\frac{dC_A}{dr}\right) = 0 \tag{4.6b}$$

Boundary Conditions:

$r = R, \quad C_A = C_{Ai}$

$r = R + \delta, \quad C_A = C_{AL}$

Integrating Equation (4.6b) twice and applying the boundary conditions, we get:

$$C_A = \frac{R(R + \delta)(C_{Ai} - C_{AL})}{r\delta} + C_{Ai} - \frac{(R + \delta)(C_{Ai} - C_{AL})}{\delta} \tag{4.7}$$

The rate of physical absorption is calculated from the flux at the interface, or:

$$N_A^\circ = K_L^\circ(C_{Ai} - C_{AL}) = -D_A \frac{dC_A}{dr}\bigg|_{r=R}$$

Evaluating $\frac{dC_A}{dr}\Big|_{r=R}$ from Equation (4.7) and substituting in the above equation, we get:

$$K_L^\circ(C_{Ai} - C_{AL}) = \frac{D_A(R + \delta)(C_{Ai} - C_{AL})}{\delta R}$$

Solving for the film thickness, we get:

$$\delta = \frac{D_A R}{(K_{L_o} R - D_A)} \tag{4.8}$$

To make Equation (4.8) dimensionless, following dimensionless variable is introduced:

$$\Omega = \frac{R}{\delta}$$

Substituting Ω in Equation (4.8), we get:

$$\Omega = \frac{K_L^\circ R - D_A}{D_A} \quad or \quad \frac{\Omega}{(1 + \Omega)} = \left[1 - \frac{D_A}{K_L^\circ R}\right] \tag{4.9}$$

Substituting for δ and $\frac{R}{\delta}$ in Equation (4.5), we get:

$$\frac{d^2a}{dx^2} + \frac{2}{(x + \Omega)}\frac{da}{dx} = M^2{}_m ab \tag{4.10}$$

Similarly, substitution of dimensionless quantities in Equation (4.4) yields:

$$\frac{d^2b}{dx^2} + \frac{2}{(x + \Omega)}\frac{db}{dx} = \frac{M^2{}_m ab}{\gamma q'} \tag{4.11}$$

where M_m is a dimensionless quantity which is defined as follows:

$$M_m = \frac{\sqrt{D_A K C_{BL}}}{K_L^o}\left(\frac{1 + \Omega}{\Omega}\right) = M\left(\frac{1 + \Omega}{\Omega}\right) \tag{4.12}$$

The dimensionless quantity M_m can be called as modified Hatta number.

Dimensionless form of Boundary Conditions:

$x = 0.$ $\quad a = 1 \quad \frac{db}{dx} = 0$

$x = 1,$ $\quad -\frac{da}{dx} = M_1 a \quad b = 1$

where

$$M_1 = \left[M^2\left\{\alpha' - \left(\frac{1}{3}\left(\frac{1}{\Omega}\right)^2 + \left(\frac{1}{\Omega}\right) + 1\right)\right\} + \xi\right]$$

$$M = \frac{\sqrt{D_A K C_{BL}}}{K_L^o}$$

$$\alpha' = \frac{\varepsilon_L K_L^o}{a D_A}\left(\frac{\Omega}{1 + \Omega}\right)$$

$$\xi = \frac{\varepsilon_L \Omega}{K_L^o a \tau_L (1 + \Omega)}$$

4.3 Approximate Analytical Solution of Model Equations

Equations (4.10) and (4.11) are coupled non-linear ordinary differential equations, thus exact analytical solution is not possible. Approximate analytical solution for the simpler case of slab geometry has been obtained by van Krevelen and Hoftizer [12]. For our case we will use the approximation approach of van Krevelen and Hoftizer [12] to obtain an approximate analytical solution of Equations (4.10) and (4.11). It is assumed that the concentration of liquid phase reactant B at the gas liquid interface is constant. Let this constant concentration be denoted as C_{Bi} and let $b_i = \frac{C_{Bi}}{C_{BL}}$. Thus, Equation (4.10) becomes:

$$\frac{d^2a}{dx^2} + \frac{2}{x + \Omega}\frac{da}{dx} = M^2{}_m a b_i$$

Since b_i is constant it can be combined with M_m to give:

$$\frac{d^2a}{dx^2} + \frac{2}{x + \Omega}\frac{da}{dx} = M_m{}'^2 a \tag{4.13}$$

where

$$M_m{}' = M_m\sqrt{b_i}$$

Equation (4.13) can now be solved for dimensionless concentration of gaseous reactant, $a(x)$.

$$a(x) = \left[\frac{a_l\{1 - M_1(\Omega + 1)\} - \Omega M'_m Sinh(M'_m)}{M'_m Cosh(M'_m)}\right]\frac{Sinh(M'_m x)}{(\Omega + x)} + \Omega\left[\frac{Cosh(M'_m x)}{(\Omega + x)}\right] \tag{4.14}$$

The expression for dimensionless concentration of liquid reactant, $b(x)$ can be

obtained by combining Equations (4.10) and (4.11) and solving for $b(x)$.

$$b(x) = \frac{a}{\gamma q'} + 1 - \frac{\Omega(1 + \Omega)E^{*}_{A}}{\gamma q'(x + \Omega)} + \frac{\Omega E^{*}_{A}}{\gamma q'} - \frac{a_l}{\gamma q'} \tag{4.15}$$

4.4 New Reaction Factor Expression

The reaction factor, E^{*}_{A} is defined as:

$$E^{*}_{A} = \frac{Rate\ of\ absorption\ of\ A\ in\ presence\ of\ chemical\ reaction}{Maximum\ rate\ of\ pure\ physical\ absorption\ of\ A}$$

Substituting for the rates of gas absorption with and without chemical reaction in the above equation and rearranging, we get:

$$E^{*}_{A} = -\left(\frac{\Omega}{1 + \Omega}\right)\frac{da}{dx}\bigg|_{x=0} \tag{4.16}$$

Evaluating $\left.\frac{da}{dx}\right|_{x=0}$ by differentiating Equation (4.14) and substituting in Equation (4.16), we get:

$$E^{*}_{A} = \frac{M_m\sqrt{b_i}\Omega}{(1 + \Omega)}\left[\frac{M_m\sqrt{b_i}Tanh(M_m\sqrt{b_i})(1 + \Omega) + \{M_1(1 + \Omega) - 1\}}{M_m\sqrt{b_i}(1 + \Omega) + \{M_1(1 + \Omega) - 1\}Tanh(M_m\sqrt{b_i})}\right] + \frac{1}{1 + \Omega} \tag{4.17}$$

The parameter b_i in Equation (4.17) is obtained from Equation (4.15) by making following substitutions:

$x = 0 \qquad b = b_i \qquad a = 1$

$$b_i = \frac{E_i - E^{*}_{A} - a_l}{E_i - 1} \tag{4.18}$$

where a_l is the dimensionless concentration of gaseous reactant in the liquid

bulk. Substituting x = 1 in Equation (4.14) and making appropriate rearrangement, we get the following expression for a_l:

$$a_l = \frac{\Omega M_m \sqrt{b_i}}{M_m \sqrt{b_i} Cosh(M_m \sqrt{b_i})(\Omega + 1) + \{M_1(\Omega + 1) - 1\} Sinh(M_m \sqrt{b_i})} \tag{4.19}$$

In order to calculate E_A^*, Equations (4.17) to (4.19) are solved simultaneously. A detailed derivation of E_A^* is given in Appendix A2. Note that the new reaction factor expression reduces to the one developed by Teramoto et al. [13] for the case of slab geometry, discussed in section 3.5, as the term $1/\Omega$ approaches zero, i.e., as $\Omega \rightarrow \infty$.

4.5 Numerical Solution of Model Equations

4.5.1 Finite Difference Approximation

In order to obtain the numerical solution, we first combine Equations (4.10) and (4.11) by substituting for b from Equation (4.15).

$$\frac{d^2a}{dx^2} + \frac{2}{(x + \Omega)\frac{da}{dx}} = M_m^2 \left[\frac{\{a^2 - aa_l + a(E_i - 1)\}(x + \Omega) + \Omega(x - 1)E_A^* a}{(E_i -)(x + \Omega)} \right] \tag{4.20}$$

Boundary Conditions:

$$x = 0, \quad a = 1$$

$$x = 1, \quad -\frac{da}{dx} = M_1 a$$

The nonlinear Equation (4.20) is solved using finite difference method combined

with quasilincarization technique [129]. Applying this technique to Equation (4.20) we get the following form of matrix Equation (for details see Appendix A2.).

$$\overline{C}\,\overline{a}_{k+1} = \overline{X} \tag{4.21}$$

where

$$\overline{C} = \begin{bmatrix} V_1 & W_1 & & & & \\ U_2 & V_2 & W_2 & & & \\ & U_3 & V_3 & W_3 & & \\ & & & & & \\ & & & & U_{N-2} & V_{N-2} & W_{N-2} \\ & & & & & U_{N-1} & V_{N-1} \end{bmatrix}$$

$$\overline{a}_{k+1} = \begin{bmatrix} a_{k+1}(1) \\ a_{k+1}(2) \\ . \\ . \\ . \\ a_{k+1}(N\text{-}1) \end{bmatrix} \qquad \overline{X} = \begin{bmatrix} X_1 - U_1 \\ X_2 \\ . \\ . \\ . \\ X_{N-1} \end{bmatrix}$$

The definitions of variables U_j's, V_j's, W_j's, $\overline{a}$, $\overline{C}$ and $\overline{X}$ in the above equation are given in Appendix A2.

4.5.2 Numerical Procedure

In order to solve Equation (4.20) and to compare the accuracy of the approximate analytical expression for E_A^* given by Equation (4.17) to (4.19), a computer code named GLRXN has been written. The flow chart of the

computer code is shown in Figure 4.2. For the given values of various dimensionless parameters (E_i, α', ξ, M, Ω), a suitable step size and the initial guess values for $a_k(i)'s$ and E_A^* are selected. Next, the matrix Equation (4.21) is solved for $a_{k+1}(i)'s$ using Thomas algorithm. If the newly obtained values of $a_{k+1}(i)'s$ do not agree with the assumed values of $a_k(i)'s$ within a prescribed tolerance, they are taken as the new initial values and the procedure is repeated until the desired accuracy is achieved. The convergence has been found to be rapid for all the numerical examples presented in this work. After the convergence for a(x) is achieved, the reaction factor is calculated by using the following Taylor series approximation:

$$E_A^* = -\frac{\Omega}{1+\Omega}\frac{4a_{k+1}(1) - a_{k+1}(2) - 3a_{k+1}(0)}{2\Delta x} \tag{4.22}$$

The accuracy of the new analytical expression for E_A^* is checked by solving the Equations (4.17) to (4.19) for E_A^* using half interval method and comparing it with the one obtained by solving the model Equations (4.10) and (4.11) numerically.

4.6 Results and Discussion

4.6.1 Asymptotic Behavior of the New Reaction Factor Expression

We have developed a new approximate analytical expression for E_A^*, given by Equations (4.17), which is based on spherical bubble geometry and an approximation approach suggested by van-Krevelen and Hoftizer [12]. The

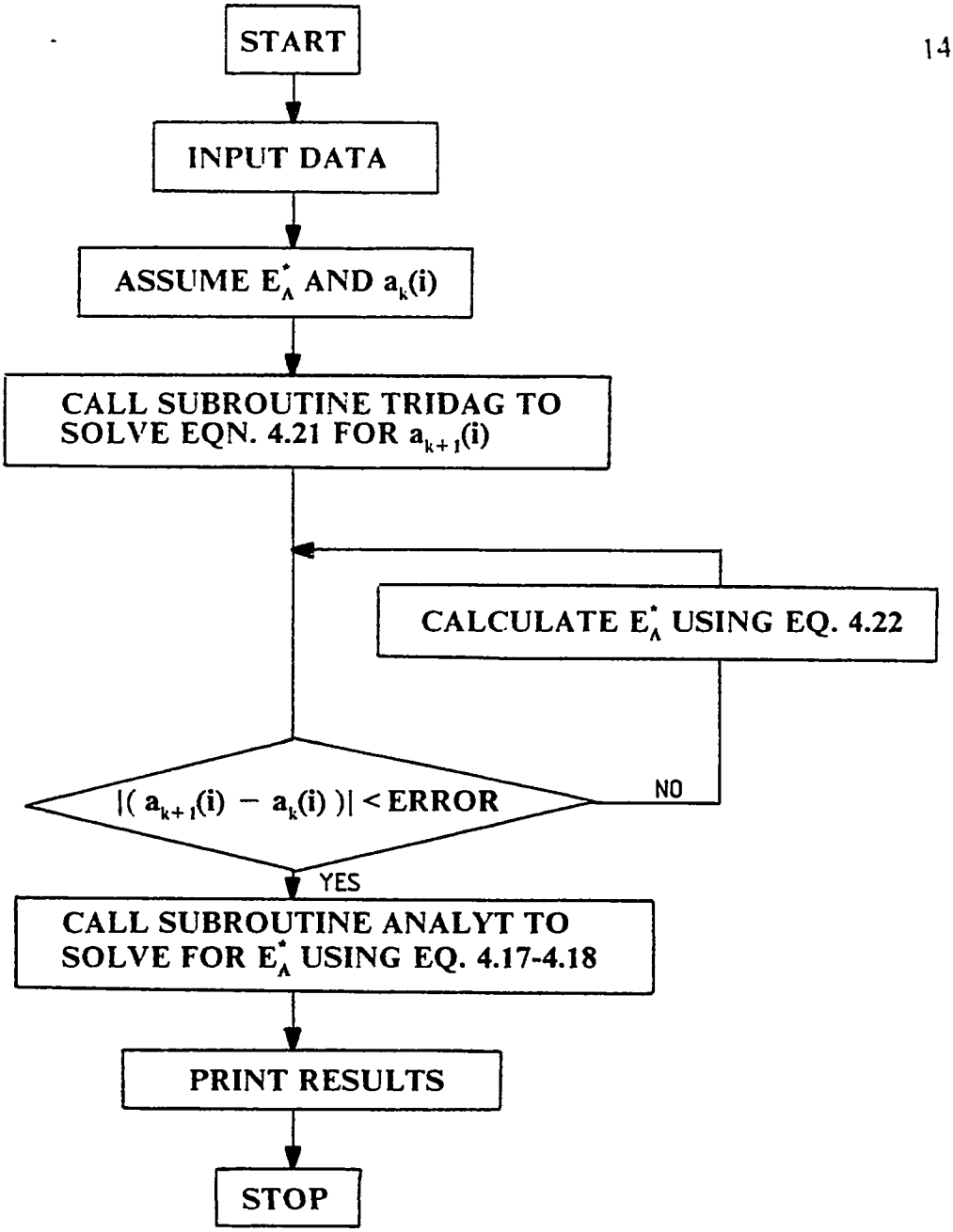

Figure 4.2 Flow Chart of the Computer Program GLRXN

asymptotic behavior of the new reaction factor expression is shown in Figure 4.3. It is clear from Figure 4.3 that the new expression is most general which in the limit reduces to the reaction factor expression developed by earlier researchers for the case of slab geometry. Note, by setting b_i equal to 1, the new expression will reduce to the reaction factor expression for first-order reaction based on spherical geometry.

4.6.2 Accuracy of the New Reaction Factor Expression

The accuracy of the new reaction factor expression has been checked by comparing its results with those obtained numerically. Table 4.1 presents a comparison of numerical and analytical values of E_A^* for a set of dimensionless parameters. It can be seen from Table 4.1 that the numerical and analytical results are in excellent agreement and in most cases the absolute percentage error is less than 2. We also note from Table 4.1 that the percentage error increases as the dimensionless number Ω decreases (or as the spherical effect increases).

Tables 4.2 to 4.4 present a comparison of analytical and numerical values of E_A^* for three different values of ξ. We note from these tables that in case of very slow reactions ($M \approx 0.01$), at relatively smaller values ξ, i.e., smaller liquid flow rates, the numerical and the analytical results differ widely. This is, possibly, because of numerical instability of the analytical expression at very low values of M, as it is highly nonlinear and involves hyperbolic functions.

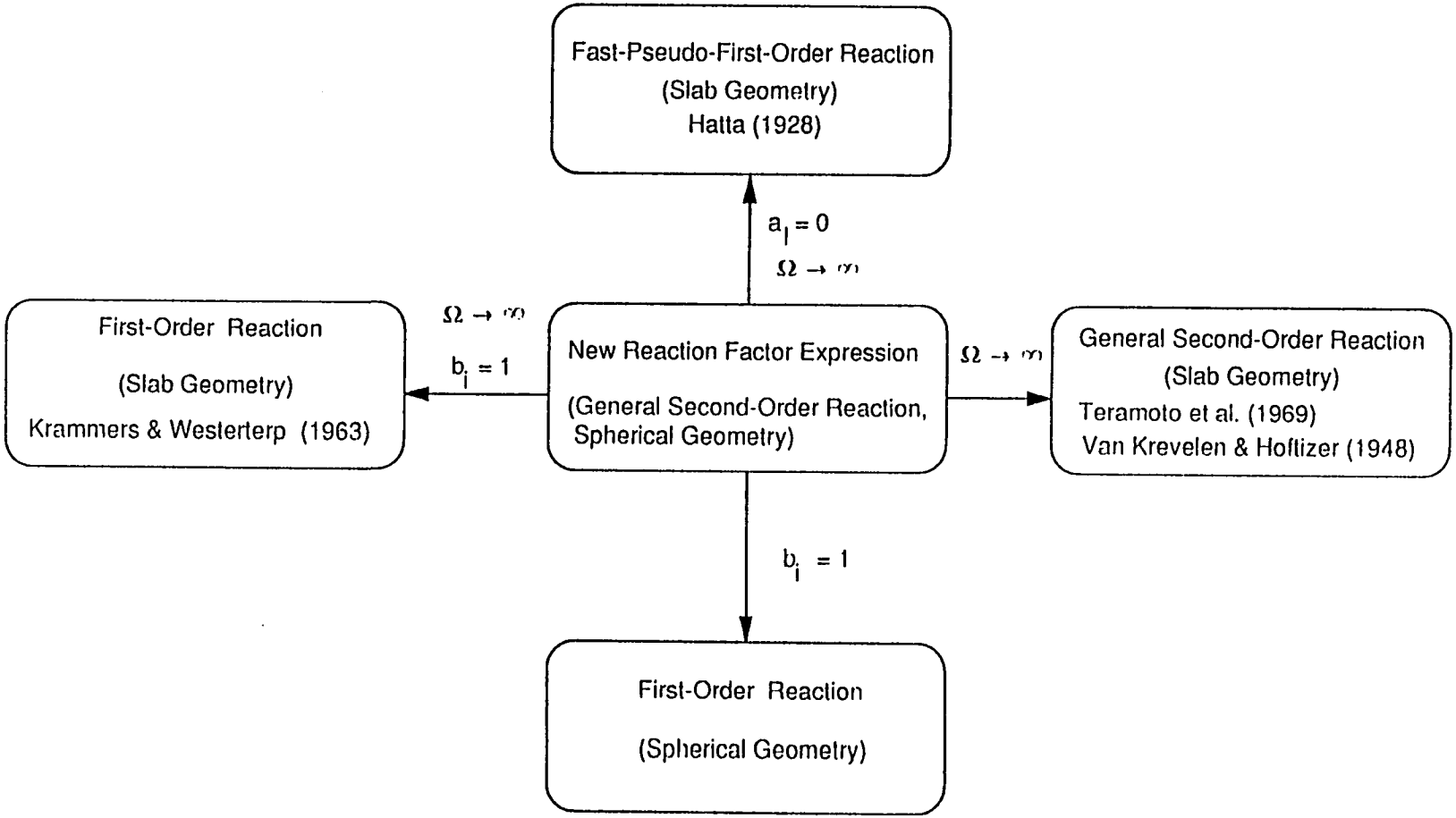

Figure 4.3 Asymptotic Behavior of the New Reaction Factor

Table 4.1 Comparison of Analytical and Numerical Values of Reaction Factor (Ei = 500, $\alpha' = 100$, $\xi = 5.0$)

M	E_A^* (Numerical)	E_A^* (Analytical)	% Error
$\Omega = 50$			
20.000	19.478	19.642	0.845
15.000	14.739	14.811	0.489
10.000	9.907	9.930	0.227
5.000	4.998	5.000	0.045
1.000	1.312	1.312	0.070
0.500	1.055	1.054	0.155
0.100	0.863	0.861	0.195
0.050	0.843	0.841	0.195
0.010	0.836	0.834	0.314
$\Omega = 1.0$			
20.000	19.432	20.113	3.508
15.000	14.945	15.284	2.269
10.000	10.271	10.405	1.304
5.000	5.441	5.478	0.670
1.000	1.527	1.534	0.453
0.500	1.128	1.133	0.420
0.100	0.862	0.865	0.373
0.050	0.839	0.842	0.406
0.010	0.831	0.834	0.359
$\Omega = 0.5$			
20.000	18.886	20.277	7.364
15.000	14.736	15.448	4.828
10.000	10.281	10.570	2.813
5.000	5.562	5.643	1.453
1.000	1.652	1.670	1.073
0.500	1.189	1.202	1.118
0.100	0.860	0.870	1.208
0.050	0.833	0.843	1.280
0.010	0.824	0.834	1.238

Table 4.2 Comparison of Analytical and Numerical Values of Reaction Factor (Ei = 50, $\alpha' = 200$, $\xi = 5.0$)

M	E_A^* (Numerical)	E_A^* (Analytical)	% Error
$\Omega = 50$			
20.000	16.494	16.545	0.312
15.000	13.026	13.046	0.157
10.000	9.149	9.150	0.013
5.000	4.827	4.821	0.125
1.000	1.314	1.313	0.085
0.500	1.067	1.067	0.044
0.100	0.880	0.879	0.183
0.050	0.849	0.847	0.192
0.010	0.837	0.834	0.309
$\Omega = 1.0$			
20.000	16.596	16.930	2.014
15.000	13.261	13.454	1.459
10.000	9.495	9.582	0.917
5.000	5.251	5.277	0.486
1.000	1.525	1.531	0.408
0.500	1.138	1.143	0.400
0.100	0.880	0.883	0.367
0.050	0.845	0.848	0.403
0.010	0.831	0.834	0.357
$\Omega = 0.5$			
20.000	16.331	17.064	4.486
15.000	13.160	13.596	3.310
10.000	9.526	9.732	2.159
5.000	5.369	5.435	1.222
1.000	1.648	1.665	1.013
0.500	1.196	1.209	1.085
0.100	0.877	0.888	1.252
0.050	0.839	0.850	1.274
0.010	0.824	0.834	1.237

Table 4.3 Comparison of Analytical and Numerical Values of Reaction Factor (Ei = 50, $\alpha' = 200$, $\xi = 0.1$)

M	E_A^* (Numerical)	E_A^* (Analytical)	% Error
$\Omega = 50$			
20.000	16.494	16.545	0.312
15.000	13.026	13.046	0.157
10.000	9.149	9.150	0.013
5.000	4.827	4.821	0.125
1.000	1.314	1.313	0.087
0.500	1.066	1.065	0.050
0.100	0.683	0.681	0.286
0.050	0.378	0.376	0.701
0.010	0.113	0.107	5.040
$\Omega = 1.0$			
20.000	16.596	16.930	2.014
15.000	13.261	13.454	1.459
10.000	9.495	9.582	0.917
5.000	5.251	5.277	0.486
1.000	1.525	1.531	0.408
0.500	1.137	1.142	0.402
0.100	0.684	0.686	0.388
0.050	0.376	0.377	0.198
0.010	0.112	0.107	4.311
$\Omega = 0.5$			
20.000	16.331	17.064	4.486
15.000	13.160	13.596	3.310
10.000	9.526	9.732	2.159
5.000	5.369	5.435	1.222
1.000	1.648	1.665	1.014
0.500	1.195	1.208	1.086
0.100	0.683	0.693	1.482
0.050	0.373	0.378	1.497
0.010	0.111	0.107	3.209

Table 4.4 Comparison of Analytical and Numerical Values of Reaction Factor (Ei = 50, $\alpha' = 200$, $\xi = 0.001$)

M	E_A^* (Numerical)	E_A^* (Analytical)	% Error
$\Omega = 50$			
20.000	16.494	16.545	0.312
15.000	13.026	13.046	0.157
10.000	9.149	9.150	0.013
5.000	4.827	4.821	0.125
1.000	1.314	1.313	0.087
0.500	1.066	1.065	0.042
0.100	0.673	0.671	0.293
0.050	0.337	0.334	0.811
0.010	0.027	0.021	23.141
$\Omega = 1.0$			
20.000	16.596	16.930	2.014
15.000	13.261	13.454	1.459
10.000	9.495	9.582	0.917
5.000	5.251	5.277	0.486
1.000	1.525	1.531	0.408
0.500	1.137	1.142	0.399
0.100	0.673	0.676	0.385
0.050	0.335	0.335	0.084
0.010	0.027	0.021	24.388
$\Omega = 0.5$			
20.000	16.331	17.064	4.486
15.000	13.160	13.596	3.310
10.000	9.526	9.732	2.159
5.000	5.369	5.435	1.222
1.000	1.648	1.665	1.014
0.500	1.195	1.208	1.088
0.100	0.672	0.682	1.494
0.050	0.332	0.337	1.391
0.010	0.028	0.021	25.217

4.6.3 Effect of Sphericity on the mass Transfer with Chemical Reaction

If the size of the gas bubble is comparable to the thickness of the concentration boundary layer around it, the mass transfer through a spherical bubble can no longer be considered same as the mass-transfer through a plane surface. The so-called spherical effect increases with decreasing size of the bubble due to component diffusion in spherical space around the bubble. In this section we will investigate the effect of sphericity on the mass transfer in presence of chemical reaction and will compare our results with those of previous investigators. All the results presented in this section are based on numerical solution of the film theory model equations.

Figures 4.4 and 4.5 show the effect of dimension less parameter Ω, which is a ratio of the bubble radius and the thickness of concentration boundary layer, on the concentration profile of gaseous and liquid reactants for two different sets of dimensionless parameters. It is clear from these figures that a decrease in Ω, i.e., an increase in spherical effect, causes the concentration gradient to steepen which in turn increases the mass transfer rate. Comparing Figures 4.4 and 4.5, we further note that the spherical effect is more pronounced in case of relatively fast reactions which is in contrast with the results reported by Nagy et al. [125] who concluded that with the increasing reaction rate, the influence of the spherical effect on the mass transfer decreases. This is because in their analysis Nagy et al. [125] did not account for the spherical effect while evaluating the thickness of the concentration boundary layer, δ, and therefore underestimated the mass transfer rate in presence of chemical reaction. Indeed,

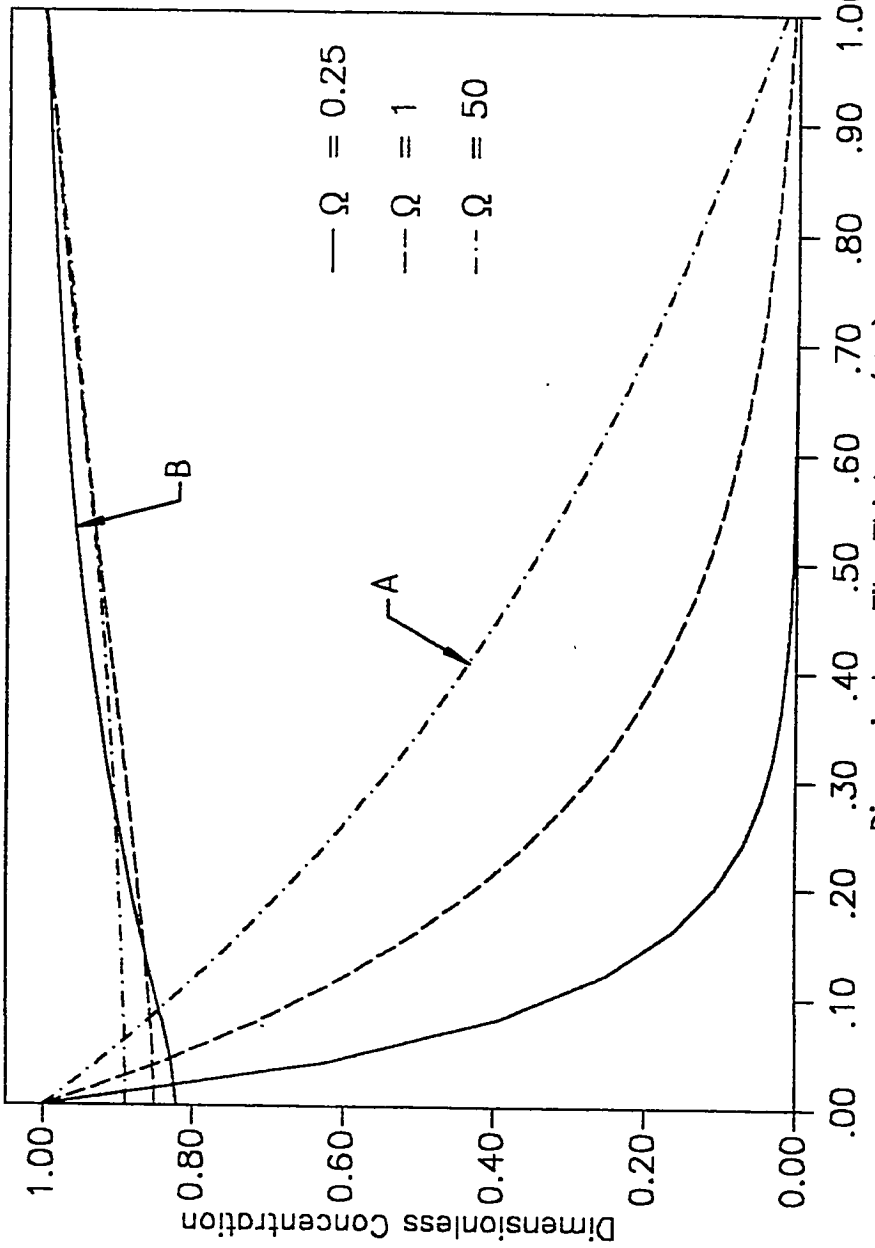

Figure 4.4 Effect of Sphericity on Concentration Profiles of Gaseous and Liquid Reactants
(Ei = 10.0, M = 2.0, α = 200, ξ = 0.001)

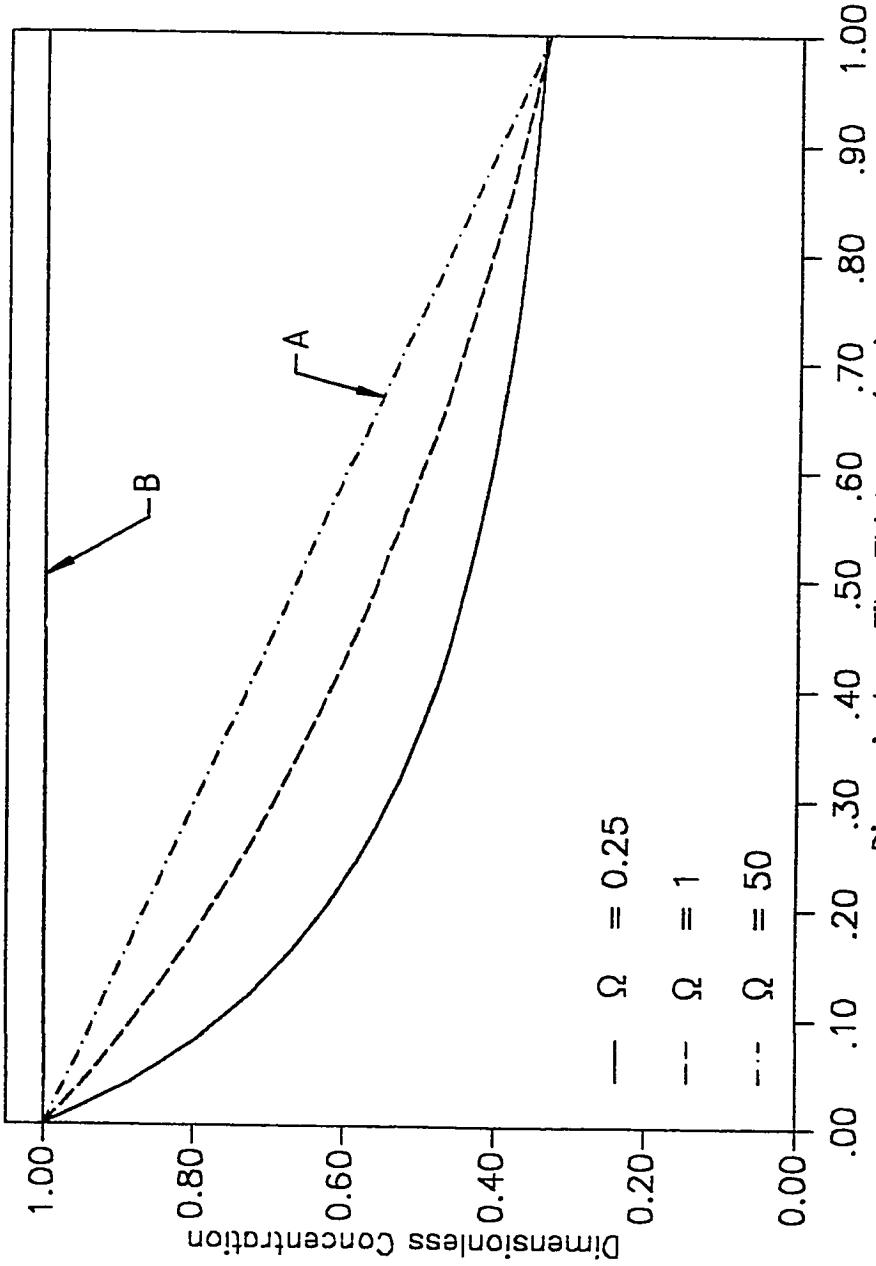

Figure 4.5 Effect of Sphericity on Concentration of Gaseous and Liquid Reactants
(Ei = 10, M = 0.1, α' = 200, ξ = 0.001)

there evaluation of δ is based on the conventional slab-geometry. Moreover, these investigators used arbitrary values of gaseous reactant in the liquid bulk and implicitly analysed the fast reaction regime. Note that in the fast reaction regime the reaction will be completed in the liquid film and there will be no gaseous reactant left in the liquid bulk as shown in Figure 4.4. Therefore in the fast reaction regime using an arbitrary value for a_l, as done by Nagy et al. [125], will lead to further underestimation of the rate of gas absorption.

The effect of sphericity on the reaction factor can be understood by analysing Equation (4.16). According to this equation as the bubble size decreases (i.e. as Ω decreases), E_A^* may increase or decrease depending on the relative magnitude of the terms $\Omega(\Omega + 1)$ and $\frac{da}{dx}\Big|_{x=0}$. Figures 4.6a-b present the effect of sphericity on the reaction factor for a given set of dimensionless parameters. Figure 4.6a shows E_A^* in the very slow reaction regime ($0.001 < M < 0.1$) and Figure 4.6b shows E_A^* in the relatively fast reaction regime ($0.1 < M < 20$). It can be seen from these figures that, depending on the reaction regime, a decrease in Ω (i.e. an increase in spherical effect) may increase or decrease the reaction factor. Here again our results are quite different from those of Nagy et al. [125] who reported that the reaction factor always decreases with the increase in the spherical effect. This difference is because they underestimated the rate of gas absorption in presence of chemical reaction due to the reason stated above. Figures 4.7a-b show the effect of sphericity on the reaction factor for a higher value of ξ. A comparison of

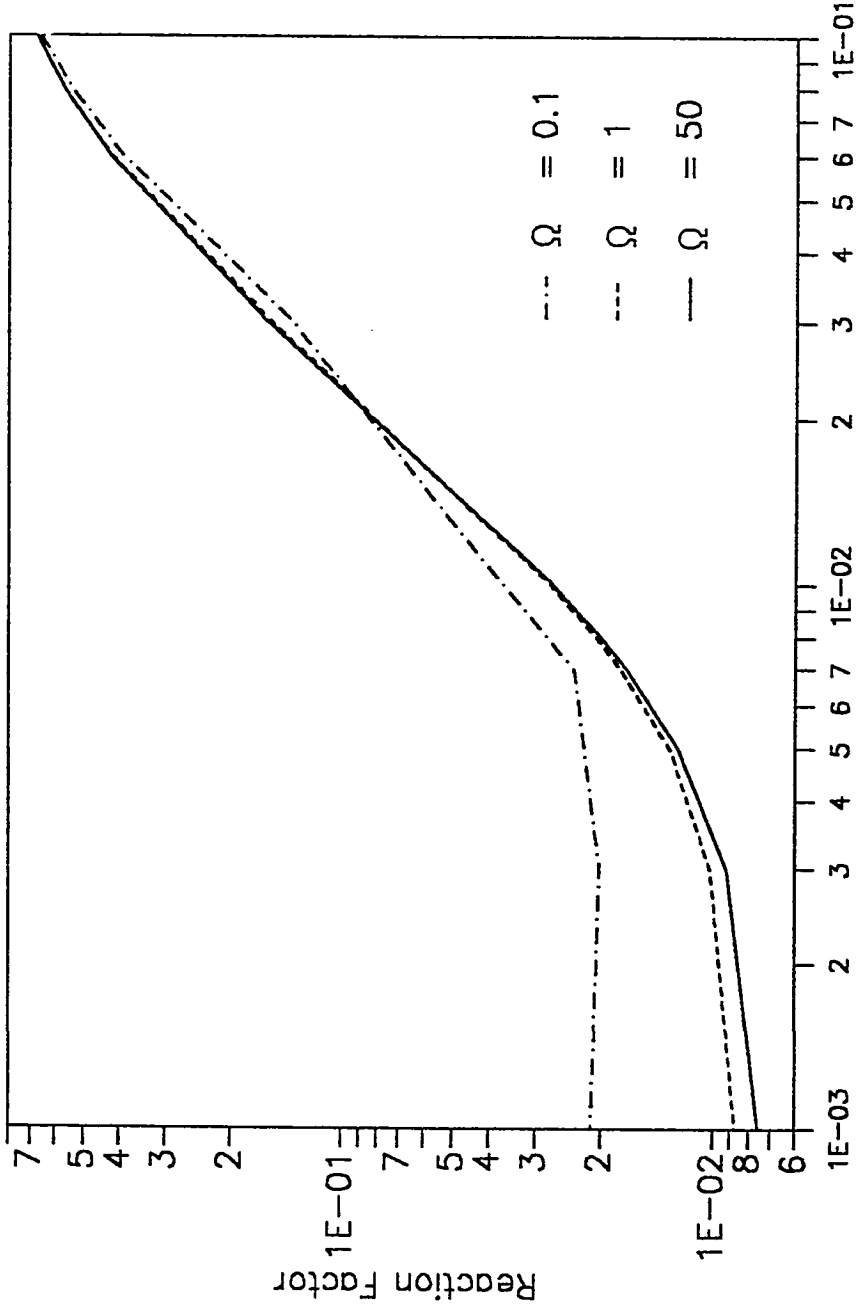

Figure 4.6a Effect of Sphericity on the Reaction Factor
(Ei 50, α' = 200, ξ = 0.001)

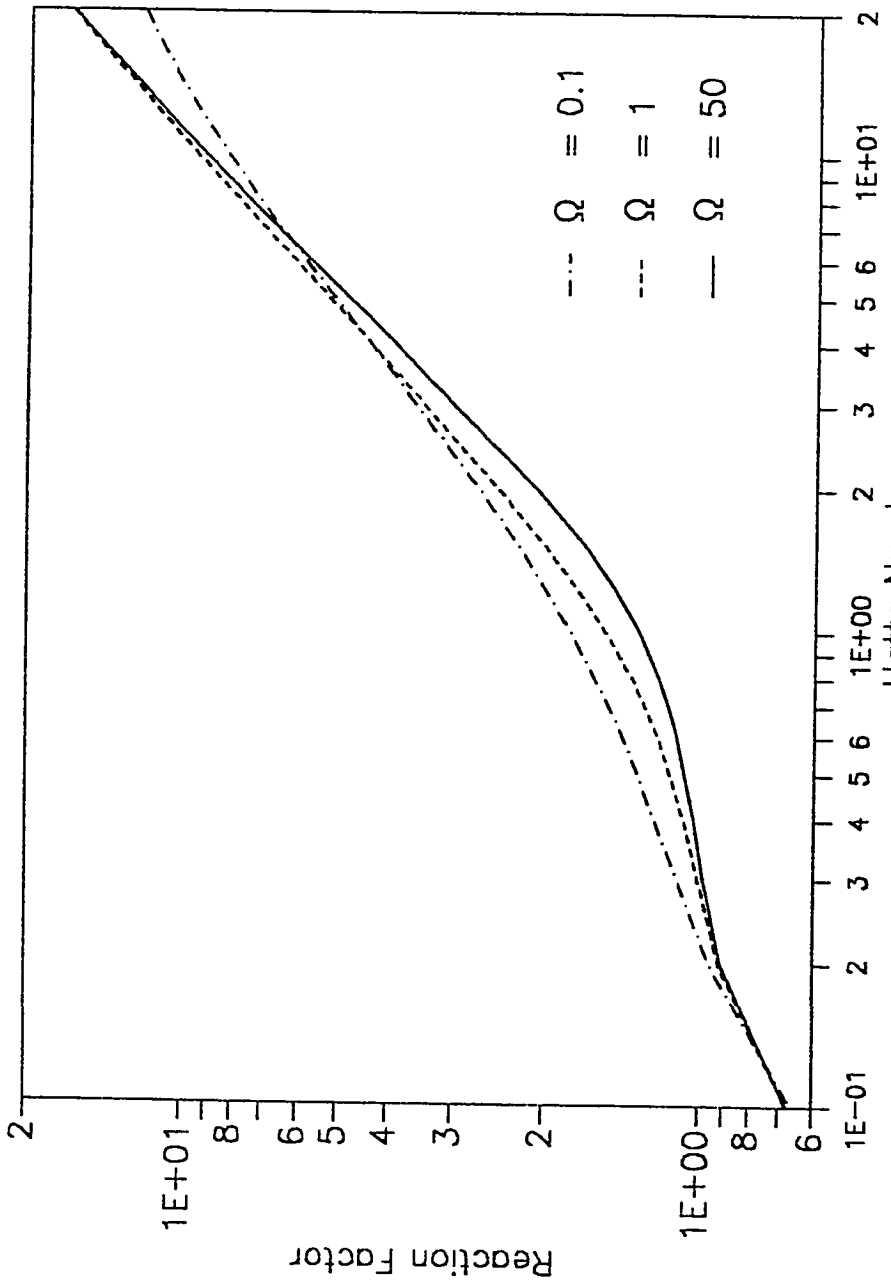

Figure 4.6b Effect of Sphericity on the Reaction Factor
(Ei 50, α' = 200, ξ = 0.001)

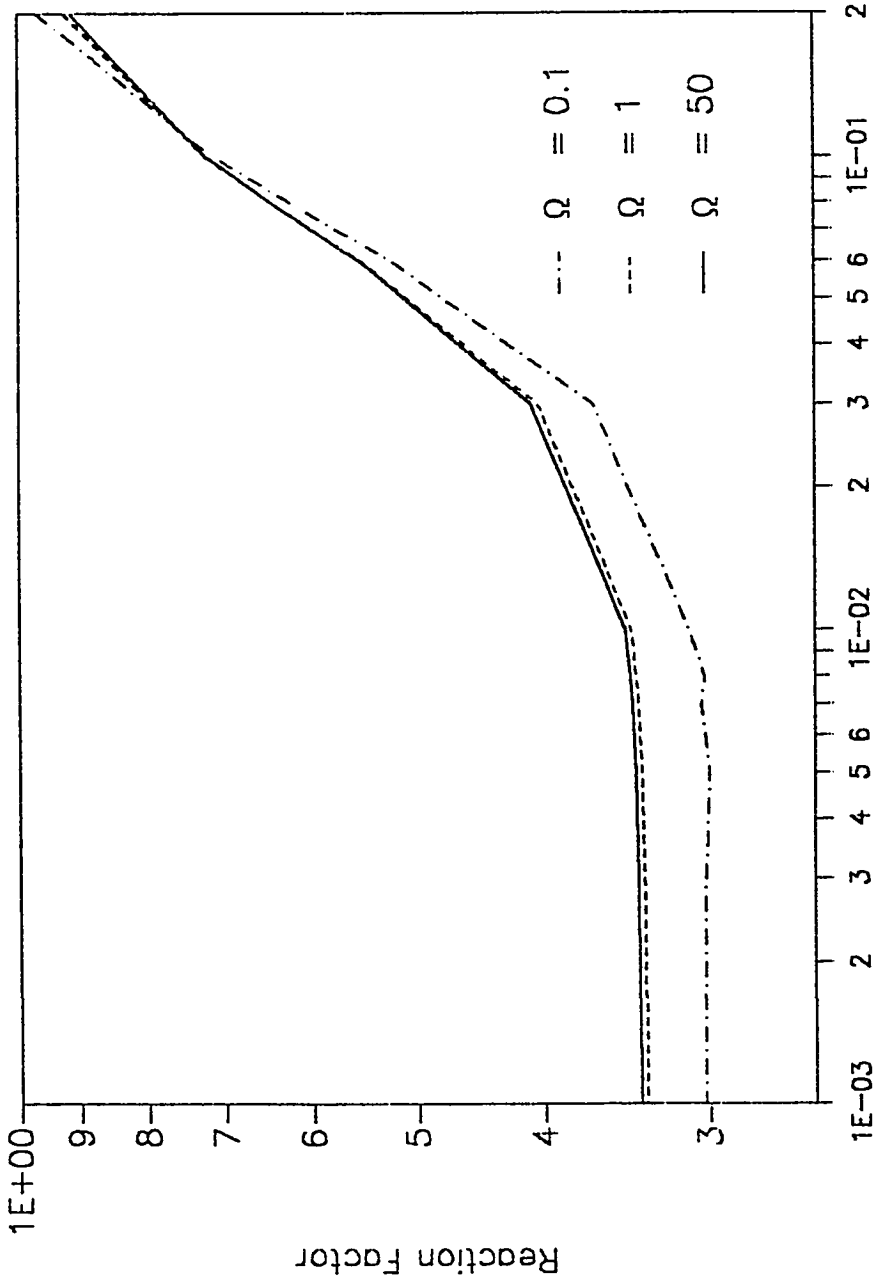

Figure 4.7a Effect of Sphericity, on the Reaction Factor
(Ei = 50, α' = 200, ξ=0.5)

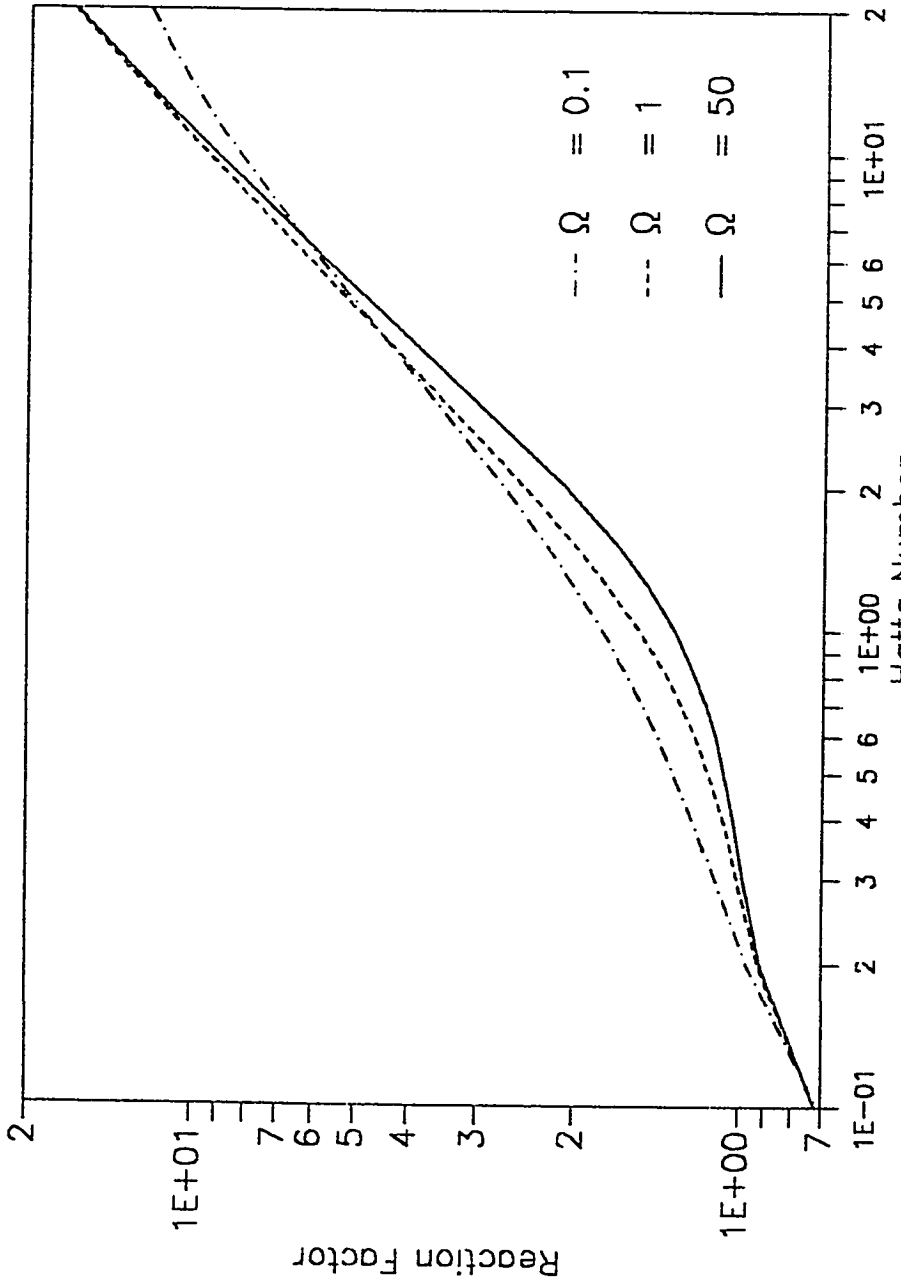

Figure 4.7b Effect of Sphericity on the Reaction Factor
(Ei = 50, α' = 200, ξ=0.5)

Figures 4.6a and Figures 4.7a reveals that in case of very slow reactions ($0.001 < M < 0.1$), for lower values of ξ, i.e., lower liquid flow rates, the reaction factor in case of spherical surface ($\Omega = 0.25$) is higher than that of the plane surface ($\Omega = 50$) whereas for higher values of ξ, i.e., higher liquid flow rates, a reverse trend is observed. Note that a change in ξ has no influence on the characteristic effect of sphericity on the reaction factor for relatively fast reactions as can be seen from Figures 4.6b and 4.7b.

From the above discussion it is clear that when the size of the gas bubble is comparable to thickness of the concentration boundary layer around it, the spherical effect, depending on the system conditions, might exert a significant influence on E_A^*. Thus for a rigorous design and analysis of gas-liquid CSTRs, the new reaction factor expression developed in this Chapter should be used.

CHAPTER 5

REACTOR SIMULATION RESULTS AND DISCUSSION

5.1 Introduction

One of the major objectives of this thesis is to study the steady state performance of non-isothermal, non-adiabatic, gas-liquid CSTRs by developing a comprehensive model which integrates various complex interactions involved in the modeling of such reactors (see Figure 1.2). A detailed discussion on the model development is presented in Chapter 3. Unique features of the new model are that it relaxes most of the crucial assumptions of previous authors and uses empirical correlations for various hydrodynamic and transport parameters and a new reaction factor expression developed for the spherical bubble geometry. An extensive review on the correlations is presented in Chapter 2. A discussion on the development of new reaction factor expression and its comparison with the numerical results is given in Chapter 4.

All previous simulation studies reported in the literature dealing with steady state multiplicity in gas-liquid CSTRs considered fixed values of the hydrodynamic and transport parameters. But in practical situations these parameters could be strongly dependent on operating conditions as we

demonstrated in Chapter 2. Therefore, the predictions of the multiplicity behavior based on the previous simplified models are conservative. This necessitates that a model be developed considering the possible variation of hydrodynamic and transport parameters to investigate the multiplicity problem from a more rigorous and realistic perspective. The new model incorporates empirical correlations for the interfacial area, gas-holdup, bubble diameter, bubble rise velocity, gas and liquid-side mass transfer coefficients, tank and jacket/coil side heat transfer coefficients, power dissipation and the minimum impeller speed for effective dispersion of gas. Also, various physico-chemical parameters such as diffusivity, viscosity, density and thermal conductivity have been represented as a function of temperature as discussed in section 5.3. These provisions enable one to study the effect of gas residence time, effect of degree of agitation and the effect of reactor and impeller geometry on the steady state multiplicity which was not possible with the simplified models used by all earlier authors. With the new model we can also study the effect of feed gas temperature, feed gas purity and the gas-side mass transfer resistance. Results of such studies are presented in section 5.4. Note that, for the case of general second-order reactions, these effects have not been investigated before.

In order to solve the complex set of non-linear algebraic model equations a computer simulation program called MULTIPLE has been developed. This program which involves tedious iterative procedure uses the half-interval method to get possible multiple roots of the model equations. The program can, in future, be used for designing gas-liquid CSTRs. A detailed discussion on the numerical procedure is given in section 5.3.

5.2 Physico-Chemical Parameters Used in Numerical Simulation

All the previous simulation studies on steady state behavior of gas-liquid CSTRs have been performed using a fixed set of values of physico-chemical and hydrodynamic parameters. These parameters, in most of the cases, were selected similar to those representing the chlorination of n-decane, which is a typical gas-liquid reaction and has been experimentally studied by Ding et al. [7]. In order to test the capability of the new model to describe real systems and to compare its results with those of previous researchers, we have also selected the data representing the chlorination of n-decane in our numerical simulations. However, in our study, wherever necessary, we have used published correlations for various temperature sensitive physico-chemical parameters, since existence of steady state multiplicity may cause a great variation in the reactor temperature. Table 5.1 presents a list of correlations for various temperature dependent physico-chemical parameters used in the numerical simulations with the new model. Various constants involved in the correlations are given in Table 5.1 and other temperature independent physico-chemical parameters are given in Table 5.2. For the numerical simulations using the old model of Shaikh et al. [26], we have used the same physico-chemical and hydrodynamic parameters as those of Huang and Varma [6]. A list of these parameters is given in Table 5.3.

5.3 Numerical Procedure

In order to perform numerical simulations using the new model a general purpose computer program named MULTIPLE has been written. This program allows the user to specify certain process and operating conditions for the

Table 5.1 Temperature Dependent Physico-Chemical Parameters

Parameter	Correlation	Reference
Diffusivity of A in B	$D_A = 0.66 \times 10^{-7} T \exp[1172(\frac{1}{273} - \frac{1}{T})]$	[130]
Sp. Heat of Liquid	$C_{pl} = 4.25 + 0.234T$	[130]
Sp. Heat of of Gas	$C_{pg} = Y_{Af} C_{PCl_2} + (1 - Y_{Af}) C_{PHCl}$ where, $C_{PCl_2} = 8.28 + 5.6 \times 10^{-4} T$ $C_{HCl} = 6.7 + 8.4 \times 10^{-4} T$	[130]
Viscosity of n-Decane	$\mu_L = 1.3\exp[-1172(\frac{1}{273} - \frac{1}{T})$	[130]
Surface Tension	$\sigma = P_c^{2/3} T_c^{1/3} Q(1 - T_r)^{11/9}$ where, $Q = 0.127(1 + T_{br} \frac{\ln P_c}{1 - T_{br}}) - 0.281$	[131]
Thermal Conductivity of n-Decane	$\lambda_L = \frac{2.64 \times 10^{-3}}{M_w^{1/2}} [\frac{3 + 20(1 - T_r)^{2/3}}{3 + 20(1 - T_{rb})^{2/3}}$	[131]
Molar Volume of n-Decane	$V = V^R [\frac{V_r^{(0)}(T_r)(1 - \omega\Gamma(T_r))}{V_r^{(0)}(T_r^R)(1 - \omega\Gamma(T_r^R))}]$ where, $T_r^R = \frac{T^R}{T_c}$ For $0.2 \le T_r \le 0.8$ $V_r^{(0)} = 0.336 - 0.34T_r + 1.52T_r^2 - 2.03T_r^3 + 1.114T_r^4$ For $0.8 < T_r < 1.0$ $V_r^{(0)} = 1 + 1.3(1 - T_r)^{1/2} \log(1 - T_r) - 0.509(1 - T_r) - 0.915(1 - T_r)^2$ For $0.2 \le T_r < 1.0$ $\Gamma = 0.296 - 0.09T_r - 0.048T_r^2$	[131]

Table 5.2 Reference Data Set for the Reactor Simulations Using New Model

Parameter	Value	Units	Reference
λ_m	2.6×10^{-3}	cal/s.cm.°K	[132]
λ_c	7.139×10^{-4}	cal/s.cm.°K	[132]
λ_{ins}	3.8×10^{-4}	cal/s.cm.°K	[132]
D_{Al}	0.0754	cm^2/s	[132]
C_{pc}	18.0	cal/gmol.°K	[132]
α_{th}	303.14×10^{-6}	1/°K	[132]
T_{cj}	617.6	°K	[131]
T_{hj}	447.3	°K	[131]
P_{cj}	20.69	atm	[131]
V_{cj}	603.0	cm^3/gmmol	[131]
Z_{cj}	0.247		[131]
ω_L	0.49		[131]
ρ_{lf}	5.13×10^{-3}	gmol/cm^3	[131]
M_{wL}	142.29	gm/gmol	[131]
M_{wG}	70.906	gm/gmol	[132]
M_{wc}	18.02	gm/gmol	[132]
H_o	0.00188	-	[6]
ρ_c	5.56×10^{-2}	gmol/cm^3	[132]
ρ_{gf}	4.2×10^{-5}	gmol/cm^3	[131]
$(-\Delta H_R)$	26000	cal/gmol	[6]
$(-\Delta H_s)$	4500	cal/gmol	[6]
E	29000	cal/gmol	[6]
T_{lf}	297	°K	
T_{ci}	293	°K	
T_{co}	303	°K	
A_{gf}	4.2×10^{-5}	gmol/cm^3	[6]
B_{lf}	5.1×10^{-3}	gmol/cm^3	[6]
V_R	400	cm^3	[7]
P_T	1.0	atm	

Table 5.3 Reference Data Set for the Reactor Simulations Using Old Model [6]

Parameter	Value	Units
$\underline{a}$	3	cm^{-1}
ε_L	0.86	-
K_L^o	0.04	cm/s
US	0.03	cal/°K.s
$D_A = D_B$	6×10^{-5}	cm^2/s
H_o	0.00188	-
ρ_{lf}	5.1×10^{-3}	$gmol/cm^3$
ρ_{gf}	4.2×10^{-5}	$gmol/cm^3$
C_{p_l}	70	cal/gmol.°K
C_{p_g}	6.5	cal/gmol.°K
$(-\Delta H_R)$	26000	cal/gmol
$(-\Delta H_s)$	4500	cal/gmol
E	29000	cal/gmol
T_{lf}	297	°K
T_c	298	°K
A_{gf}	4.2×10^{-5}	$gmol/cm^3$
B_{lf}	5.1×10^{-3}	$gmol/cm^3$
V_R	400	cm^3

reactor and other accessories such as the impeller, gas sparger and the heat exchange device. Our program with little modifications can, in future, be used for designing isothermal gas-liquid CSTRs. A flow chart of the simulation program is shown in Figure 5.1 and a step by step description is given below.

1. Read input data.

   Input to the program includes various thermodynamic, kinetic and physical property data and certain operating variables such as gas and liquid feed temperatures, pressures and compositions, cooling water temperature and flow rate, vessel diameter and the impeller speed.

2. Calculate various geometrical parameters.

   For a given reactor diameter the program calls a subroutine GEOMET which is based on the standard configuration as discussed in Chapter 2 to calculate the vessel dimensions and the dimensions and locations of impeller, gas sparger and the heat exchange device.

3. Read gas flow rate.

4. Check the superficial gas velocity.

   If the gas superficial velocity is not within the practical operating range the gas flow rate is accordingly adjusted.

5. Read liquid residence time.

6. Assume a suitable liquid bulk temperature.

7. Calculate temperature dependent physico-chemical parameters.

   Various parameters such as liquid viscosity, gas and liquid phase diffusivities, surface tension, gas and liquid densities, liquid thermal conductivity, and gas and liquid heat capacities are calculated using

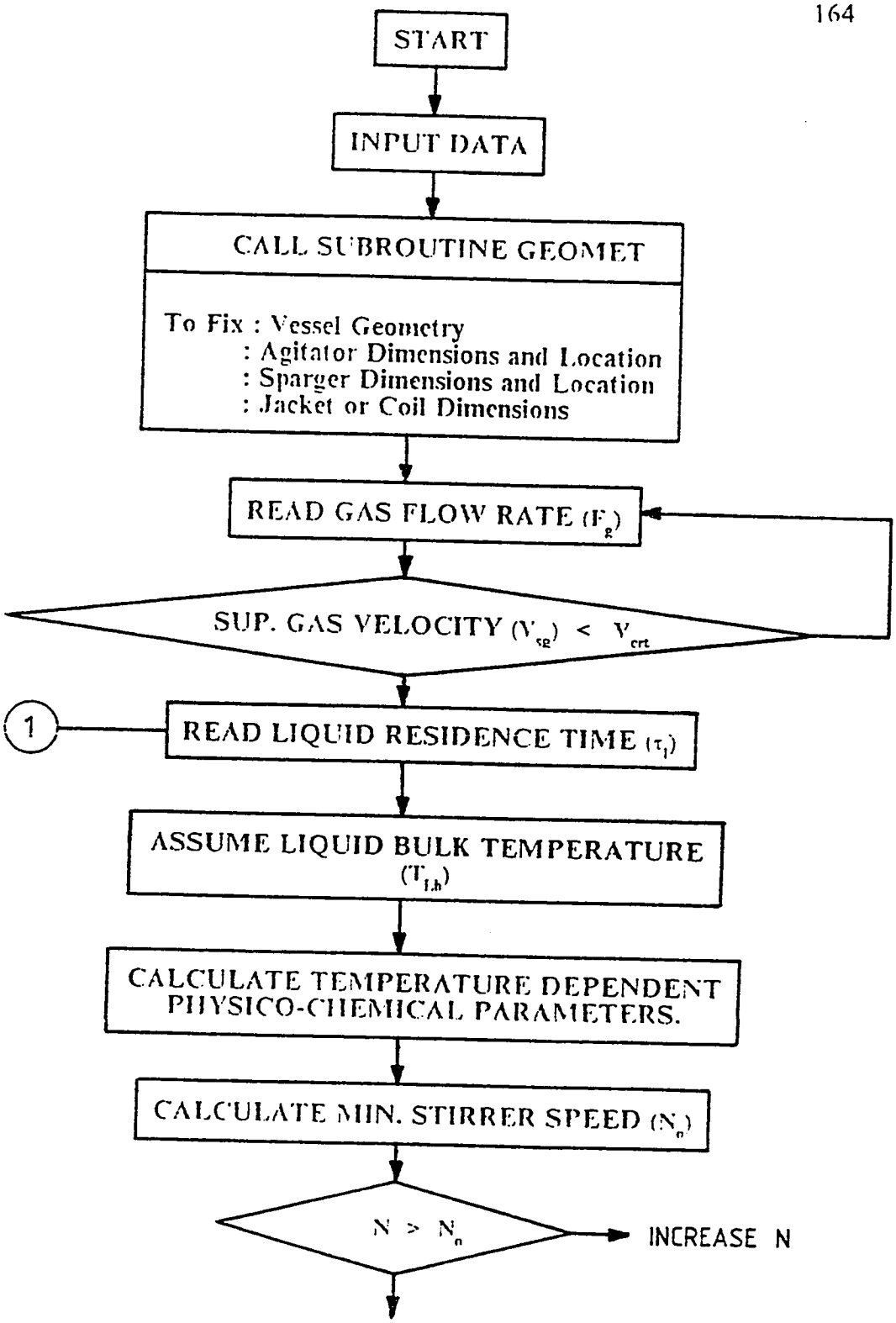

Figure 5.1 Flow Chart for the Reactor Simulation Program.

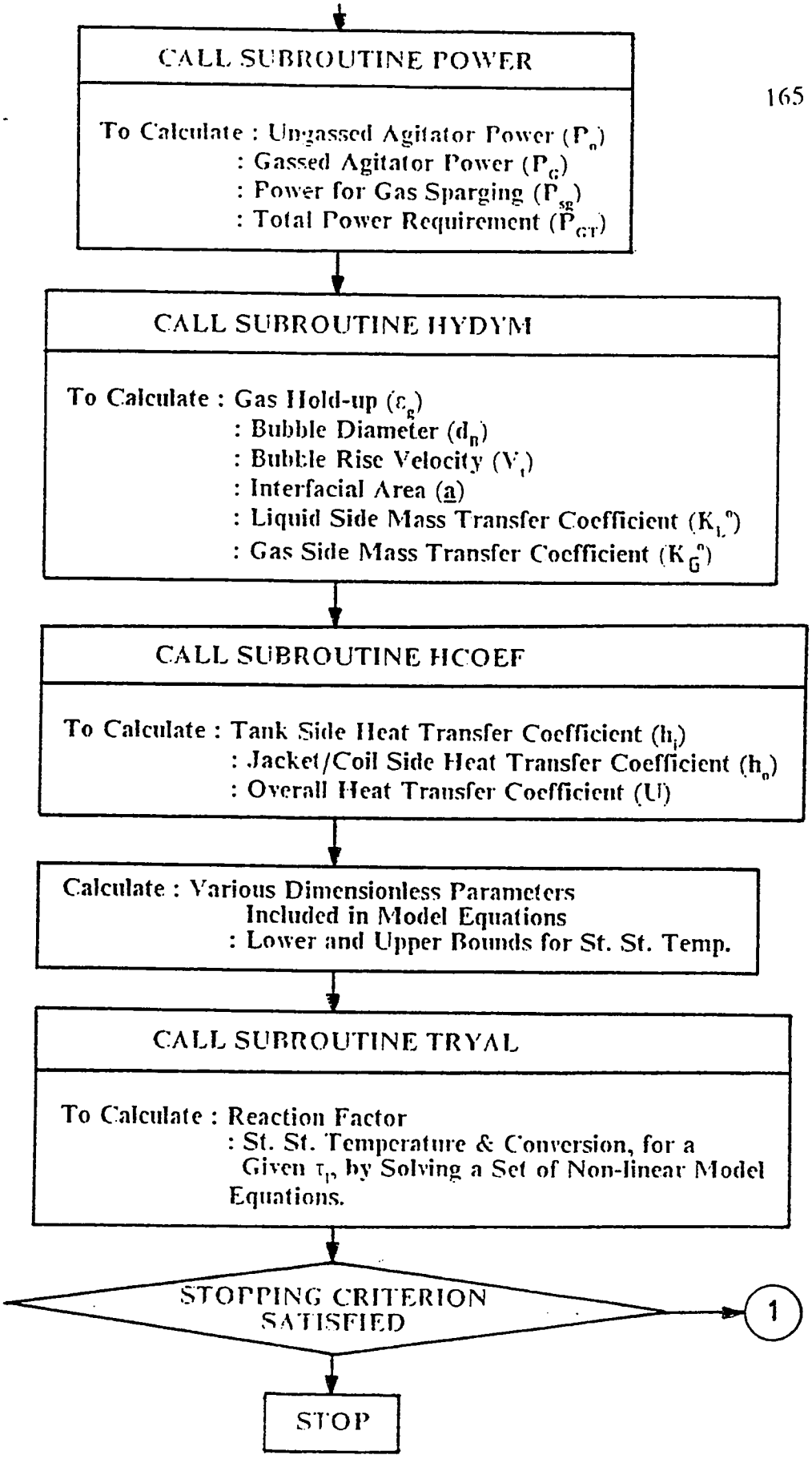
CALL SUBROUTINE POWER
To Calculate : Ungassed Agitator Power (P_u)
: Gassed Agitator Power (P_G)
: Power for Gas Sparging (P_{sg})
: Total Power Requirement (P_{GT})
CALL SUBROUTINE HYDYM
To Calculate : Gas Hold-up (ε_g)
: Bubble Diameter (d_B)
: Bubble Rise Velocity (V_t)
: Interfacial Area (a)
: Liquid Side Mass Transfer Coefficient (K_L^o)
: Gas Side Mass Transfer Coefficient (K_G^o)
CALL SUBROUTINE HCOEF
To Calculate : Tank Side Heat Transfer Coefficient (h_i)
: Jacket/Coil Side Heat Transfer Coefficient (h_o)
: Overall Heat Transfer Coefficient (U)
Calculate : Various Dimensionless Parameters
Included in Model Equations
: Lower and Upper Bounds for St. St. Temp.
CALL SUBROUTINE TRYAL
To Calculate : Reaction Factor
: St. St. Temperature & Conversion, for a
Given τ_1, by Solving a Set of Non-linear Model
Equations.
STOPPING CRITERION SATISFIED
1
STOP

correlations listed in Table 5.1

8. Evaluate minimum impeller speed.

   For the given gas flow rate, minimum impeller speed for complete gas dispersion is calculated using Equation (3.43). If calculated impeller speed is less than the given value in step 1, it is set equal to the calculated minimum stirrer speed.

9. Calculate total power input to the system.

   To calculate power input, the program calls a subroutine POWER in which first the ungassed power input is evaluated using Equations (3.38) and (3.39) and then power input in presence of gas is estimated from Equations (3.35) to (3.37). Next, the power input due to gas sparging is calculated using Equation (3.40). Finally, using Equations (3.41) and (3.42). the total power input to the system is evaluated.

10. Calculate various hydrodynamic and mass transport parameters.

    These parameters are estimated using subroutine HYDEM. Since the correlations for gas hold-up, bubble diameter, interfacial area and the bubble rise velocity are implicit, they have to be solved using some iterative procedure. In this subroutine first a suitable value for bubble diameter is assumed and then the bubble terminal velocity is calculated using Equation (3.34). Next, a suitable initial guess for ε_G is made and Equation (3.31) is solved for ε_G. If the newly obtained value of ε_G does not agree with the assumed value of ε_G within a prescribed tolerance, it is taken as the new initial value and is then used to calculate the bubble diameter from Equation (3.33) and the procedure is repeated until the desired

accuracy is achieved. After the convergence for ε_G is achieved, interfacial area is calculated from Equation (3.32). Finally, liquid and gas-side mass transfer coefficients are calculated using Equations (3.29) and (3.30) respectively.

11. Calculate over-all heat transfer coefficient.

The over-all heat transfer coefficient is calculated by calling a subroutine HCOEF. This subroutine first calculates various dimensionless groups for the tank-side and the jacket-side heat transfer coefficients. Next, assuming a suitable wall temperature (T_w), the viscosity of the reaction fluid at T_w is evaluated and then using Equations (3.23) and (3.25) heat transfer coefficients h_T and h_j are calculated. With these values of individual heat transfer coefficients, the wall temperature is estimated and then compared with the assumed value T_w. If the new value of T_w does not agree with the assumed value within a prescribed tolerance, it is taken as the new initial value and the same procedure is repeated until the required accuracy is achieved. Finally, the over all heat transfer coefficient is calculated using Equation (3.27). If an internal coil is used instead of the jacket, as the heat exchange device, the same procedure is adopted and in place of Equations (3.23), (3.25) and (3.27), Equations (3.24), (3.26) (3.28) are used.

12. Calculate various dimensionless parameters involved in the model equations and evaluate upper and lower temperature bounds through Equations (3.19) and (3.20), respectively.

13. Determine steady state temperature and conversion.

For a given set of physico-chemical, hydrodynamic and transport

parameters, steady state temperature and conversion are calculated by solving dimensionless model Equations (3.13) to (3.18). The iterative computational scheme used here starts from $\theta = \theta_{lb}$ with a suitable step size in θ. Then a suitable guess on a_l is made and a subroutine named TRYAL is called. This subroutine solves Equation (3.21a-c) for E_A^*, b_i and a_l using an iterative procedure. After the convergence for E_A^*, b_i and a_l is achieved all these values along with other dimensionless parameters are substituted in Equation (3.17) to check whether the assumed value of θ is a solution. For the next value of θ, the last convergence value of a_l is set as the starting assumed value and the same procedure is repeated until the complete range of θ between the lower and upper temperature bounds is searched for any possible roots of Equation (3.17). Within a step size, the possible solutions of Equation (3.17) are located using the half-interval method.

14. Make correction for liquid bulk temperature.

    This is done by comparing the steady state temperature, θ, obtained in step 12, with the assumed liquid bulk temperature in step 5. If this computed value of θ does not agree with the assumed value within a prescribed tolerance, it is set to be the new assumed value for the liquid bulk temperature and the procedure is repeated starting from step 6.

15. Print results.

5.4 Parametric Study

5.4.1 Effect of Reactivity

Figures 5.2 and 5.3 show the regions and patterns of multiplicity obtained at different values of reaction rate constant with respect to gas and liquid residence times. Three multiplicity patterns: S-shaped, mushroom and *isola* have been identified as indicated by regions b, c and d in Figures 5.2 and 5.3. Region 'a' in these plots means that the uniqueness is assured for all values of τ_G. Note that for any value of $\tau_G < \tau_G^L$ and $\tau_G > \tau_G^U$ corresponding to Figure 5.2 and $\tau_L < \tau_L^L$ and $\tau_L > \tau_L^U$, corresponding to Figure 5.3, a unique steady state is assured for all values of K. We also note that for any $K > K^U$ and $K < K^L$, uniqueness is guaranteed for all values of τ_G and τ_L.

5.4.2 Effect of Gas and Liquid Residence Times

Effect of gas residence time on steady state multiplicity has not been studied before. This is because all previous researchers worked with fixed values of hydrodynamic and transport parameters and did not attempt to study the effect of gas residence time possibly because the gas superficial velocity has a strong influence on these parameters. With the new model, however, one can study the effect of gas residence time because it uses the empirical correlations to evaluate various parameters involved in the model.

Figure 5.4 presents an example of an S-shaped multiplicity pattern, showing the effect of gas and liquid flow rates on reactor temperature. Corresponding

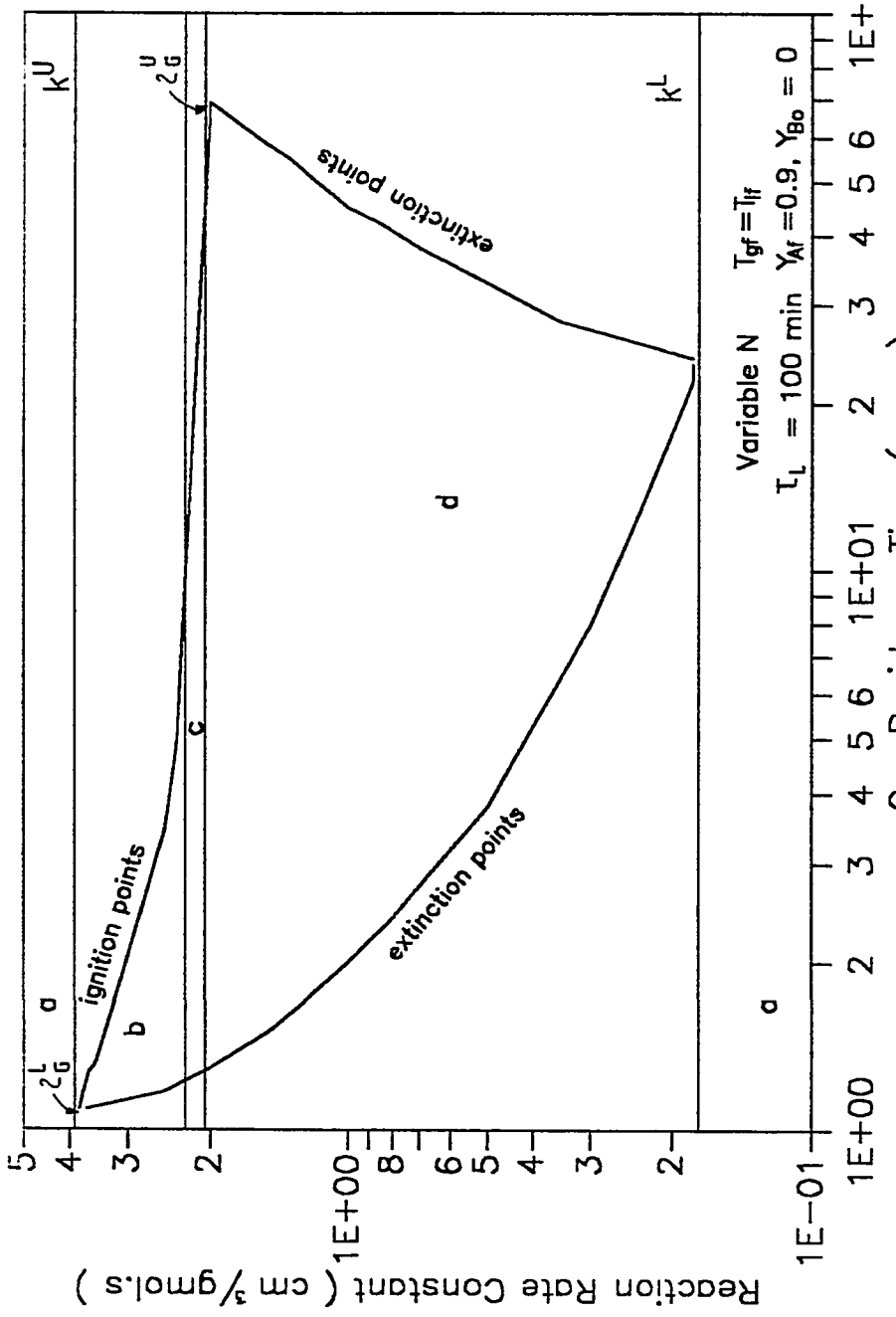

Figure 5.2 Effect of Reactivity on the Regions and Patterns of Multiplicity

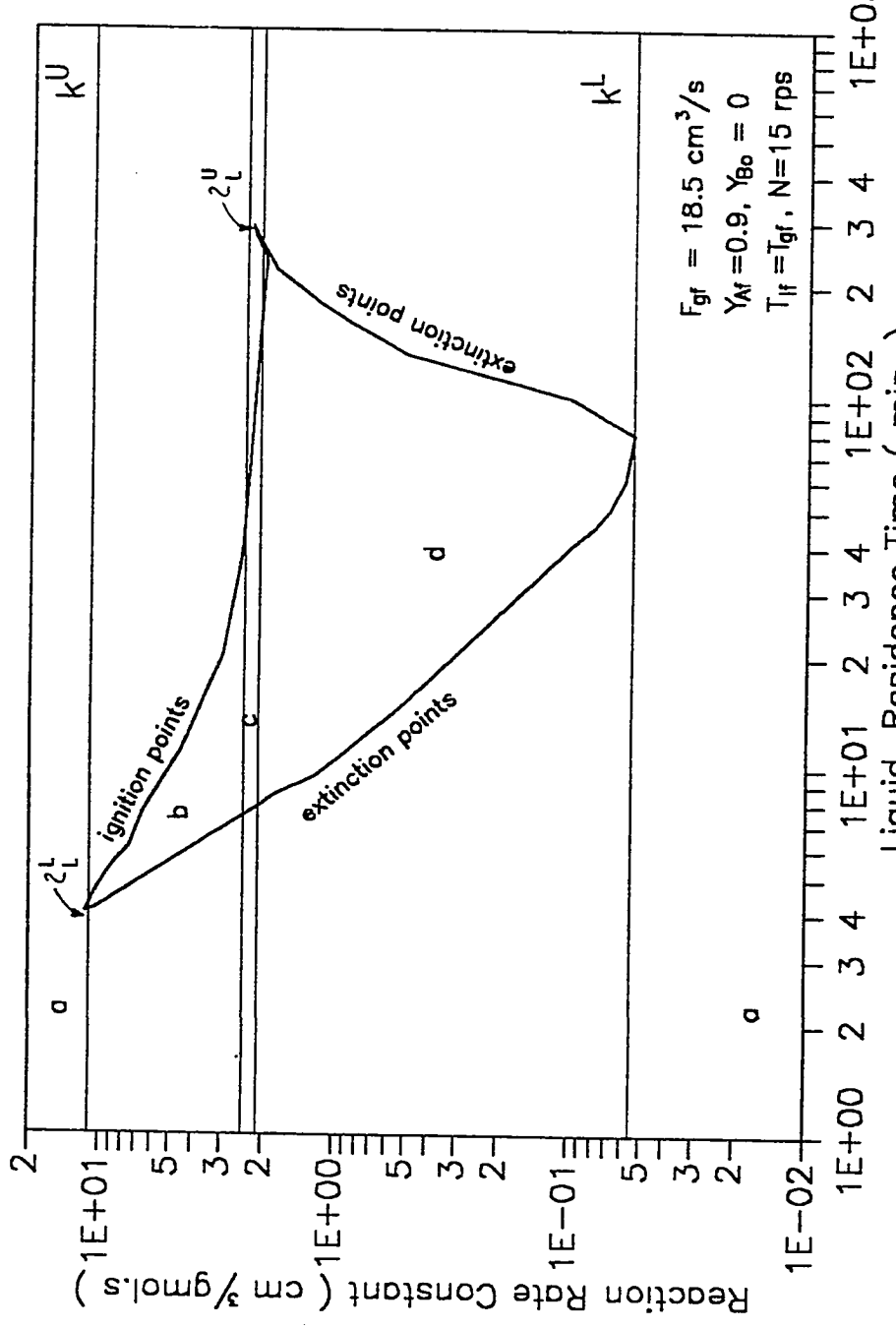

Figure 5.3 Effect of Reactivity on the Regions and Patterns of Steady State Multiplicity

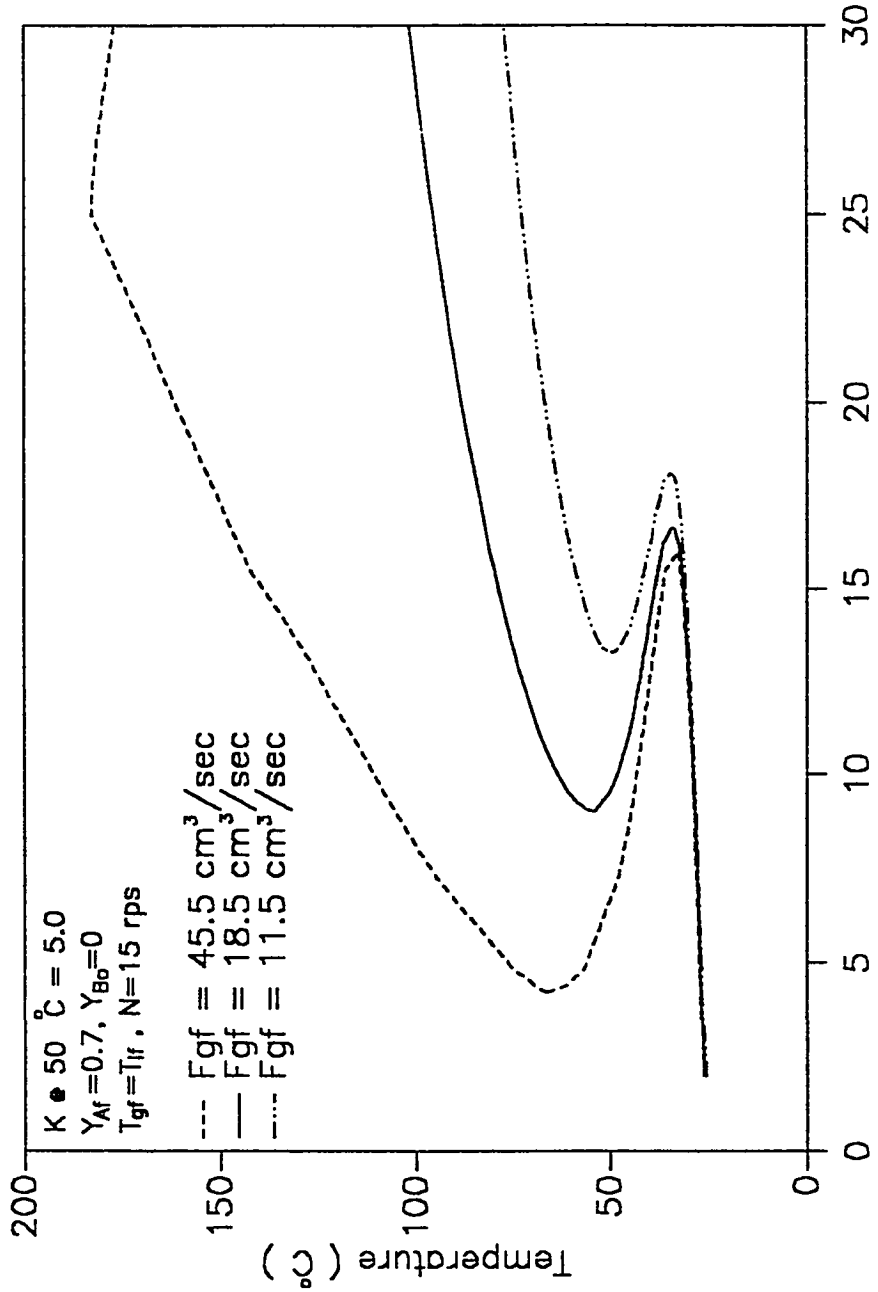

Figure 5.4 Effect of F_{gf} on Temperature

plots for steady state conversion of liquid and gaseous reactants are shown in Figures 5.5 and 5.6. It can be seen from Figure 5.4 that the region of multiplicity expands with the increase in gas flow rate. Both the ignition and the extinction points are shifted towards lower liquid residence time as the gas flow rate is increased. The shift in the extinction point, however, is much higher compared to the ignition point. A comparison of ignition and extinction points for different gas flow rates is given in Table 5.4. It is observed that the gas to liquid flow rate ratio at which the ignition to upper temperature branch occurs exhibits a sharp increase with the increase in gas flow rate. The gas to liquid flow rate ratio corresponding to extinction point, however, shows only a slight increase with the gas flow rate. It is seen in Figure 5.4 that the upper temperature branch is more sensitive to gas flow rate. This is because in that region reaction rate increases with the increases in gas flow rate as shown in Figures 5.7 and 5.8. In Figure 5.4 we also note that the steady state temperature corresponding to $F_g = 45.5 cm^3/\text{sec}$ reaches a maximum and starts decreasing sharply if we further increase the liquid residence time. This is because at this point the conversion of liquid reactant is almost complete (see Figure 5.5) and the liquid reactant is exhausted, as a result the rate of reaction decreases and so does the steady state temperature. Figure 5.7 also shows that at low temperature branch, the reaction factor decreases with the increase in gas flow rate. This indicates that at high gas flow rate and low temperature conditions, the rate of absorption of gaseous reactant is very high compared to its consumption in the liquid film. As a result all the gaseous reactant goes into the liquid bulk as shown in Figure 5.8. It is clear from Figure 5.7 and 5.8 that

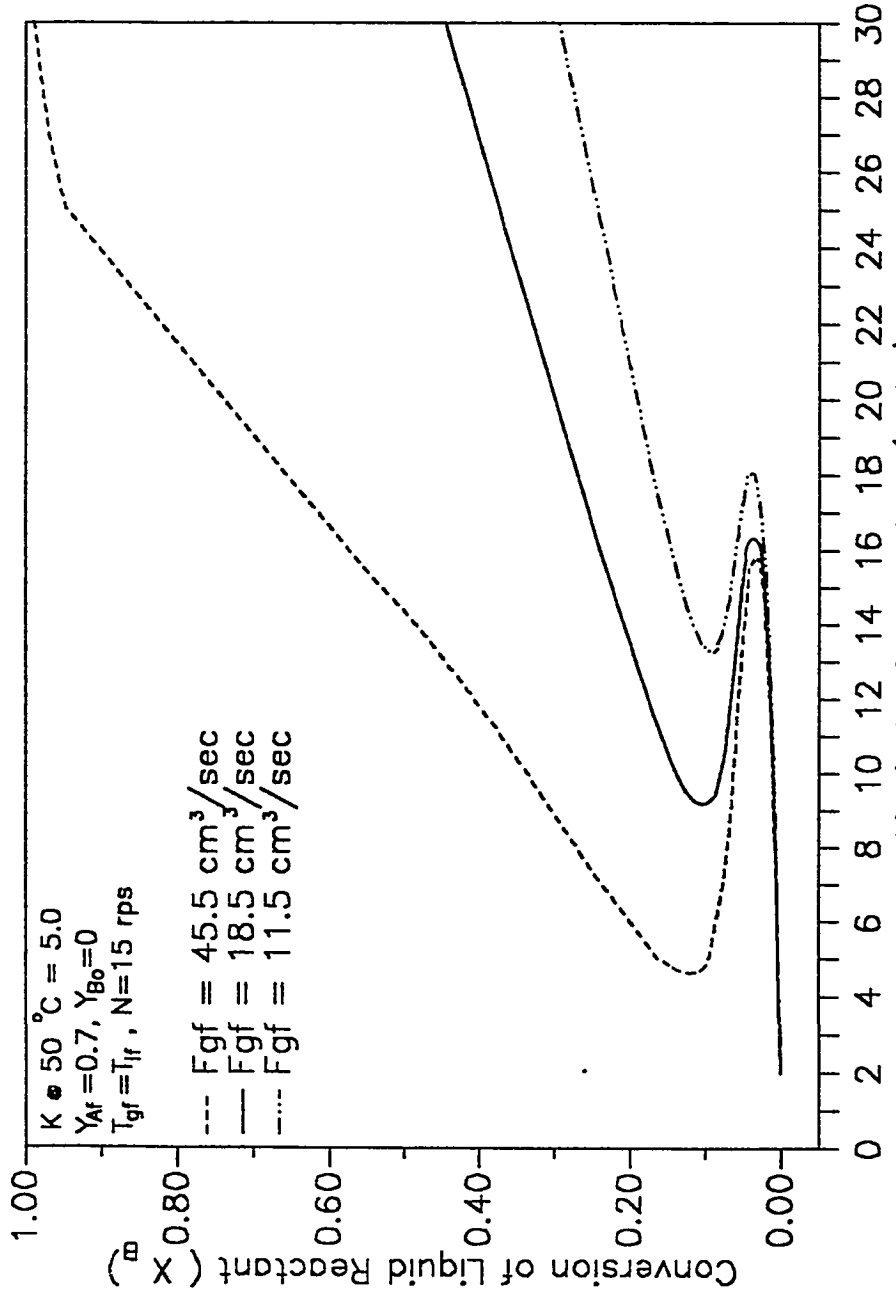

Figure 5.5 Effect of F_{gf} on Dimensionless Conversion of Liquid Reactant

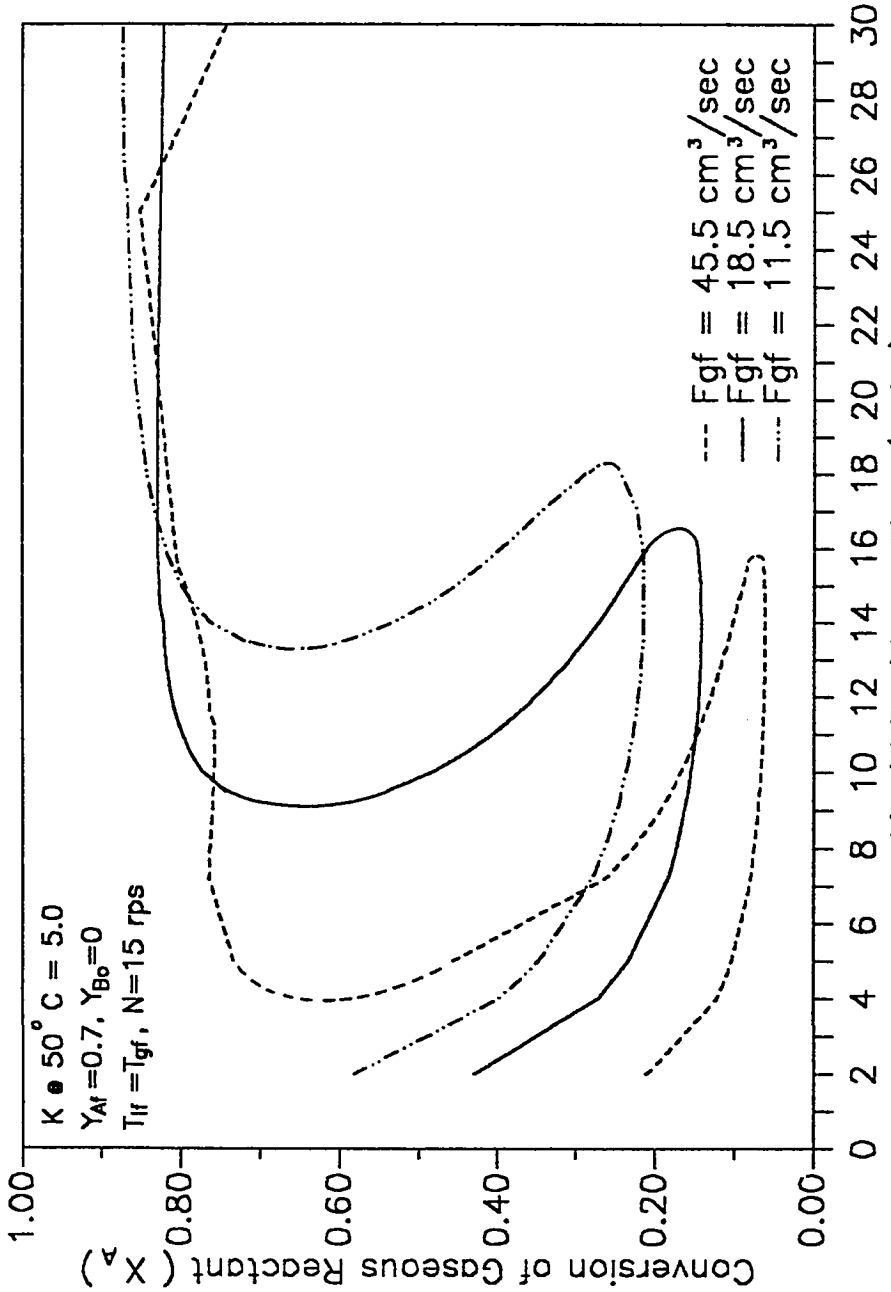

Figure 5.6 Effect of F_{gf} on Dimensionless Conversion of Gaseous Reactant

Table 5.4 Comparison of Ignition and Extinction Points at Different Gas Flow Rates

F_{gf} cm^3/s	Extinction Points (F_{gf}/F_{lf})	Ignition Points (F_{gf}/F_{lf})
11.5	23.12	31.40
18.5	25.23	46.06
45.5	29.34	107.85

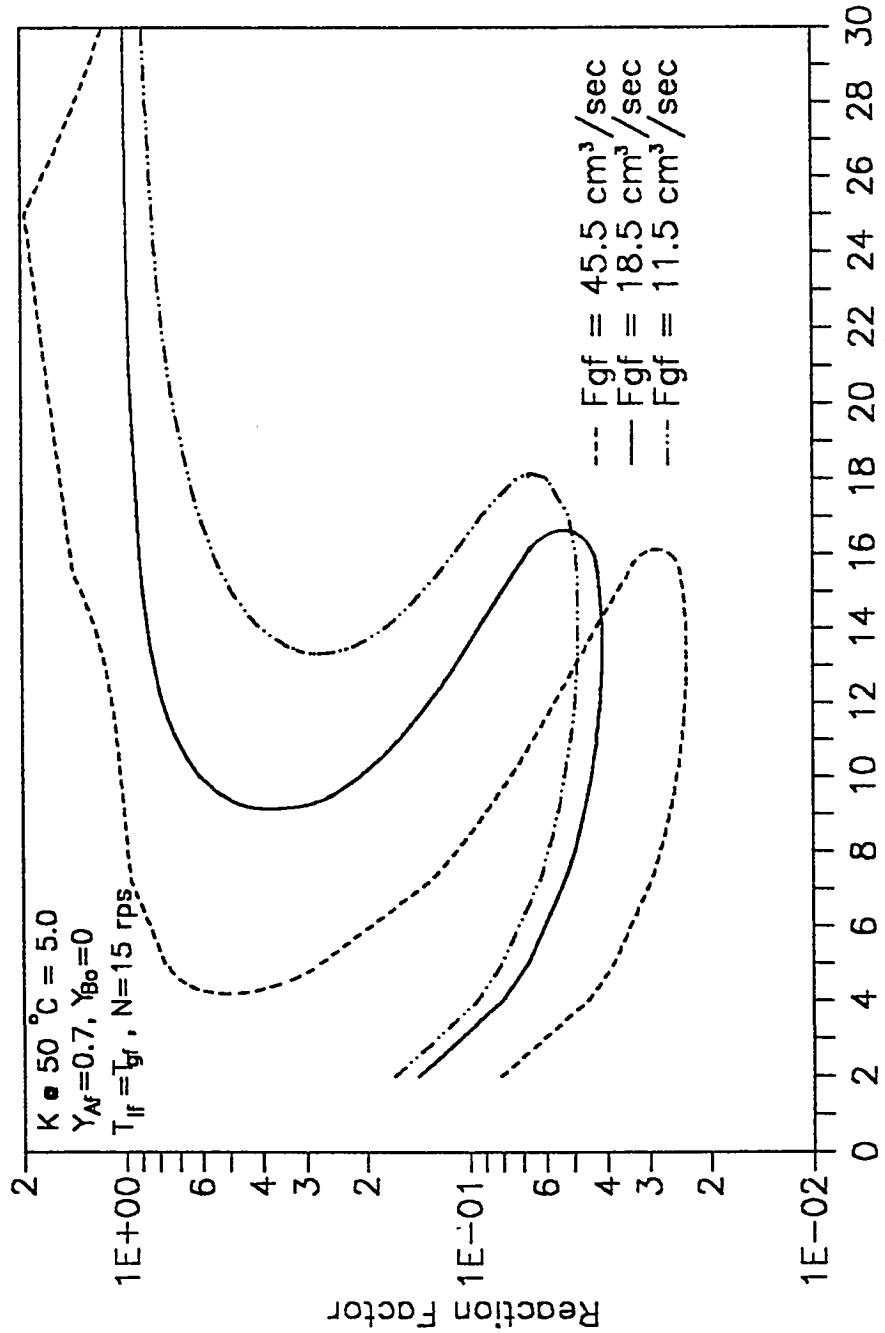

Figure 5.7 Effect of F_{gf} on Reaction Factor

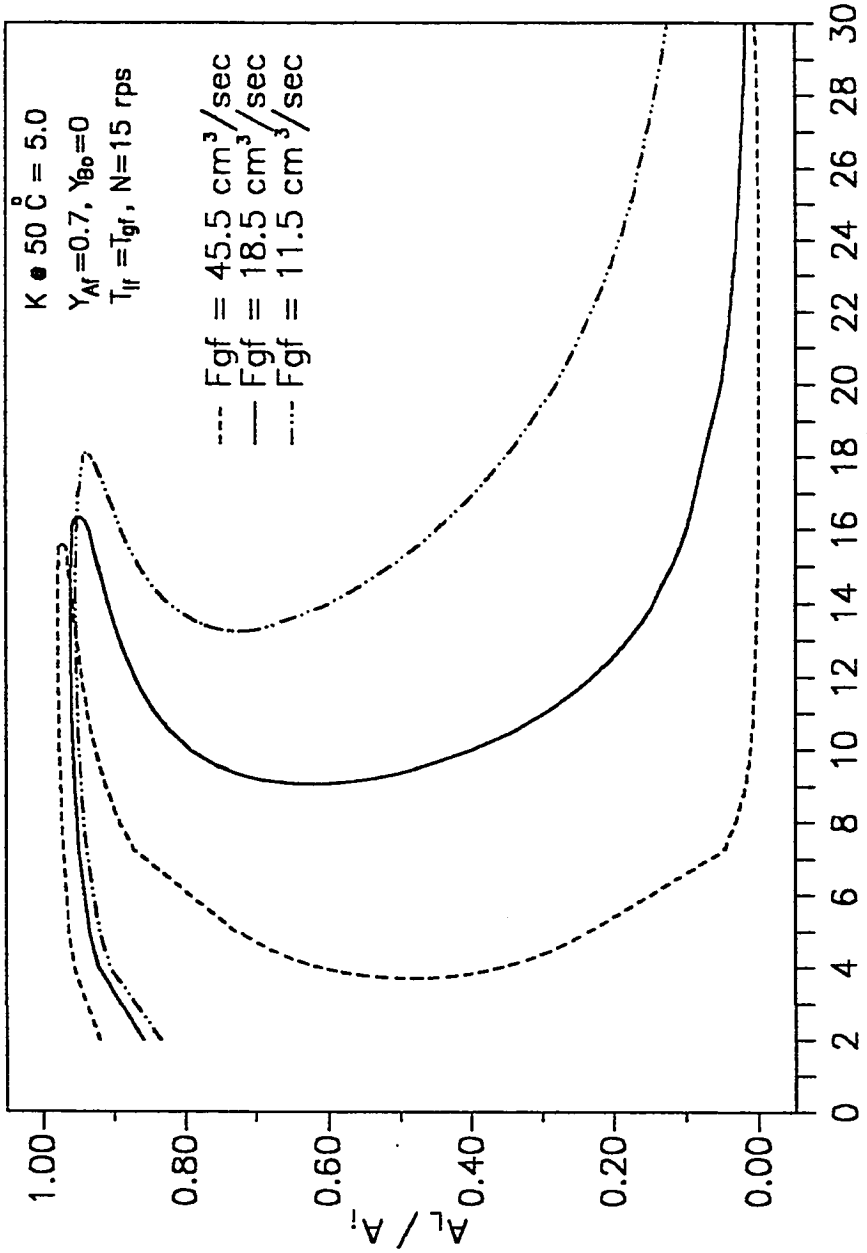

Figure 5.8 Effect of F_{gf} on Dimensionless Concentration of A in Liquid Bulk

corresponding to upper temperature branch, the increase in gas flow rate causes a sharp increase in the rate of reaction due to the change in physico-chemical, hydrodynamic and transport parameters as shown below.

Figure 5.9 shows the effect of change in operating conditions on the power input to the reactor. It can be seen that an increase in gas flow rate increases the total specific power input and decreases the power input due to agitation. This is because, the presence of gas reduces the drag coefficient of the impeller blade by forming gas cavities at the rear of each blade. It is also seen that the reduction in power drawn by the impeller is higher at higher gas flow rate. This is because at higher gas flow rates the size of the gas cavities is larger and thus the drag coefficient is smaller. The middle and the lower branch in each curve of Figure 5.9 demonstrate the effect of change in physico-chemical properties, mainly the viscosity in this case, due to the change in steady state temperature.

Figures 5.10 and 5.11 show that an increase in gas flow rate increases the interfacial area and gas hold-up due to increase in superficial gas velocity and total specific power input as shown in Figure 5.9. Figure 5.12 shows that the mean bubble diameter also increases with the increase in gas flow rate despite the fact that the total specific power input is increased, indicating that under present conditions the effect of superficial gas velocity, to which bubble diameter is directly proportional, is dominating. It is clear from Figures 5.10 to 5.12 that the interfacial area, gas hold-up and bubble diameter are greatly influenced by the change in steady state temperature: an increase in steady state temperature decreases the surface tension which in turn decreases the bubble diameter and

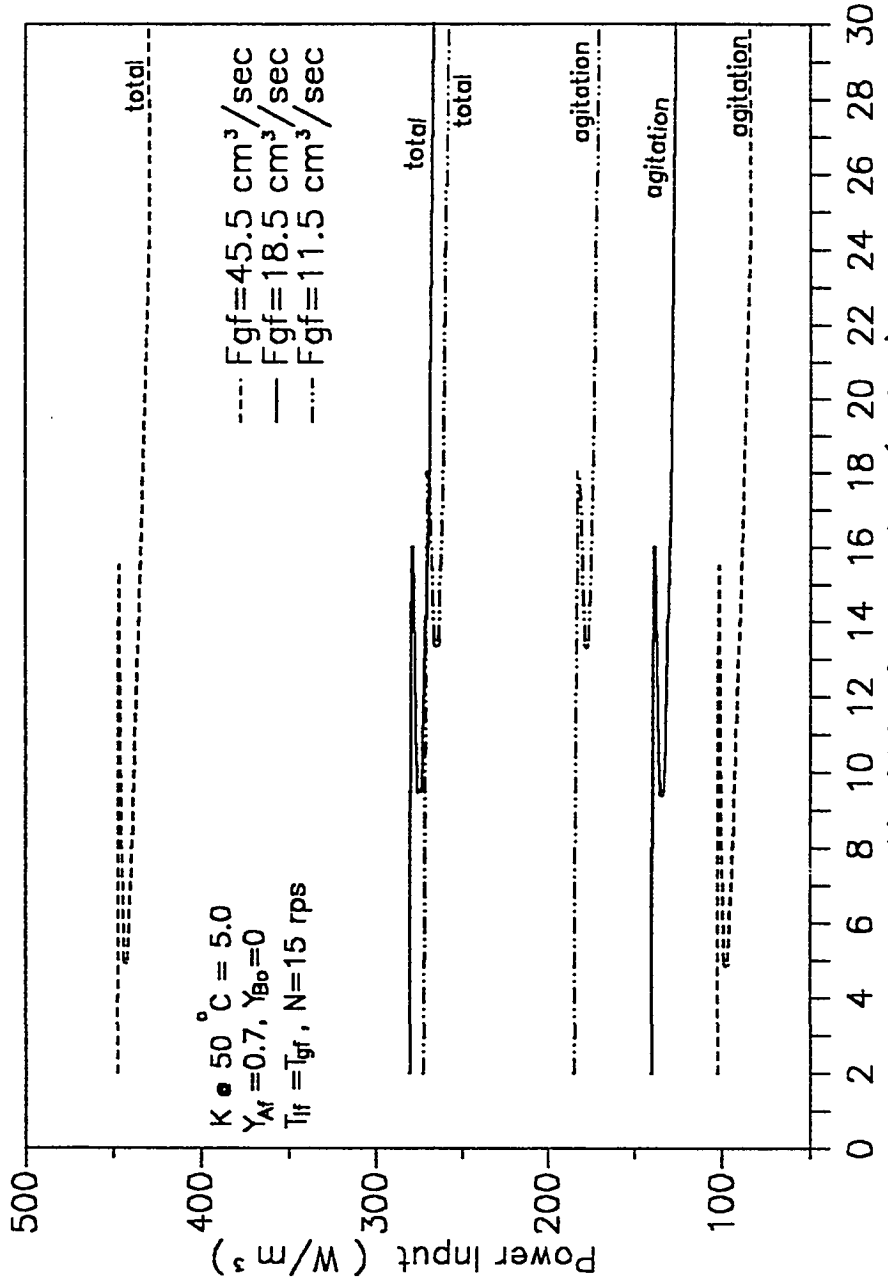

Figure 5.9 Effect of F_{gf} on Power Input

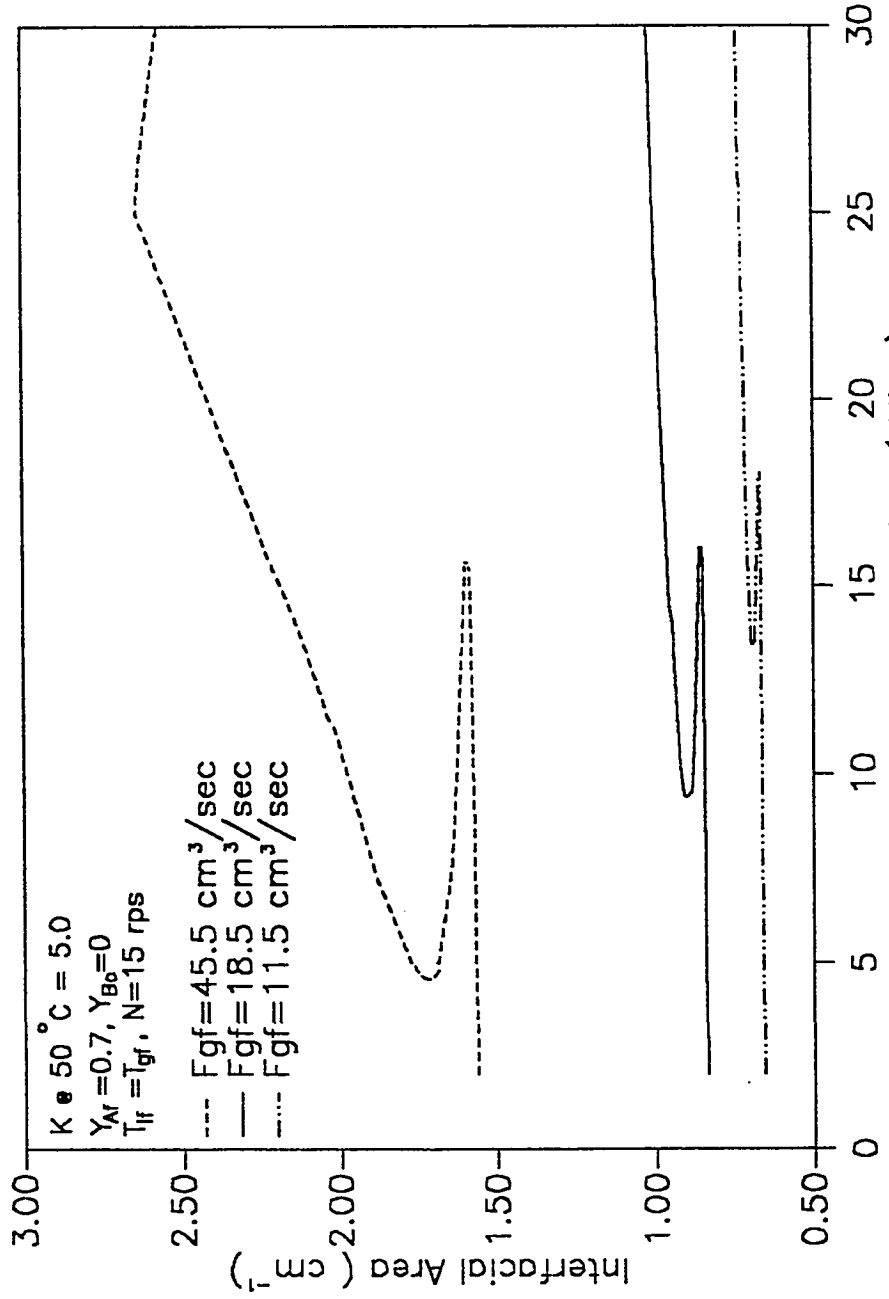

Figure 5.10 Effect of F_{gf} on Interfacial Area

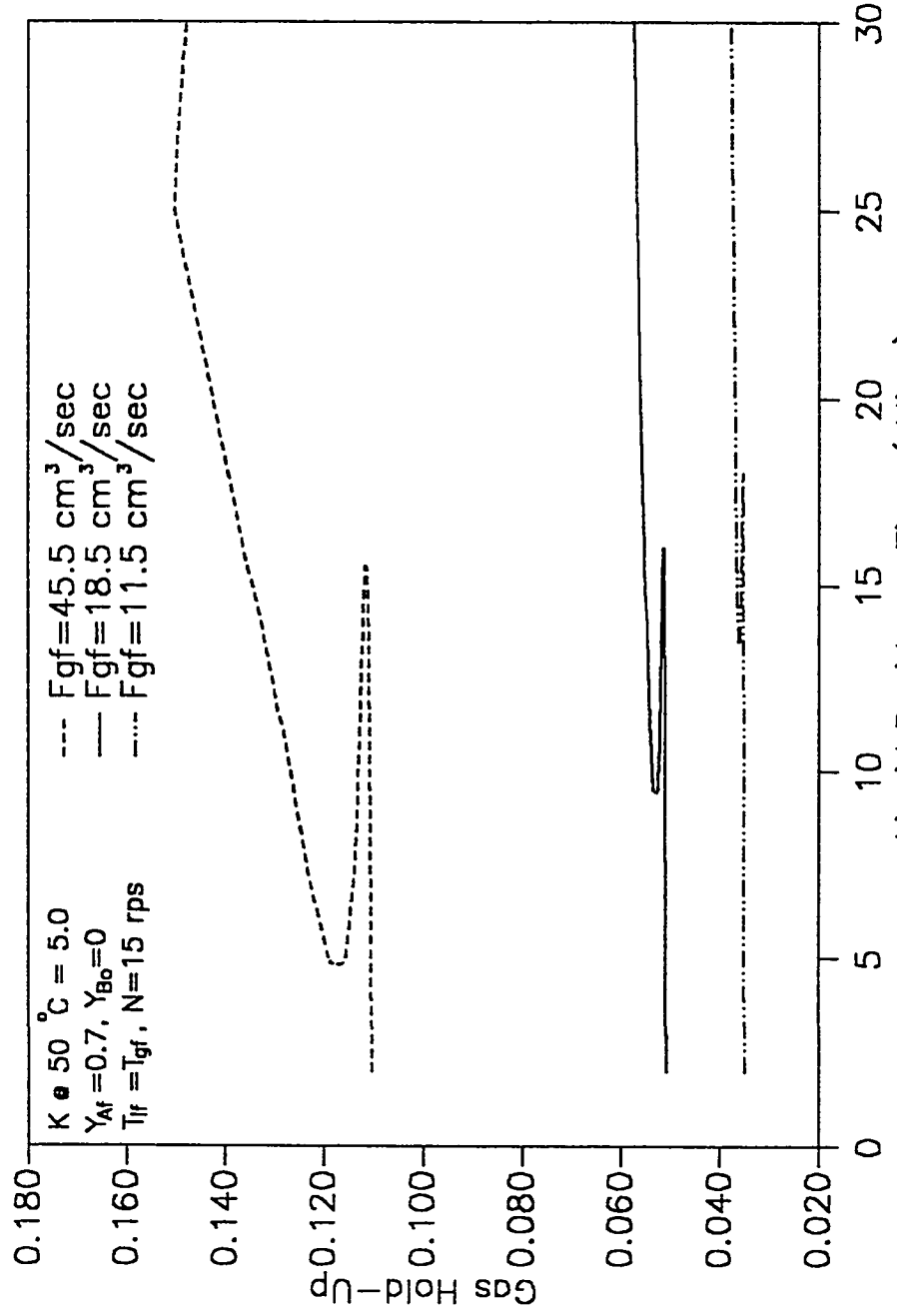

Figure 5.11 Effect of F_{gf} on Gas Hold-Up

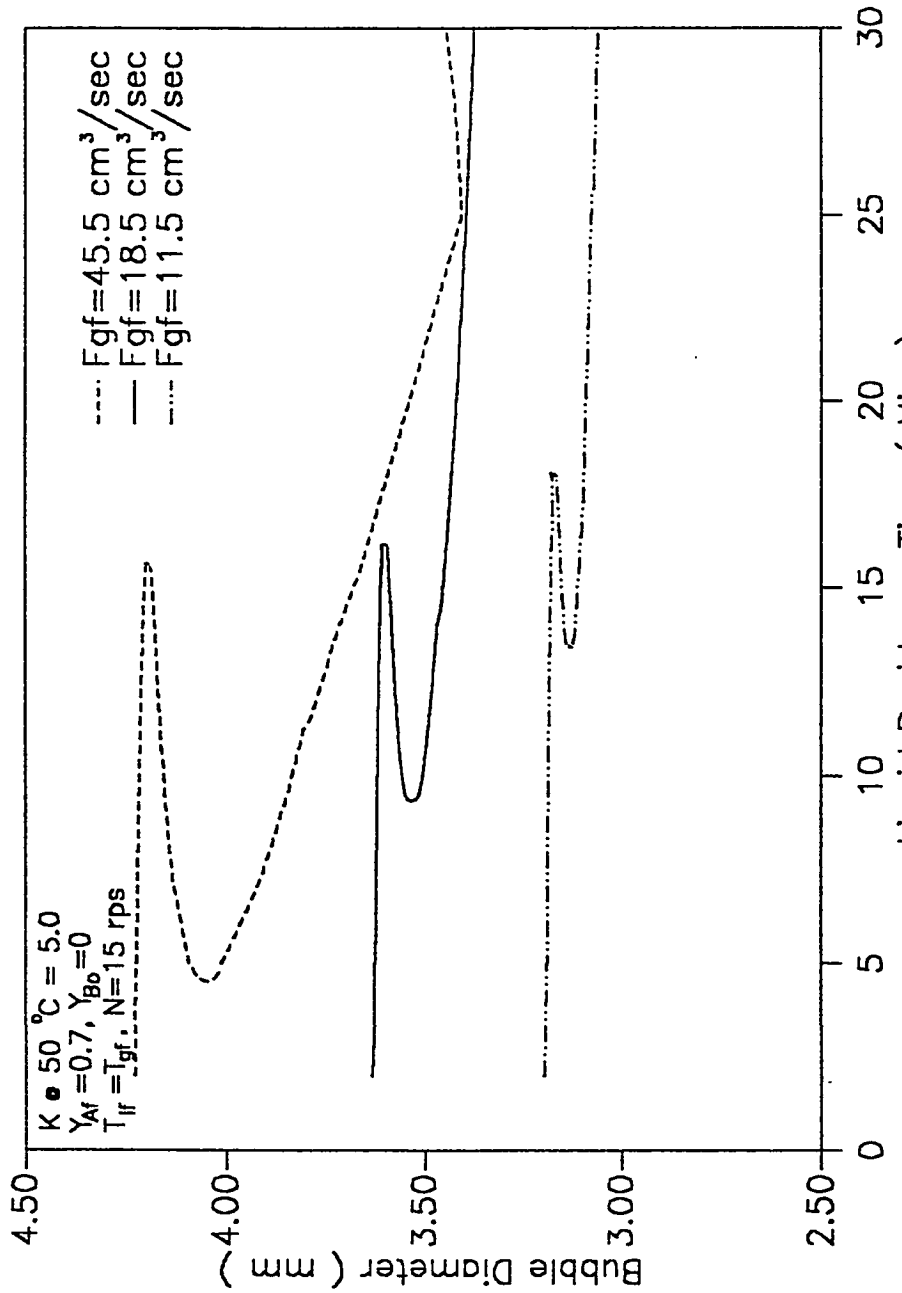

Figure 5.12 Effect of F_{gf} on Bubble Diameter

increase the interfacial area and gas hold-up.

It can be seen from Figure 5.13 that the gas flow rate has no significant influence on the liquid-side mass transfer coefficient, K_L^o. However, K_L^o rapidly increases with the increase in temperature, because both diffusivity and viscosity are greatly affected by the change in temperature. Figure 5.14 shows that the gas-side mass transfer coefficient, K_G^o, decreases with the increase in gas flow rate. This is because at higher gas flow rates relatively larger size bubbles are formed, as shown in Figure 5.12. At higher temperatures the value of K_G^o is higher due to smaller bubble size and higher gas diffusivity.

Figures 5.15 and 5.16 show the variation in tank-side and over-all heat transfer coefficients with respect to gas and liquid flow rate and steady state temperature. We note that the increase in gas flow rate increases the heat transfer coefficient due to increased turbulence created by the extra energy input by the aeration. The upper and the middle branches in the curves shown in Figure 5.15 illustrate the effect of change in physical properties on the heat transfer coefficient due to the change in steady state temperature. It can be seen from Figure 5.16 that although the tank-side heat transfer coefficient varies significantly with the gas flow rate and the steady state temperature, the over-all heat transfer coefficient does not change much.

From the above discussion it can be concluded that the variations in gas flow rate and the temperature can significantly influence the hydrodynamic and transport parameters. Variations in liquid flow rate, however, have little

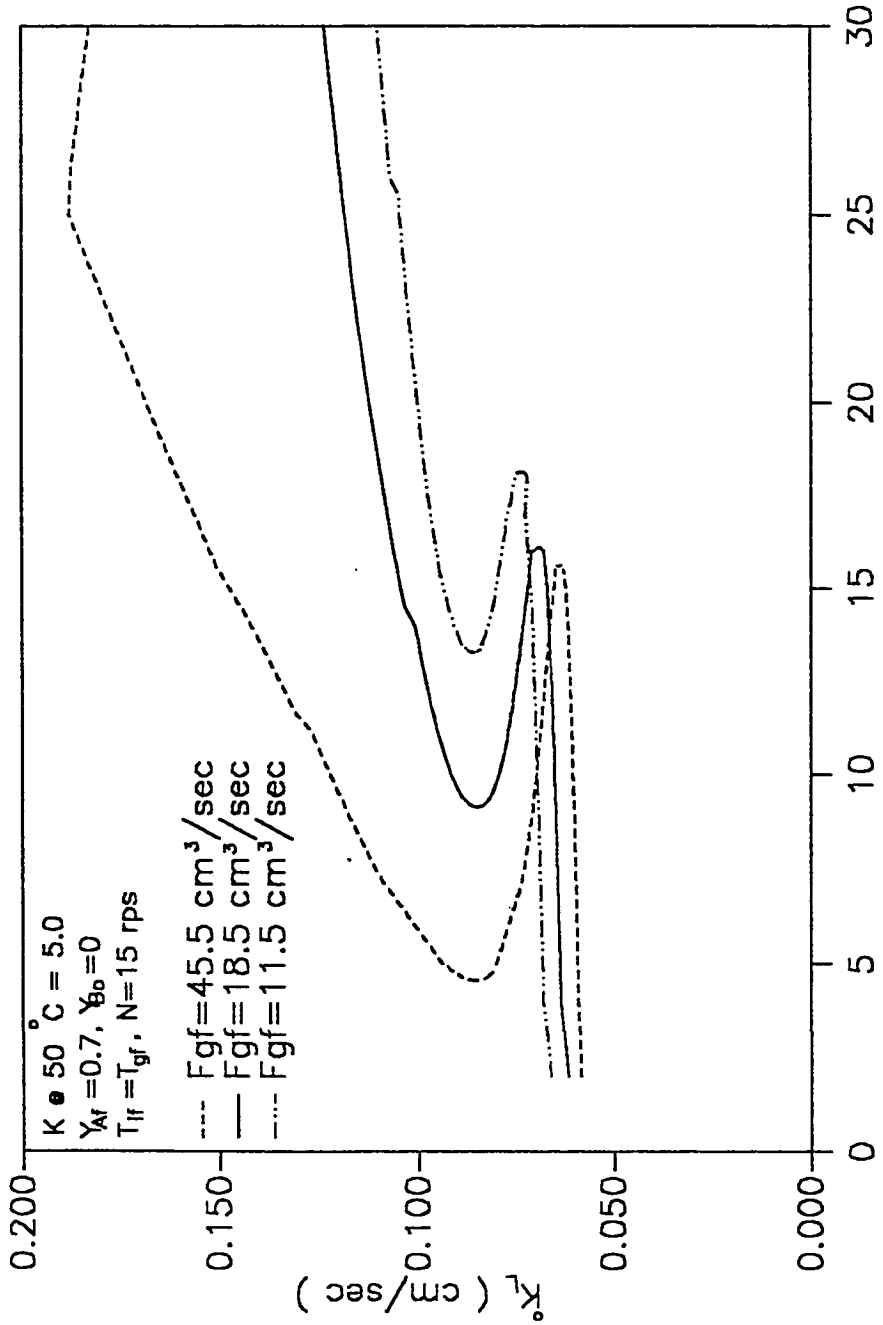

Figure 5.13 Effect of F_{gf} on Liquid-Side Mass Transfer Coefficient

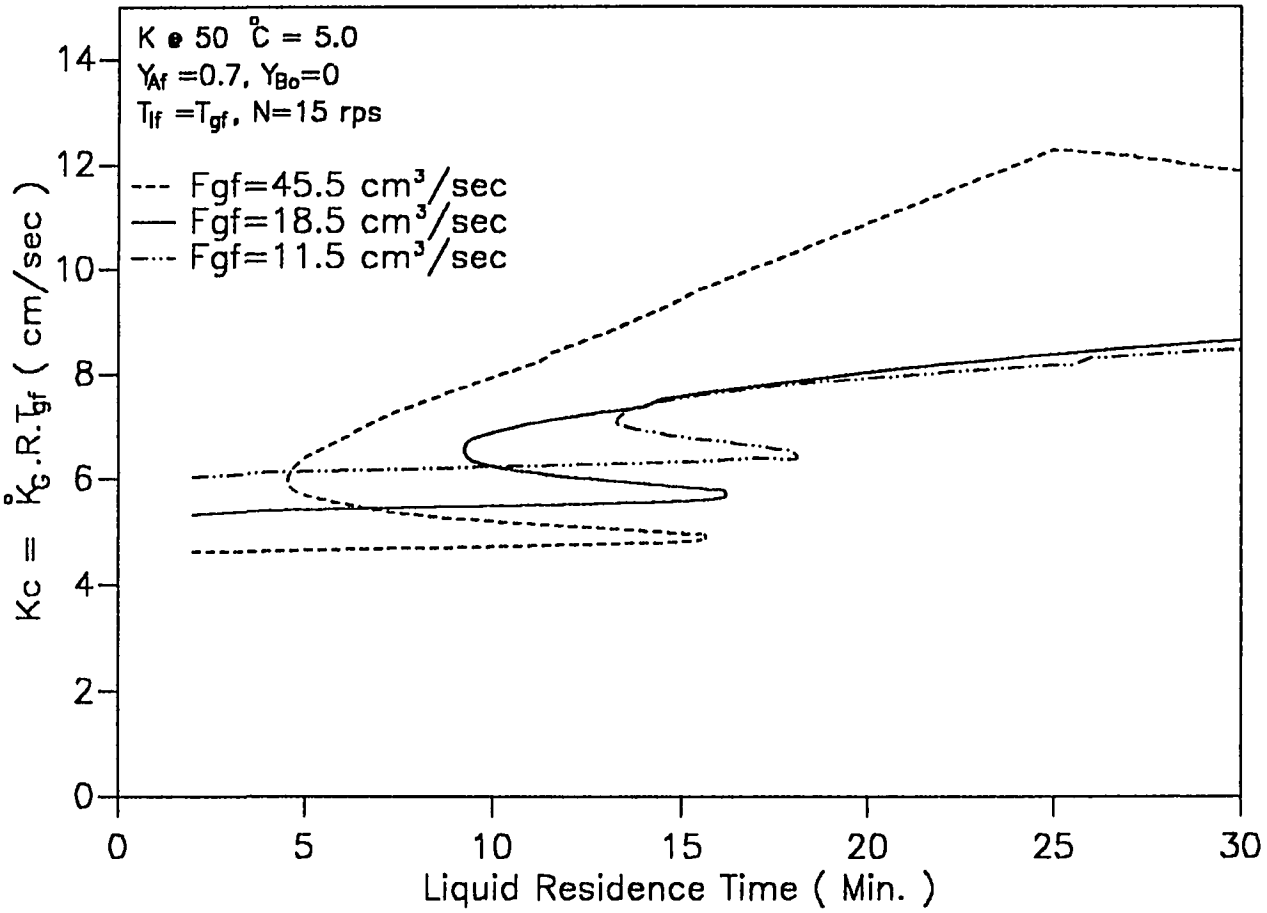

Figure 5.14 Effect of F_{gf} on Gas–Side Mass Transfer Coefficient

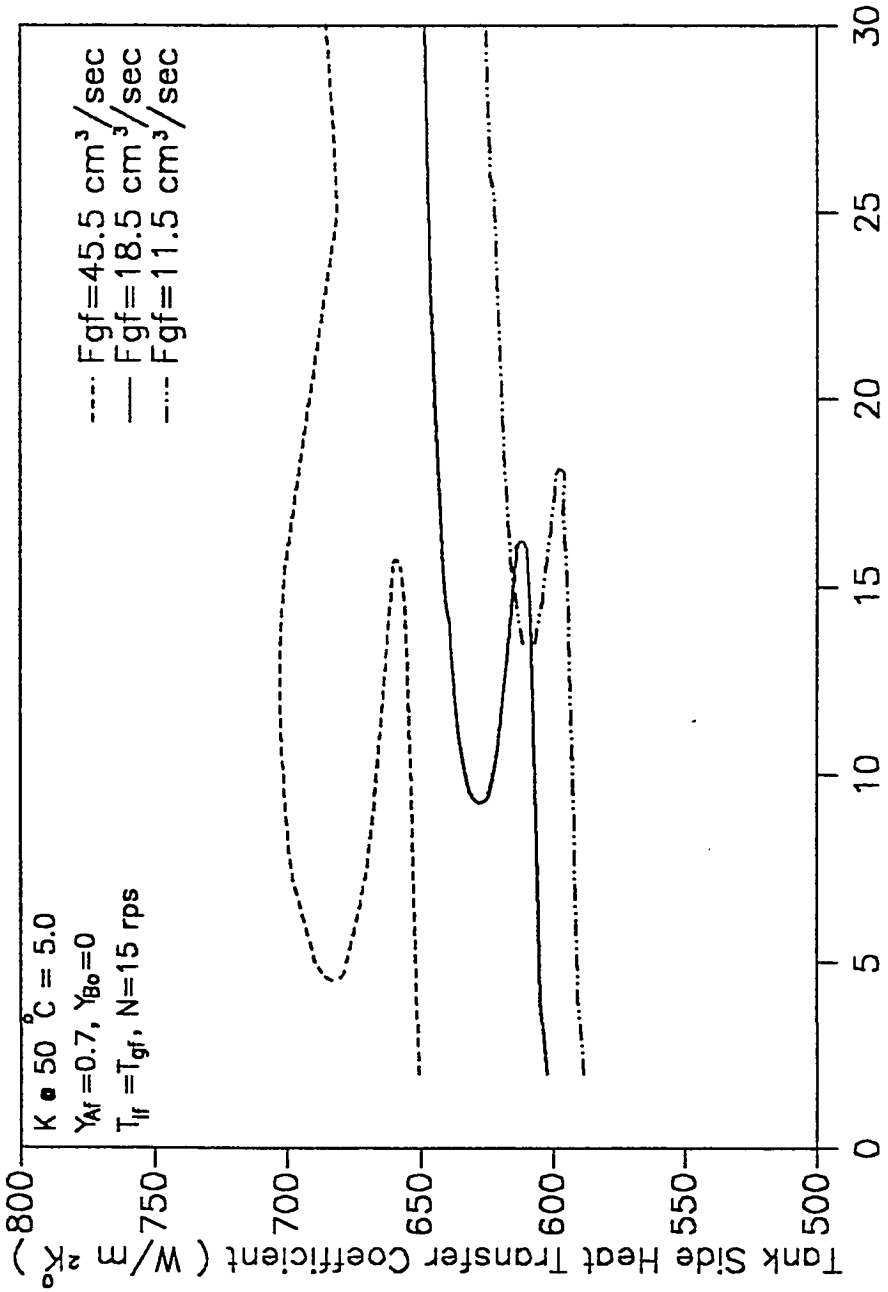

Figure 5.15 Effect of F_{gf} on Tank–Side Heat Transfer Coefficient

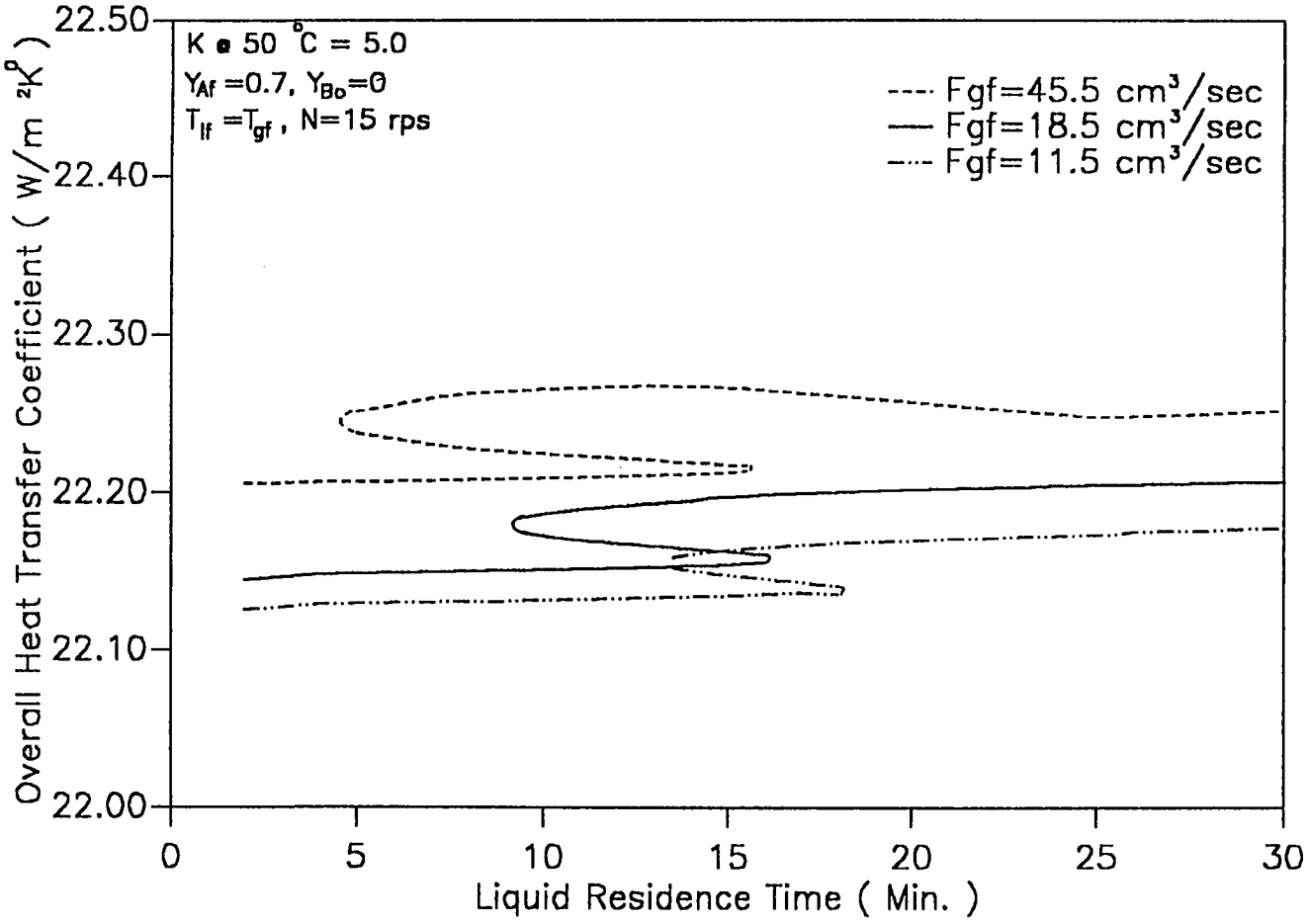

Figure 5.16 Effect of F_{gf} on Overall Heat Transfer Coefficient

influence on these parameters.

5.4.3 Effect of Feed Gas Purity

Effect of feed gas purity on the steady state multiplicity with general second-order kinetics has not been studied even with simplified model. Shaikh and Varma [22] were the first to study the effect of nature of feed gas in case of the fast pseudo-first-order reaction regime. They noted that the likelihood of multiple steady state is strongly dependent on the richness of the gas feed in the reactive species. Numerical simulation results on the effect of feed gas purity with the new and old models for the case of general second order reaction regime are shown in Figures 5.17 to 5.20. It can be seen from these figures that the nature of feed gas has a very strong influence on the occurrence of multiplicity, a decrease in the purity of feed gas moves the system toward the low temperature uniqueness region which is in accordance with the conclusion of Shaikh and Varma [22] based on simplified model.

Figure 5.19 and 5.20 present the effect of feed gas purity with the simplified old model and the new model for the same reaction rate constant. We note, though their behavioral features are similar, the size of the multiplicity region predicted by the old model is much higher as compared to the new model. Moreover, under similar conditions, the old model predicts a change in the multiplicity pattern when the feed gas purity is increased from 70% to 99%, whereas the new model predicts no change in the multiplicity pattern.

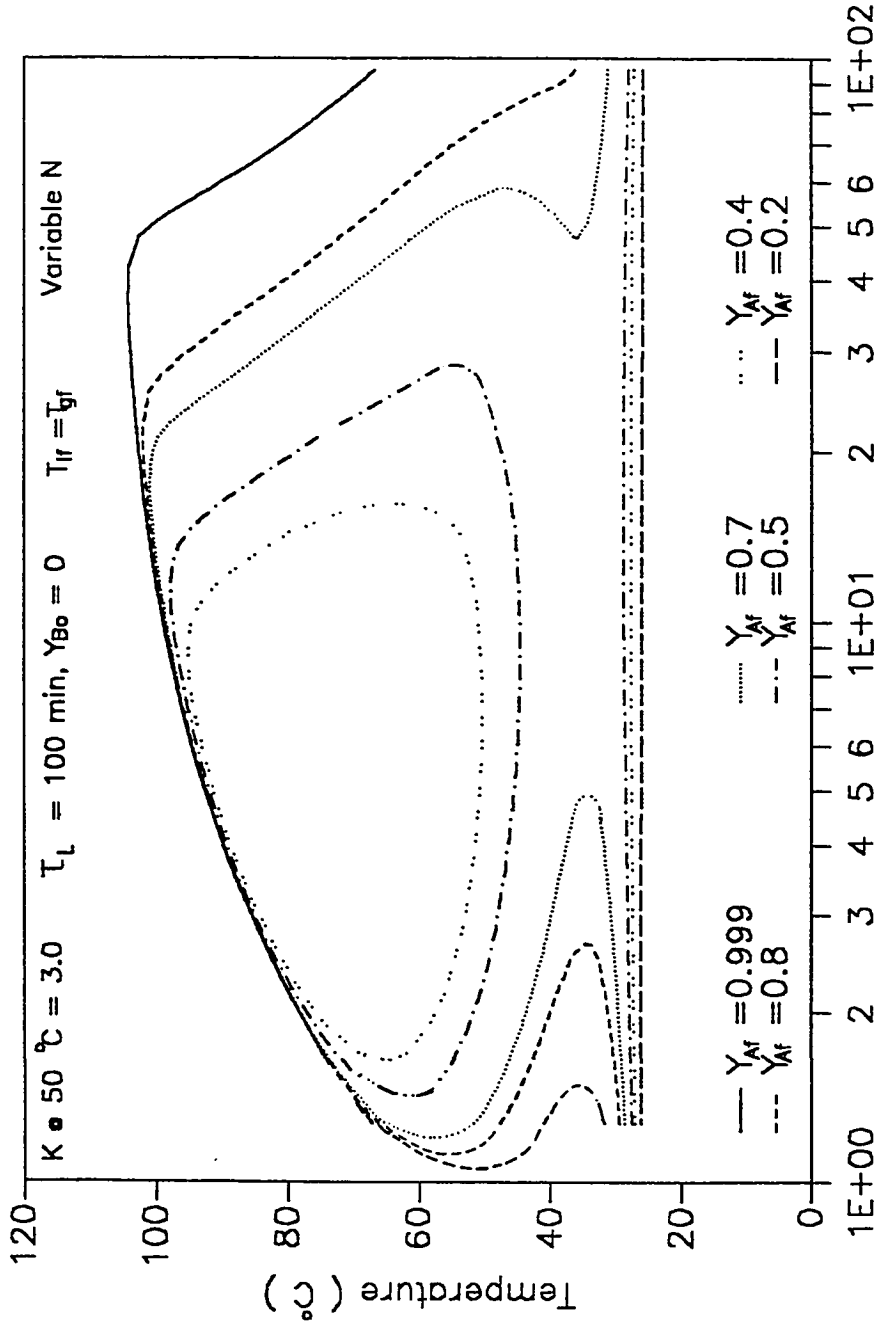

Figure 5.17 Effect of Feed Gas Purity on Steady State Multiplicity

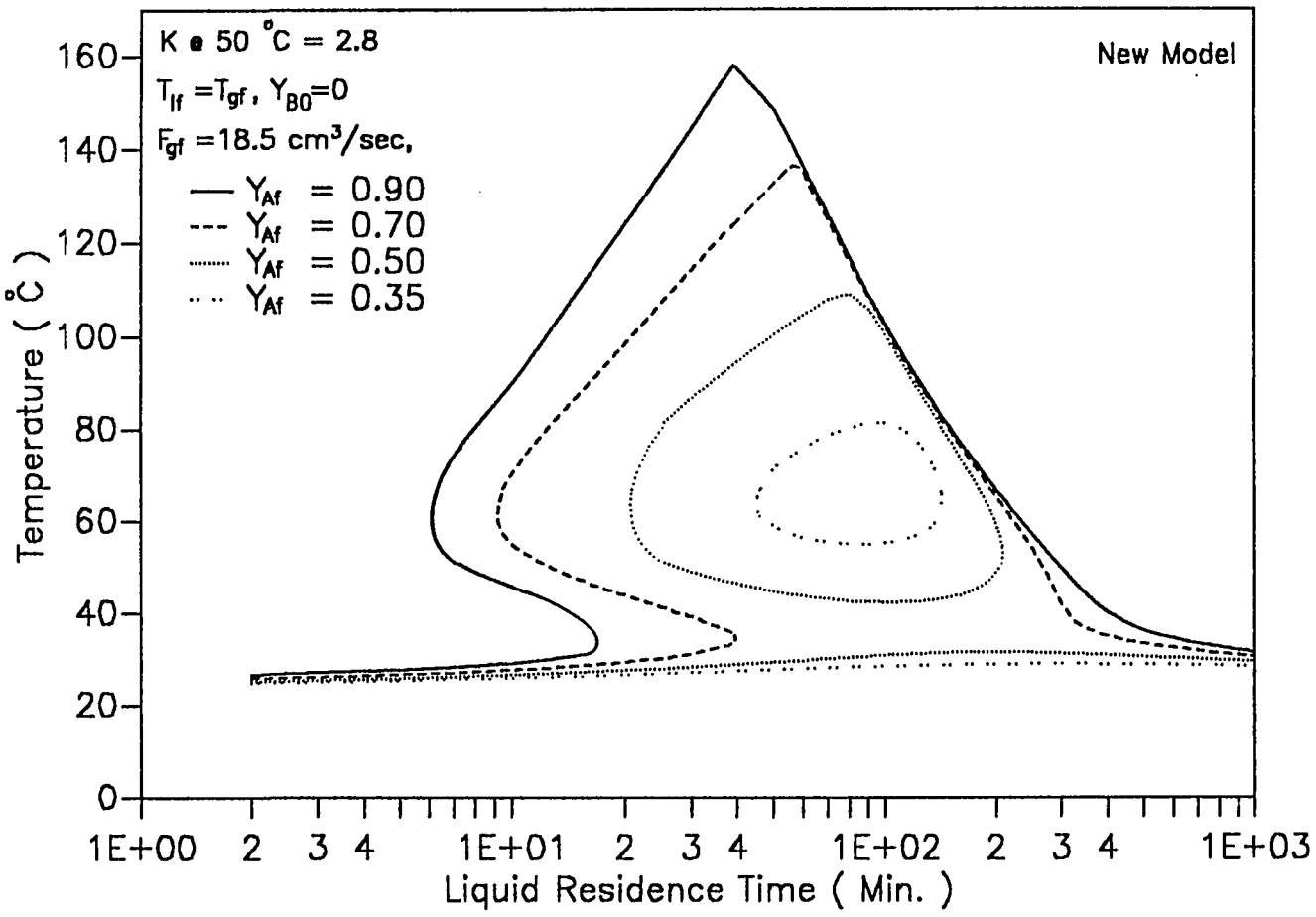

Figure 5.18 Effect of Feed Gas Purity on Steady State Multiplicity

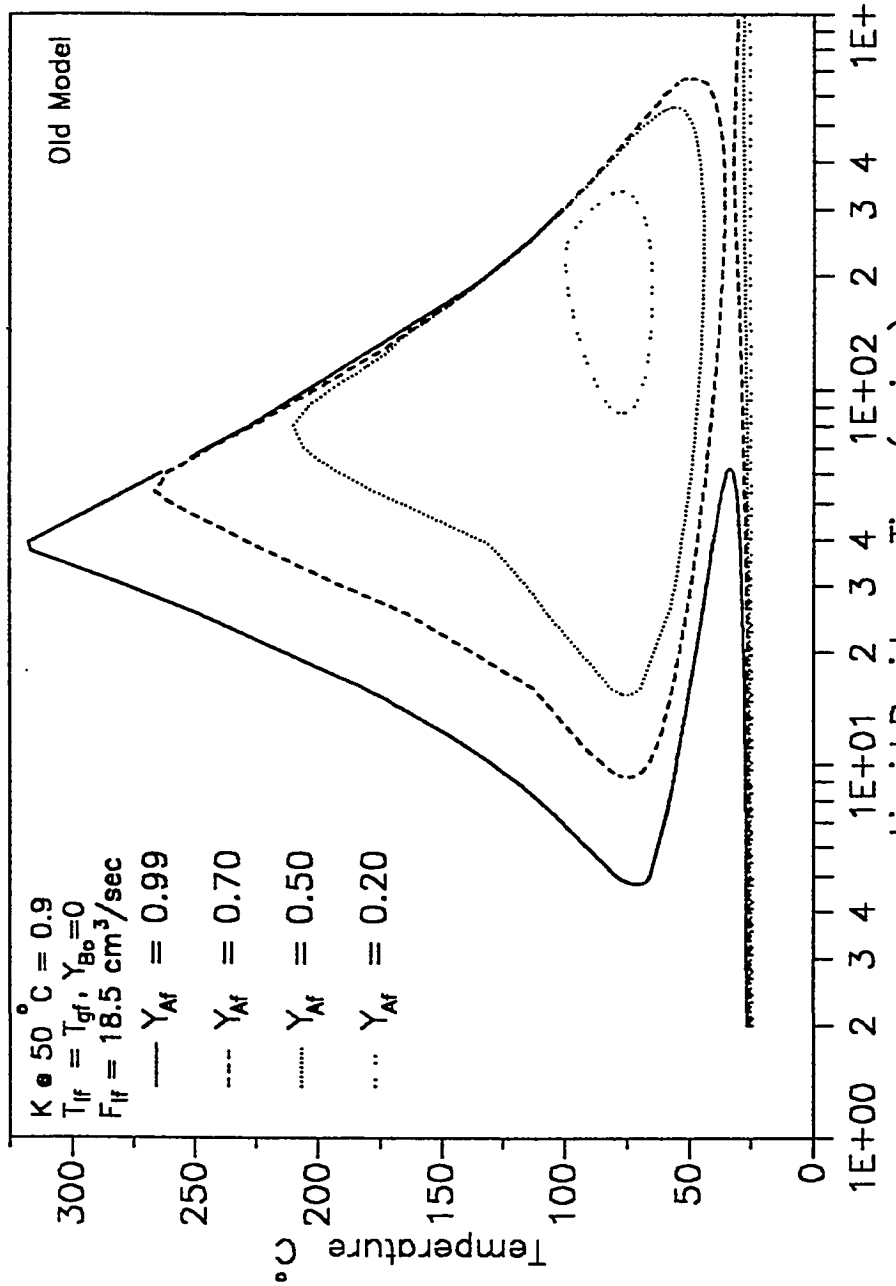

Figure 5.19 Effect of Feed Gas Purity on Steady State Multiplicity Using Old Model

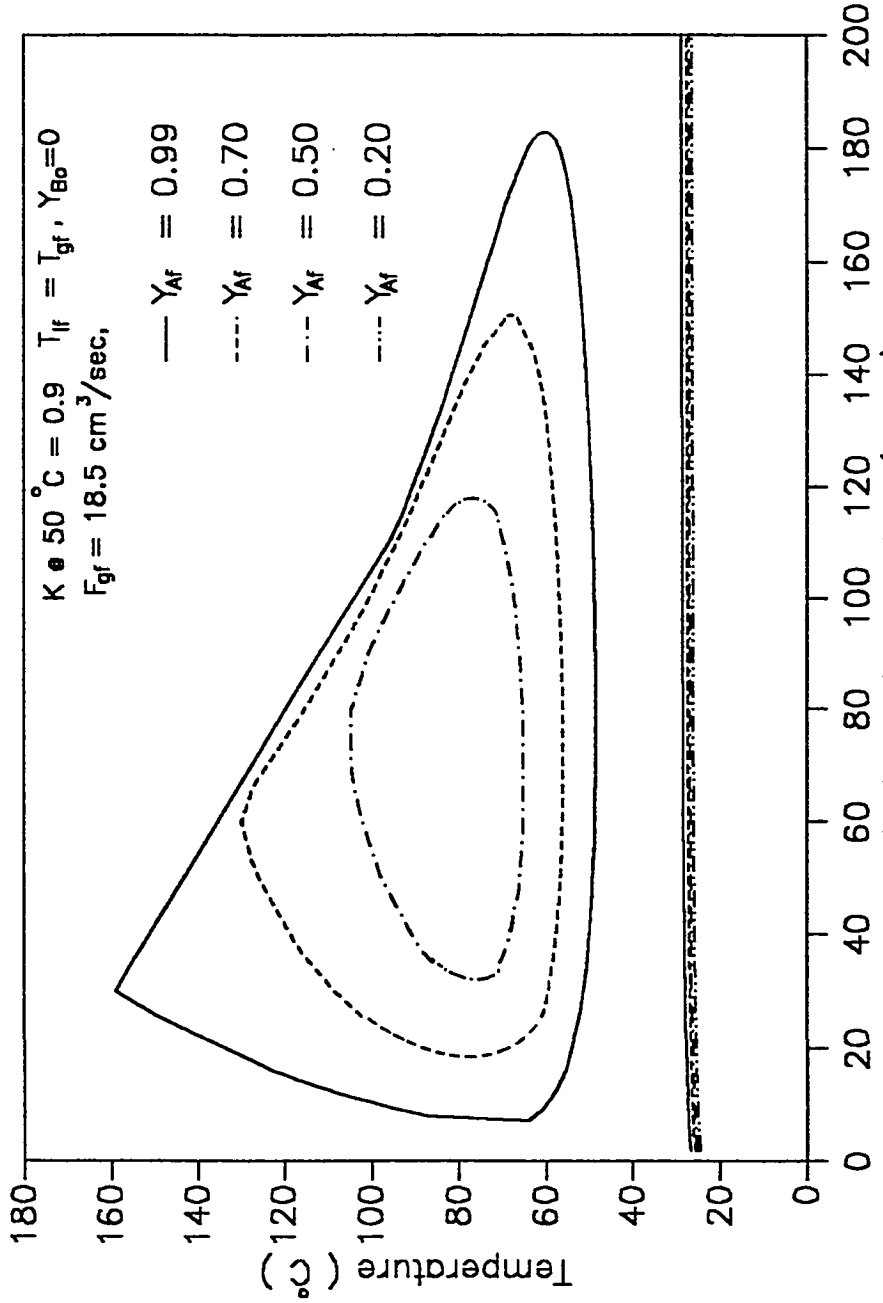

Figure 5.20 Effect of Feed Gas Purity on SSM with Variable Liquid Residence Time Using New Model

5.4.4 Effect of Feed Gas Temperature

The study of the effect of feed gas temperature on the steady state behavior of the reactor becomes important in cases where the ratio of the volumetric flow rate of the gas to that of liquid and the pressures are very high. Singh et al. [21] were the first to study the effect of feed gas temperature on the steady state behavior of a gas-liquid CSTR with fast pseudo first order kinetics. They pointed out that there exists a minimum feed gas temperature beyond which uniqueness is assured. Shaikh and Varma [22] made a more realistic analysis of the effect of feed gas temperature by introducing the nature of feed gas in the analysis. These authors also studied the case of fast pseudo-first-order kinetics and concluded that effect of feed gas temperature on the multiplicity depends on the nature of feed gas, a parameter not considered by Singh and et al. [21]. However, no study has been done on the effect of feed gas temperature with general second-order kinetics, because in this case it is not possible to derive an analytic criteria for multiplicity as in the case of the fast reaction regime and numerical simulation is necessary.

Figures 5.21 and 5.22 show the effect of feed gas temperature on steady state multiplicity by changing liquid and gas residence times, respectively. According to Figure 5.21, the upper temperature branch is most sensitive to the change in feed gas temperature, with the increase in feed gas temperature the upper temperature moves downward and the lower temperature branch moves upward, whereas the intermediate branch is more or less unaffected. This confirms the conclusions drawn by Singh et al. [21]. During our simulation

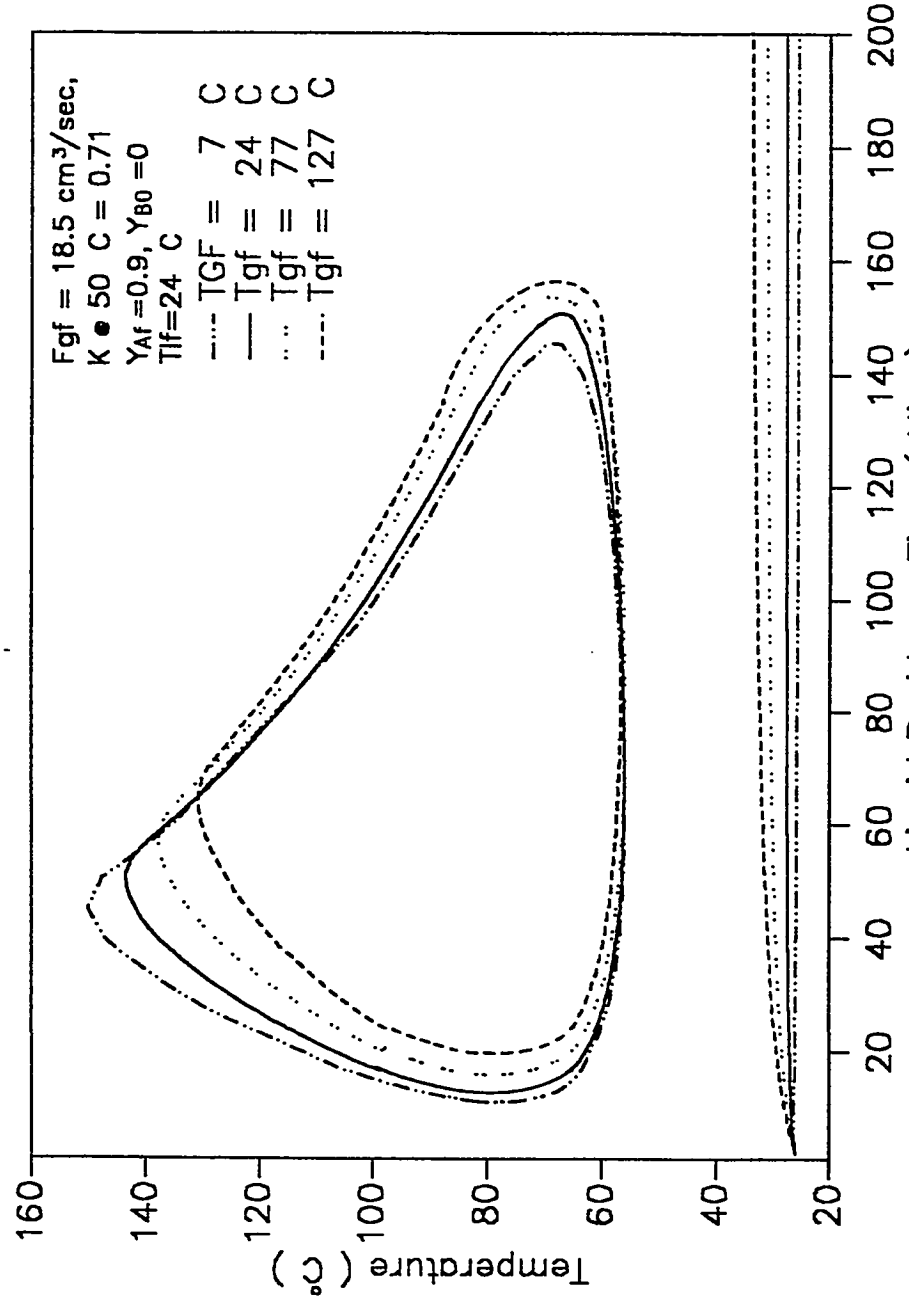

Figure 5.21 Effect of Feed Gas Temperature on Steady State Multiplicity with Variable Liquid Residence Time

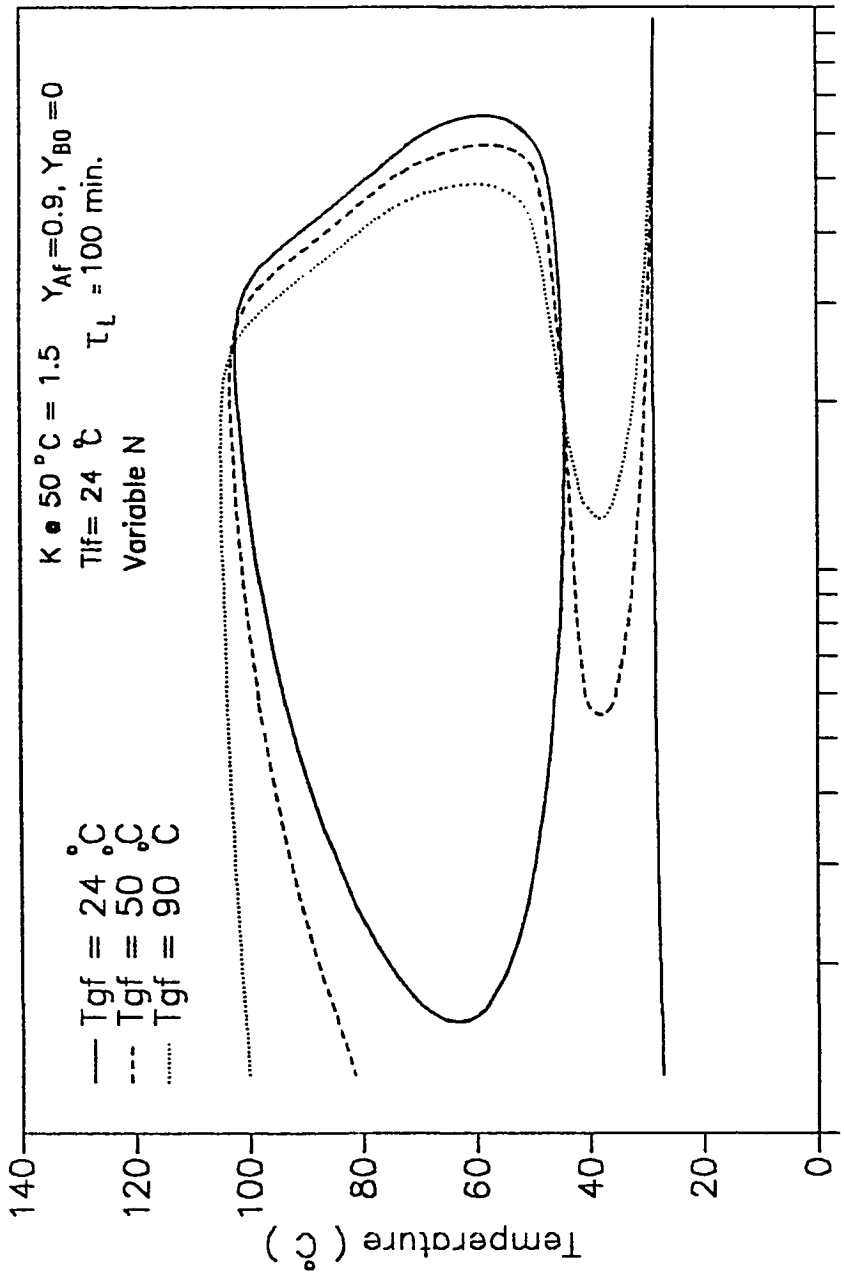

Figure 5.22 Effect of Feed Gas Temperature on SSMwith Variable Gas Residence Time

study, we noticed that the effect of feed gas temperature on the multiplicity behavior of the reactor is independent of feed gas purity which is not in accordance with the analysis of Shaikh and Varma [22]. However further investigation needs to be done to prove it conclusively. It should noted that the nature of feed gas greatly influences the multiplicity patterns as discussed in the previous section. A better picture of the effect of feed gas temperature on multiplicity is obtained if the steady state temperature is plotted against the gas residence time, as shown in Figure 5.22, with increase in feed gas temperature the multiplicity pattern is changed from an *isola* to an inverted-S-shaped multiplicity. It can be seen from Figure 5.22, that at higher ratios of volumetric flow rates of gas to liquid, a high temperature unique steady state is obtained indicating that in such a case a significant amount of heat is contributed by the gas phase. At a very low ratio of flow rates, the effect of feed gas temperature on the steady state behavior of the reaction is negligible. Figures 5.21 and 5.22 show a shift in the region of multiplicity as the feed gas temperature is increased. At higher feed gas temperature the multiplicity starts and ends at higher liquid residence time, whereas with respect to gas residence time, at higher feed gas temperature, the region of multiplicity shrinks.

Figures 5.23 and 5.24 show the effect of liquid feed temperature on steady state multiplicity with change in liquid and gas residence times. These graphs indicate that steady state behavior of a gas-liquid CSTR is <u>*very sensitive*</u> to liquid feed temperature, which is due to the higher heat carrying capacity of liquid phase as compared to the gas phase. By increasing the liquid feed temperature multiplicity is changed from an *isola* to a high temperature unique

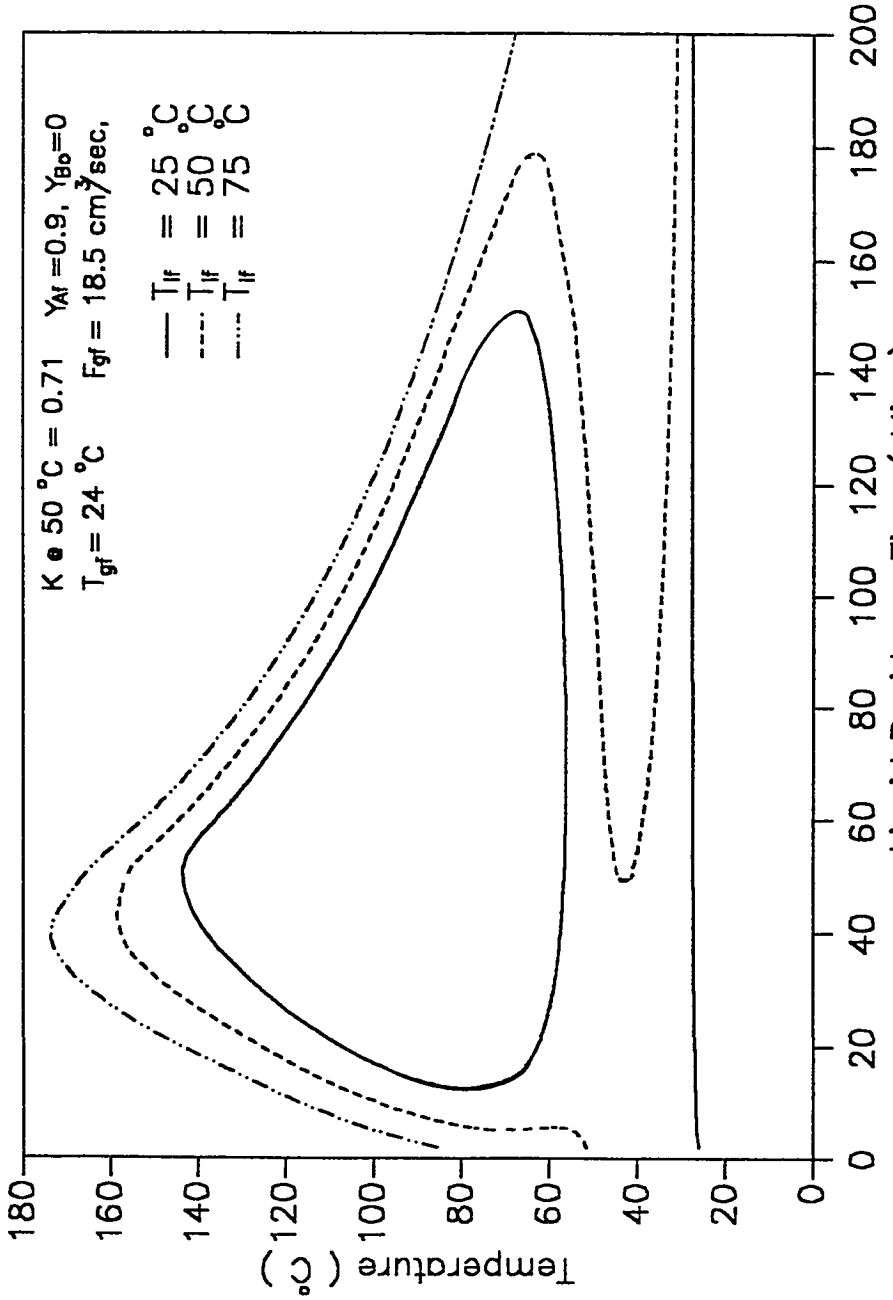

Figure 5.23 Effect of Liquid Feed Temperature on Steady State Multiplicity

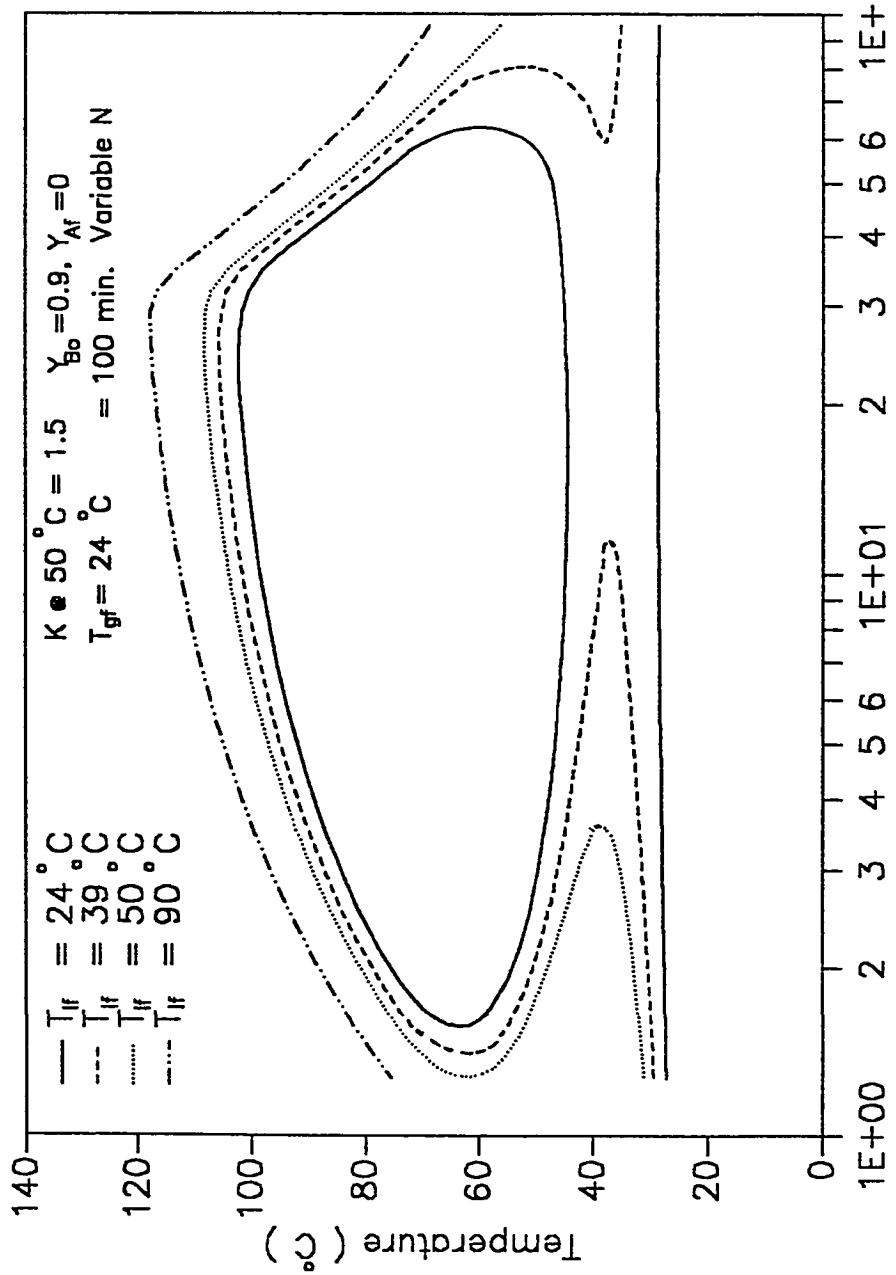

Figure 5.24 Effect of Liquid Feed Temperature on SSM with Variable Gas Residence Time

steady state.

5.4.5 Effect of Impeller Speed

Figures 5.25 and 5.26 show the effect of impeller speed on steady state multiplicity with respect to gas and liquid residence times. We note from Figure 5.25 that the region of multiplicity expands with the increase in impeller speed towards higher gas residence time. We also note that the increase in impeller speed has no effect on the multiplicity in case of relatively higher gas flow rates, i.e. lower gas residence time. This can be explained as follows. Firstly, at higher gas residence times, i.e. at lower gas flow rates, an increase in the impeller speed increases the value of dimensionless parameter H_p in Equation (3.18), indicating that in such a condition the contribution of heat dissipated by agitation becomes significant in the over all heat build-up of the system. Secondly, at low gas flow rates, the values of interfacial area, gas hold-up and the mass transfer coefficients are much higher at high impeller speed compared to low impeller speed. Therefore, a change in the degree of agitation may change the regions and patterns of multiplicity due to the change in rate of reaction caused by the combined effect of above two reasons.

Figure 5.26 shows the effect of impeller speed on the steady state temperature with respect to liquid residence time. Here again we note that the effect of impeller speed is more pronounced in the region of low gas to liquid flow rate ratios due to the same reasons discussed above. We further note that there exists a maximum impeller speed beyond which the multiplicity region is

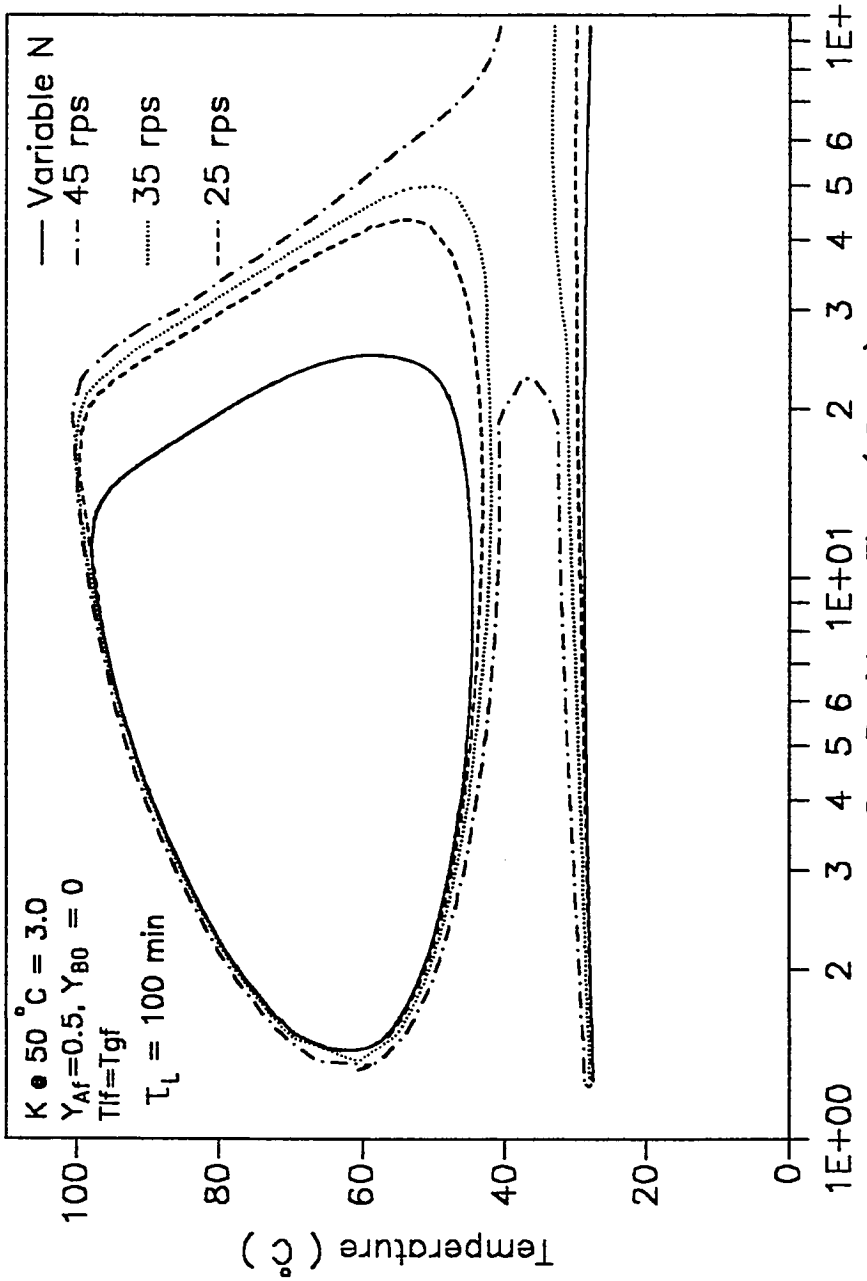

Figure 5.25 Effect of Impeller Speed on Steady State Multiplicity with Variable Gas Residence Time

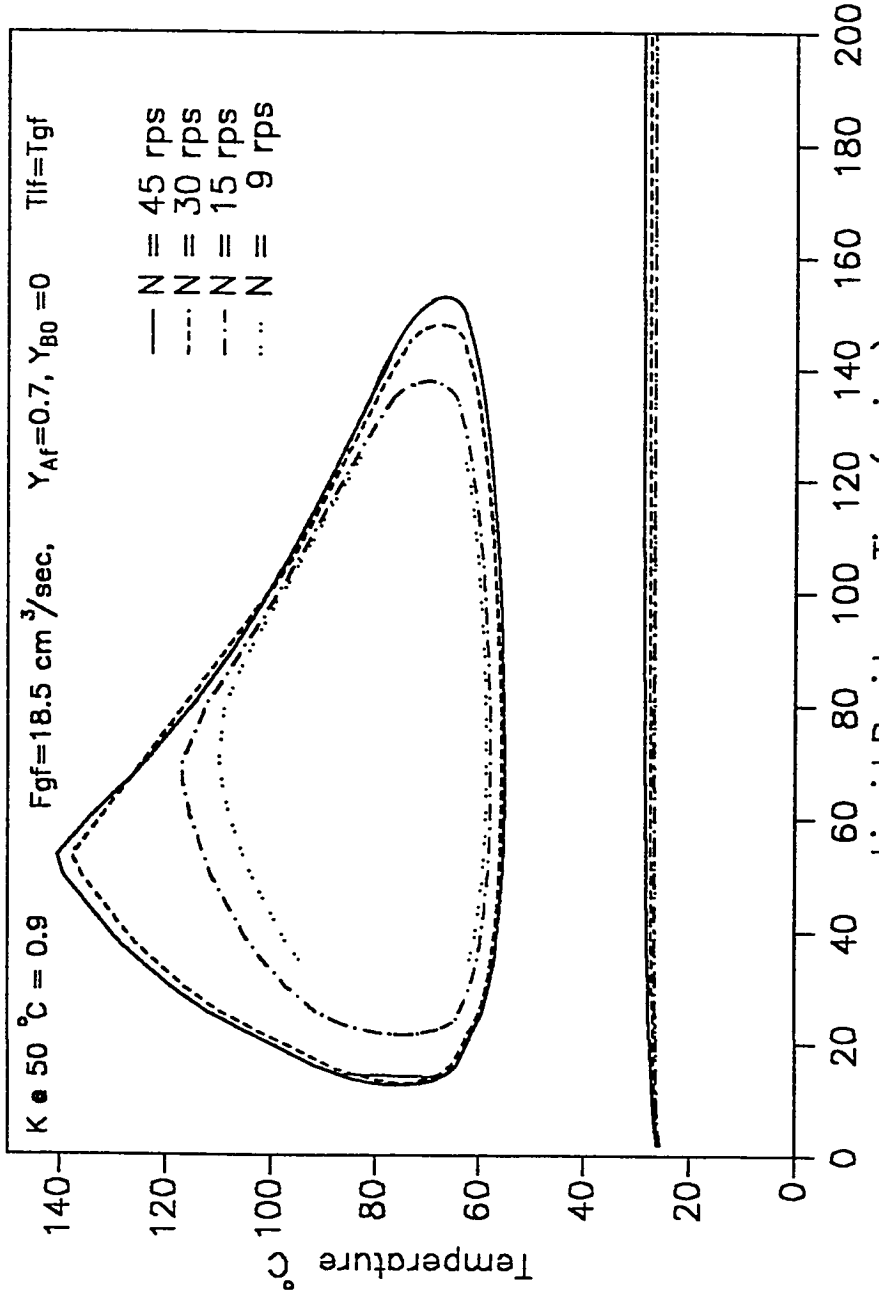

Figure 5.26 Effect of Impeller Speed on Steady State Multiplicity with Variable Liquid Residence Time

not affected by the impeller speed.

5.5 Model Discrimination : Old Versus New Model

5.5.1 Variable Gas Residence Time

Figure 5.27 presents a comparison of the multiplicity regions predicted by the new model developed in this thesis and an old model used by Shaikh et al. [26]. It can be seen from Figure 5.27 that the region in the parameter space of K versus τ_G for which the new model predicts multiplicity is much smaller compared to that predicted by simplified model. A comparison of model predictions in the high temperature uniqueness region is shown in Figure 5.28. We see that a much higher temperature is predicted by the old model because, as will be shown later, the change in operating conditions greatly influences the hydrodynamic and transport parameters which in turn affect the rates of heat generation and heat removal of the system.

A comparison of various multiplicity patterns predicted by new and simplified model is given in Figures 5.29 to 5.31. It is clear from these graphs that new model predicts all three types of multiplicity patterns reported before. Note that in all the cases shown in Figures 5.29 to 5.31, the regions and the patterns of multiplicity predicted by new model are *remarkably different* from the predictions of simplified model. For example in Figure 5.30, new model predicts a mushroom-type multiplicity whereas old model predicts a unique steady state. We also note that in all the cases presented here, the upper temperature branch predicted by new model is always lower than that predicted

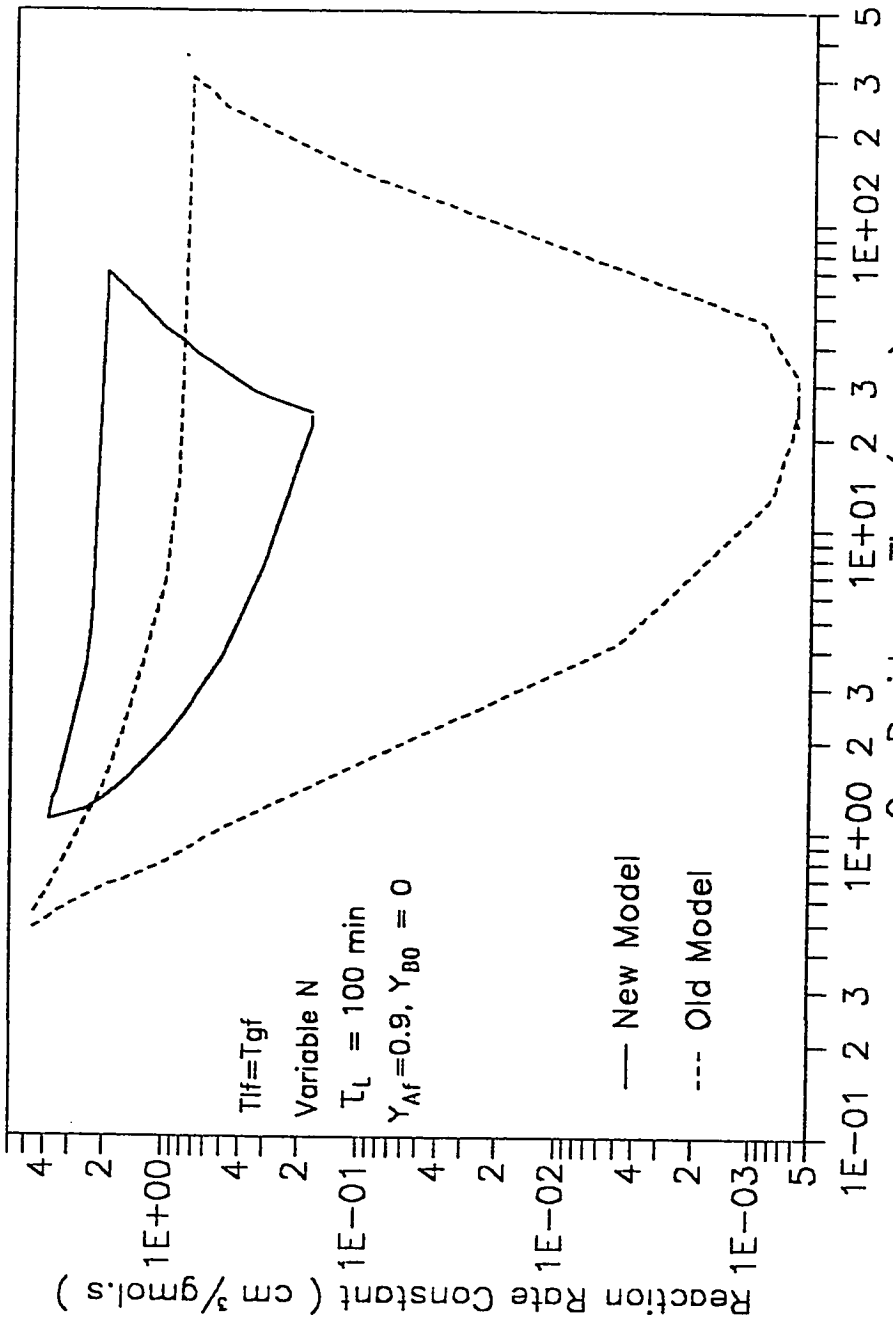

Figure 5.27 Comparison of the Multiplicity Regions of New and Old Models

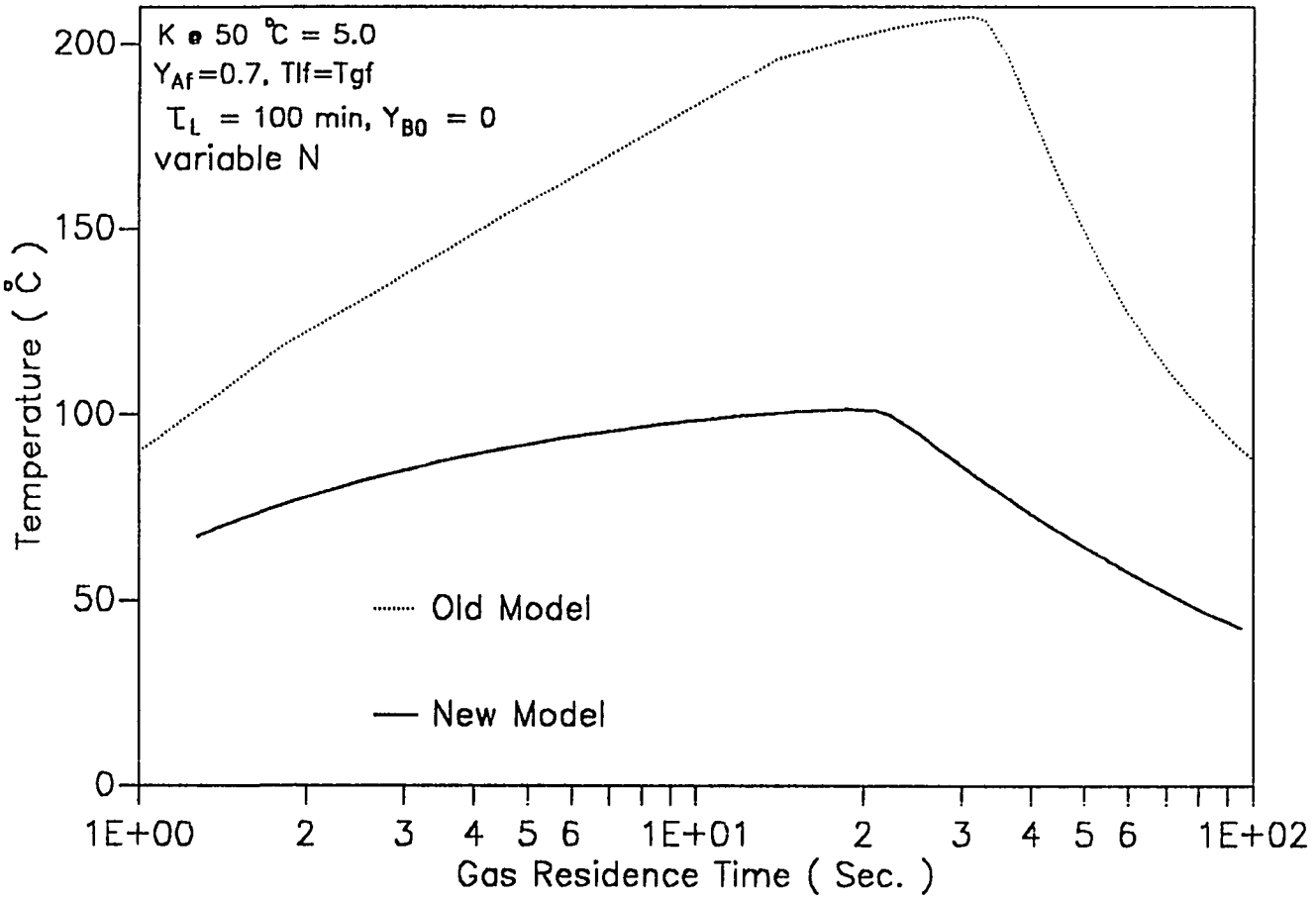

Figure 5.28 Comparison of Steady State Temperatures Predicted by New and Old Models

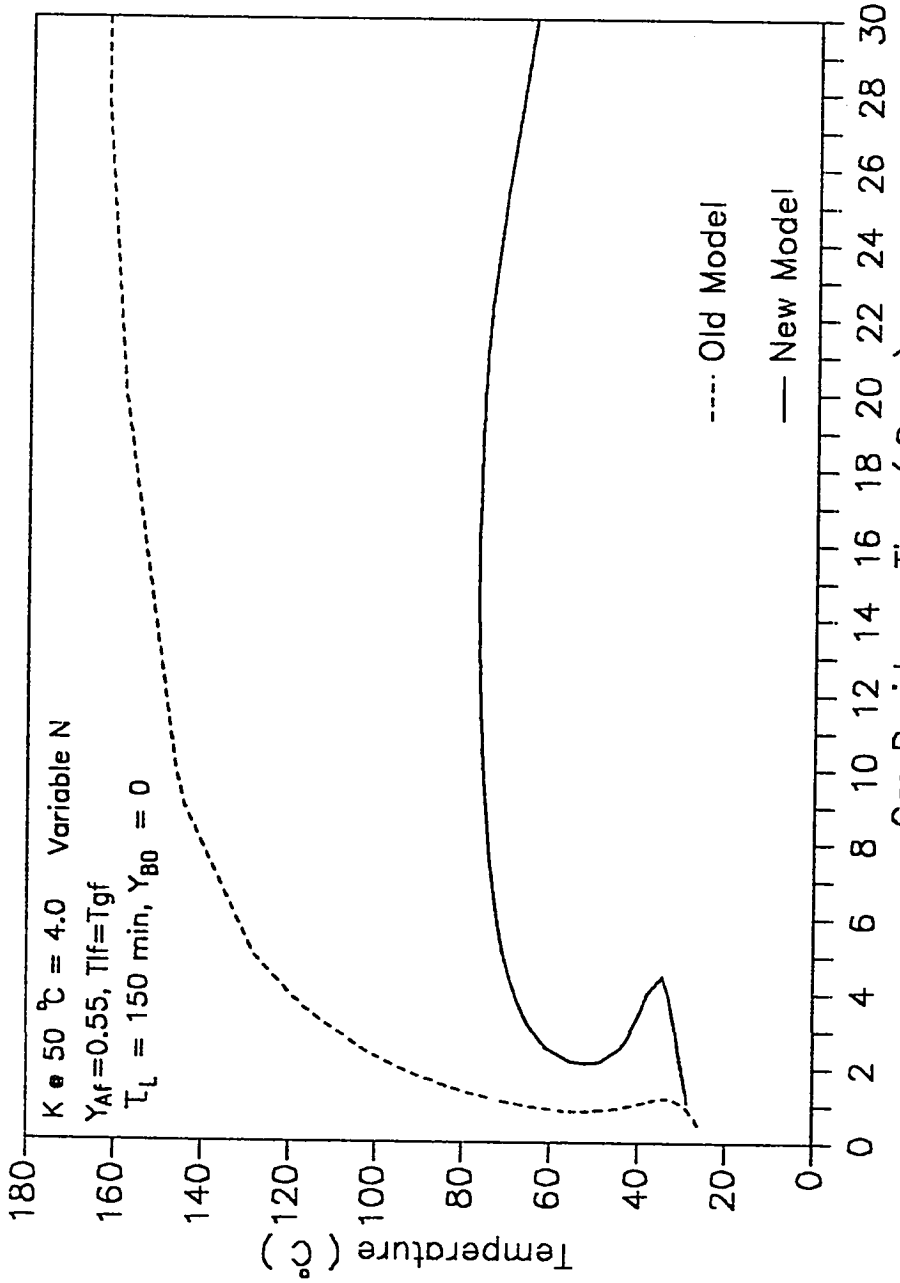

Figure 5.29 Comparison of Steady State Temperature Predicted by New and Old Models

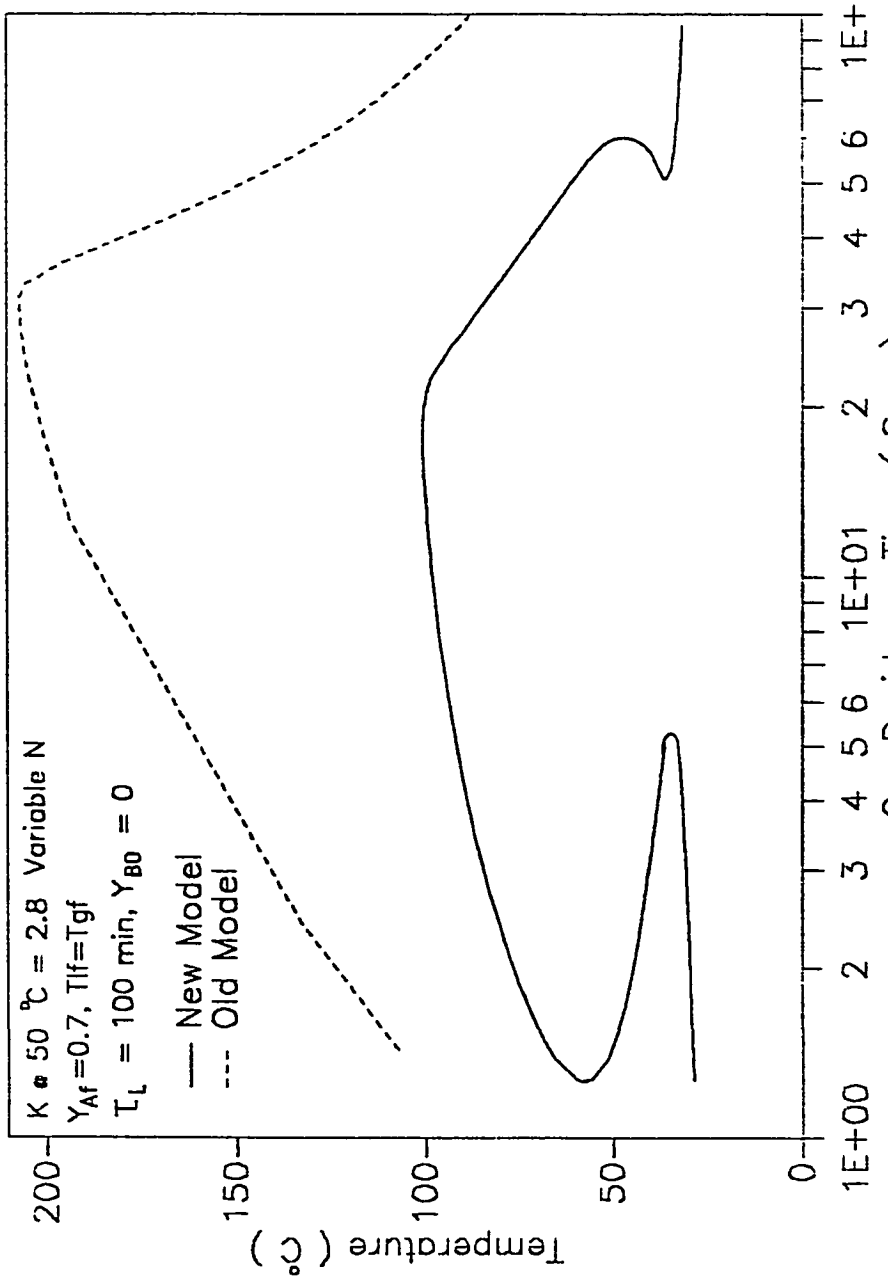

Figure 5.30 Comparison of Steady State Temperatures Predicted by New and Old Models

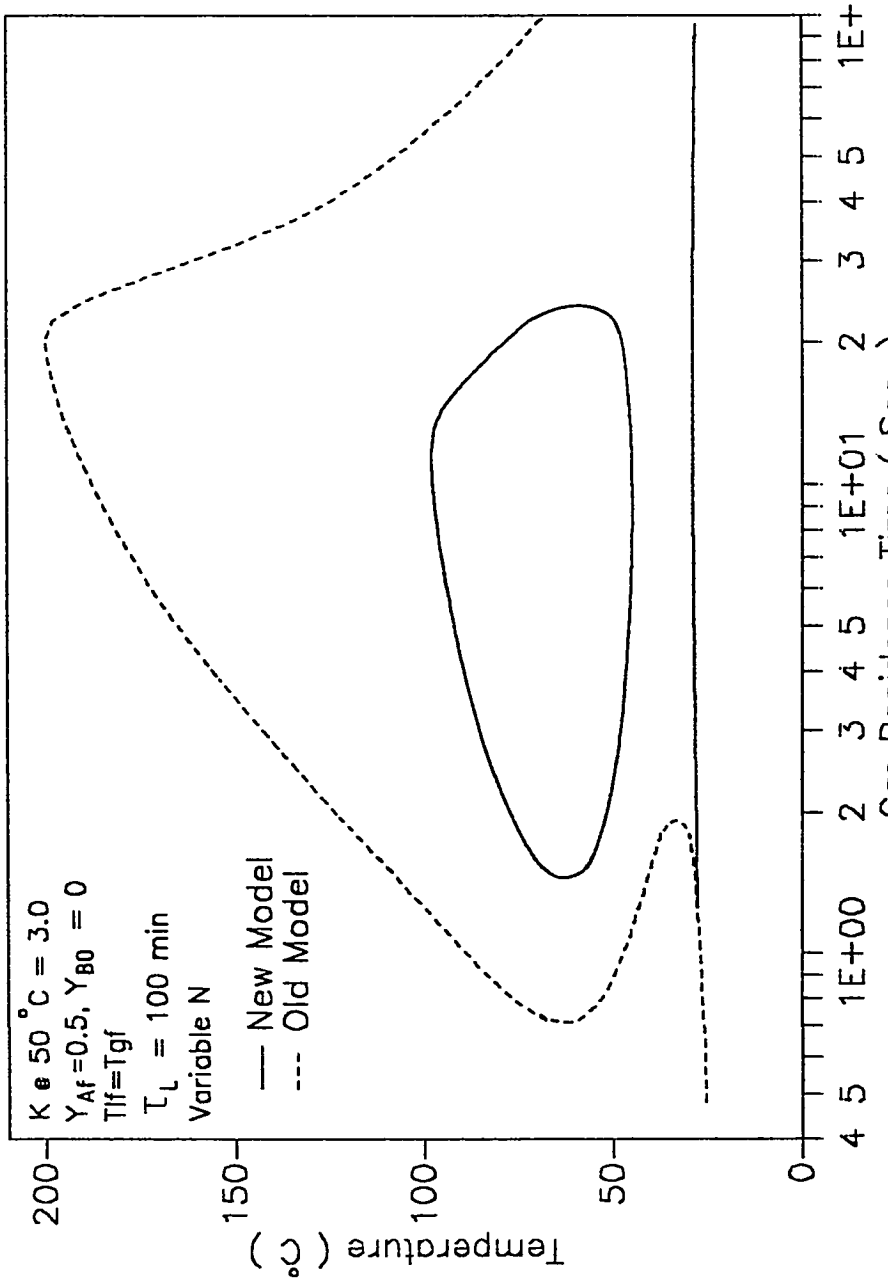

Figure 5.31 Comparison of Steady State Temperatures Predicted by New and Old Models

by simplified model. Such a large difference between the predictions of the two models is due to the fact that the new model, which has been developed to represent a more realistic situation, (by combining reaction kinetics and interphase mass transfer with gas-liquid dispersion, power dissipation, bubble behavior and reactor and impeller geometry, and by relaxing most of the crucial assumptions of the simplified model) predicts significantly different values of hydrodynamic and transport parameters than those used in the simulation based on the simplified model. Also, the simulation results of the new model show a great variation in the values of these parameters as the operating conditions (i.e., the gas flow rate) and the temperature change. This can be further clarified by analysing the behavior of various hydrodynamic, transport and other important dimensionless parameters with respect to change in gas residence time. A discussion on the behavior of these variables corresponding to the case shown in Figure 5.31 is presented below.

Figure 5.32 shows that in a practical situation when the gas flow rate is decreased the minimum impeller speed to achieve complete gas dispersion is also decreased. As a consequence the specific power input to the reaction medium, which along with the superficial gas velocity has a strong influence on most of the hydrodynamic and transport parameters, is significantly reduced as shown in Figure 5.33. The effect of the these changes on various parameters is illustrated in Figures 5.34 to 5.38. From these plots we note that the values of interfacial area, gas hold-up, mass and heat transfer coefficients predicted by the new model are quite different than those used with the simplified model and they show a definite variation with respect to the operating variables. Thus, it is

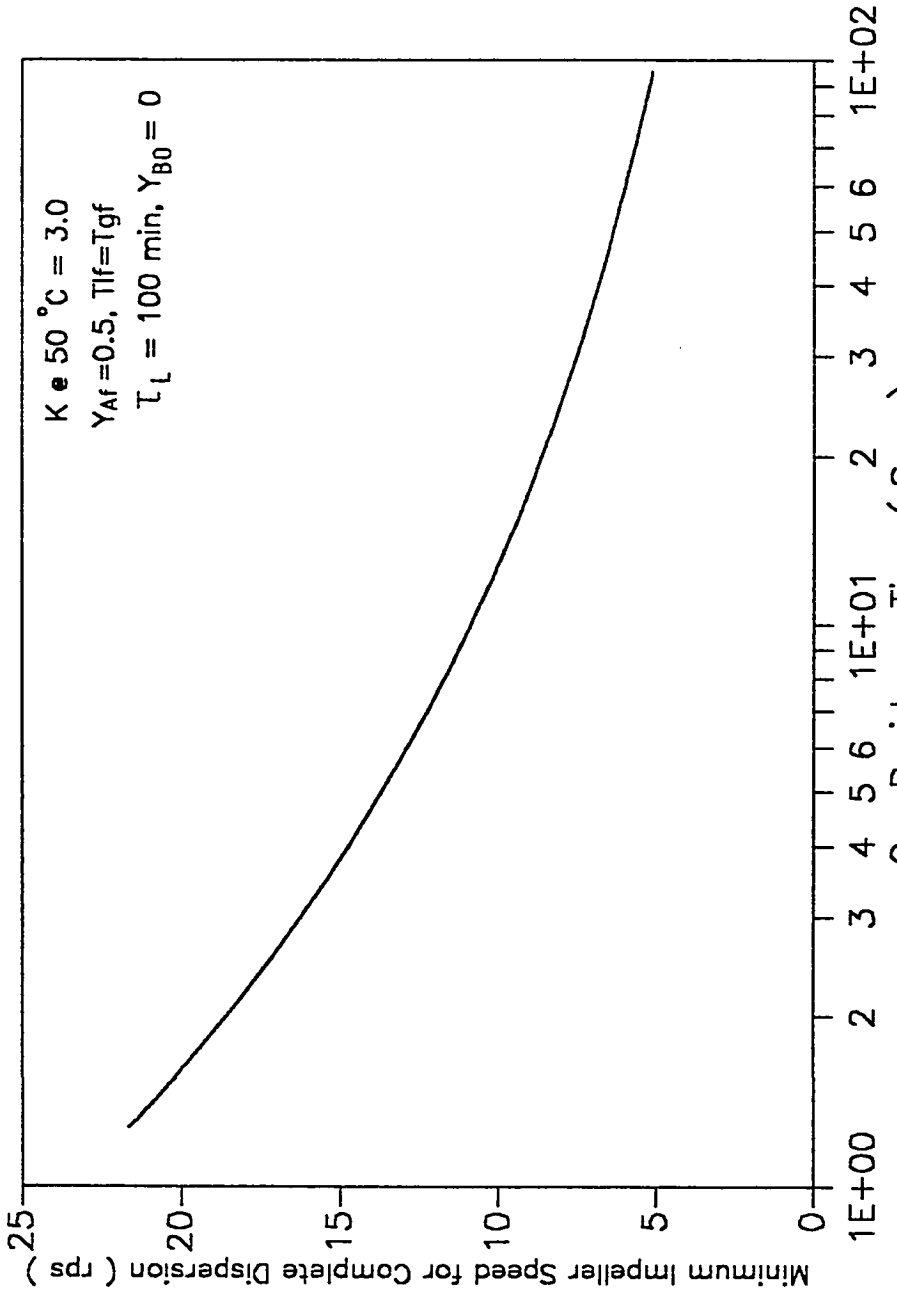

Figure 5.32 Minimum Impeller Speed versus Gas Residence Time

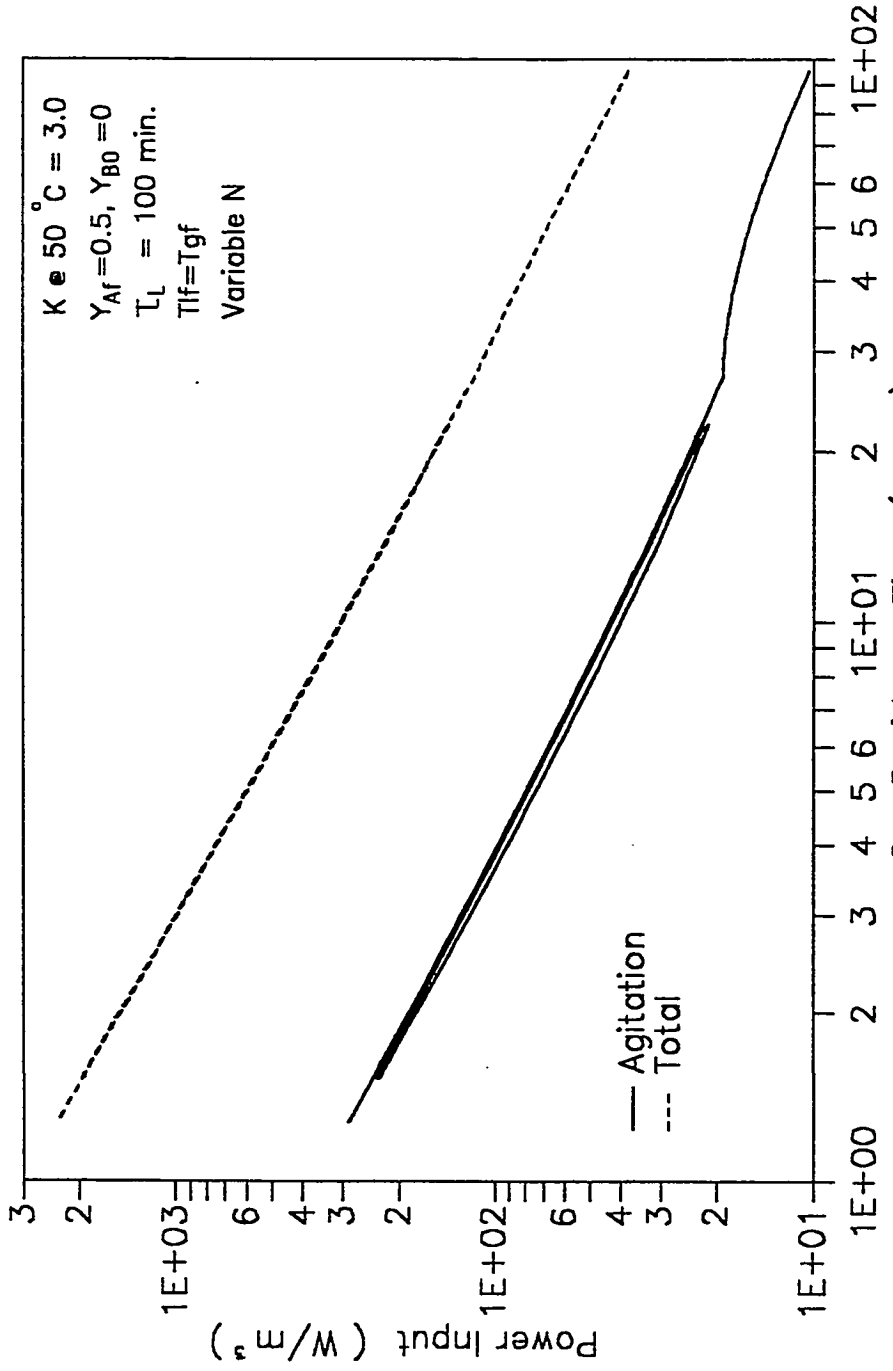

Figure 5.33 Power Input versus Gas Residence Time

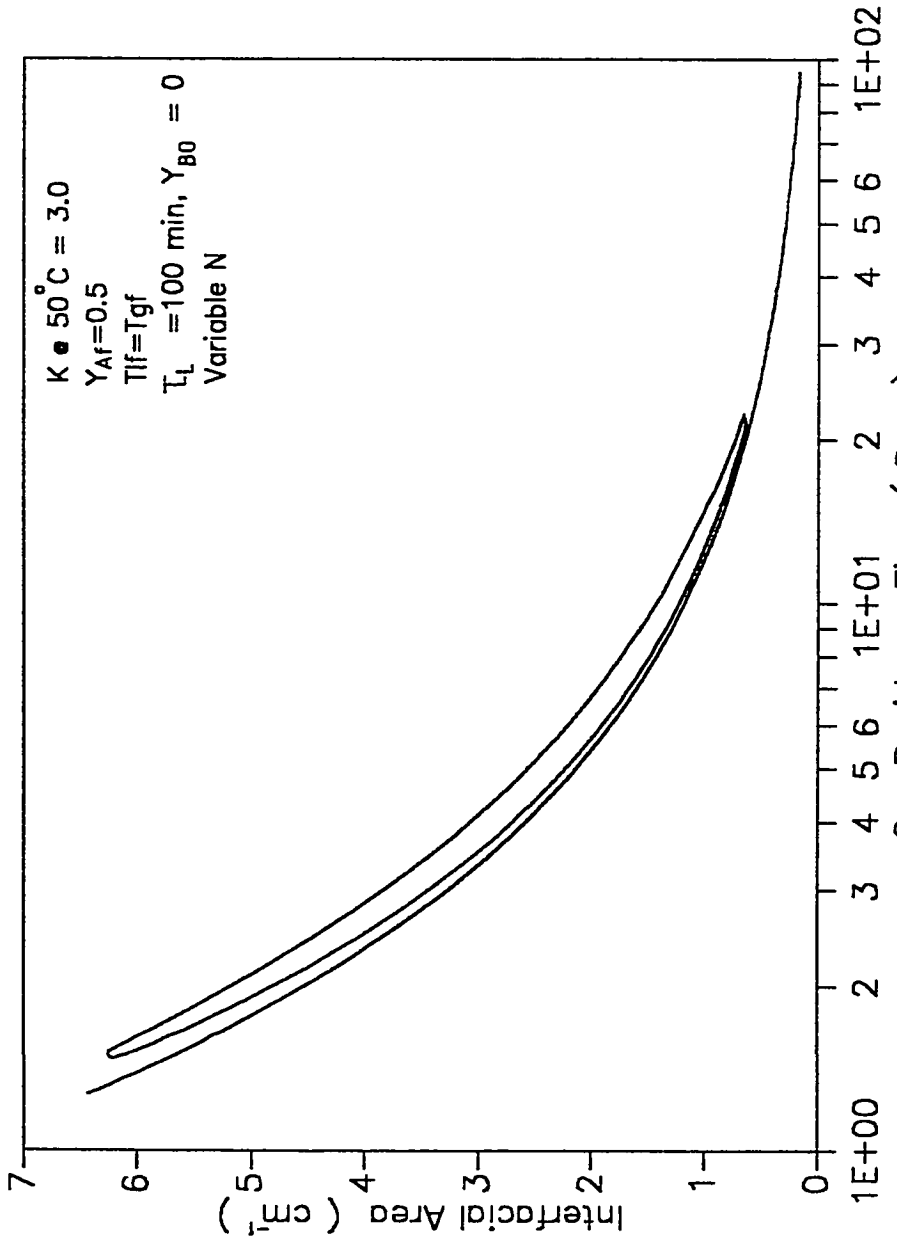

Figure 5.34 Interfacial Area versus Gas Residence Time

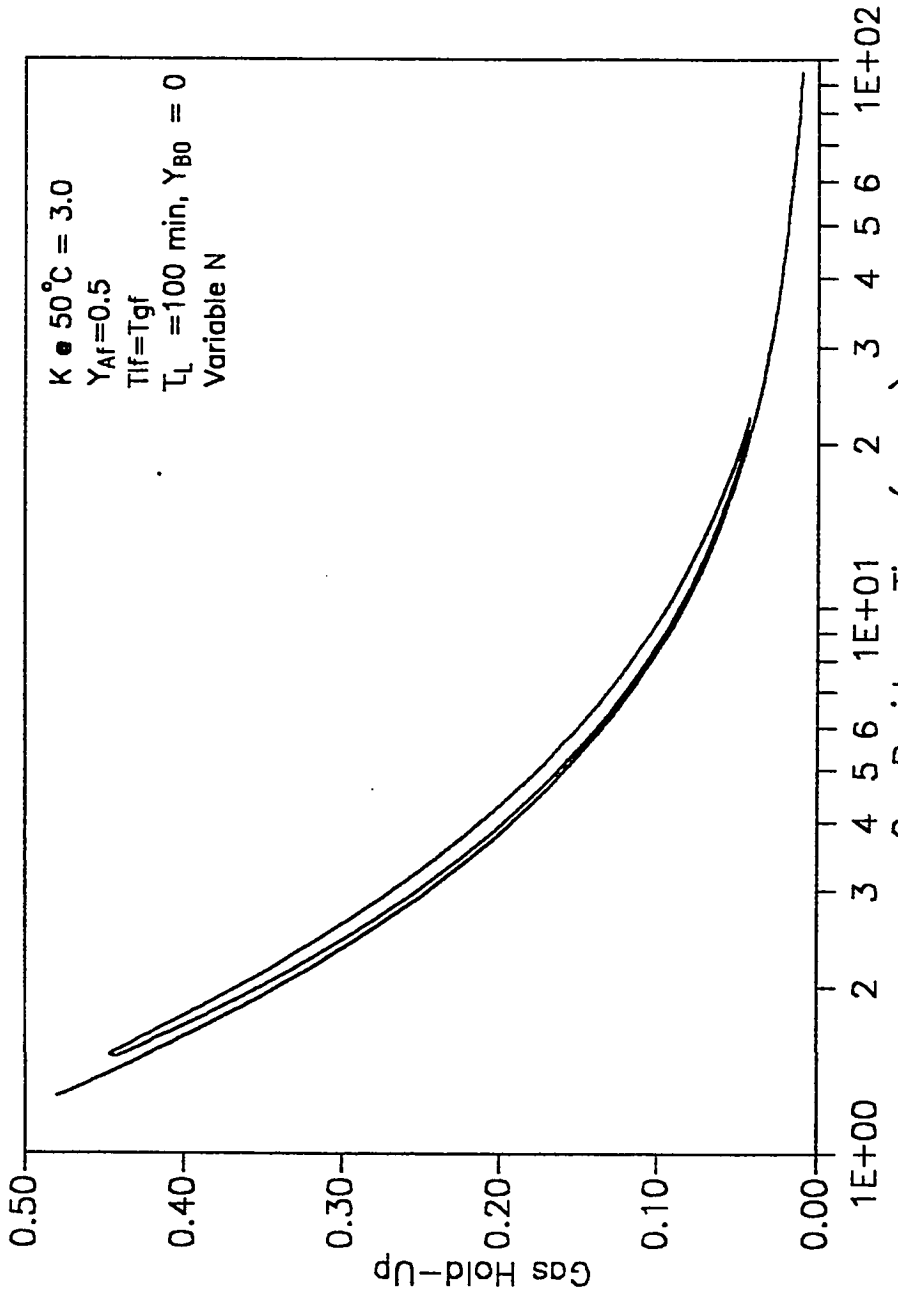

Figure 5.35 Gas Holdup versus Gas Residence Time

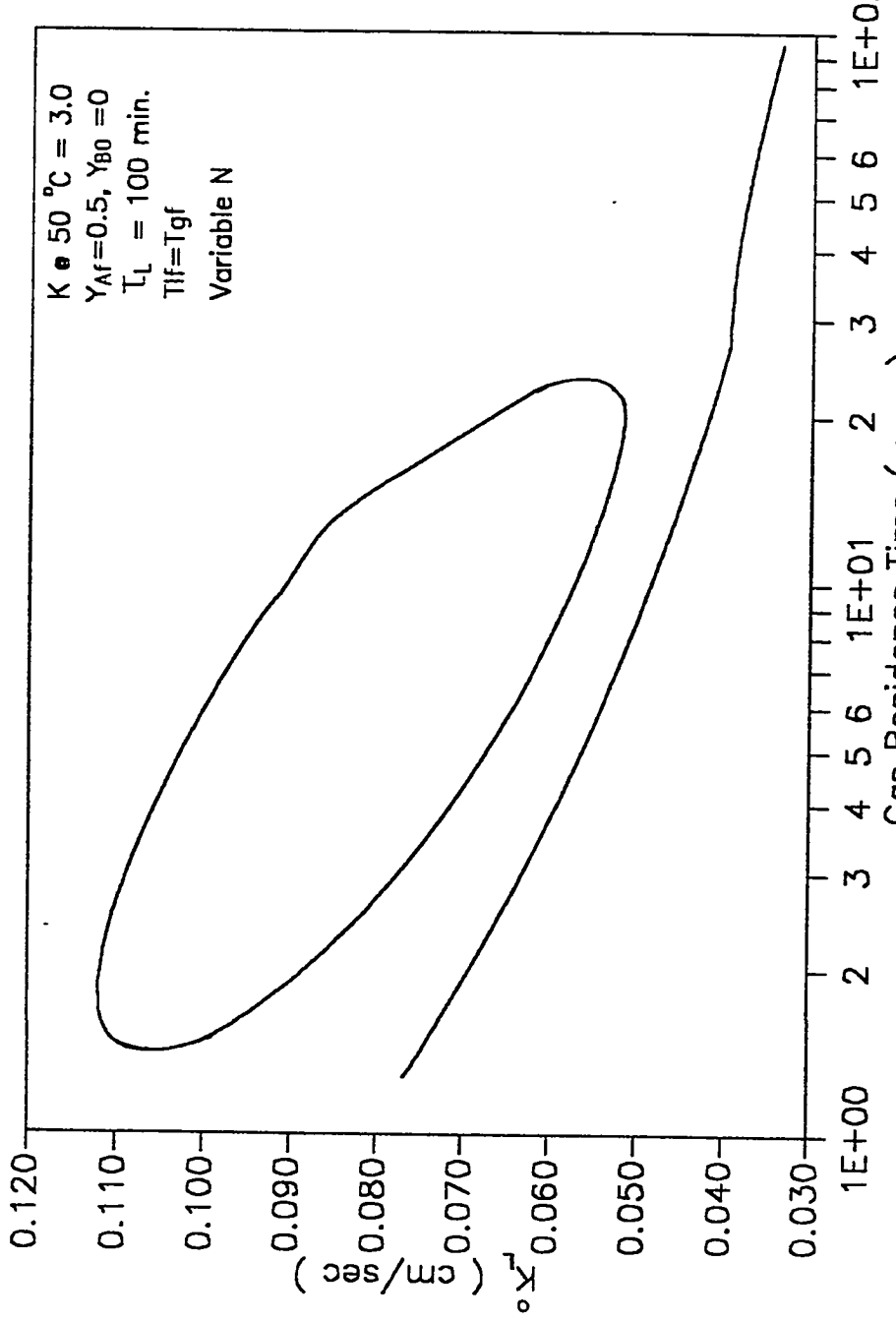

Figure 5.36 Liquid–Side Mass Transfer Coefficient versus Gas Residence Time

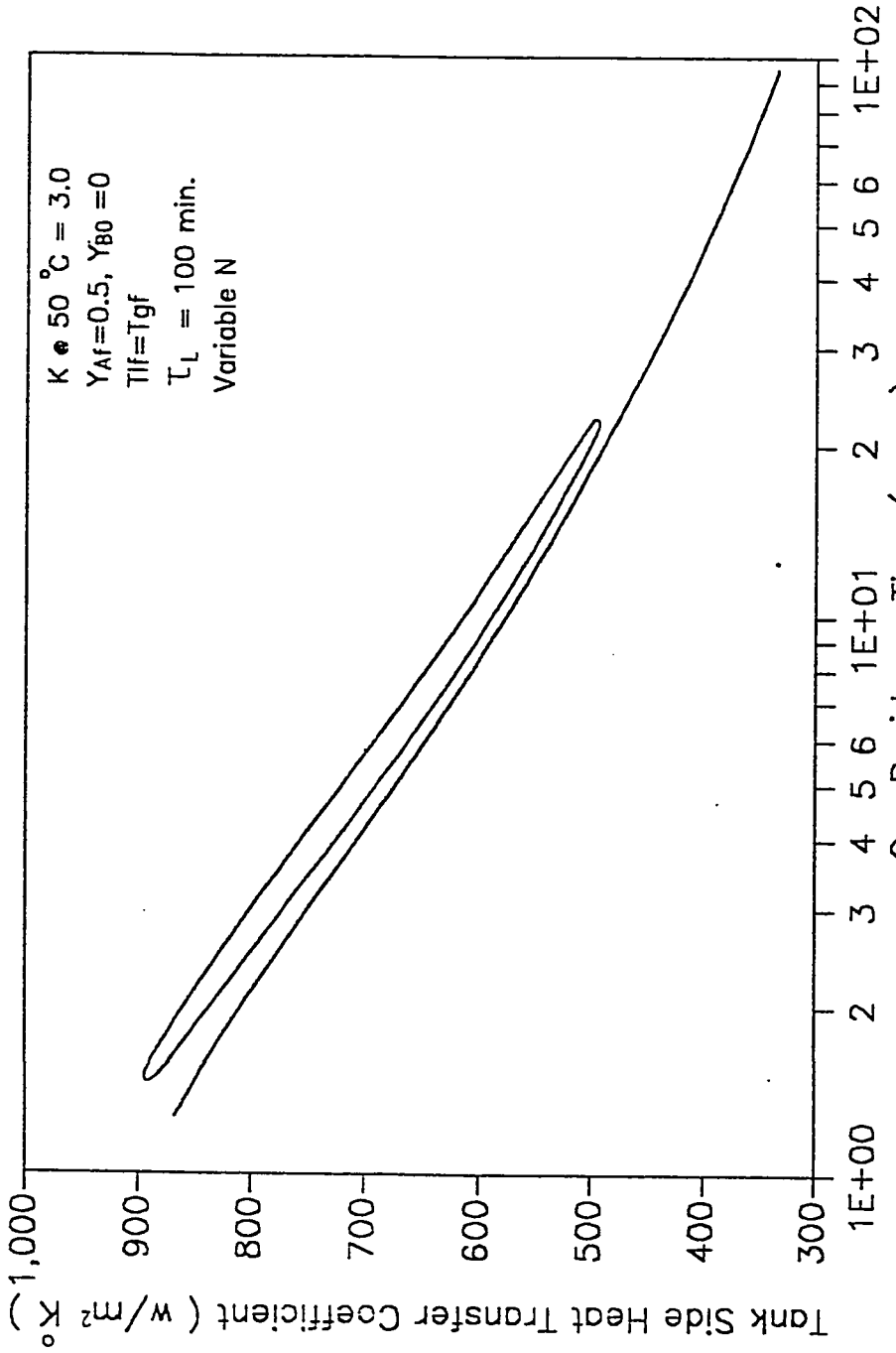

Figure 5.37 Tank–Side Heat Transfer Coefficient versus Gas Residence Time

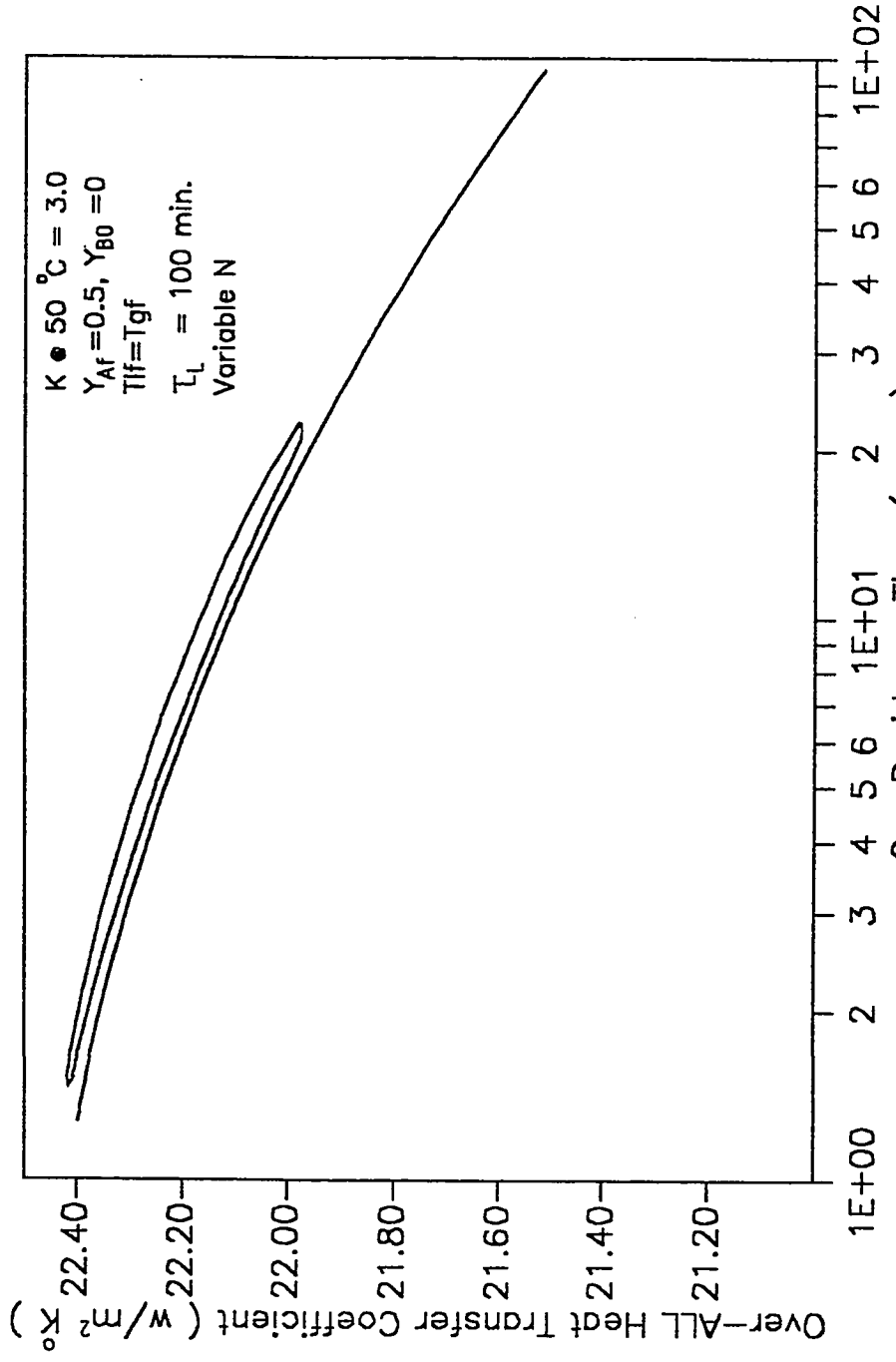

Figure 5.38 Overall Heat Transfer Coefficient versus Gas Residence Time

not reasonable to assume that the hydrodynamic and transport parameters do not change with the change in the operating conditions, because the change in these variable will effect the rate of heat generation and the rate of heat removal which in turn will affect the region and patterns of multiplicity.

Figures 5.39 and 5.40 show that the gas-side mass transfer coefficient and the mean bubble diameter, parameters not considered in the old model, suffer significant variation with respect to gas residence time. The upper and the middle curves in these graphs indicate the effect of change in physico-chemical properties due to the change in steady state temperature. We note that the bubble diameter decreases with the increase in gas residence time and the steady state temperature. As a result, the gas-side mass transfer coefficient increases.

Figures 5.41 and 5.42 show that the conversions of liquid and gaseous reactants predicted by the new model are lower than those predicted by the simplified model. This is because in the new model the predicted values of Hatta number and the reaction factor, as shown in Figures 5.43 and 5.44, are much smaller compared to the simplified model, This indicates that compared to old model, the new model predicts a slower rate of reaction. The large difference in the Hatta number values and the reaction factor predicted by the two models arises because the new model uses more representative values of hydrodynamic and transport parameters, as explained earlier. Figure 5.45 shows that for all values of gas residence time the concentration of gaseous reactant in the liquid bulk predicted by the new model is much higher than that predicted by the old model. It is also seen that for certain values of τ_G, the old model predicts that

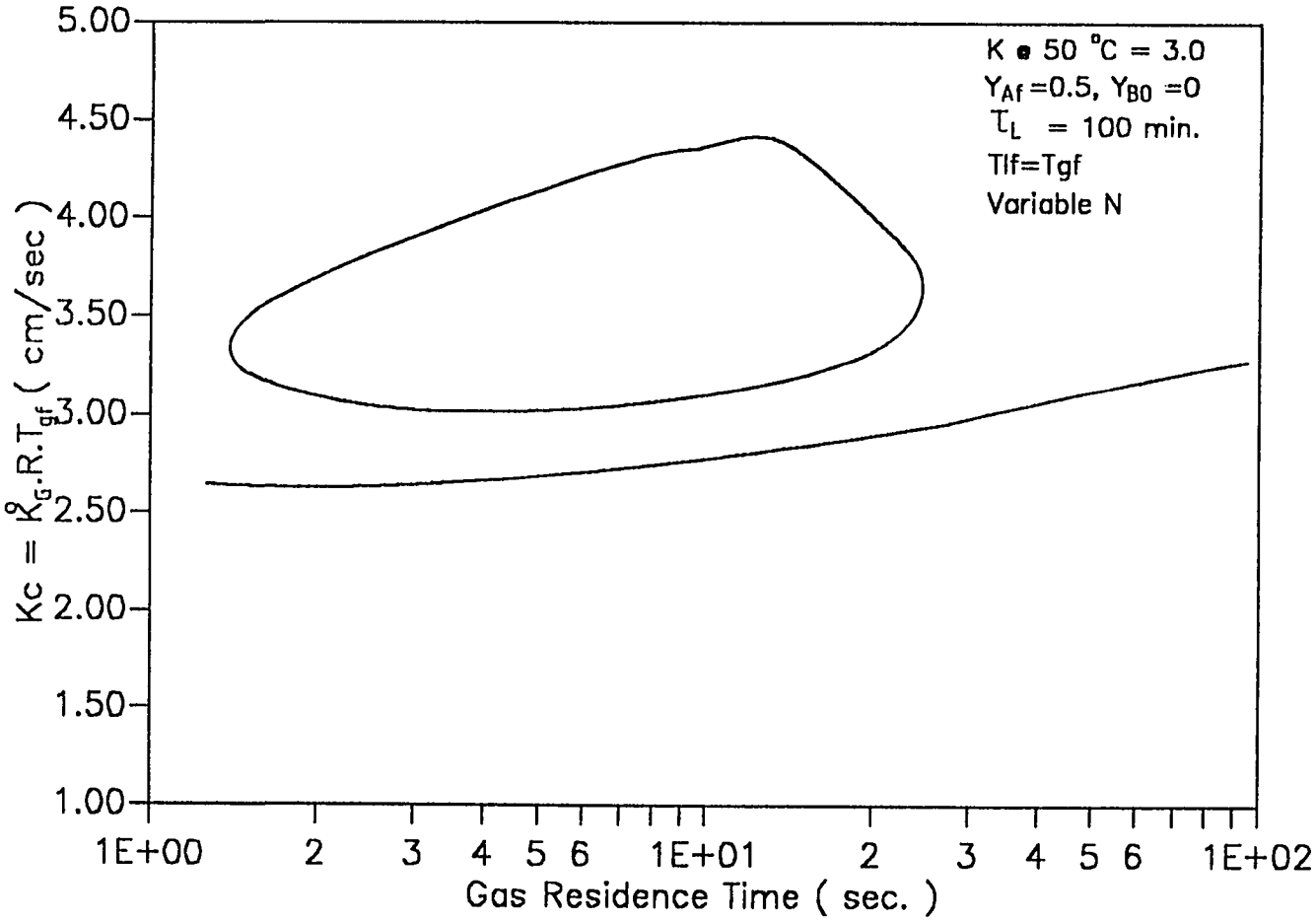

Figure 5.39 Gas–Side Mass Transfer Coefficient versus Gas Residence Time

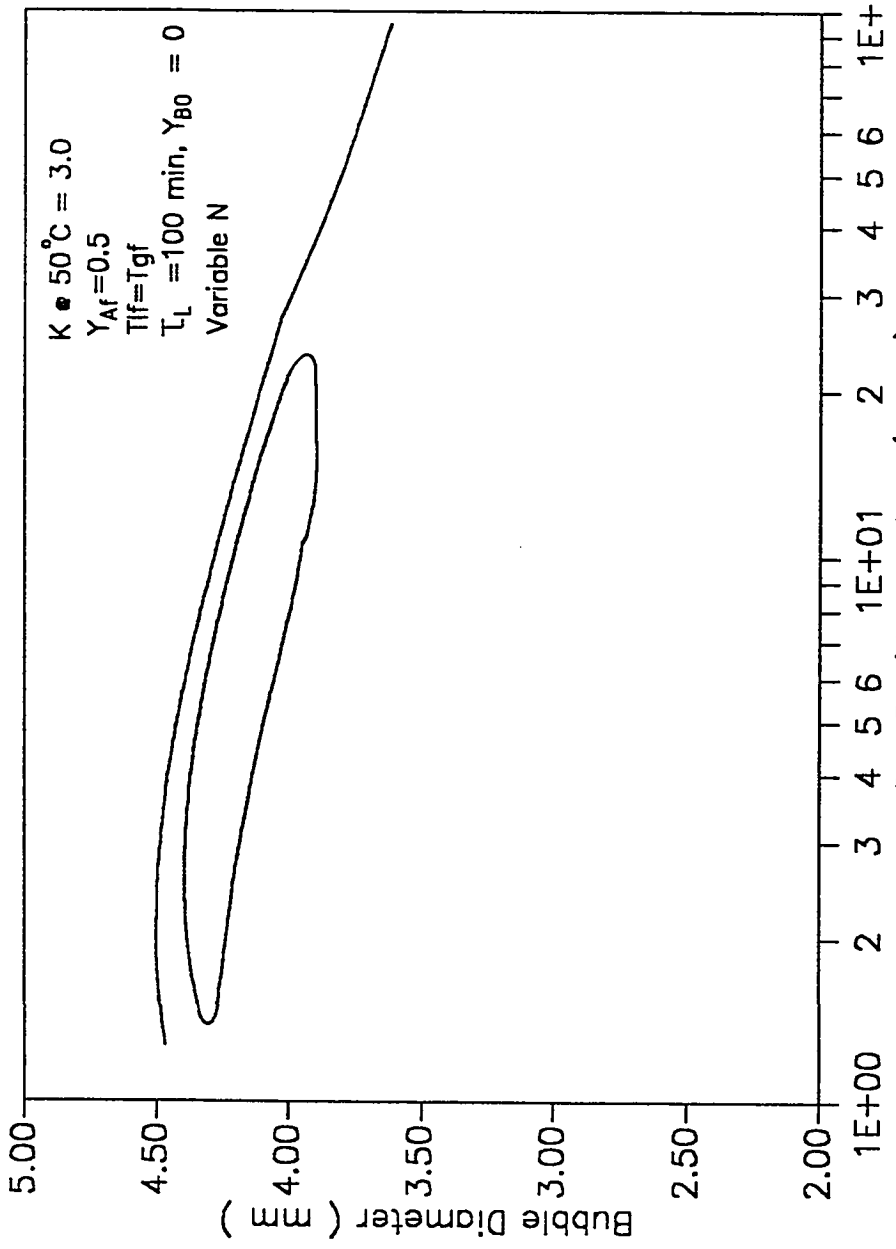

Figure 5.40 Bubble Diameter versus Gas Residence Time

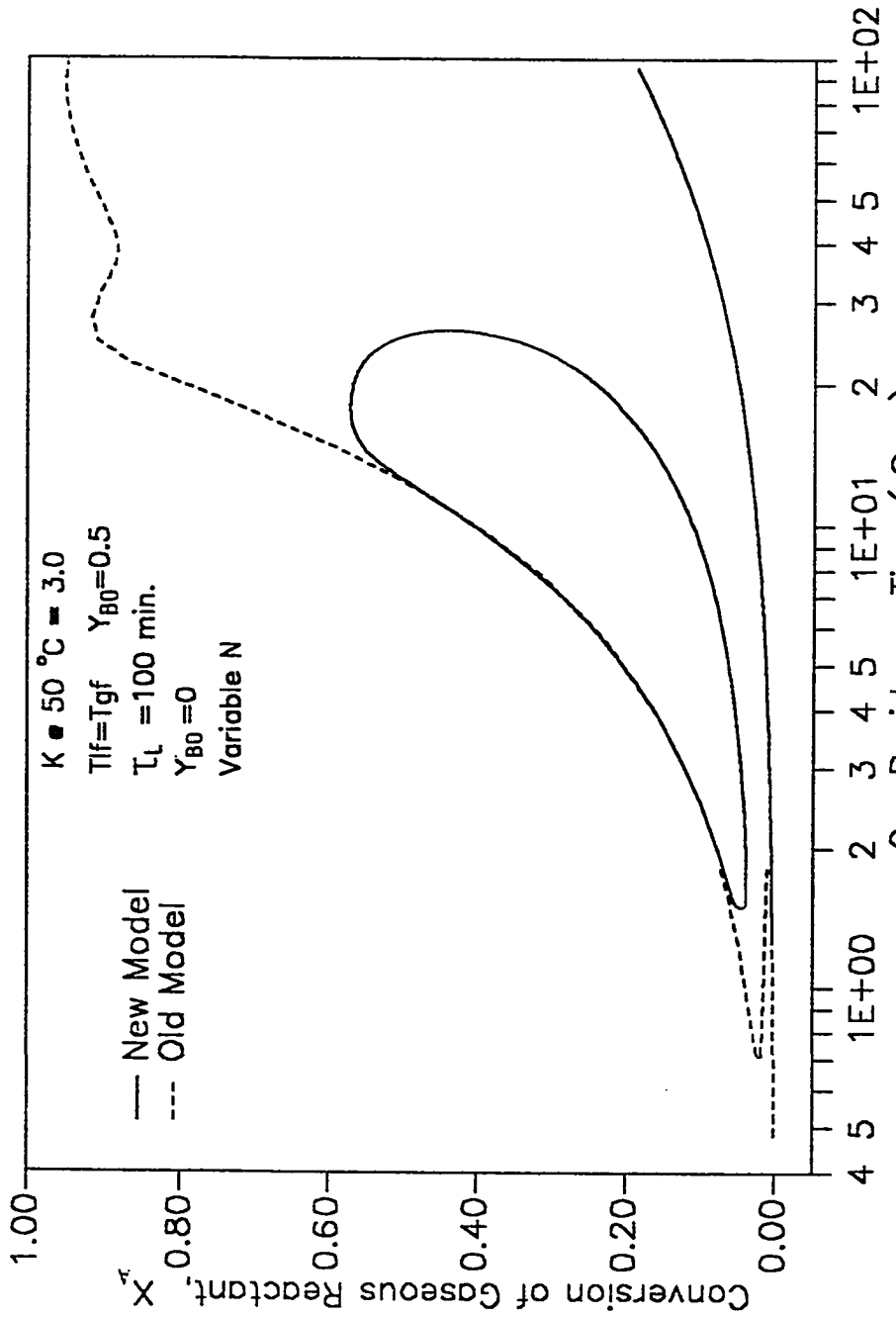

Figure 5.41 Comparison of Steady State Conversions of Gaseous Reactant Predicted by Old and New Models

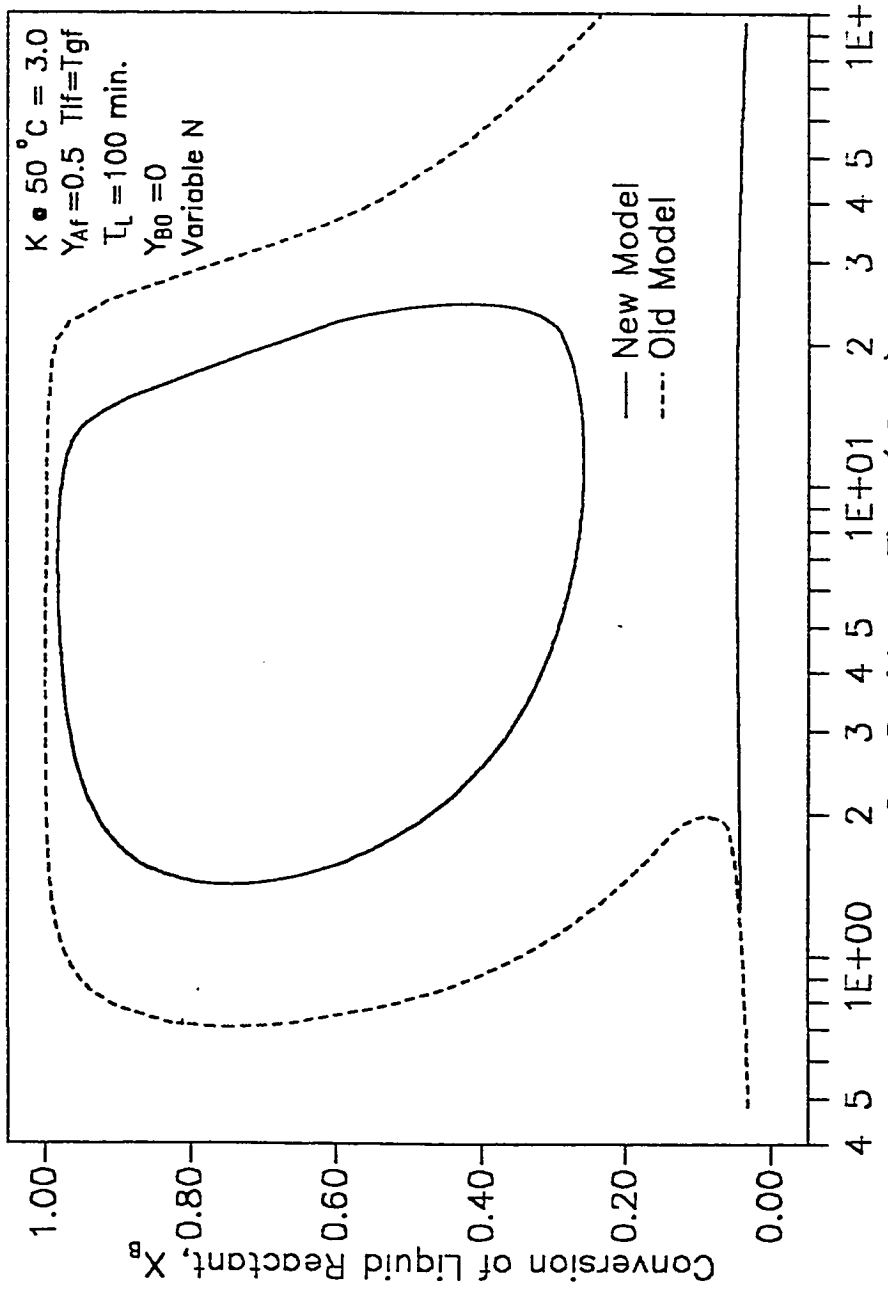

Figure 5.42 Comparison of Steady State Conversions of Liquid Reactant Predicted by Old and New Models

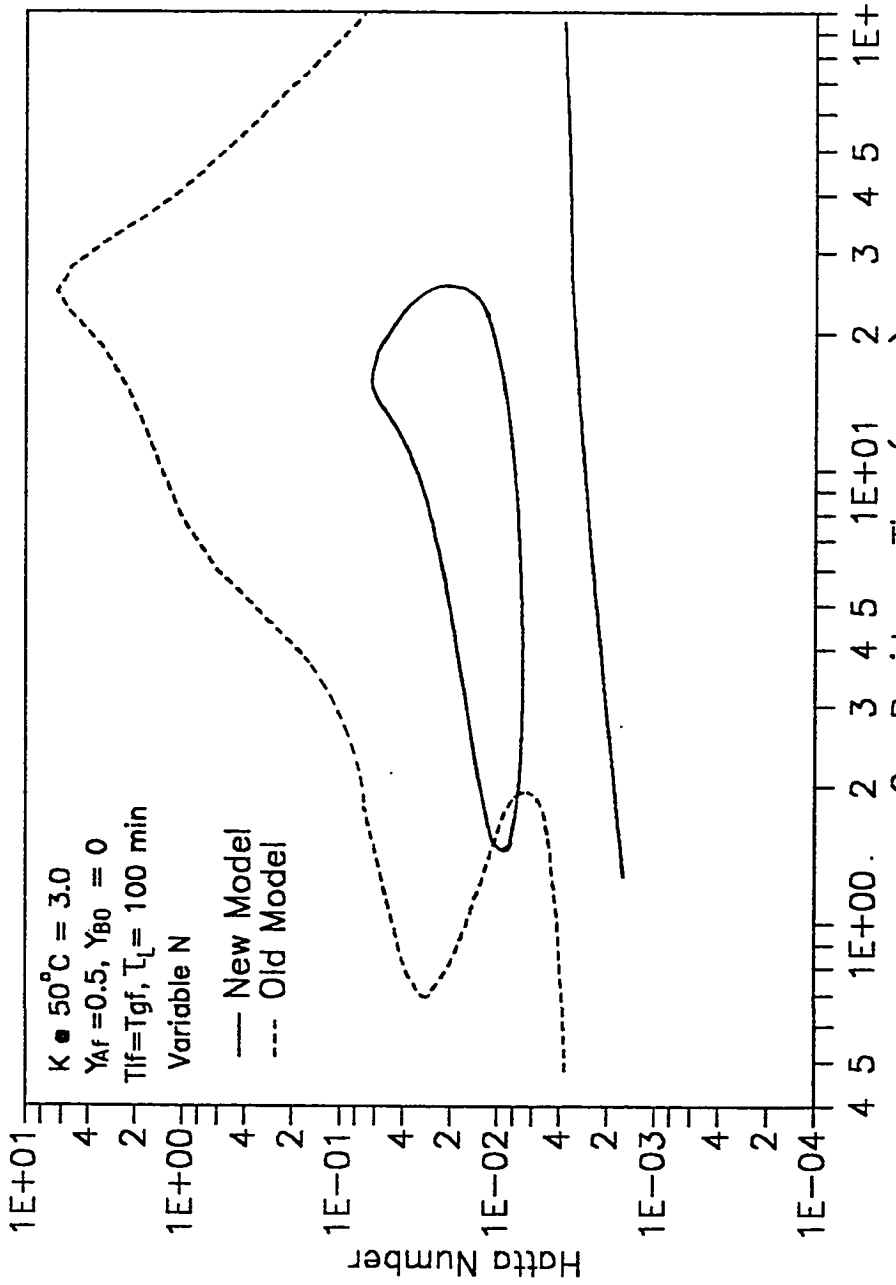

Figure 5.43 Hatta Number versus Gas Residence Time: Predictions of Old and New Models

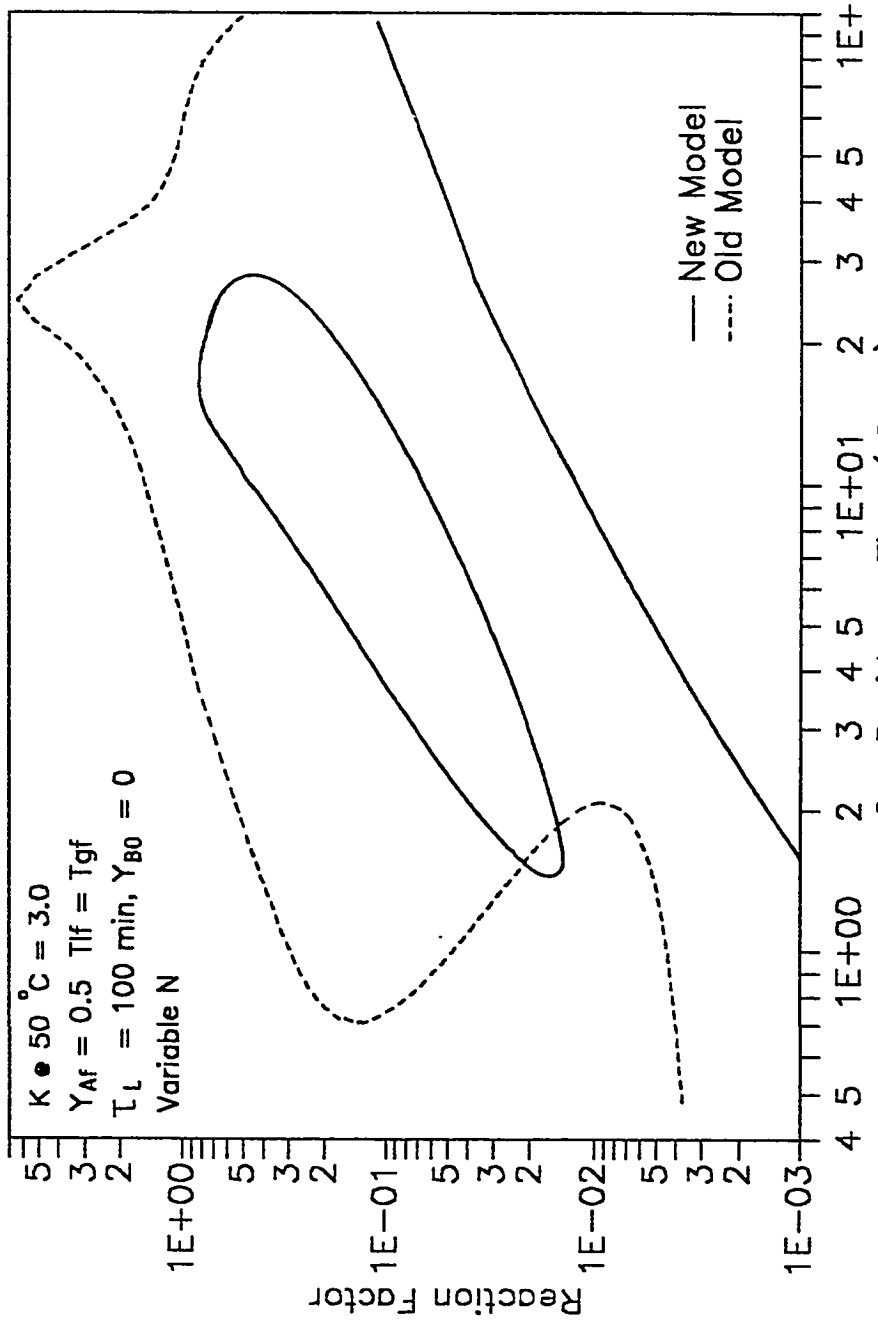

Figure 5.44 Reaction Factor versus Gas Residence Time: Predictions of Old and New Models

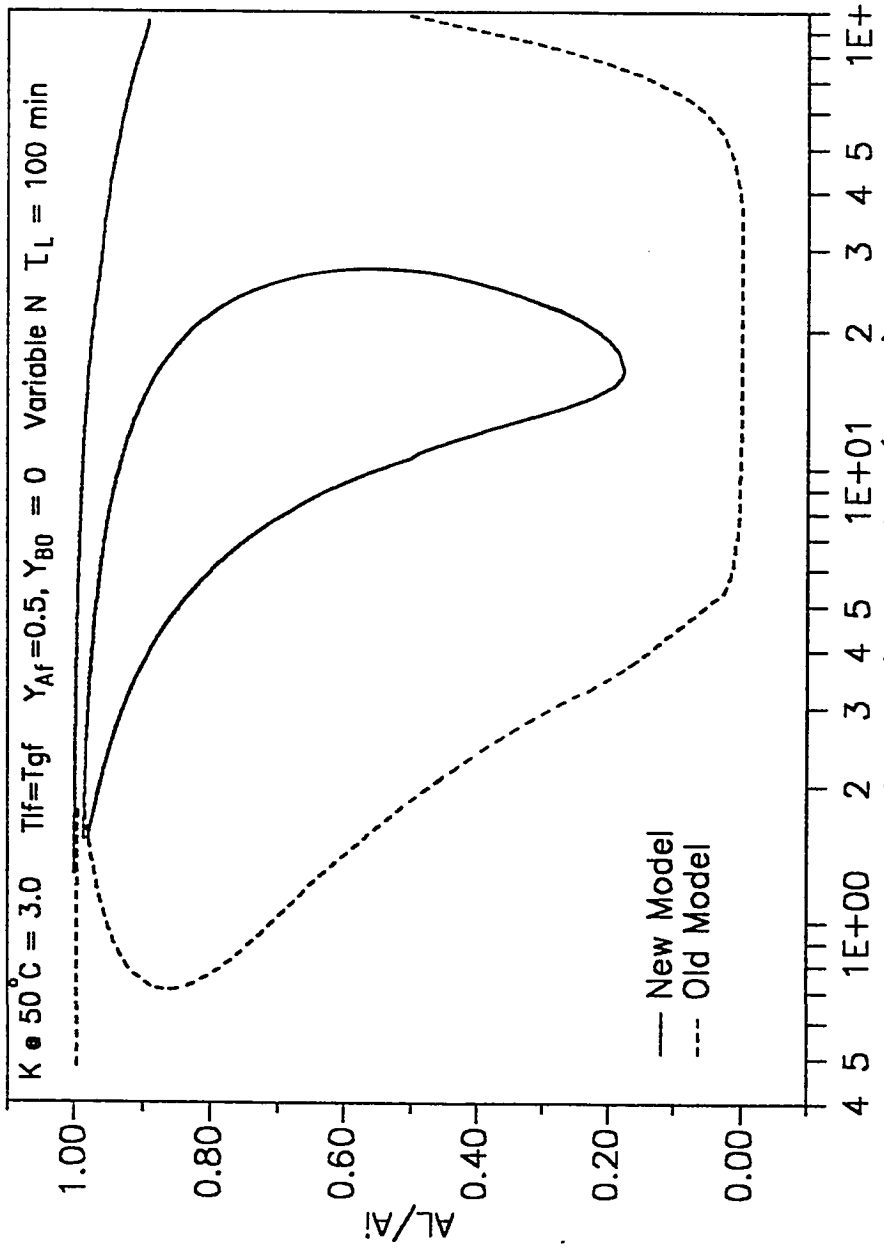

Figure 5.45 Dimensionless Concentration of A in Liquid Bulk versus Gas Residence Time: Predictions of Old and New Models

the reaction is completed within the liquid film (i.e. $a_l = 0$) whereas the new model predicts that there is always a substantial quantity of the dissolved gaseous reactant left in the liquid bulk. This further indicates that the rate of reaction predicted by the new model is slow compared to that predicted by old model.

5.5.2 Variable Liquid Residence Time

Figure 5.46 compares the multiplicity regions predicted by our model and the simplified model in the parameter space of K versus τ_L. It is seen that the multiplicity region predicted by new model is smaller than that by simplified model. Figures 5.47 to 5.49 show various multiplicity patterns predicted by the new and old models. From these figures we note that the multiplicity patterns predicted by new model are the same as those predicted by old model. However, for exactly the same parameters, the two models might predict different multiplicity patterns as shown in Figures 5.47 and 5.49.

Figures 5.50 to 5.63 present a case study of the behavior of various parameters with respect to liquid residence time for new and old model. Although, the variation in hydrodynamic and transport parameters with respect to liquid residence time is not significant, we note that their behavioral features are quite similar to those of the corresponding Figures 5.31 to 5.45. Therefore, same description of their behavior and relationships for the case of varying gas residence time can be applied here as well.

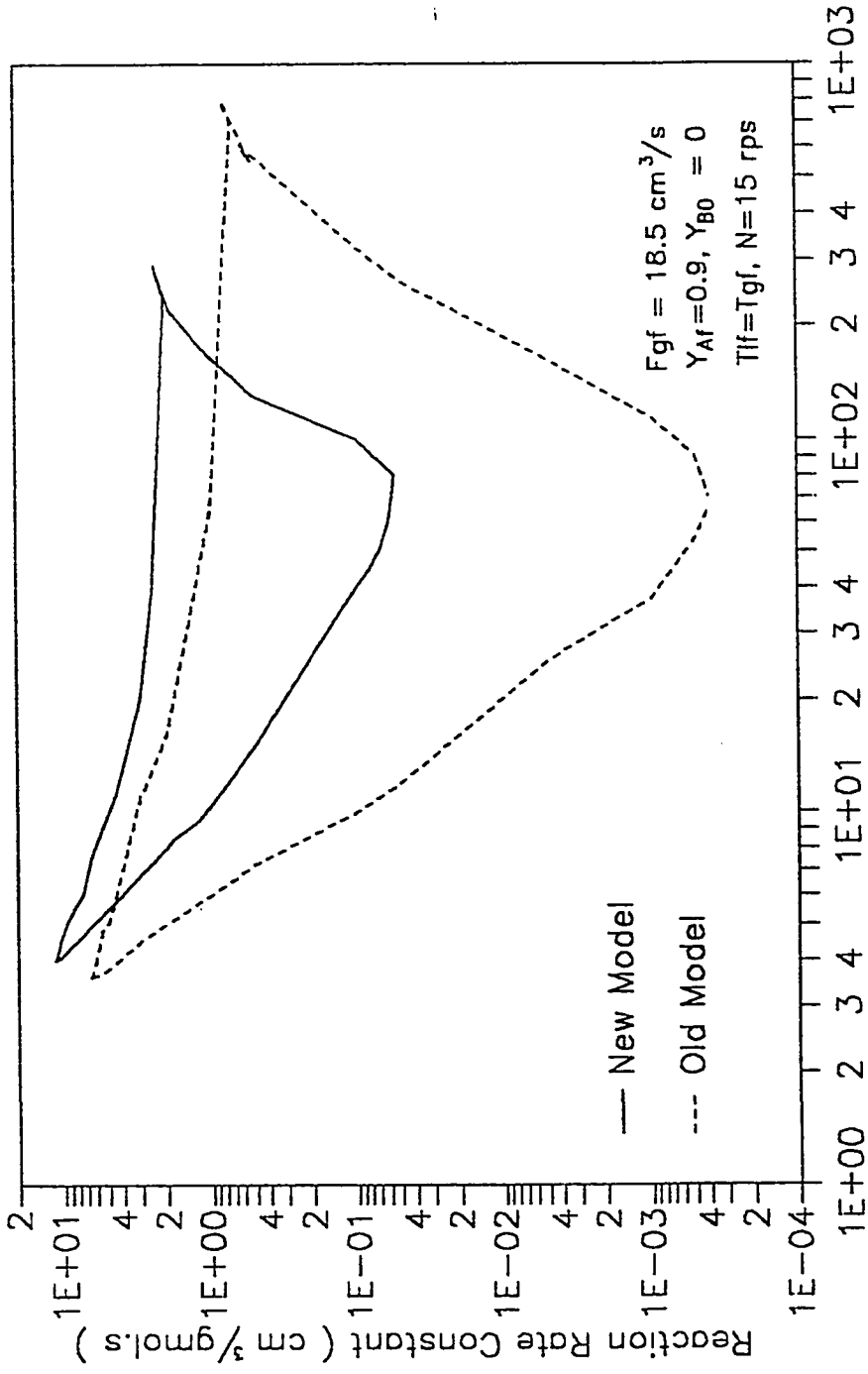

Figure 5.46 Comparison of the Multiplicity Regions Predicted by New and Old Models

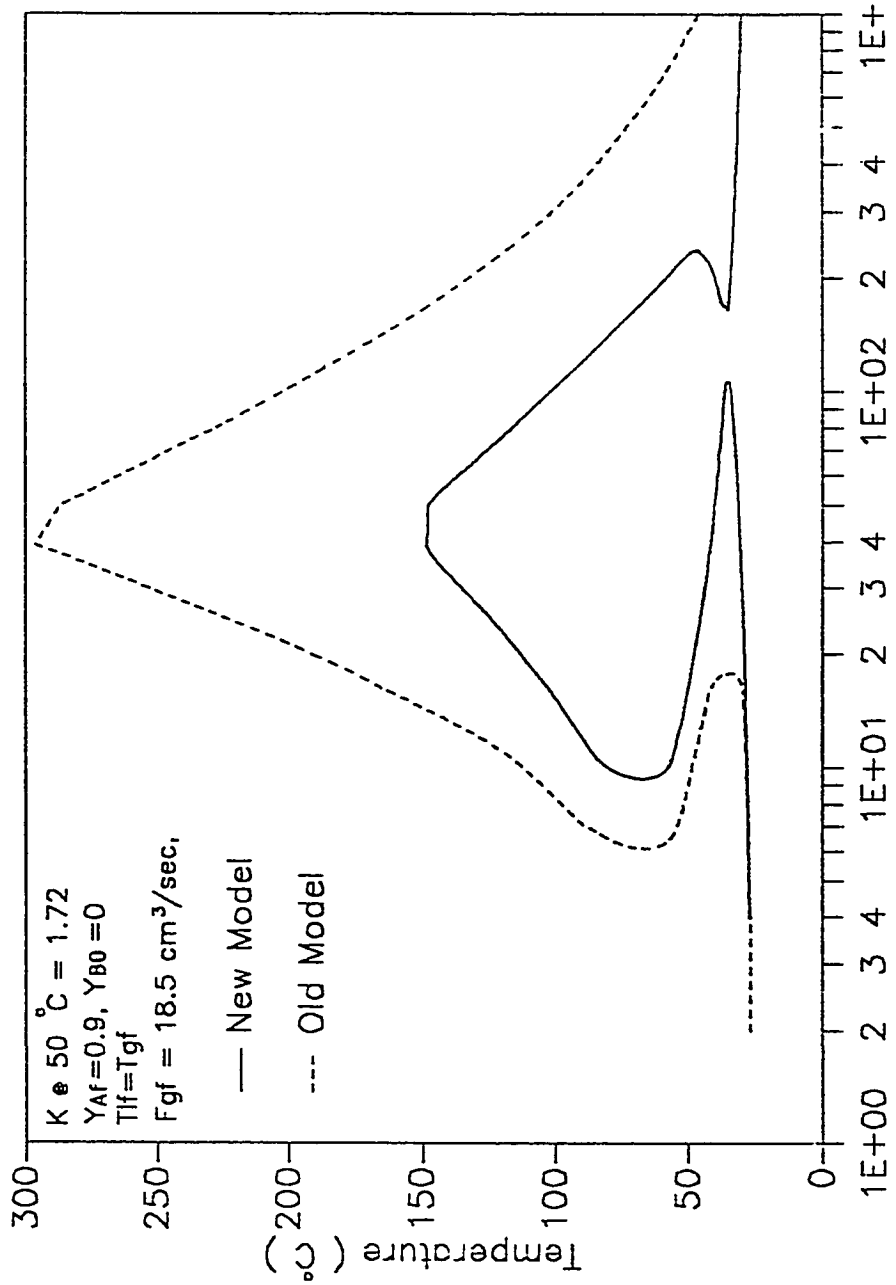

Figure 5.47 Comparison of Steady State Temperatures Predicted by New and Old Models

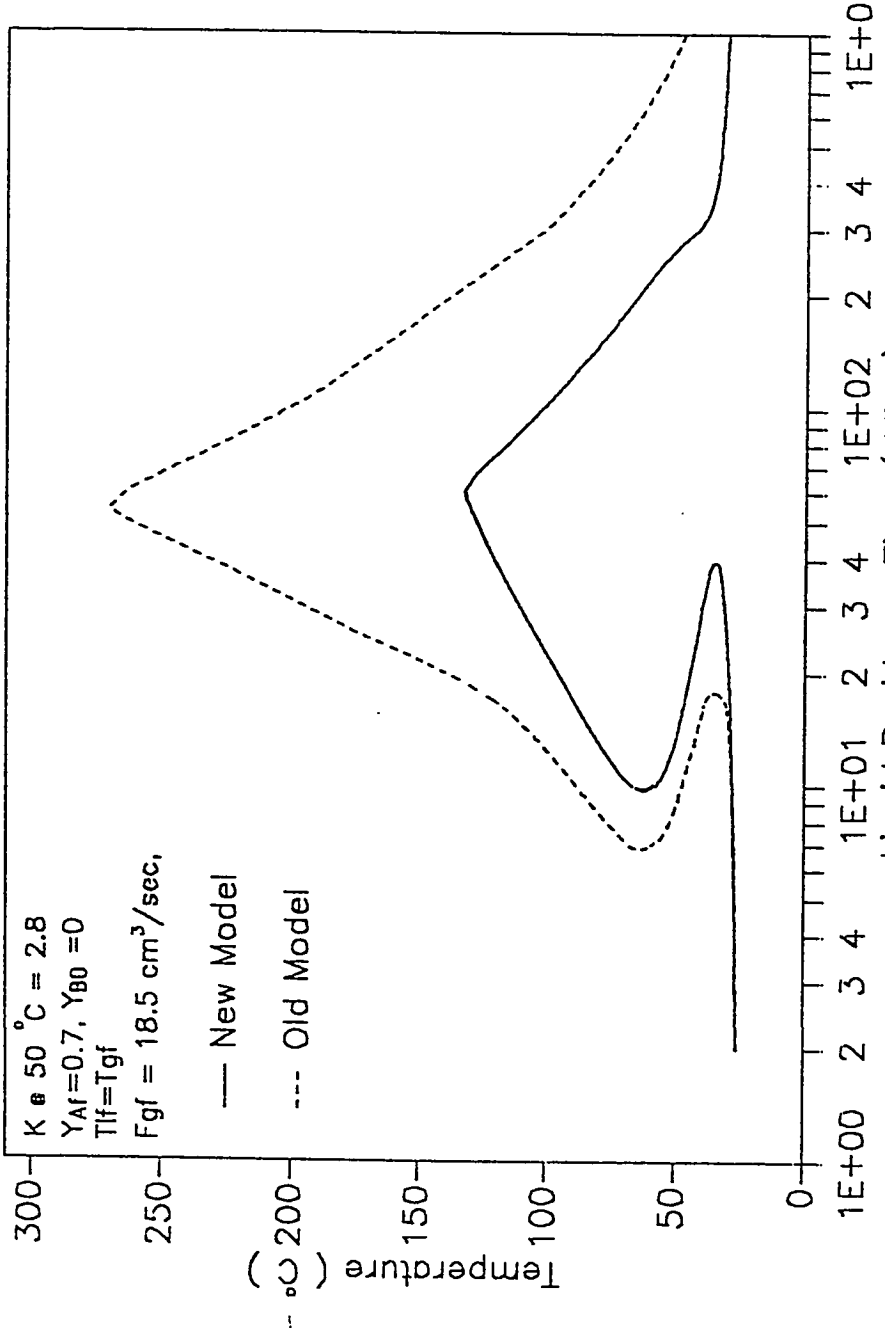

Figure 5.48 Comparison of Steady State Temperature Predicted by New and Old Models

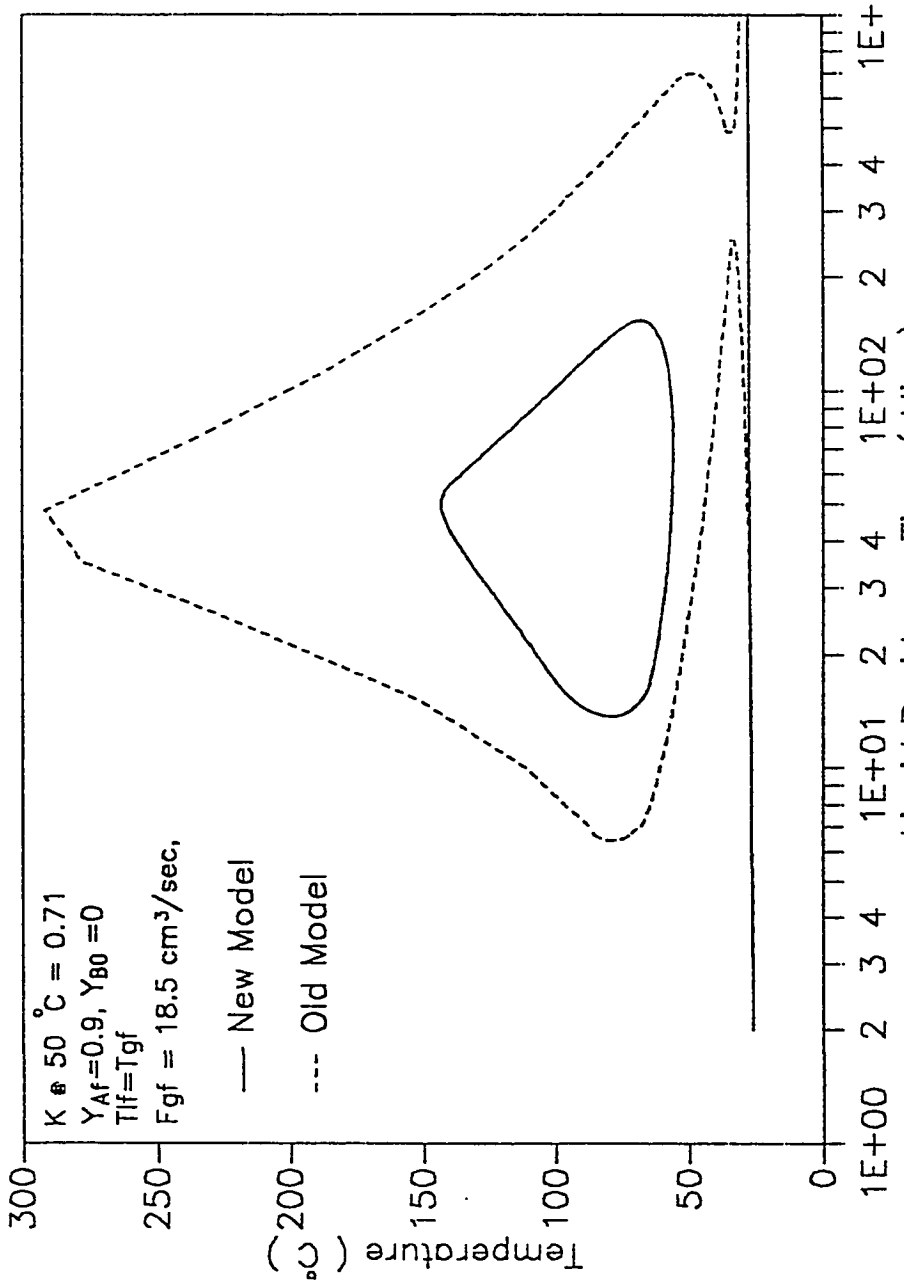

Figure 5.49 Comparison of Steady State Temperatures Predicted by New and Old Model

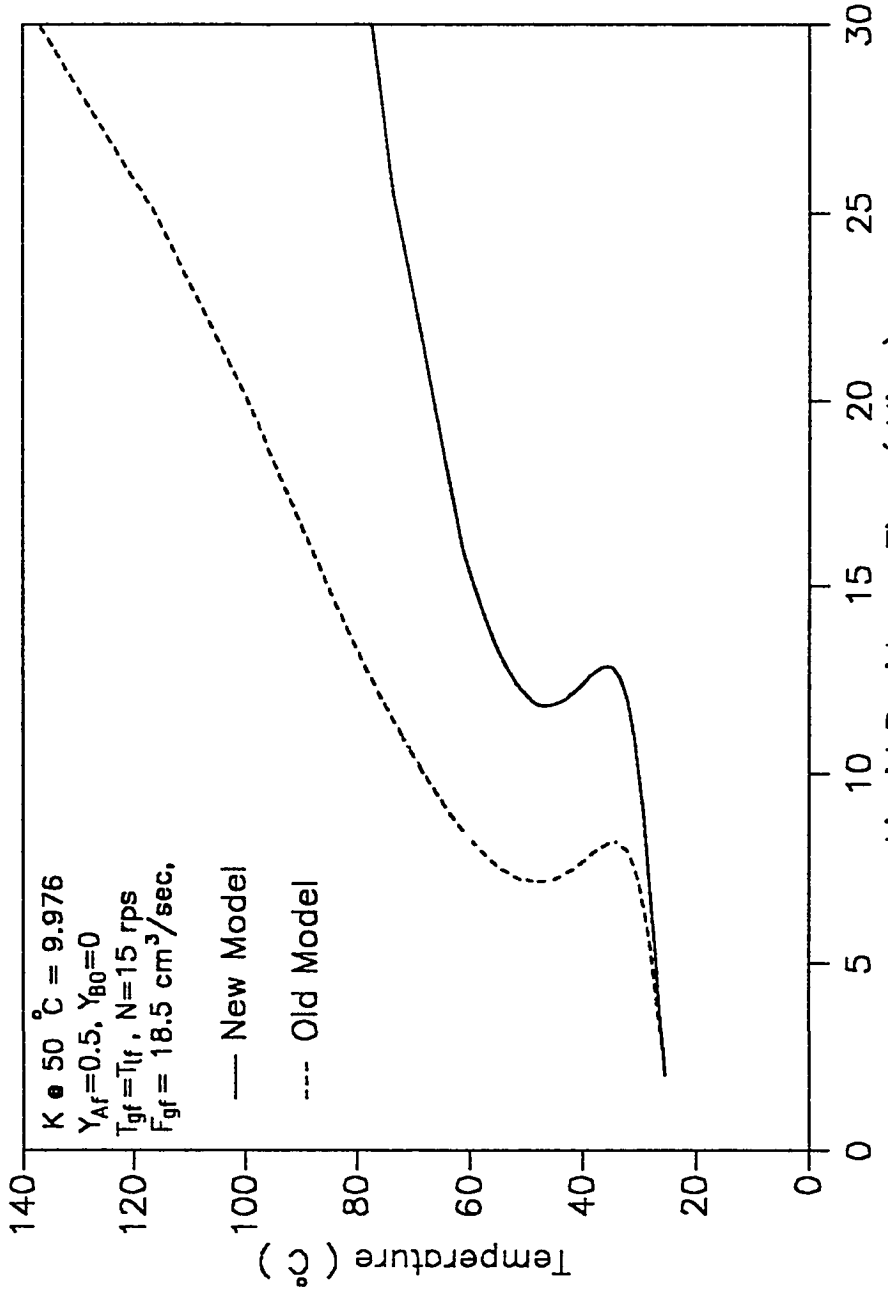

Figure 5.50 Steady State Reactor Temperature versus Liquid Residence Time: Predictions of Old and New Models

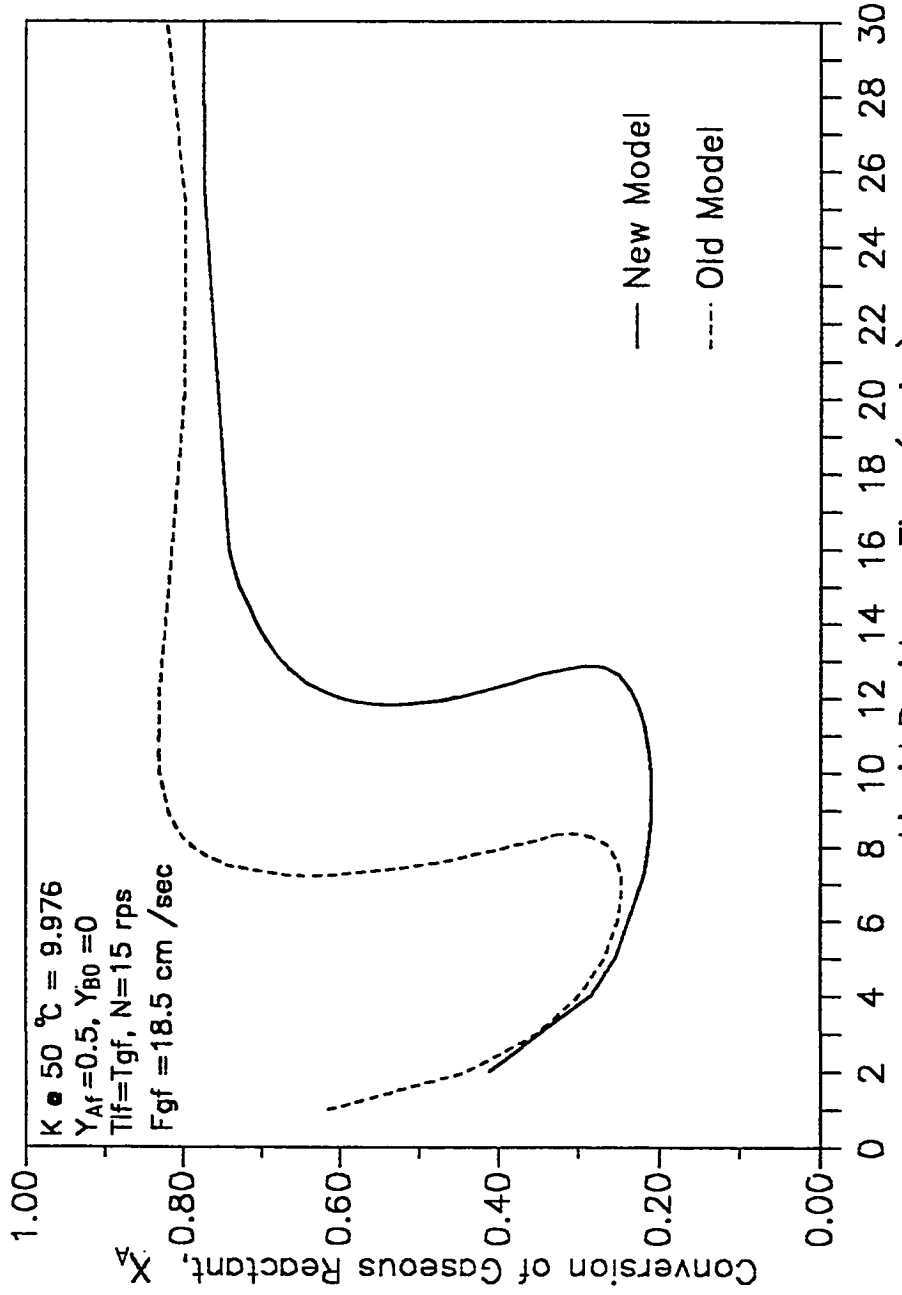

Figure 5.51 Conversion of Gaseous Reactant versus Liquid Residence Time: Predictions of Old and New Models

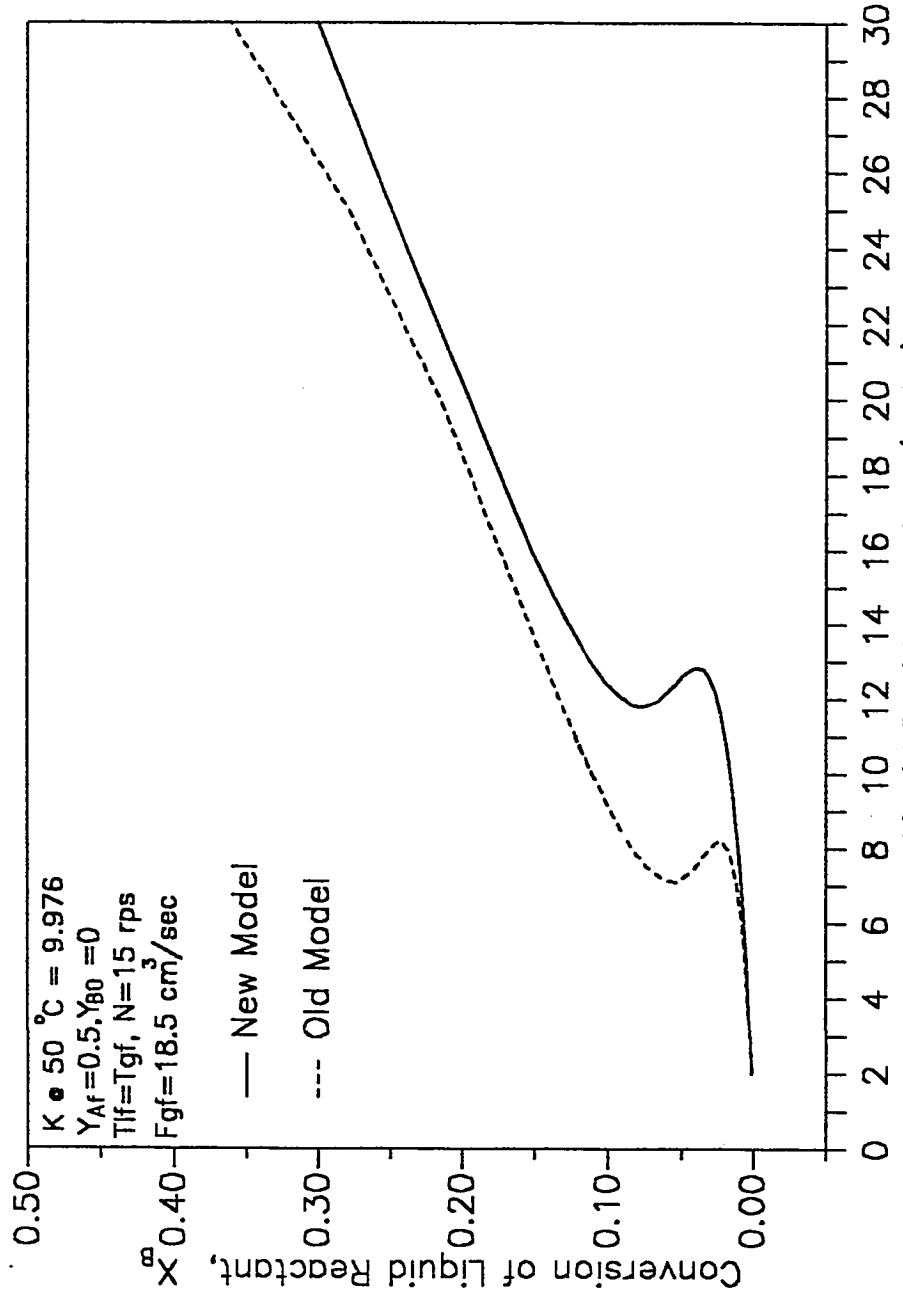

Figure 5.52 Conversion ofLiquid Reactant versus Liquid Residence Time: Predictions of Old and New Models

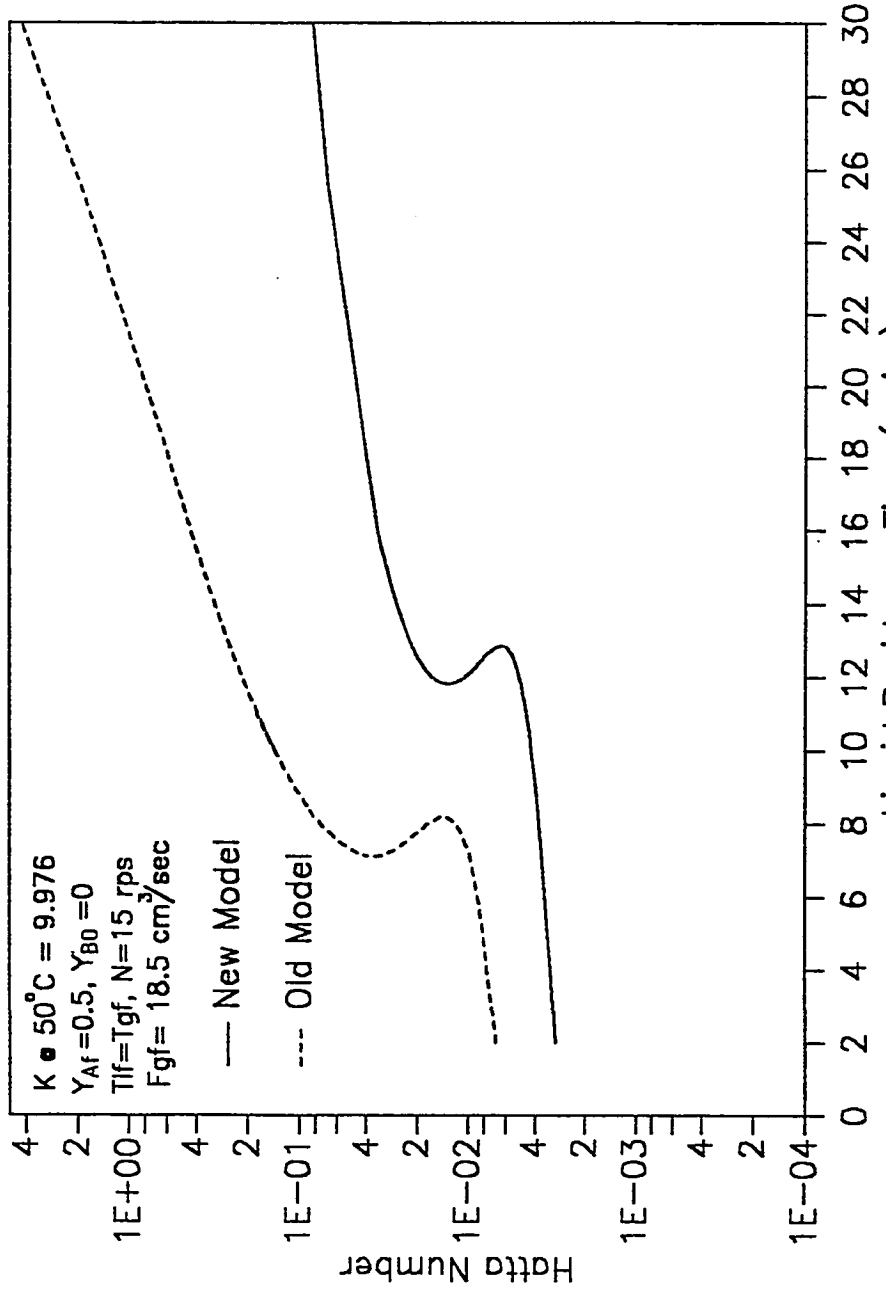

Figure 5.53 Hatta Number versus Liquid Residence Time: Predictions of Old and New Models

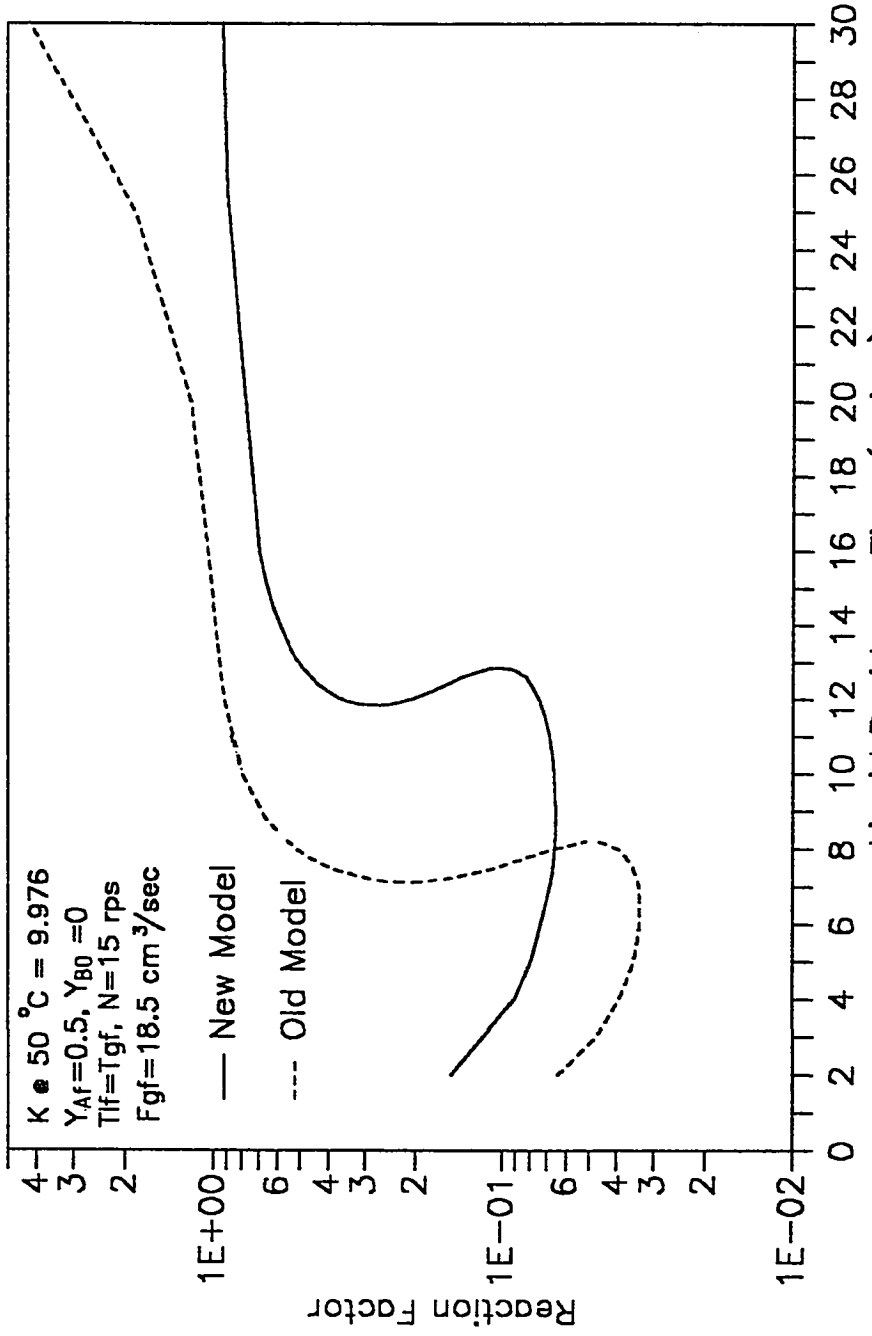

Figure 5.54 Reaction Factor versus Liquid Residence Time Predictions of Old and New Models

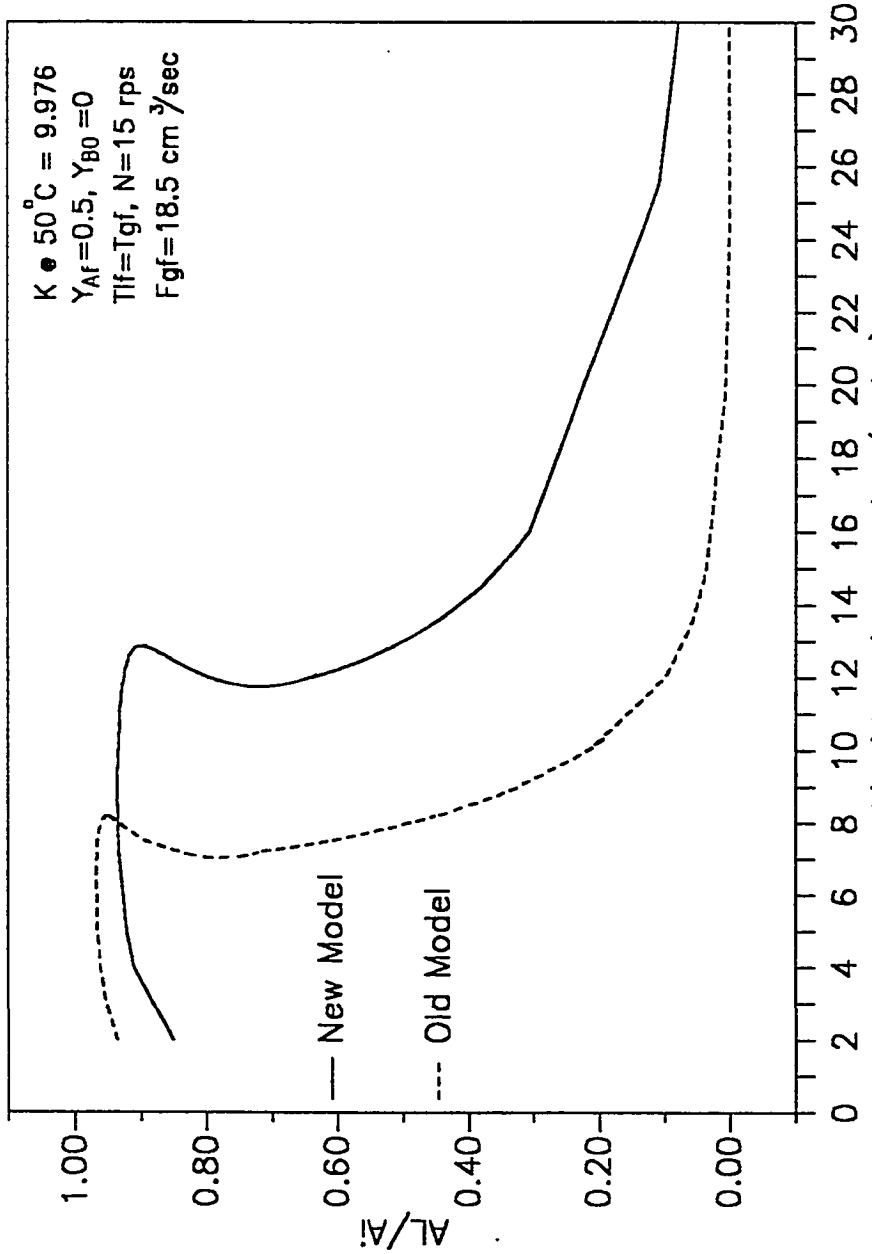

Figure 5.55 Dimensionless Concentration of A in the liquid Bulk versus Liquid Residence Time: Predictions of Old and New Models

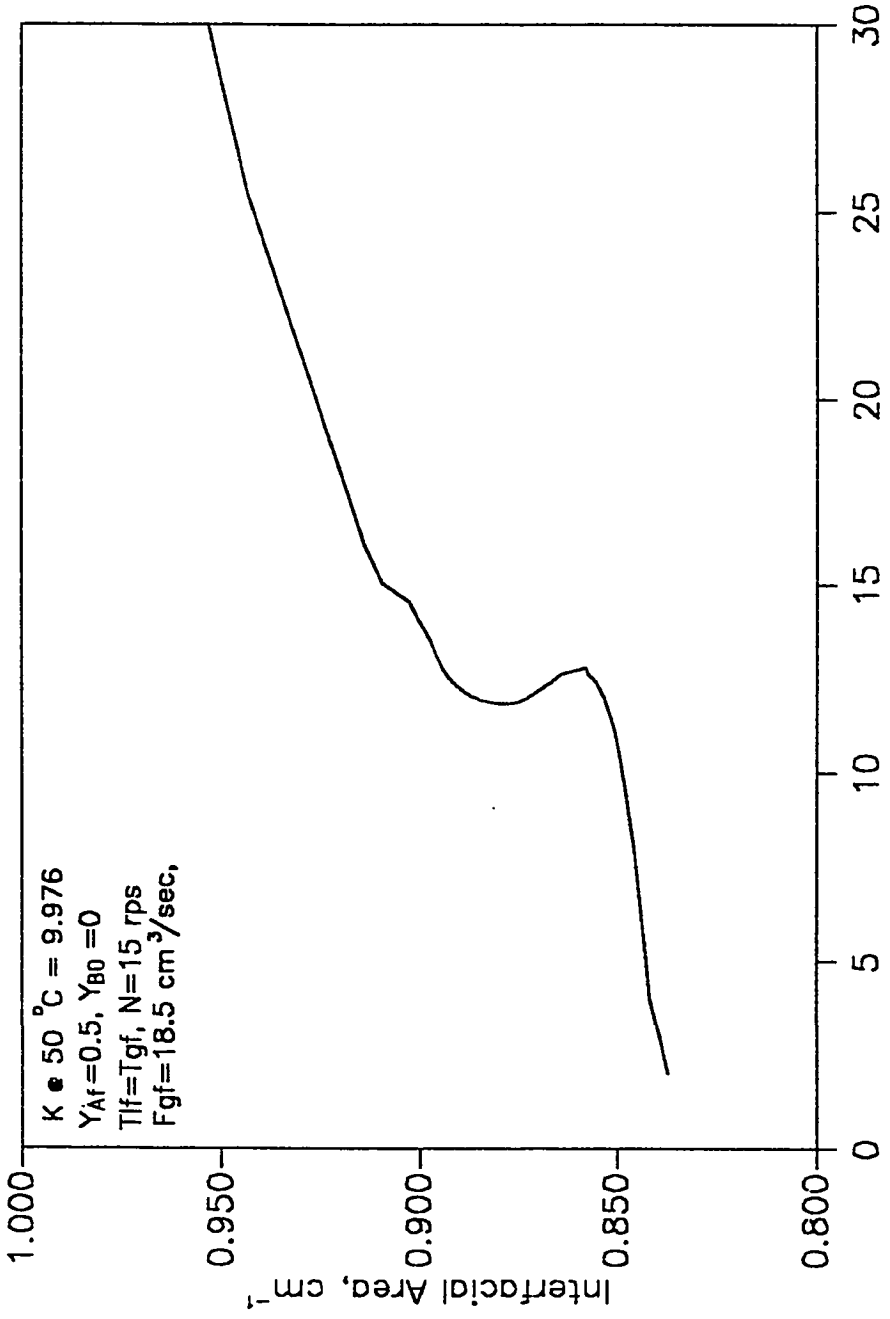

Figure 5.56 Interfacial Area versus Liquid Residence Time

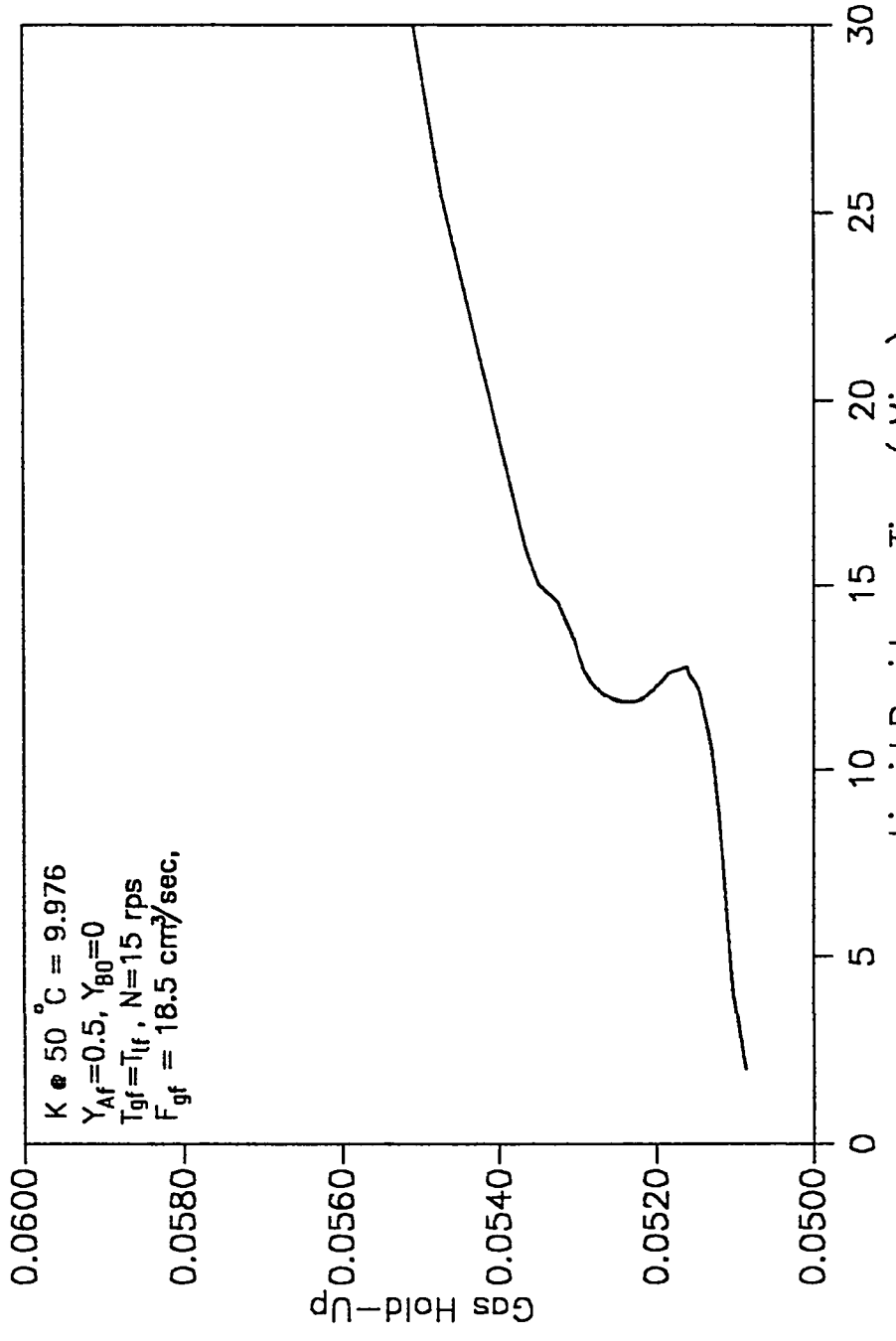

Figure 5.57 Gas-Holdup versus Liquid Residence Time

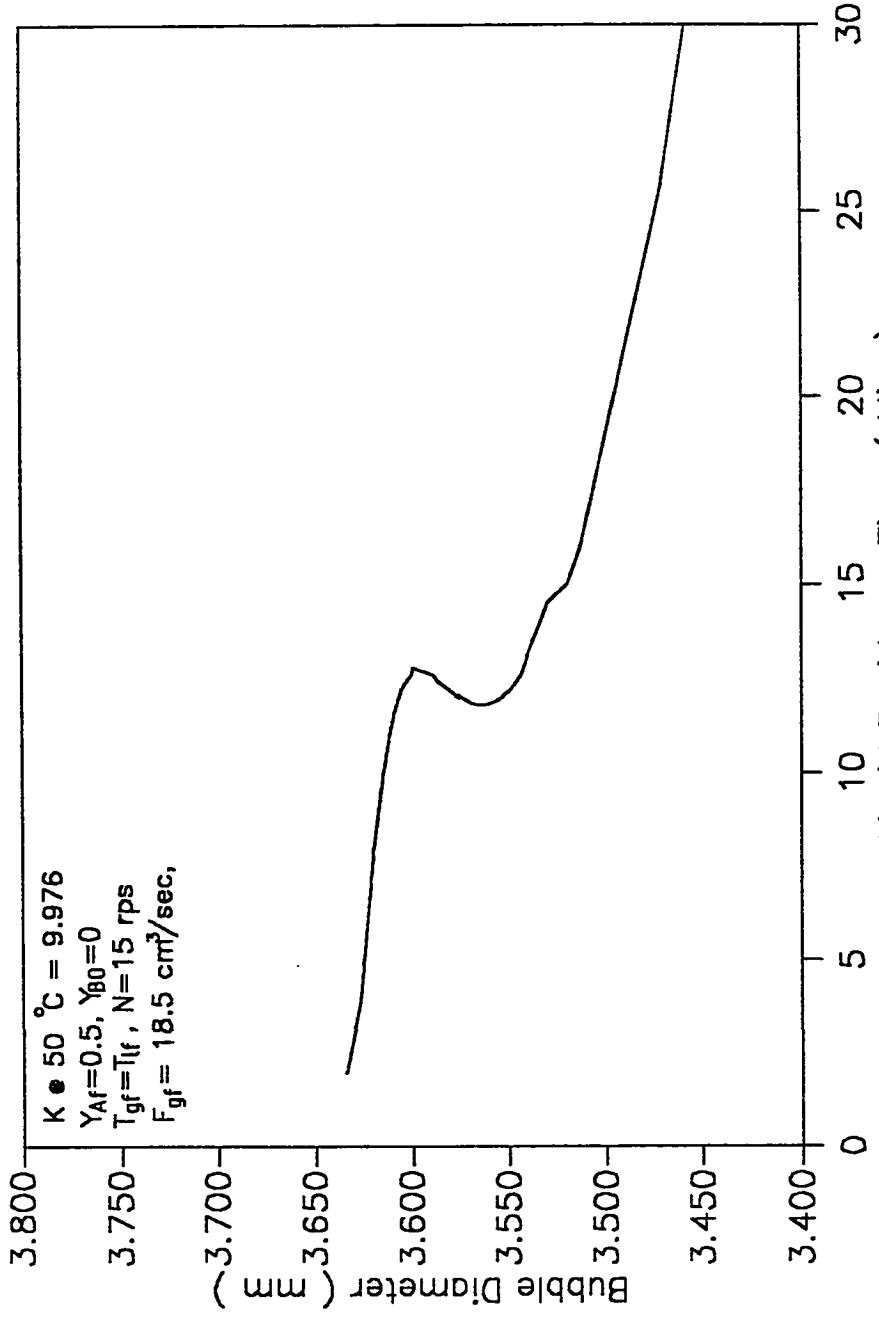

Figure 5.58 Bubble Diameter versus Liquid Residence Time

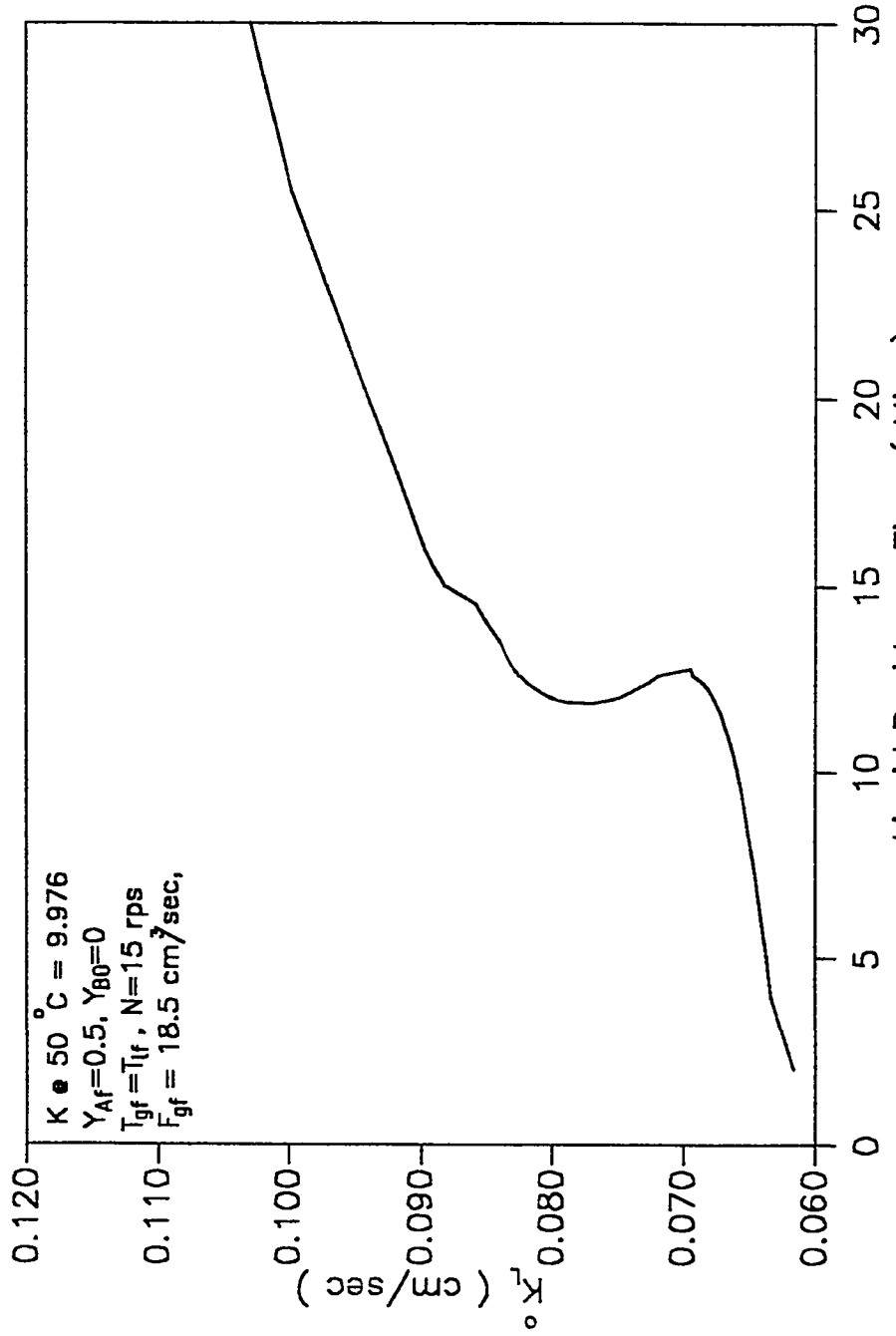

Figure 5.59 Liquid-Side Mass Transfer Coefficient versus Liquid Residence Time

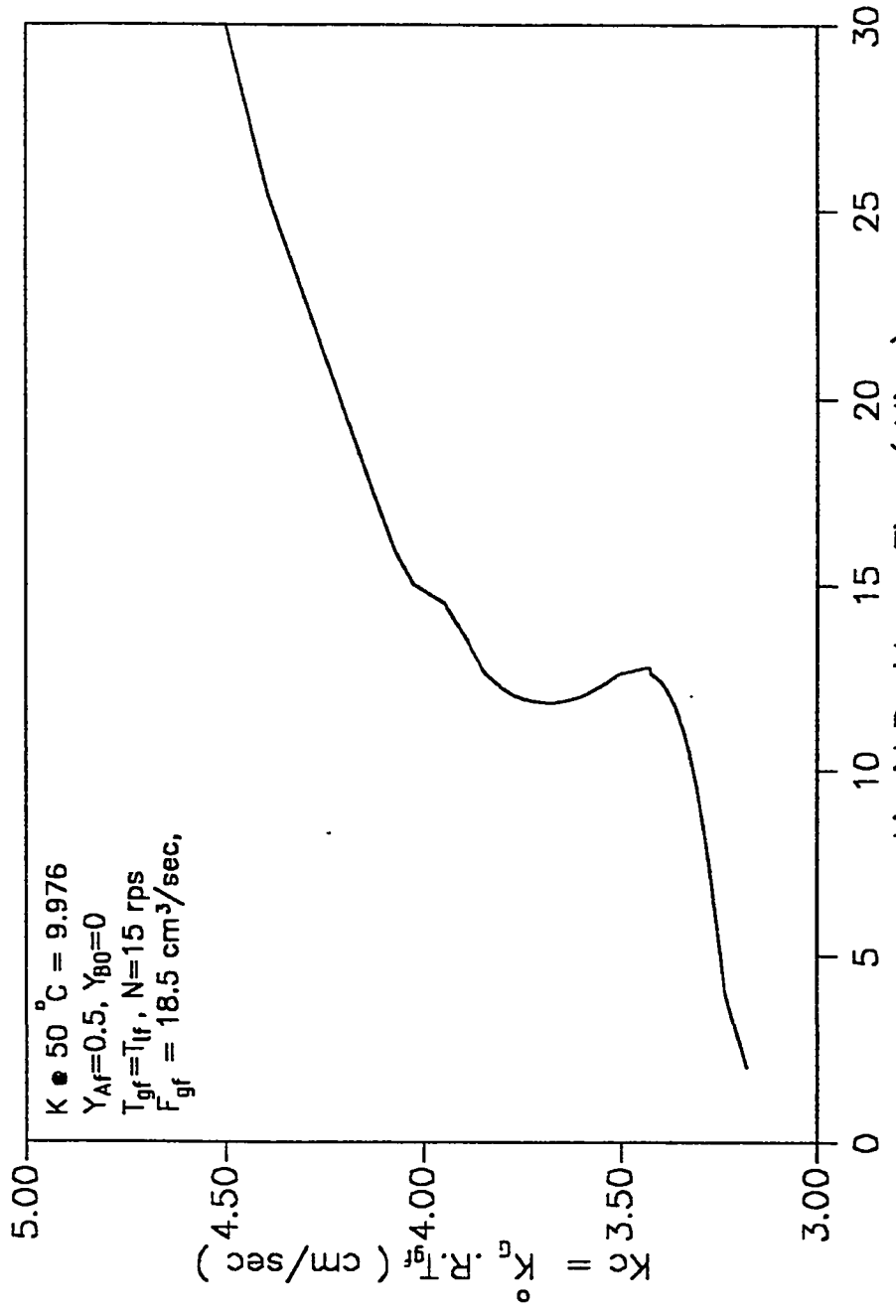

Figure 5.60 Gas–Side Mass Transfer Coefficient versus Liquid residence Time

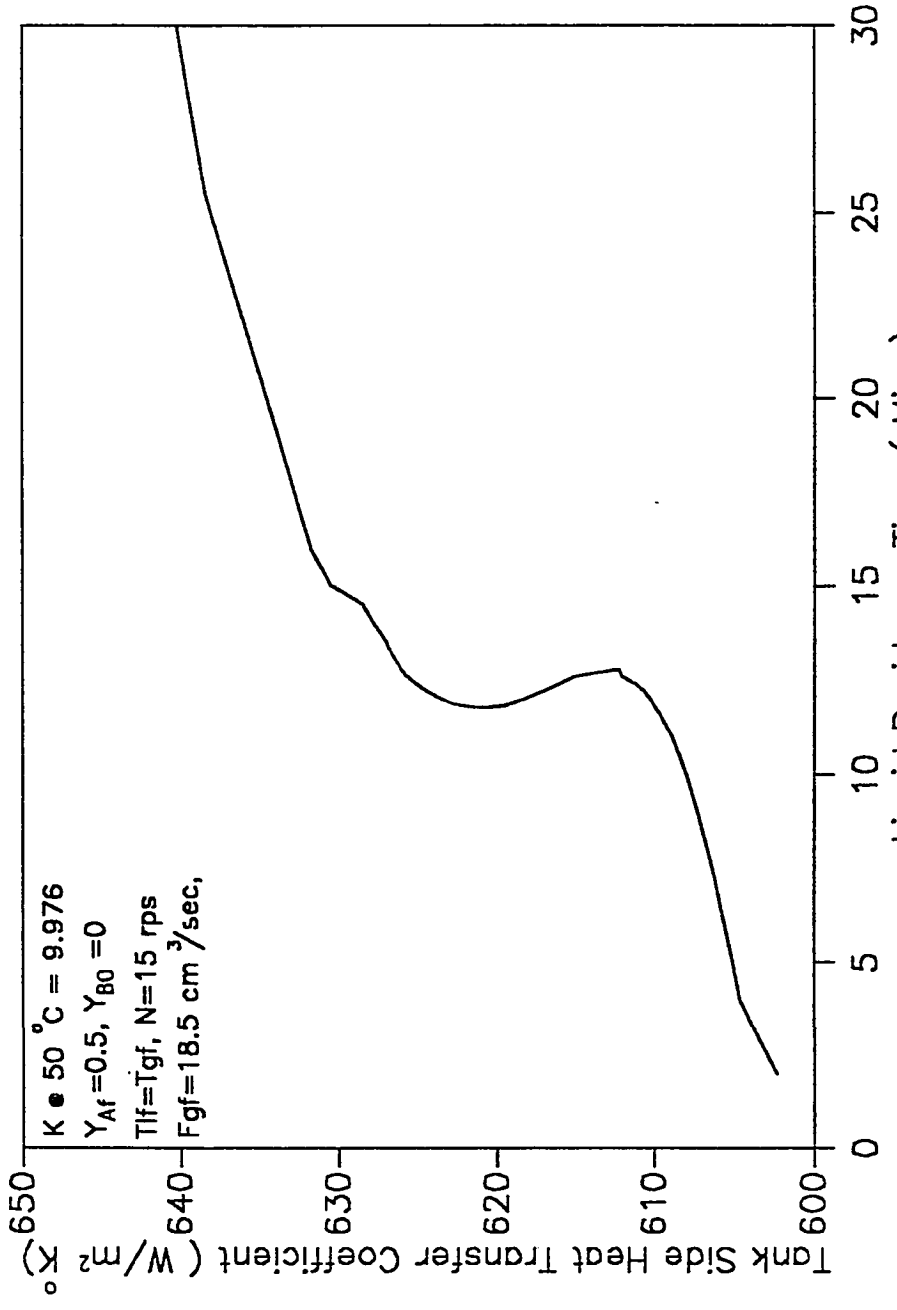

Figure 5.61 Tank–Side Heat Transfer Coefficient versus Liquid Residence Time

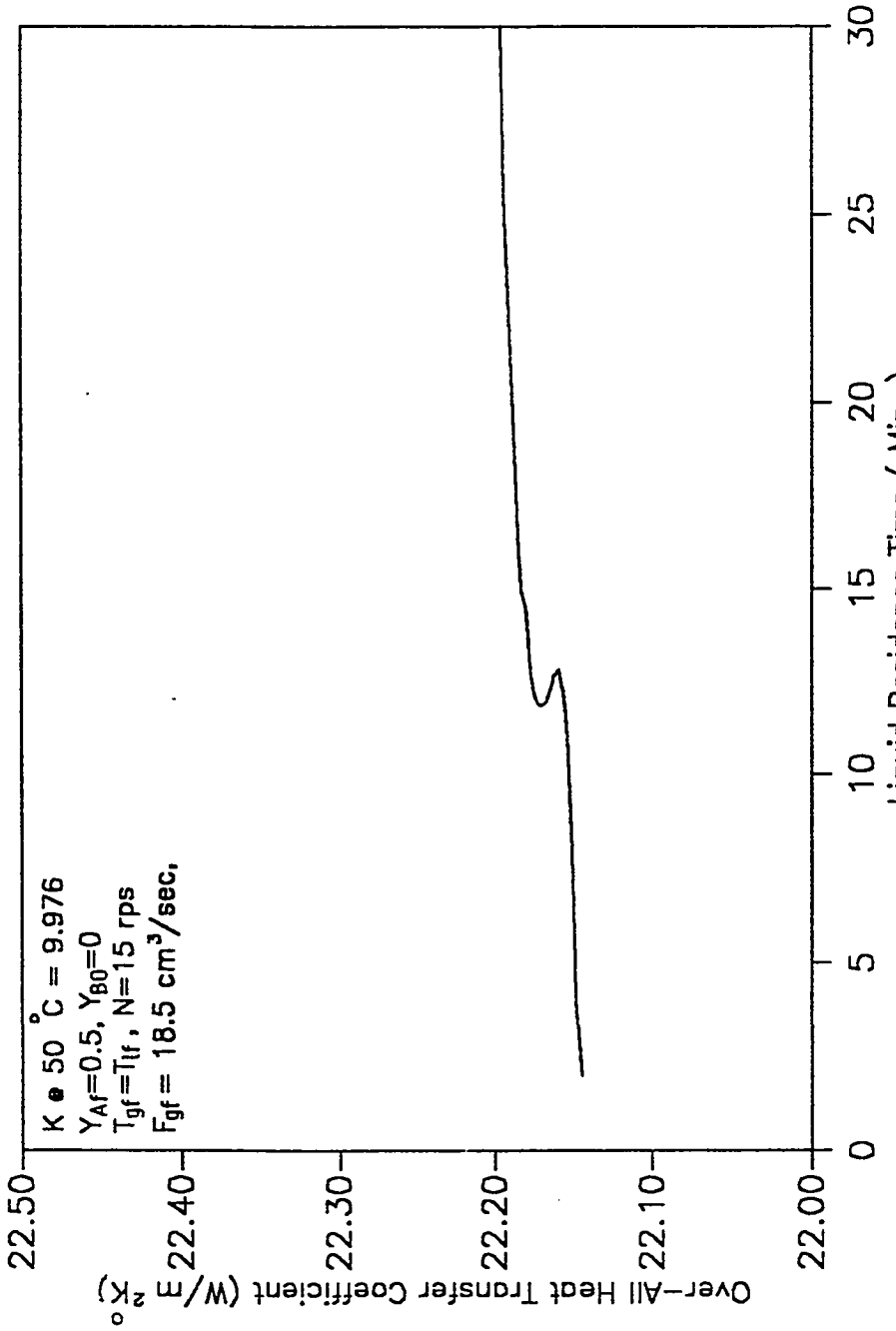

Figure 5.62 Overall Heat Transfer Coefficient versus Liquid Residence Time

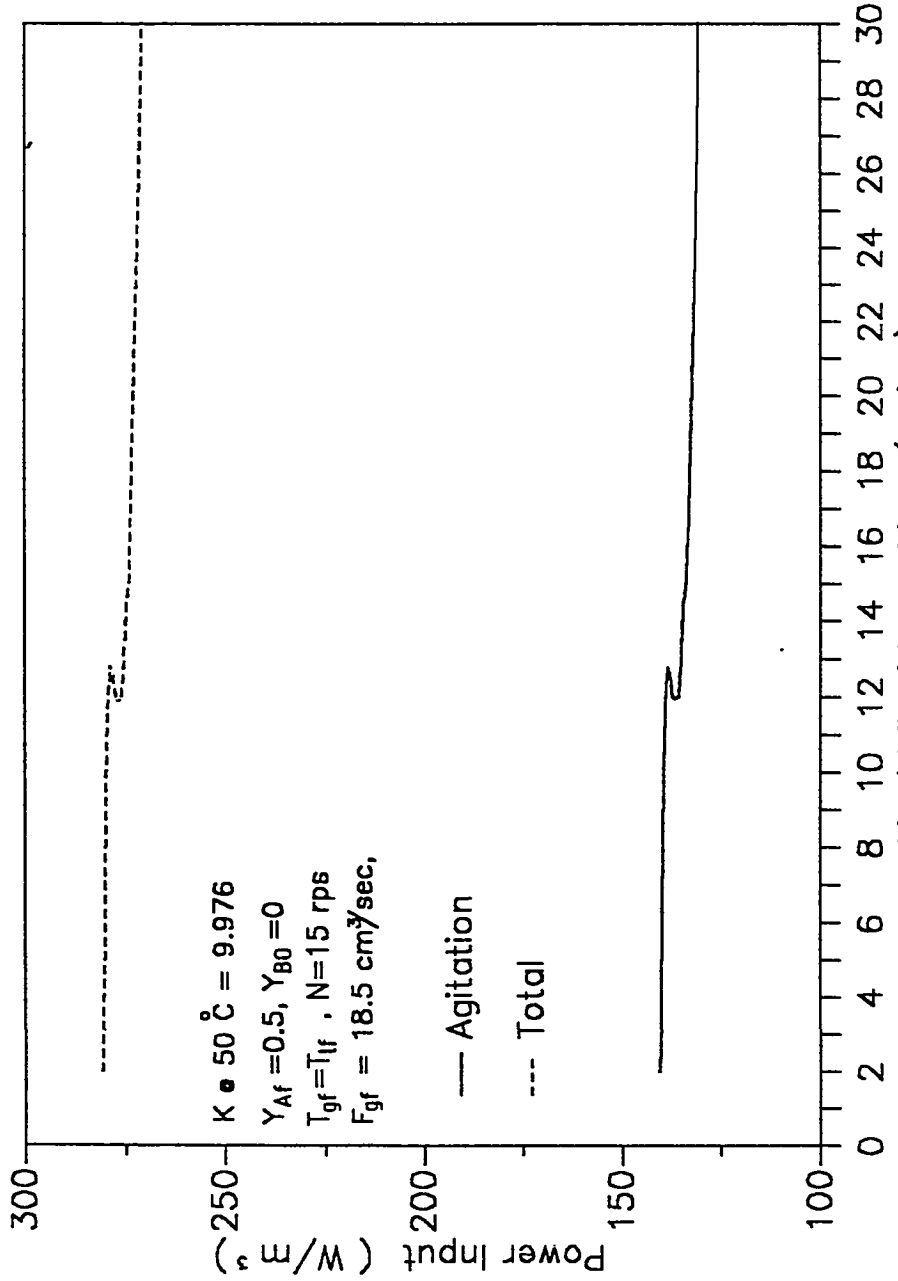

Figure 5.63 Power Input versus Liquid Residence Time

CHAPTER 6

CONCLUSIONS AND RECOMMENDATIONS

1. A comprehensive model for the study of steady state performance of non-isothermal, non-adiabatic, gas-liquid CSTRs has been developed. Unique features of the new model are that it not only relaxes most of the assumptions of the previous researchers but also for the first time combines various complex interactions involved in the modeling of such reactors, i.e, reaction kinetics, interphase mass transfer, physical contacting and the reactor and impeller geometry.

2. In order to account for the influence of chemical reaction on the gas absorption rate, a new approximate reaction factor expression has been derived. The new expression is developed for general second-order kinetics and spherical bubble geometry which in the limit reduces to the reaction factor expressions developed by previous authors.

3. The accuracy of the new reaction factor expression was checked numerically. To do this, a computer program named GLRXN was developed, which solves coupled non-linear ordinary differential equations

using finite difference method combined with a quasi-linearization technique. Reaction factor values obtained by the new approximate analytical expression are in excellent agreement with the values obtained numerically.

4. Parametric study on the local film model, based on spherical geometry shows that when the size of the gas bubble is comparable to the thickness of concentration boundary layer around it, the spherical effect depending on the system conditions may significantly increase or decrease the reaction factor values. Therefore for a rigorous design and analysis of gas-liquid CSTRs reaction factor based on spherical geometry should be used.

5. A comprehensive review of empirical correlations for interfacial area, gas hold-up, bubble diameter, bubble rise velocity, gas and liquid-side mass transfer coefficients, tank and jacket/coil side heat transfer coefficient, power dissipation and the minimum impeller speed for effective gas dispersion is presented and selected correlations for each of the above variables have been incorporated in the model. This review presents a current state of the art concerning research in the area of developing correlations for the hydrodynamic, transport and associated parameters covering varying experimental conditions. These correlations should be developed based on a consistent and coherent experimental design.

6. The comprehensive reactor model developed in this thesis gives rise to a complex set of highly non-linear algebraic equations. A computer program called MULTIPLE has been developed to simulate reactor performance,

which allows the user to specify certain process and operating conditions for the reactor and the coupled heat exchange device to predict and analyse the steady state behavior of the reactor. The computer program can, in future, be used for designing isothermal gas-liquid CSTRs by making slight modifications.

7. Extensive parametric studies have been carried out and the predictions of the new reactor model have been compared with those of the earlier simplified model [26]. The results show that with the new model, regions in different parameter spaces in which multiplicity exists are considerably reduced. Although the new model predicts the same multiplicity patterns and same maximum number of multiple steady states, the conditions under which they occur differ significantly for the two models. Moreover, in certain cases the new model predicts uniqueness while the simplified model predicts multiplicity or vice versa.

8. The numerical reactor simulation results show that the hydrodynamic and transport parameters can change significantly with the change in operating conditions, particularly with varying gas residence times, which indicates that the simulation results with the new model are more realistic and the previous studies over-predicted the regions of multiplicity. Therefore, earlier results on steady state multiplicity can be considered conservative.

9. The nature of feed gas has been found to have a very strong influence on the occurrence of multiplicity. The likelihood of steady state multiplicity decreases with the decrease in feed gas purity which is in line with the work

of Shaikh and Varma [21] for the fast reaction case.

10. Feed gas temperature has been found to effect the regions and pattern of multiplicity. An increase in the feed gas temperature brings down the upper temperature branch and moves up the lower temperature branch, without affecting the middle temperature branch. At higher gas to liquid volumetric flow rate ratios the upper and lower temperature branches merge and a high temperature unique steady state is obtained. The effect of gas temperature at low gas to liquid volumetric flow rate ratios has been found to be negligible. The steady state behavior is very sensitive to liquid feed temperature, an increase in the liquid feed temperature increases the likelihood of multiplicity.

11. The contribution of heat due to agitation in the over-all energy balance of the reactor and the effect of degree of agitation on the the steady state performance of gas-liquid CSTRs has been analysed for the first time in this thesis. It has been found that, depending on the operating conditions, a change in the degree of agitation may influence the regions and patterns of multiplicity. With the increase in impeller speed, the region of multiplicity expands toward higher gas residence time. At very low gas residence time, however, the impeller speed has no effect on the multiplicity.

12. One of the assumptions in our model is that gas and liquid are perfectly mixed. This assumption is justified in our case since we have worked with relatively simple kinetics, at high impeller speeds and with a low viscosity

liquid. However, in case of viscous liquid and the cases involving complex kinetics, micro-mixing should also be considered in the modeling of a CSTR.

13. The literature gives only one report of experimental data showing multiple steady states. This study, however, is based on a consecutive second-order reaction in a laboratory reactor. Therefore, the predictions of the new model are left for the future experimental verification preferably in pilot-plant or laboratory reactor employing second-order gas-liquid reactions. Such experiments should be so designed that they confirm to the requirement of model development.

NOMENCLATURE

A	gaseous reactant
A_{lm}	jacket height, cm
a_i	dimensionless concentration, A_i/B_{lf}
$\underline{a}$	interfacial area per unit reactor volume, 1/cm
B	liquid phase reactant
B_{lm}	jacket width, cm
B	dimensionless quantity, $(\Delta H_s - \Delta H_R)A_{gf}/\rho_l C_{pl} T_{lf}$
b_i	dimensionless concentration, B_i/B_l
C_A	concentration of gaseous reactant, gm/cm^3
C_B	concentration of liquid phase reactant, gm/cm^3
C_p	specific heat, cal/gmol.°K
D_A, D_B, D_{AI}	diffusion coefficients of species A , B and inerts respectively, cm^2/s
D_c	mean or centerline diameter of internal coil helix, cm
D_{ip}	inner diameter of jacket inlet pipe, cm
D_g	equivalent diameter of jacket, cm
D_{gf}	dimensionless quantity, $K_L^o \underline{a}\, V_R H_o/F_{gf}$
D_I	impeller diameter, cm
D_o	sparger orifice diameter, cm
D_S	sparger diameter, cm

D_T tank diameter, cm

d_b bubble diameter, cm

d_{ci} inner diameter of cooling coil, cm

d_{co} outer diameter of cooling coil, cm

d_{cm} log mean diameter cooling coil, cm

E activation energy, cal/gmol

E_A^* reaction factor

E_o Iotvos number, $\frac{gd_b(\rho_l - \rho_g)}{\sigma}$

E_i dimensionless quantity, $\gamma q' + 1$

F volumetric flow rate, cm^3/s

F_N flow number, $\frac{gd_b^{8/3}\Delta\rho\rho_l^{2/3}}{\mu_l^{4/3}\sigma^{1/3}}$

F_{rr} Froude number (rotation), $\frac{N^2 D_I}{g}$

F_{rg} Froude number (gas), $\frac{V_{sg}^2}{gD_T}$

f_J fouling factor inside jacket, cm^2 °K.s/ cal

f_T fouling factor inside tank, cm^2 °K.s/ cal

G_a Galileo number, $\frac{\rho_l g D_I^3}{\mu_l^2}$

g acceleration due to gravity, cm/s^2

H_A Henry's law constant, atm-cm^3/gmol

H_{ag} heat due to agitation, cal/s

H_L clear liquid height, cm

H_c dimensionless quantity, RT_{gf}/H_A

H_p dimensionless quantity, $\frac{H_{ag}}{\rho_l C_{pl} T_{lf} F_{gf}}$

ΔH_R heat of reaction, negative if heat is liberated with reac-

tion, cal/gmol

ΔH_s heat of solution, negative if heat is liberated with dissolution, cal/gmol

ΔH_v heat of vaporization, negative cal/gmol

h_{ci} coilside heat transfer coefficient referred to inside coil area, cal/s. °K. cm^2

h_{co} coilside heat transfer coefficient referred to outside coil area, cal/s. °K. cm^2

h_j jacketside heat transfer coefficient, cal/s. °K. cm^2

h_s distance between impeller and tank bottom, cm

h_T tankside heat transfer coefficient, cal/s. °K. cm^2

K second-order rate coefficient, cm^3/gmol-s.

K_G^o gas-side physical mass transfer coefficient for species B, gmol/cm^2-s-atm

K_L^o liquid-side physical mass transfer coefficient cm s

k_o second-order Arrhenius factor, cm^3/gmols-s.

L_I impeller blade length, cm

M Hatta number, $(KD_A C_{BL})^{1/2}/K_L^o$

M_m modified Hatta number, $\{(KD_A C_{BL})^{1/2}/K_L^o\}(\frac{1+\Omega}{\Omega})$

M_r Morton number, $\frac{g\mu_l}{\rho_l \sigma^3}$

M_w molecular weight

N impeller speed, 1/s

N_A aeration number, $\frac{F_G}{ND_I^3}$

$N_c or N_p$	Newton number or power number, $\frac{P_o}{\rho_l N^3 D_I^5}$
N_m	minimum impeller speed for complete dispersion of gas, 1/s
N_g	molar gas flow rate, gmol/s
N_{uT}	Nusselt number (tank), $\frac{h_T D_T}{\lambda_L}$
P_c	critical pressure, atm
P_T	total pressure in reactor, atm
P_{GT}	total power input, $gmcm^2/s^3$
P_G	power input in presence of gas, $gmcm^2/s^3$
P_o	power input in the absence of gas, $gmcm^2/s^3$
P_{sG}	power input due to gas sparging, $gmcm^2/s^3$
p_A, p_B	partial pressures of species A and B, respectively, atm.
p	dimensionless quantity, $(-\Delta H_R)F_l A_{gf} / \rho_l C_{pl} T_{lf} F_{gf}$
Q	dimensionless quantity, F_{gf}/F_l
q	dimensionless quantity, B_{lf}/A_{gf}
R	universal gas constant
R_{en}	Reynolds number (rotation), $\frac{\rho_l N D_I^2}{\mu_l}$
R_{eb}	Reynolds number (bubble), $\frac{\rho_l V_T d_b}{\mu_l}$
r	dimensionless quantity, $\rho_{gf} C_{pg} / \rho_l C_{pl}$
r_A	reaction rate, gmol/cm^3-s.
S	reactor cooling area, cm^2
S_c	Schmidt number, $\frac{\mu_l}{\rho_l D_A}$
S_h	Sherwood number, $\frac{K_L^o D_I}{D_A}$

T	temperature, °K
T_b	boiling point temperature, °K
T_c	critical temperature, °K
T_r	reduced temperature, T/T_c
U	overall heat transfer coefficient, cal/°K.cm^3.s
U_i	overall heat transfer coefficient based on inside area, cal/°K.cm^3.s
U_o	overall heat transfer coefficient based on outside area, cal/°K.cm^3.s
V_{cl}	critical molal volume of liquid, $cm^3/gmol$
V_L	liquid volume in the reactor,
V_N	velocity number, $\frac{V_T d_b^{2/3} \rho_l^{2/3}}{\mu_l^{1/3} \sigma^{1/3}}$
V_R	reactor volume, $V_L + V_G$,cm^3
V_T	bubble rise velocity, cm/s
v	dimensionless quantity, $(-\Delta H_v)\rho_{gf}/\rho_l C_{pl} T_{lf}$
W_b	baffle width, cm
W_l	impeller blade length, cm $\rho_l N^2 D_j^3 \sigma$
W_{en}	Weber number (rotation),
X_A	dimension less conversion of gaseous reactant
X_B	dimension less conversion of liquid phase reactant
Y_{Bo}	dimensionless quantity, $Y_{Bo}/(1 - Y_{Bo})$
y_A,y_B	mole fraction in gas phase of species A and B, respectively

Z_c	compressibility factor at the critical point

Greek Symbols

α	dimensionless quantity, (1/Q) + r
α'	dimensionless parameters in the reaction factor expression. $\{\varepsilon_L K_L^o/\underline{a}D_A\}(\Omega/1 + \Omega)$
β	dimensionless quantity, $US/F_{gf}\rho_l C_{pl}$
δ	dimensionless quantity, $(\Delta H_s)/RT_{lf}$
ε_G	fractional gas holdup, V_G/V_R
ε_L	fractional liquid holdup, V_L/V_R
γ	dimensionless quantity, $D_B/\nu D_A$
λ_c	thermal conductivity of cooling water, cal/s.cm.°K
λ_{ins}	thermal conductivity of insulation, cal/s.cm.°K
λ_L	thermal conductivity of liquid, cal/s.cm.°K
λ_m	thermal conductivity of reactor material, cal/s.cm.°K
μ	viscosity, cp
ν	stoichiometric coefficient
Ω	dimension less quantity $(K_L^o R - D_A)/D_A$
Ψ'	dimensionless quantity, $K_L^o/K_G^o H_A$
θ	dimensionless reactor temperature, $(T - T_{lf})/T_{lf}$
θ_c	dimensionless quantity, $(T_c - T_{lf})/T_{lf}$
θ_r	ratio of feed temperatures, T_{gf}/T_{lf}
τ_l	liquid residence time, s
τ_G	gas residence time, s

ξ	dimensionless parameters in the reaction factor expression, $\varepsilon_L \Omega / \underline{a} K_l^{\circ} \tau_l (1 + \Omega)$

Subscripts

c	cooling water
f	feed
G or g	gas phase
i	gas-liquid interface
L or l	liquid phase
lb	lower bound
ub	upper bound
w	at tank wall

REFERENCES

1. Doraiswamy, L.K. and Sharma, M.M. "Heterogeneous Reactions: Analysis, Examples and Reactor Design," Volume 2. John Wiley & Sons, N.Y., (1984).

2. Midoux, N. and Charpentier, J.C., "Mechanical Agitated Gas-Liquid Reactors. Part 1. Hydrodynamics," Int. Chem. Eng., **24**, 249 (1984).

3. Trambouze, P., Van Landengham, H. and Wauquier, J.P., "Chemical Reactors: Design/Engineering/Operation," Editions Technip, Paris, p. 251-295 (1988).

4. Mann, R., "Gas-Liquid Contacting in Mixing Vessels," The Institute of Chemical Engineers, England, (1983).

5. Sharma, S., Hoffman, L.A. and Luss, D.,"Steady State Multiplicity of Adiabatic Gas-Liquid Reactors," AIChE J., **22**, 324 (1976).

6. Huang, D.T.J. and Varma, A., "Steady State Uniqueness and Multiplicity of Nonadiabatic Gas-Liquid CSTRs: Part I: Second Order Reaction Model," AIChE J., **27**, 481 (1981).

7. Ding, J.S.Y., Sharma, S. and Luss, D., "Steady State Multiplicity and Control of the Chlorination of n-Decane in an Adiabatic CSTR," Ind. Eng.

Chem. Fundam., **13**, 76 (1974) .

8. Hancock M.D. and Kenney, C.N., "The Stability and Dynamics of a Gas-Liquid Reactor," Chem. Eng. Sci., **32**, 629 (1977).

9. Perlmutter, D.D., " Stability of Chemical Reactors," Prentice-Hall Inc., Englewood Cliffs, N.J. (1972).

10. Denn, M.M., "Stability of Reaction and Transport Process," Prentice-Hall Inc., Englewood Cliffs, N.J. (1975).

11. Shaikh, A.A.,"Effect of Gas Side Resistance on Steady State Multiplicity in Gas-Liquid CSTRs," Chem. Eng. Comm., **52**, 331 (1987).

12. Van Krevelen, D.W. and Hoftijzer, P.J.,"Kinetics of Gas-Liquid Reactions: General Theory," Rev. Chim. Pays-Bas, **67**, 563 (1948).

13. Teramoto, M., Nagayasu, T., Matsui, K., Hashimoto, K., and Nagota, S., "Selectivity of Consecutive Gas-liquid Reactions," J. Chem. Eng. Japan, **2**, 186 (1969)

14. Zarook, S.M.,"Modeling of Non-Isothermal Bubble Column Reactors," M. S. Thesis, King Fahd University of Petroleum and Minerals, Dhahran, Saudi Arabia, (1989).

15. Schmitz R.A. and Amundson N.R., "An Analysis of Chemical Reactor Stability and Control," Chem. Eng. Sci., **8**, 265,391,415,447 (1963).

16. Hoffman, L.A., Sharma, S., and Luss, D.,"Steady State Multiplicity of

Adiabatic Gas-Liquid Reactors I: The Single Reaction Case.," AIChE J., **21**, 318 (1975).

17. Raghuram, S. and Shah, Y.T., "Criteria for Unique and Multiple Steady States for a Gas-Liquid Reaction in an Adiabatic CSTR," Chem. Eng. J., **13**, 81 (1977).

18. Raghuram, S., Shah, Y.T., and Tierney, J.W., "Multiple Steady States in Gas-Liquid Reactors," Chem. Eng. J., **17**, 63 (1979).

19. Huang, D.T.J. and Varma, A., "Steady State and Dynamic Behavior of Fast Gas-Liquid Reactions in Non-adiabatic Continuous Stirred Tank Reactors," Chem. Eng. J., **21**, 47 (1981).

20. Huang, D.T.J. and Varma, A., "Steady State Uniqueness and Multiplicity of Nonadiabatic Gas-Liquid CSTRs; Part II: Discrimination among Rival Reaction Models," AIChE J., **27**, 489 (1981).

21. Singh, C.P.P., Shah, Y.T., and Carr, N.L., "The Effect of Gas Feed Temperature on the Steady State Multiplicity of an Adiabatic CSTR with a Fast Pseudo-First-Order Reaction," Chem. Eng. J., **23**, 101 (1982).

22. Shaikh, A.A., and Varma, A., "On Steady State Uniqueness and Multiplicity in Gas-Liquid Continuous Stirred Tank Reactors with Fast Reactions," Chem. Eng. J., **29**, 59 (1984).

23. White, D. and Johns, L.E., "Gas-Liquid Reaction System: A Heuristic Model and its Steady Solutions," AIChE J., **32**, 981 (1986)

24. Westerterp, K.R., Vanswaaij, W.P.M. and Beenackers, A.A.C.M., "Chemical Reactors Design and Operation," John Wiley & Sons, N.Y., (1984).

25. Westerterp, K.R. and Crombeen, P.R.J.J., "Thermal Behavior of Agitated Gas-Liquid Reactors with A Vaporizing Solvent/Air Oxidation of Hydrocarbons," Chem. Eng. Sci., **38**, 1331 (1983).

26. Shaikh, A.A., Batran, S.H. and Zarook, S.M., " Effect of Liquid Reactant Volatility on the Behavior of Gas-liquid CSTRs," Proc. Third Saudi Engineering Conference, Riyadh, Saudi Arabia, (1991).

27. Balakotaiah, V. and Luss, D., "Multiplicity Features of Reacting Systems: Dependence of Steady State on The Residence Time," Chem. Eng. Sci., **38**, 1709 (1983).

28. Balakotaiah, V., and Luss, D.," Analysis of The Multiplicity Patterns of a CSTR," Chem. Eng. Comm., **13**, 111 (1981); **19**, 185 (1982).

29. Uppal, A.W., Ray, W.H. and Poore, A. B., "Classification of Dynamic Behavior of Continuous Stirred Tank Reactors - Influence of Residence Time," Chem. Eng. Sci., **31**, 205 (1976).

30. Leib, T.M. and Luss, D. "Exact Uniqueness and Multiplicity Criteria for n-th Order Reaction in a CSTR," Chem. Eng. Sci., **36**, 210 (1981).

31. Luss, D., "Steady State Multiplicity and Stability", in "Multiphase Chemical Reactors - Volume 1," Eds.: A. E. Rodrigues, J. M. Calo and N.

H. Sweed, Sijthoff E. Noordhoff. The Hague, p. 405 (1981).

32. Joshi, J.B., Patil, T.A., Ranade. V.V. and Shah, Y.T., "Measurement of Hydrodynamic Parameters in Multiphase Sparged Reactors," Rev. Chem. Eng., **6**, 76 (1990).

33. Oyevaar, M.H. and Westerterp. K.R., "The Use of the Chemical Method for the Determination of Interfacial Areas in Gas-Liquid Contactors," Chem. Eng. Sci., **44**, 2691 (1989).

34. Ridgway, D. and Sharma, R.N. and Hanley, T.R., "Determination of Mass Transfer Coefficients in Agitated Gas-Liquid Reactors By Instantaneous Reaction," Chem. Eng. Sci., **44**, 2935 (1989).

35. Schugerl, K., Lubbert, A., Korte, T. and Diekmann, J., "Measuring Techniques for Characterizing Gas/Liquid Reactors," Int. Chem. Eng., **27**, 583 (1987).

36. Bondy, F. and Lippa, S., "Heat transfer in Agitated Vessels," Chem. Eng., 62. (April,4 1983).

37. Uhl, V.W. and Gray, J.B., "Mixing Theory and Practice," Vol. I, Academic Press, N.Y., (1966).

38. Nagata, S., "Mixing Principles and Applications," John Wiley & Sons, N.Y., (1975).

39. Harnaby, N., Edwards, M.F., "Mixing in the Process Industries,"

Butterworths, London, (1985).

40. Dickey, D.S. "Succeed at Stirred-Tank Reactor Design," Chem. Eng. Prog., 22 (Dec. 1991).

41. Steiff, A., Poggemann, R. and Weinspach, P.M., "Heat Transfer in Agitated Vessels with Multiphase Systems," Ger. Chem. Eng., **4**, 30 (1981).

42. Rushton, J.H., Costick, E.W. and Everett, H.J., "Power Characteristics of Mixing Impellers," Chem. Eng. Prog., **46**, 395 (1950).

43. Holland, F.A. and Chapman, F.S., "Liquid Mixing and Processing in Stirred Tanks," Reinhold Publishing Corporation, N.Y. (1966).

44. Gianetto, A. and Silveston, P., "Multiphase Chemical Reactors: Theory, Design, Scale-up," Hemisphere Publishing Corporation , N.Y., (1986).

45. Litz, L.M., "A Novel Gas-Liquid Stirred Tank Reactor," Chem. Eng. Prog., 36 (Nov. 1985).

46. van't Riet, K. and Smith, J.M., "The Trailing Vortex System Produced by Rushton Turbine Agitators," Chem. Eng. Sci., **30**, 1093 (1975).

47. Nienow, A.W., Wisdom, D.T. and Middleton, J.C.,"The Effect of Scale and Geometry on Flooding, Recirculation and Power in Gas Stirred Vessels," Proc. 2nd Euro. Conf. on Mixing, BHRA Fluid Engineering, Cranfield, F1., (1977).

48. Nienow, A.W. and Wisdom, D.J., "Flow Over Disc Turbine Blade," Chem.

Eng. Sci., **29**, 1994 (1974).

49. Calabrese, R.V. and Stoots, C.M., "Flow in the Impeller Region of a Stirred Tank," Chem. Eng. Prog., 43 (May 1989).

50. Bruijn, W., van't Riet, K. and Smith, J.M., "Power Consumption with Aerated Rushton Turbines," Trans. Inst. Chem. Engrs., **52**, 88 (1974).

51. Warmoeskerken, M.M.C.G. and Smith, J.M., "The Flooding Transition with Gassed Rushton Turbines," Inst. Chem. Engrs. Symp. Ser., **89**, 59 (1981).

52. Ismail, A.F., Nagase, Y. and Imon, J., "Power Characteristics and Cavity Formation in Aerated Agitations," AIChE J., **30**, 487 (1984).

53. Nienow, A.W., Warmoeskerken, M.M.C.G., Smith, J.M. and Konno, M., "The Flooding /Loading Transition and the Complete Dispersal Condition in Aerated Vessels Agitated by a Rushton Turbine," Proc. 5th Euro. Conf. on Mixing, BHRA Fluid Engineering, Cranfield, 143 (1985).

54. Nienow, A.W., "Gas Dispersion Performance in Fermenter Operation," Chem. Eng. Prog., 61 (Feb. 1990).

55. Greaves, M. and Kobaccy, K.A.H., "Power Consumption and Impeller Dispersion Efficiency in Gas-Liquid Mixing," Inst. Chem. Engrs. Symp. Ser., **64**, L1 (1981).

56. Mann, R., "Gas-Liquid Stirred Vessel Mixers: Towards A Unified Theory

Based on Networks-of-Zones," Chem. Eng. Res. Des., **64**, 23 (1986).

57. Westerterp, K.R., Van Dierendonck, L.L. and De Kraa, J.A. "Interfacial Areas in Agitated Gas-Liquid Contactors," Chem. Eng. Sci., **18**, 157 (1963).

58. Mikulcova, E., Kudrna, V. and Vlacek, J., "Determination of the Boundary Conditions for Flooding of a Stirrer," Sb. Vys. Sk. Chem. Technol. Praze, (Oddil): Chem. Inz. Autom. K1, 167 (1967).

59. Dierendonck, L.L. van, Fortuin, J.M.H. and Venderbos, D., "The Specific Contact Area in Gas-Liquid Reactors," Proc. 4th Euro. Symp. Chem. Reaction Eng., 205 (1968).

60. Smith, J.M., Van't Reit, K. and Middleton, J.C., "Scale-Up of Agitated Gas-Liquid Reactors for Mass Transfer," Proc. 2nd Euro. Conf. Mixing, F4 (1977).

61. Dickey, D.S., "Turbine Agitated Gas Dispersion - Power, Flooding, and Hold-Up," AIChE 72nd Annula Meeting San Francisco, (1975).

62. Wiedmann, J.A., Steiff, A. and Weinspach, P.M., "Investigation of Power Consumption, Suspension and Flooding Characteristics of Stirred Slurry Reactors," Ger. Chem. Eng. **3**, 303 (1980).

63. Warmoeskerken, M.M.C.G. and Smith, J.M., "Flooding of Disc Turbines in Gas-Liquid Dispersion: A New Description of the Phenomenon," Chem. Eng. Sci., **40**, 2063 (1985).

64. Wong, C.W., Wang, J.P. and Huang, S.T., "Fluid Dynamics of Stirred Three-Phase Reactors," Proc. ROC - Japan Joint Symp. Three Phase Reactors, Taipei 208 (1986).

65. Wiedmann, J.A., "The Flooding Behavior of Two and Three-Phase Stirred Reactors," Int. Chem. Eng., **26**, 189 (1986).

66. Lu, W.M. and Chen, H., "Flooding and Critical Impeller Speed for Gas Dispersion in Aerated Turbine Agitated Vessels," Chem. Eng. J., **33**, 57 (1986).

67. Desplanches, H., Essayem, F. and Chevalier, J.L., "Hydrodynamics and Heat Transfer in Agitated, Aerated Newtonian and Highly Viscous Liquids, in the Transitional Flow Regime," Proc. 6th Euro. Conf. on Mixing, BHRA Fluid Engineering, Springer-Verlag, London, 479 (1988).

68. Lu, W.M. and Ju, S.J., "Cavity Configuration, Flooding and Pumping Capacity of Disc-Type Turbines in Aerated Stirred Tanks," Chem. Eng. Sci., **44**, 333 (1989).

69. Barona, N., "Design CSTR Reactors This Way," Hydrocarbon Processing, 179 (July 1979).

70. Calderbank, P.H. and Moo-Young, M.B., Trans. Inst. Chem. Engrs., **39**, 22 (1961). Cited in Mann [4].

71. Joshi, J.B., Pandit, A.B. and Sharma, M.M.," Mechanically Agitated Gas-Liquid Reactors," Chem. Eng. Sci., **12**, 813 (1982).

72. Michel, B.J. and Miller, S.A., "Power Requirement of Gas-Liquid Agitated Systems," AIChE J., **8**, 262 (1962).

73. Calderbank, P.H., "Physical Rate Processes in Industrial Fermentation. Part 1: The Interfacial Area in Gas-Liquid Contacting with Mechanical Agitation," Trans. Inst. Chem. Engrs., **36**, 443 (1958).

74. Pharamond, J.C., Roustan, M. and Roques, H., "Determination De La Puissance Consommee Dans Une Cuve Aeree Et Agitee" Chem. Eng. Sci., **30**, 907 (1975).

75. Hassan, I.T.M. and Robinson, C.W., "Stirred-Tank Mechanical Power Requirement and Gas Holdup in Aerated Aqueous Phase," AIChE J., **23**, 48 (1977).

76. Luong, H.T. and Volesky, B., "Mechanical Power Requirements of Gas-Liquid Agitated Systems," AIChE J., **25**, 893 (1979).

77. Hughmark, G.A., "Power Requirements and Interfacial Area in Gas-Liquid Turbine Agitated Systems," Ind. Eng. Chem. Proc. Des. Dev., **19**, 638 (1980).

78. Brown, D.E., "Impeller Power Input Measurements in a Production-Scale Fermenter," Inst. Chem. Engrs. Symp. Ser. **64**, N1 (1981).

79. Miller, D.N., "Scale-Up of Agitated Vessels Gas-Liquid Mass Transfer," AIChE J., **20**, 445 (1974).

80. Grace, J.R., "Shapes and Velocities of Bubble Rising in Infinite Liquids," Trans. Inst. Chem. Engrs., **51**, 116 (1973).

81. Abou-El-Hassan, M.E., "A Generalized Bubble Rise Velocity Correlation," Chem. Eng. Commun., **22**, 243 (1983).

82. Rushton, J.H. and Bimbinet, J.J., "Holdup and Flooding in Air Liquid Mixing," Can. J. Chem. Eng., **46**, 16 (1968).

83. Figueiredo, M. and Calderbank, P.H., " Some Effects of Agitator Configuration on Mass Transfer in a Larger Aerated Mixing Vessels, Proc. Int. Symp. on Mixing, Faculte Polytechnique de Mons., Belgium, (1978).

84. Roustan, M., " The Study of Agitation and Mass Transfer in Gas-Liquid Reactors," Thesis University de Toulouse, France (1978).

85. Loiseau, B., Midoux, N. and Charpentier, J.C., "Some Hydrodynamics and Power Input Data in Mechanically Agitated Gas-Liquid Contactors," AIChE J., **27**, 931 (1977).

86. Young, C.N., Wong, C.W. and Chang, C.L., "The Prediction of Power Consumption in the Agitation of Gas-Liquid System," Can. J. Chem. Eng., **57**, 672 (1979).

87. Midoux, N. and Charpentier, J.C., "Mechanical Agitated Gas-Liquid Reactors. Part 2. Interfacial Area," Int. Chem. Eng., **24**, 452 (1984).

88. Sridhar, T. and Potter, O.E. "Interfacial Areas in Gas-Liquid Stirred

Vessels," Chem. Eng. Sci., **35**, 683 (1979).

89. Oyevaar, M.H., Bos, R. and Westerterp, K.R. "Interfacial Areas and Gas Hold-Ups in Gas Liquid Contactors at Elevated Pressures from 0.1 to 8.0 MPa," Chem. Eng. Sci., **46**, 1217 (1991).

90. Albal, R.S., Shah, Y.T. and Schumpe, A., "Mass Transfer in Multiphase Agitated Contactors," Chem. Eng. J., **27**, 61 (1983).

91. Calderbank, P.H. and Moo-Young, M.B., "The Continuous Phase Heat and Mass Transfer Properties of Dispersion," Chem. Eng. Sci., **16**, 39 (1961).

92. Prasher B.D. and Wills, G.B., "Mass Transfer in an Agitated Vessels," Ind. Eng. Chem. Proc. Des. Dev., **12**, 351 (1973).

93. Yagi, H. and Yoshida, F., "Gas Absorption by Newtonian and Non-Newtonian Fluids in Sparged Agitated Vessels," Ind. Eng. Chem. Proc. Des. Dev., **14**, 351 (1975).

94. Van't Riet, K., "Review of Measuring Methods and Results in Non-Viscous Gas-Liquid Mass Transfer in Stirred Vessels," Ind. Eng. Chem. Proc. Des. Dev., **18**, 367 (1979).

95. Lopes De Figueiredo, M.M. and Calderbank, P.H., "The Scale-Up of Aerated Mixing Vessels for Specified Oxygen Dissolution Rates," Chem. Eng. Sci., **34**, 1333 (1979).

96. Chandrasekharan, K. and Calderbank, P.H., "Further Observations on the Scale-Up of Aerated Mixing Vessels," Chem. Eng. Sci., **36**, 819 (1981).

97. Andrew, S.P.S., "Gas-Liquid Mass Transfer in Microbiological Reactors," Trans. Inst. Chem. Engrs., **60**, 3 (1982).

98. Judat, H., "Gas-Liquid Mass Transfer in Stirred Vessels - A Critical Review," Ger. Chem. Eng., **60**, 357 (1982).

99. Linek, V., Vacek, V. and Benes, P., "A Critical Review and Experimental Verification of the Correct Use of the Dynamic Method for the Determination of Oxygen Transfer in Aerated Agitated Vessels to Water, Electrolyte Solutions and Viscous Liquids," Chem. Eng. J., **34**, 11 (1987).

100. Schmitz, M., Steiff, A. and Weinspach, P.M., "Gas-Liquid Interfacial Area per Unit Volume and Volumetric Mass Transfer Coefficient in Stirred Slurry Reactors," Chem. Eng. Technol., **10**, 204 (1987).

101. Linek, V. and Vacek, V., "Volumetric Mass Transfer Coefficient in Stirred Reactors," Chem. Eng. Technol., **11**, 249 (1988).

102. Hickman, A.D., "Gas-Liquid Oxygen Transfer and Scale-Up. A Novel Experimental Technique with Results for Mass Transfer in Aerated Agitated Vessels," Proc. 6th Euro. Conf. on Mixing, BHRA Fluid Engineering, Springer-Verlag, London, 369 (1988).

103. Calderbank, P.H., "Physical Rate Process in Industrial Fermentation Part 2: Mass Transfer Coefficient in Gas-Liquid Contacting with and without

Mechanical Agitation," Trans. Inst. Chem. Engrs., 37, 173 (1959).

104. Newman, A.B., AIChE Trans., 27, 310 (1931). Cited in Barona [69].

105. Rase, H.F., "Chemical Reactor Design for Process Plants," Vol. 1, John Wiley & Sons, N.Y. (1977).

106. Sharma, M.M. and Mashelkar, R.A., "Mass Transfer with Reaction," Inst. Chem. Engrs. Symp. ser., 28, 10 (1968).

107. Rao, K.B. and Murti, P.S., "Heat Transfer in Mechanically Agitated Gas-Liquid Systems," Ind. Eng. Chem. Proc. Des. Dev., 12, 190 (1973).

108. Steif, A. and Weinspach, P.M., "Heat transfer in Stirred and Non-Stirred Gas-Liquid Reactors," Ger. Chem. Eng., 1, 150 (1978).

109. Pollard, R. and Topiwala, H.H.,"Heat Transfer Coefficient and Two-Phase Dispersion Properties in a Stirred Tank Fermento," Boitech. and Bioeng., 18, 1517 (1976).

110. Zlokarnik, M., " Heat Transfer in Gas-Liquid Agitated Vessels," Chem. Ing. Tech., 38, 717 (1966).

111. Maerteleire, E. D.,"Heat Transfer to a Helical Cooling Coil in Mechanically Agitated Gas-Liquid Dispersions," Chem. Eng. Sci., 33, 1107 (1978).

112. Nagata, S., Nishikawa, M., Itaya, M. and Ashiwake, K., "Study of Heat Transfer for Aerated Mixing Vessel and Aerated Tower," Heat Transfer-

Jpn Res., **5**, 75 (1976).

113. Edney, H.G.S.and Edwards, M.F.,"Heat Transfer to Non-Newtonian and Aerated Fluids in Stirred Tanks," Trans. Inst. Chem. Engrs, **54**. 160 (1976).

114. Kurpiers, P., Steif, A., Weinspach, P.M., " Heat Transfer in Stirred Multiphase Reactors," Ger. Chem. Eng., **8**, 48 (1985).

115. Kurpiers, P., Steif, A., Weinspach, P.M., "Reactor Wall/Fluid Heat Transfer in a Stirred Single or Multi-phase Reactor Using Single or Two-stage Disk Stirrers," Ger. Chem. Eng., **9**, 190 (1986).

116. Kurpier, P., Steif, A. and Weinspach, P.M., "Heat Transfer and Scale-up in Stirred Single and Multiphase Reactors with Immersed Heating Elements," Ger. Chem. Eng., **8**, 267 (1985).

117. Rose, L.M., "Chemical Reactor Design in Practice," Elsevier Scientific Publishing Company, N.Y., (1981).

118. Lehrer, I.H., "Jacket-Side Nusselt Number," Ind. Eng. Chem. Proc. Des. Dev., **9**, 553 (1970).

119. Bolliger, D.H., "Assessing Heat Transfer in Process Vessel Jackets," Chem. Eng., 95 (Sept., 20 1983).

120. Stein, W.A. and Schmidt, W., "Heat Transfer in Agitated Tank Jackets with Liquid Media," Ger. Chem. Eng., **9**, 362 (1986).

121. Dankwerts P.V.,"Gas Liquid Reactions," McGraw Hill N.Y., (1970).

122. Juvekar, R.A. and Sharma, M.M., "Some Aspects of Process Design of Gas-Liquid Reactors," Trans. Inst. Chem. Engrs., **55**, 77 (1977).

123. Alper, E., "Mass Transfer with Chemical Reaction in Multiphase System," Vol. 1, NATO ASI Series, Martinus Nijhoff Publishers, (1983).

124. Carberry, J.J., "Chemical and Catalytic Reaction Engineering," McGraw Hill N.Y., 244-306 (1976).

125. Nagy, E.,"Mass Transfer Through Spherical Surface Accompanied by Chemical Reaction," Hung. J. Ind. Chem., **14**, 163 (1986).

126. Ruckenstein, E.V., Dang, D. and Gill, W.W., "Mass Transfer with Chemical Reaction from Spherical one or Two Components Bubbles or Drops, " Chem. Eng. Sci., **26**, 647 (1971).

127. Nienow, A.W., "Agitated Vessel Particle-Liquid Mass Transfer: A Comparison between Theories and Data," Chem. Eng. J. **9**, 153 (1975).

128. Johnson, A.I. and Akeheta, T., "Mass Transfer with Chemical Reaction from Single Spheres," Can. J. Chem. Eng., **47**, 88 (1969).

129. Lee, E.S, "Quasilincarization, Difference Approximation, and Nonlinear Boundary Value Problems," AIChE J. **14**, 90 (1968).

130. Hoffman, L.A., MSc. Thesis, " Theoretical Study of Steady State Multiplicity and Stability in Gas-Liquid Continuous Stirred Tank

Reactors," Univ. Houstan, Texsas, (1974).

131. Robert, C.R., Prausnitz, J.M. and Sherwood, T.K., "The Properties of Gases and Liquids," 3rd ed., McGraw-Hill Book Company, N.Y. (1977).

132. Robert, C.W., "Handbook of Chemistry and Physics," 49th ed., The Chemical Rubber Co., Ohio, (1968).

APPENDIX A1

DERIVATION OF REACTOR MODEL

Mass Balance of The Gaseous Reactant, A

Moles of A in the Gas Feed = $N_{gf}Y_{Af}$

Moles of A in the Effluent Gas = $N_{go}Y_{Ao}$

Moles of A Consumed in the Reaction = $R_A V_R$

Moles of A in the Effluent Liquid = $F_l A_l$

Steady state mole balance of Gaseous reactant A across the reactor:

Moles of A in Gas Feed − *Moles of A in Effluent Gas* = *Moles of A consumed in the Reaction* + *Moles of A in Effluent Liquid*

$$N_{gf}Y_{Af} - N_{go}Y_{Ao} = R_A V_R + F_l A_l \qquad (A1.1)$$

Mass Balance of The Liquid Reactant, B

Moles of B in the Liquid Feed = $F_l B_{lf}$

Moles of B in the Liquid Effluent = $F_l B_l$

Moles of B Consumed in the Reaction = $R_B V_R$ or $\nu R_A V_R$

Moles of B in the Effluent Gas = 0 (Condensate is returned to reactor)

Steady state mole balance of Liquid reactant B across the reactor:

Moles of B in Liquid Feed − *Moles of B in Liquid Effluent* = *Moles of B consumed in the Reaction* + *Moles of B in Effluent Gas*

$$F_l B_{lf} - F_l B_l = \nu R_A V_R + 0$$

$$F_l(B_{lf} - B_l) = \nu R_A V_R \qquad \text{(A1.2)}$$

Mass Balance of The Gaseous Inerts

Moles of Inerts in the Gas Feed = $N_{gf}(1 - Y_{Af})$

Moles of Inerts in the Effluent Gas = $N_{go}(1 - Y_{Ao} - Y_{Bo})$

Moles of Inerts in the Liquid Effluent = 0 (Inerts are not absorbed in liquid)

Steady state mole balance of gaseous inerts across the reactor:

Moles of Inerts in Gas Feed = *Moles of Inerts in Effluent Gas* + *Moles of Inerts in Liquid Effluent*

$$N_{gf}(1 - Y_{Af}) = N_{go}(1 - Y_{Ao} - Y_{Bo}) \qquad \text{(A1.3)}$$

Energy Balance

Heat Input (Gas Feed) = $N_{gf} C_{pg} T_{gf}$

Heat Input (Liquid feed) = $F_l \rho_l C_{pl} T_{lf}$

Heat Generated (Reaction) = $(-\Delta H_R) R_A V_R$

Heat Generated (Absorption) = $(-\Delta H_s)[R_A V_R + F_l A_l]$

Heat Generated (Agitation) = $0.239 \times 10^{-7} P_{GT} = H_{ag}$

Heat Output (Effluent Gas) = $N_{go}(1 - Y_{Bo}) C_{pg} T$

Heat Output (Liquid Effluent) = $F_l \rho_l C_{pl} T$

Heat Loss (Cooling) = $U S(T - T_c)$

Heat Loss (Liquid Evaporation) = $N_{go}Y_{Bo}(-\Delta H_v)$

Steady state energy balance across the reactor:

$$\underset{(Liquid+Gas)}{Heat\ Input} + \underset{(Reactn+Absptn+Agitn)}{Heat\ Generated} = \underset{(Liquid+Gas)}{Heat\ Output} + \underset{(Cooling+Evaporation)}{HeatLoss}$$

$$F_l\rho_l C_{pl}T_{lf} + N_{gf}C_{pg}T_{gf} + [(-\Delta H_s) + (-\Delta H_R)]R_A V_R + (-\Delta H_s)F_l A_i + H_{og} =$$

$$F_l\rho_l C_{pl}T + N_{go}(1 - Y_{Bo})C_{pg}T + US(T - T_c) + N_{go}Y_{Bo}(-\Delta H_v)$$

Rearranging we get:

$$F_l\rho_l C_{pl}(T_{lf} - T) + N_{gf}C_{pg}T_{gf} + [(-\Delta H_s) + (-\Delta H_R)]R_A V_R + H_{og} +$$

$$(-\Delta H_s)F_l A_i - N_{go}(1 - Y_{Bo})C_{pg}T - N_{go}Y_{Bo}(-\Delta H_v) - US(T - T_c) = 0 \quad (A1.4)$$

Rate of absorption of gaseous reactant A in terms of liquid-side mass transfer coefficient:

$$N_A = \underline{a}K^{\circ}_L V_R A_i E^{*}_A = (R_A V_R + F_l A_i)$$

Substituting for $(R_A V_R + F_l A_i)$ from Equation (A1.1) in the above equation and rearranging, we get:

$$N_A = \underline{a}K^{\circ}_L V_R A_i E^{*}_A = N_{gf}Y_{Af}\left[1 - \frac{N_{go}Y_{Ao}}{N_{gf}Y_{Af}}\right] = N_{gf}Y_{Af}X_A \quad (A1.5)$$

Rate of absorption of gaseous reactant A in terms of gas-side mass transfer coefficient:

$$N_A = \underline{a}K^{\circ}_G V_R(p_{Ab} - p_{Ai}) \quad (A1.6)$$

From Henry's law, $p_{Ai} = H_A \exp(-\Delta H_s/RT)A_i$

From ideal gas law, $p_{Ab} = A_b RT$

Substituting for p_{Ai} and p_{Ab} in Equation (A1.6) and solving for A_i, we get:

$$A_i = \frac{K^{\circ}_G A_b RT}{K^{\circ}_L E^{*}_A + H_A \exp\left(\frac{-\Delta H_s}{RT}\right) K^{\circ}_G}$$

Concentration of gaseous reactant A in the gas bulk, $A_b = \frac{Y_{Ao} N_{go}}{F_g}$

Substituting for A_b and rearranging to get:

$$A_i = \frac{Y_{Ao} N_{go} RT \exp\left(\frac{\Delta H_s}{RT}\right)}{F_g \left[\exp\left(\frac{\Delta H_s}{RT}\right) \frac{K^{\circ}_L E^{*}_A}{K^{\circ}_G} + H_A\right]} \qquad \text{(A1.7)}$$

From ideal gas law:

Gas flow rate at the reactor outlet, $F_g = \frac{N_{go} RT}{P}$

Gas flow rate at the reactor Inlet, $F_{gf} = \frac{N_{gf} RT_{gf}}{P_f}$

Assuming P = P_f, we get the following relation.

$$F_g = \frac{F_{gf} N_{go} T}{N_{gf} T_{gf}}$$

Substituting for F_g in Equation (A1.7)

$$A_i = \left(\frac{N_{gf}}{N_{go}}\right)\left(\frac{Y_{Ao} N_{go}}{F_{gf}}\right) \frac{RT_{gf} \exp\left(\frac{\Delta H_s}{RT}\right)}{\left[\exp\left(\frac{\Delta H_s}{RT}\right) \frac{K^{\circ}_L E^{*}_A}{K^{\circ}_G} + H_A\right]} \qquad \text{(A1.8)}$$

Conversion of gaseous reactant A, $X_A = \frac{Moles\ of\ A\ in - Moles\ of\ A\ out}{Moles of A in}$

$$X_A = \frac{N_{gf} Y_{Af} - N_{go} Y_{Ao}}{N_{gf} Y_{Af}} \quad \text{or} \quad N_{go} = \frac{N_{gf}(1 - X_A) Y_{Af}}{Y_{Ao}}$$

Substituting for N_{go} in Equation (A1.3) and rearranging, we get:

$$\frac{N_{gf}}{N_{go}} = \frac{(1 - Y_{Bo})}{(1 - Y_{Af}X_A)}$$

Substituting for N_{go} and $\frac{N_{gf}}{N_{go}}$ in Equation (A1.8):

$$A_i = \frac{N_{gf}Y_{Af}(1 - Y_{Bo})(1 - X_A)RT_{gf}\exp\left(\frac{\Delta H_s}{RT}\right)}{F_{gf}(1 - Y_{Af}X_A)\left[\exp\left(\frac{\Delta H_s}{RT}\right)\frac{K^{\circ}_L E^{*}_A}{K^{\circ}_G} + H_A\right]} \qquad \text{(A1.9)}$$

Substituting following dimensionless quantities in Equation (A1.9), we get:

$$\delta = \frac{\Delta H_s}{RT_{lf}} \quad \text{and} \quad \theta = \frac{T - T_{lf}}{T_{lf}}$$

$$A_i = \frac{N_{gf}Y_{Af}(1 - Y_{Bo})(1 - X_A)RT_{gf}\exp\left(\frac{\delta}{1 + \theta}\right)}{F_{gf}(1 - Y_{Af}X_A)\left[\exp\left(\frac{\delta}{1 + \theta}\right)\frac{K^{\circ}_L E^{*}_A}{K^{\circ}_G} + H_A\right]} \qquad \text{(A1.10)}$$

Combining Equations (A1.5) and (A1.10) and rearranging, we obtain following expression for the conversion of gaseous reactant:

$$X_A = \frac{(1 - X_A)(1 - Y_{Bo})}{(1 - Y_{Af}X_A)\left[\frac{F_{gf}}{\underline{a}V_R RT_{gf}K^{\circ}_G} + \frac{H_A F_{gf}}{\underline{a}K^{\circ}_L V_R E^{*}_A RT_{gf}}\exp\left(-\frac{\delta}{1 + \theta}\right)\right]} \qquad \text{(A1.11)}$$

Substituting following dimensionless quantities in Equation (A1.11) and rearranging, we get:

$$H_o = \frac{RT_{gf}}{H_A}, \quad D_{gf} = \frac{\underline{a}K^{\circ}_L V_R H_o}{F_{gf}} \quad \text{and} \quad \Psi = \frac{K^{\circ}_L}{K^{\circ}_G H_A}$$

$$X_A = \frac{D_{gf}(1 - X_A)(1 - Y_{Bo})}{(1 - Y_{Af}X_A)}\left[\Psi + \left\{\frac{\exp\left(-\frac{\delta}{1 + \theta}\right)}{E^{\cdot}_A}\right\}\right]^{-1} \qquad \text{(A1.12)}$$

Combining Equations (A1.1) and (A1.2):

$$\nu(N_{gf}Y_{Af} - N_{go}Y_{Ao}) = F_l(B_{lf} - B_l) + \nu F_l A_l$$

Substituting $X_B = 1 - \frac{B_l}{B_{lf}}$, $X_A = \left(1 - \frac{N_{go}Y_{Ao}}{N_{gf}Y_{Af}}\right)$ and $N_{gf} = \frac{F_{gf}A_{gf}}{Y_{Af}}$ in the above equation and rearranging, an expression for X_B is obtained.

$$X_B = \nu\left[\frac{F_{gf}A_{gf}}{F_l B_{lf}}X_A - \frac{A_l}{B_{lf}}\right]$$

Substituting $Q = \frac{F_{gf}}{F_l}$, $q = B_{lf}/A_{gf}$ and $a_l = A_l/B_{lf}$ in the above equation.

$$X_B = \nu\left(\frac{Q}{q}X_A - a_l\right) \qquad \text{(A1.13)}$$

In order to obtain a relation for θ, we substitute for A_i from Equation (A1.10), % $\frac{N_{go}}{N_{gf}}$ from Equation (A1.3) and $\theta_r = \frac{T_{gf}}{T_{lf}}$ in the energy balance Equation (A1.4) to get:

$$F_l\rho_l C_{pl}(T_{lf} - T) + F_{gf}\rho_{gf}C_{pg}T_{gf}\left[1\text{-}(1 - Y_{Af}X_A)\left(\frac{1 + \theta}{\theta_r}\right)\right] + [(-\Delta H_s) + (-\Delta H_r)] \times$$

$$\left[\frac{aK^{\circ}_L V_R E^{\cdot}_A N_{gf}Y_{Af}(1 - X_A)(1 - Y_{Bo})}{F_{gf}(1 - Y_{Af}X_A)}RT_{gf}K^{\circ}_G\left\{K^{\circ}_L E^{\cdot}_A + K^{\circ}_G H_A \exp\left(-\frac{\delta}{1 + \theta}\right)\right\}^{-1}\right]$$

$$- \frac{N_{gf}(1 - Y_{Af}X_A)(-\Delta H_v)Y_{Bo}}{(1 - Y_{Bo})} - (-\Delta H_R)F_l A_l - US(T - T_c) + H_{as} = 0 \text{(A1.14)}$$

Introducing following dimensionless quantities in Equation (A1.14) and dividing it by $F_{gf}\rho_l C_{pl}T_{lf}$ we get:

$$\beta = \frac{US}{F_{gf}\rho_l C_{pl}} \qquad Q = \frac{F_{gf}}{F_l} \qquad H_p = \frac{H_{os}}{F_{gf}\rho_l C_{pl}}$$

$$p = \frac{(-\Delta H_R)F_l A_{gf}}{\rho_l C_{pl} T_{lf} F_{gf}} \qquad v = \frac{(-\Delta H_v)\rho_{gf}}{\rho_l C_{pl} T_{lf}}$$

$$q = \frac{B_{lf}}{A_{gf}} \qquad r = \frac{\rho_{gf} C_{pg}}{\rho_l C_{pl}}$$

$$B = \frac{[(-\Delta H_s) + (-\Delta H_R)]A_{gf}}{\rho_l C_{pl} T_{lf}} \qquad \theta_c = \frac{(T_c - T_{lf})}{T_{lf}}$$

$$-\theta\left[\frac{1}{Q} + r - Y_{Af}X_A r\right] + r(\theta_r - 1) + rY_{Af}X_A - \frac{vY_{Bo}(1 - Y_{Af}X_A)}{(1 - Y_{Bo})} - pqa_l - \beta(\theta - \theta_c)$$

$$H_p + \quad + B\left[\frac{D_{gf}(1 - X_A)(1 - Y_{Bo})}{(1 - Y_{AF}X_A)}\left\{\Psi + \frac{\exp\left(-\frac{\delta}{1 + \theta}\right)}{E^*_A}\right\}^{-1}\right] = 0 \quad \text{(A1.15)}$$

Combining Equations (A1.12) and (A1.15) and solving for θ and X_A, we obtain the following relations:

$$\theta = \frac{\{B + Y_{Af}(r + vY^*_{Bo})\}X_A + \beta\theta_c + r(\theta_r - 1) - pqa_l - vY^*_{Bo} + H_p}{(\alpha + \beta - rY_{Af}X_A)} \quad \text{(A1.16)}$$

$$X_A = \frac{(\alpha + \beta)\theta + pqa_l - \beta\theta_c - r(\theta_r - 1) + vY^*_{Bo} - H_p}{B + (1 + \theta)ry_{Af} + Y_{Af}vY^*_{Bo}} \quad \text{(A1.17)}$$

where

$$\alpha = \frac{1}{Q} + r \quad \text{and} \quad Y^*_{Bo} = \frac{Y_{Bo}}{(1 - Y_{Bo})}$$

APPENDIX A2

DERIVATION OF REACTION FACTOR EXPRESSION

Dimensional Form of Mass Balance Equations

Mass balances around a differential element of fluid, of thickness Δr, located in the liquid film, of thickness δ, surrounding a spherical gas bubble, of radius R, yield the following equations.

Mass balance for reactant A:

$$D_A\left[\frac{d^2C_A}{dr^2} + \frac{2}{r}\frac{dC_A}{dr}\right] = KC_AC_B \qquad \text{(A2.1)}$$

Mass balance for reactant B:

$$D_B\left[\frac{d^2C_B}{dr^2} + \frac{2}{r}\frac{dC_B}{dr}\right] = \nu KC_AC_B \qquad \text{(A2.2)}$$

Boundary Conditions:

$$r = R, \quad C_A = C_{Ai} \quad \text{and} \quad \frac{dC_B}{dr} = 0$$

$$r = R + \delta, \quad C_B = C_{BL}$$

and

$$-D_A n 4\pi(R + \delta)^2\frac{dC_A}{dr} = KC_AC_B\left[V_L - n\frac{4}{3}\pi\{(R + \delta)^3 - R^3\}\right] + F_iC_A$$

Dimensionless Form of Mass Balance Equations

In order to make Equations (A2.1) and (A2.2) dimensionless, the following dimensionless variables are introduced:

$$a = \frac{C_A}{C_{Ai}}, \qquad b = \frac{C_B}{C_{BL}}$$

$$x = \frac{r - R}{\delta}, \qquad \gamma = \frac{D_B}{\nu D_A}, \qquad q' = \frac{C_{BL}}{C_{Ai}}$$

Substituting the above dimensionless quantities in Equation (A2.1), we get:

$$\frac{d^2a}{dx^2} + \frac{2}{(x + R/\delta)}\frac{da}{dx} = \frac{\delta^2 K C_{Bl} ab}{D_A} \tag{A2.3}$$

The term δ in Equation (A2.3) is not known and is obtained by making a mass balance around a differential element of thickness Δr located in the spherical liquid film, of thickness δ, surrounding a gas bubble, of radius R, in the absence of chemical reaction, in a manner similar to that used in the conventional plane surface case. The governing equation in such a case is:

$$D_A\left[\frac{d^2C_A}{dr^2} + \frac{2}{r}\frac{dC_A}{d}r\right] = 0$$

Above equation can also be written as follows:

$$\frac{d}{dr}\left(r^2\frac{dC_A}{dr}\right) = 0 \tag{A2.4}$$

Boundary Conditions:

$$r = R, \quad C_A = C_{Ai}$$

$$r = R + \delta, \quad C_A = C_{AL}$$

Integrating Equation (A2.4) twice and applying the boundary conditions, we get:

$$C_A = \frac{R(R + \delta)(C_{Ai} - C_{AL})}{r\delta} + C_{A} - \frac{(R + \delta)(C_{Ai} - C_{AL})}{\delta} \qquad \text{(A2.5)}$$

The rate of physical absorption is calculated from the flux at the interface, or:

$$N^{o}_{A} = K^{o}_{L}(C_{Ai} - C_{AL}) = -D_A \frac{dC_A}{dr}\bigg|_{r=R}$$

Evaluating $\frac{dC_A}{dr}\Big|_{r=R}$ from Equation (A2.5) and substituting in the above equation, we get:

$$K^{o}_{L}(C_{Ai} - C_{AL}) = \frac{D_A(R + \delta)(C_{Ai} - C_{AL})}{\delta R}$$

Solving for the film thickness, we get:

$$\delta = \frac{D_A R}{(K^{o}_{L} R - D_A)} \qquad \text{(A2.6)}$$

To make Equation (A2.6) dimensionless, the following dimensionless variable is introduced:

$$\Omega = \frac{R}{\delta}$$

Substituting Ω in Equation (A2.6), we get:

$$\Omega = \frac{K^{o}_{L} R - D_A}{D_A} \quad or \quad \frac{\Omega}{(1 + \Omega)} = \left[1 - \frac{D_A}{K^{o}_{L} R}\right]$$

Substituting for δ and $\frac{R}{\delta}$ in Equation (A2.3), we get:

$$\frac{d^2a}{dx^2} + \frac{2}{(x + \Omega)}\frac{da}{dx} = M^2_m ab \qquad \text{(A2.7)}$$

Similarly Equation (A2.2) yields:

$$\frac{d^2b}{dx^2} + \frac{2}{(x + \Omega)}\frac{db}{dx} = \frac{M^2_m ab}{\gamma q'} \qquad \text{(A2.8)}$$

where M_m is a dimensionless quantity which is defined as follows:

$$M_m = \frac{\sqrt{D_A K C_{BL}}}{K^\circ_L}\left(\frac{1 + \Omega}{\Omega}\right) = M\left(\frac{1 + \Omega}{\Omega}\right)$$

The dimensionless quantity M_m can be called the modified Hatta number.

Dimensionless form of Boundary Conditions:

$$x = 0, \quad a = 1 \qquad \frac{db}{dx} = 0$$

$$x = 1, \quad -\frac{da}{dx} = M_1 a \qquad b = 1$$

where

$$M_1 = \left[M^2\left\{\alpha' - \left(\frac{1}{3}\left(\frac{1}{\Omega}\right)^2 + \left(\frac{1}{\Omega}\right) + 1\right)\right\} + \xi\right]$$

$$M = \frac{\sqrt{D_A K C_{BL}}}{K^\circ_L}$$

$$\alpha' = \frac{\varepsilon_L K^\circ_L}{\underline{a} D_A}\left(\frac{\Omega}{1 + \Omega}\right)$$

$$\xi = \frac{\Omega}{K^\circ_L \underline{a} \tau_L (1 + \Omega)}$$

Approximate Analytical Solution

In order to obtain approximate analytical solution of Equations (A2.7) and (A2.8), it is assumed that the concentration of liquid phase reactant B at the gas

liquid interface is constant. Let this constant concentration be denoted as C_{Bi}. With this assumption, the rate expression becomes:

$$(-r_A) = KC_AC_{Bi} \tag{A2.9}$$

let $b_i = \frac{C_{Bi}}{C_{BL}}$

Introducing b_i in Equation (A2.7), we get:

$$\frac{d^2a}{dx^2} + \frac{2}{x + \Omega}\frac{da}{dx} = M^2{}_m ab_i$$

Since b_i is constant, it can be combined with M_m to give:

$$\frac{d^2a}{dx^2} + \frac{2}{x + \Omega}\frac{da}{dx} = M_m{}'^2 a \tag{A2.10}$$

where

$$M_m{}' = M_m\sqrt{b_i}$$

let $p = a(\Omega + x)$ (A2.11)

Taking first and second derivative of Equation (A2.11):

$$\frac{da}{dx} = \frac{1}{(1 + \Omega)}\frac{dp}{dx} - \frac{p}{(\Omega + x)^2}$$

$$\frac{d^2a}{dx^2} = \frac{1}{(\Omega + x)}\frac{d^2p}{dx^2} - \frac{2}{(\Omega + x)^2}\frac{dp}{dx} + \frac{2p}{(\Omega + x)^3}$$

Substituting for $\frac{da}{dx}$ and $\frac{d^2a}{dx}$ in Equation (A2.10) and rearranging

$$\frac{d^2p}{dx} = M_m{}'^2 p \tag{A2.12}$$

Boundary Conditions:

$x = 0, \qquad p = \Omega$

$$x = 1, \qquad -\frac{dp}{dx} = \frac{\{M_1(\Omega + x)p\}}{(\Omega + x)}$$

Solving Equation (A2.12), we get:

$$p = C_1\sinh(M'_m x) + C_2\cosh(M'_m x) \tag{A2.13}$$

Applying boundary conditions in Equation (A2.13) and substituting the value of $p\Big|_{x=1}$ from Equation (A2.11), we get:

$$C_1 = \frac{-M_1(\Omega + 1)a_l + a_l - \Omega M'_m\sinh(M'_m)}{M'_m\cosh(M'_m)} \qquad C_2 = \Omega$$

Substituting for C_1, C_2 and p in Equation (A2.13) an expression for dimension less concentration is obtained.

$$a(x) = \left[\frac{a_l\{1 - M_1(\Omega + 1)\} - \Omega M'_m\sinh(M'_m)}{M'_m\cosh(M'_m)}\right]\frac{\sinh(M'_m x)}{(\Omega + x)} + \Omega\left[\frac{\cosh(M'_m x)}{(\Omega + x)}\right] \tag{A2.14}$$

Substituting x = 1 in Equation (A2.14) and rearranging we get an explicit expression for a_l.

$$a_l = \frac{\Omega M_m\sqrt{b_i}}{M_m\sqrt{b_i}\cosh(M_m\sqrt{b_i})(\Omega + 1) + \{M_1(\Omega + 1) - 1\}\sinh(M_m\sqrt{b_i})} \tag{A2.15}$$

The parameter b_i in Equation (A2.14) is unknown, therefore to get an expression for b_i we multiply Equation (A2.8) by $-\gamma q'$ and add it with the Equation (A2.7).

$$\frac{d^2}{dx^2}(a - \gamma q' b) + \frac{2}{x + \Omega}\frac{d}{dx}(a - \gamma q' b) = 0 \tag{A2.16}$$

Boundary conditions:

$$x = 0, \quad a = 1 \quad or \quad -\frac{da}{dx}\bigg|_{x=0} = \left(\frac{1+\Omega}{\Omega}\right)E^{\bullet}_{A}$$

$$x = 1, \quad a = 1 \qquad b = 1$$

Equation (A2.16) can also be written in the following form:

$$\frac{1}{(x+\Omega)^2}\frac{d}{dx}\left[(x+\Omega)^2\frac{d}{dx}(a - \gamma q' b)\right] = 0 \tag{A2.17}$$

Integrating Equation (A2.17) twice, we get:

$$a - \gamma q' b = -C_3\left(\frac{1}{x+\Omega}\right) + C_4 \tag{A2.18}$$

Applying boundary conditions to Equation (A2.18).

$$C_3 = -\Omega(1+\Omega)E^{\bullet}_{A} \qquad C_4 = a_l - \gamma q' - \Omega E^{\bullet}_{A}$$

Substituting for C_3 and C_4 in Equation (A2.18) and rearranging.

$$b(x) = \frac{a}{\gamma q'} + 1 - \frac{\Omega(1+\Omega)E^{\bullet}_{A}}{\gamma q'(x+\Omega)} \div \frac{\Omega E^{\bullet}_{A}}{\gamma q'} - \frac{a_l}{\gamma q'} \tag{A2.19}$$

In order to get an expression for b_i, we substitute x = 0 and a = 1 in Equation (A2.19) and make appropriate rearrangement to get the following relation:

$$b_i = \frac{E_i - E^{\bullet}_{A} - a_l}{E_i - 1} \tag{A2.20}$$

The reaction factor, $E^{\bullet}_{A}$ is defined as:

$$E^{\bullet}_{A} = \frac{\textit{Rate of absorption of A in presence of chemical reaction}}{\textit{Maximum rate of pure physical absorption of A}}$$

Rate of absorption of gaseous component A :

$$N_A = -D_A\frac{dC_A}{dr}\bigg|_{r=R}$$

In terms of dimensionless concentration N_A can be represented as:

$$N_A = C_{Ai}K^{\circ}_{L}\left(\frac{\Omega}{1+\Omega}\right)\frac{da}{dx}\bigg|_{x=0}$$

Maximum rate of pure physical absorption of component A:

$$N^{\circ}_{A} = K^{\circ}_{L}C_{Ai}$$

Thus,

$$E^{\cdot}_{A} = -\left(\frac{\Omega}{1+\Omega}\right)\frac{da}{dx}\bigg|_{x=0} \qquad \text{(A2.21)}$$

Evaluating $\left.\frac{da}{dx}\right|_{x=0}$ from Equation (A2.14) and substituting in Equation (A2.21), we get:

$$E^{\cdot}_{A} = \left(\frac{\Omega}{1+\Omega}\right)\left[\frac{M_1(\Omega+1)a_l - a_l + \Omega M_m\sqrt{b_i}\sinh\left(M_m\sqrt{b_i}\right)}{\Omega\cosh\left(M_m\sqrt{b_i}\right)} + \frac{1}{\Omega}\right]$$

Substituting for a_l from Equation (A2.15) in the above equation and rearranging we get:

$$E^{\cdot}_{A} = \frac{M_m\sqrt{b_i}\Omega}{(1+\Omega)}\left[\frac{M_m\sqrt{b_i}\tanh\left(M_m\sqrt{b_i}\right)(1+\Omega) + \{M_1(1+\Omega)-1\}}{M_m\sqrt{b_i}(1+\Omega) + \{M_1(1+\Omega)-1\}\tanh\left(M_m\sqrt{b_i}\right)}\right] + \frac{1}{1+\Omega} \qquad \text{(A2.22)}$$

Numerical Solution of Equations (A2.7) and (A2.8)

In order to solve the film theory model equations, we first combine Equations (A2.7) and (A2.8) by substituting for b from Equation (A2.19).

$$\frac{d^2a}{dx^2} + \frac{2}{(x+\Omega)\frac{da}{dx}} = M_m{}^2\left[\frac{\{a^2 - aa_1 + a(E_i - 1)\}(x+\Omega) + \Omega(x-1)E^*_A a}{(E_i -)(x+\Omega)}\right]$$

(A2.23)

where

$$E_i = \gamma q' + 1$$

Equation (A2.23) is non-linear which can be solved using finite difference method combined with quasi-linearization technique [12]. The non-linear term, a^2, in the right hand side of Equation (A2.23) can be linearized by using the following expansion formula:

$$F(f) = F(g) + (f - g)F'(g) \qquad \text{(A2.24)}$$

Equation (A2.24) is a taylor series expansion of function F(f) with second and higher order neglected. If we let $f = a_{k+1}$ and $g = a_k$ Equation (A2.24) becomes:

$$F(a_{k+1}) = F(a_k) + (a_{k+1} - a_k)F'(a_k) \qquad \text{(A2.25)}$$

where subscript k represents the k^{th} iteration. Now, linearizing the non-linear term a^2 of Equation (A2.23) by using Equation (A2.25).

$$a^2_{k-1} = 2f_k f_{k+1} - f_k^2 \qquad \text{(A2.26)}$$

For the sake simplicity let:

$$A(x) = (x+\Omega)(E_i - 1) \qquad \text{(A2.27)}$$

$$B(x) = E^*_A(x-1)\Omega \qquad \text{(A2.28)}$$

Combining Equation (A2.23), (A2.26), (A2.27) and (A2.28) and rearranging we get:

$$\frac{d^2a_{k+1}}{dx^2} + \frac{2}{(x + \Omega)d\frac{a_{k+1}}{dx}} = \frac{M_m^2 a_{k+1}}{A(x)}\left[\frac{(2a_k - a_k@|_{x=1})A(x)}{(E_i - 1)} + A(x) + B(X)\right] +$$

$$\frac{a_k^2 M_m^2}{E_i - 1} = 0$$

(A2.29)

Boundary Conditions:

$x=0,\ a_{k+1} = 1.0$

$x=1,\ -\frac{da_{k+1}}{dx} = M_1 a_{k+1}$

Assuming suitable guess values for $a_{k=0}(x)$, Equation (A2.29) is solved for $a_{k=1}(x)$ using finite difference method. If the newly obtained values of $a_{k+1}(i)'s$ do not agree with the assumed values within a prescribed tolerance, they are taken as the new initial values and next iteration is performed. This iterative procedure is continued until the required accuracy is achieved.

Finite Difference Scheme:

Writing finite difference approximation for Equation (A2.29), we get:

$$\frac{1}{\Delta x^2}a_{k+1}(i\text{-}1) + \left[\frac{\text{-}2}{\Delta x^2} - \frac{2}{(i\Delta x^2 + \Omega\Delta x)} - \frac{M_m^2(2a_k(i) - a_k(N))}{(E_i - 1)} - M_m^2 - \frac{M_m^2 B(i\Delta x)}{A(i\Delta x)}\right] \times$$

$$a_{k+1}(i) + \left[\frac{1}{\Delta x^2} + \left(\frac{2}{i\Delta x^2 + \Omega\Delta x}\right)\right]a_{k-1}(i + 1) = -\frac{M_m^2 a_k^2(i)}{E_i - 1}$$

(A2.30)

$i = 1,2,3...N\text{-}1$

Boundary Conditions:

$a_{k+1}(0) = 1$

For the second boundary condition we use backward difference formula to get:

$$a_{k+1}(N) = \frac{a_{k+1}(N\text{-}1)}{(1 + M_1\Delta x)}$$

Let

$$U_i = \frac{1}{\Delta x^2} \tag{A2.31}$$

$$V_i = \left[\frac{-2}{\Delta x^2} - \frac{2}{(i\Delta x^2 + \Omega\Delta x)} - \frac{M_m^2\{2a_k(i) - a_k(N)\}}{(E_i - 1)} - M_m^2\left\{1 + \frac{B(i\Delta x)}{A(i\Delta x)}\right\}\right] \tag{A2.32}$$

$$W_i = \left[\frac{1}{\Delta x^2} + \frac{2}{i\Delta x^2 + \Omega\Delta x}\right] \tag{A2.33}$$

$$X_i = \left[-\frac{M_m^2}{E_i - 1}a_k^2(i)\right] \tag{A2.34}$$

Substituting Equations (A2.31) to (A2.34) in Equation (A2.30), we get:

$$U_i a_{k+1}(i - 1) + V_i a_{k+1}(i + 1) + W_i a_{k+1}(i + 1) = X_i \tag{A2.35}$$

$i = 1,2,3....N\text{-}1$

Equation (A2.35) represents a system of linear equations which can be written in the following form of matrix equation:

$$\overline{C}\,\overline{a}_{k+1} = \overline{X} \tag{A2.36}$$

where

$$\overline{C} = \begin{bmatrix} V_1 & W_1 & & & & \\ U_2 & V_2 & W_2 & & & \\ & U_3 & V_3 & W_3 & & \\ & & & & & \\ & & & & U_{N-2} & V_{N-2} & W_{N-2} \\ & & & & & U_{N-1} & V_{N-1} \end{bmatrix}$$

$$\overline{a}_{k+1} = \begin{bmatrix} a_{k+1}(1) \\ a_{k+1}(2) \\ . \\ . \\ . \\ a_{k+1}(N\text{-}1) \end{bmatrix}$$

$$\overline{X} = \begin{bmatrix} X_1 - U_1 \\ X_2 \\ X_3 \\ . \\ . \\ . \\ X_{N-1} \end{bmatrix}$$

The reaction factor, E_A^*, is calculated using the following equation:

$$E_A^* = -\frac{\Omega}{1+\Omega}\frac{4a_{k+1}(1) - a_{k+1}(2) - 3a_{k+1}(0)}{2\Delta x} \qquad \text{(A2.37)}$$

APPENDIX B1

COMPUTER CODE FOR SOLVING REACTOR MODEL EQUATIONS

```
C-------------------------------------------------------------------------
C
C SIMULATION CODE NAME : MULTIPLE
C
C WRITTEN BY                    : AQIL JAMAL
C
C THIS COMPUTER CODE IS WRITTEN TO PERFORM NUMERICAL
C SIMULATION OF STEADY STATE BEHAVIOR OF A NONADIABATIC.
C NON-ISOTHERMAL GAS-LIQUID CSTRSs WITH AN IRREVERSIBLE
C SECOND-ORDER REACTION.
C
C-------------------------------------------------------------------------
C
      REAL N,NO,MUL,MUG,MUC,LAMDAL,LAMDAM,LAMDAC,LAMDAI
      REAL SOL1(1000,19),SOL2(1000,19),SOL3(1000,19),SOL4(1000,19)
      REAL SOL5(1000,19),SOL6(1000,19),SOL7(1000,19)
      COMMON /DATA/CK0,H0,G1,G2,ABT,BEYC,B,SP,AGF,BLF,Q,SQ,D,CKL,
     $          ALFAP,ZETAP,BL,BI,ISIGNAL,YAF,SR,YR,FG,RAOLF,RAOGF,
     $          VR,PTOT,AV,SV,TF,ERR1,ERR2,ERR3
C
C
C
      READ(1,*)MODEL
      READ(1,*)ITYPE
      READ(1,*)ITAU
      READ(1,*)IGEOMET
      READ(1,*)TLF
      READ(1,*)TGF
      IF(IGEOMET .EQ. 1) THEN
      DT = 7.6
      LAMDAM = 2.6E-3
      ELSEIF(IGEOMET .EQ. 2)THEN
      DT = 30.5
      LAMDAM = 0.03824
```

```
ELSEIF(IGEOMET .EQ. 3)THEN
DT = 61.0
LAMDAM = 0.03824
ELSEIF(IGEOMET .EQ. 4)THEN
DT = 122.0
LAMDAM = 0.03824
ENDIF
G = 981.
E = 29.E3
DETHR = 26.E3
TCI = 20. + 273.
TCO = 30. + 273.
H0 = 0.00188
R2 = 82.05
ICOUNT1 = 0
RAOC = 5.56E-2
AMWG = 70.906
AMWL = 142.29
AMWC = 18.02
R = 1.987
RAOGF = (4.46E-5)*(273./TGF)
DETHS = 4500.
CPC = 18.0
TSTAR = 323.1
PTOT = 1.
MUG = 132.7E-6
TRL = 617.55
TBL = 447.3
PCL = 20.69
VRL = 194.9
OMEGA = 0.49
ZCL = .247
LAMDAC = 7.139E-4
LAMDAI = 3.8E-4
DAIT1 = 0.0754
IWRITE = 0
IF(IGEOMET .EQ. 1) THEN
CALL GEOMET1(HL,VL,TH,DI,SH,GBL,W,BLM,DM,ALM,DCP,DCI,
DCO,DC,S,DT,MUG,SE,RAOGF,AMWG,ITYPE,TTH,VO,THI,JTH,SAI,SAO,
RAOC,AMWC,QC,DO)
ELSEIF(IGEOMET .EQ. 2)THEN
CALL GEOMET2(HL,VL,TH,DI,SH,GBL,W,BLM,DM,ALM,DCP,DCI,
DCO,DC,S,DT,MUG,SE,RAOGF,AMWG,ITYPE,TTH,VO,THI,JTH,SAI,SAO,
RAOC,AMWC,QC,DO)
ELSEIF(IGEOMET .EQ. 3)THEN
CALL GEOMET3(HL,VL,TH,DI,SH,GBL,W,BLM,DM,ALM,DCP,DCI,
DCO,DC,S,DT,MUG,SE,RAOGF,AMWG,ITYPE,TTH,VO,THI,JTH,SAI,SAO,
RAOC,AMWC,QC,DO)
```

```
      ELSEIF(IGEOMET .EQ. 4)THEN
      CALL GEOMET4(HL,VL,TH,DI,SH,GBL,W,BLM,DM,ALM,DCP,DCI,
     DCO,DC,S,DT,MUG,SE,RAOGF,AMWG,ITYPE,TTH,VO,THI,ITH,SAI,SAO,
     RAOC,AMWC,QC,DO)
      ENDIF
      READ(1,*)CK
      READ(1,*)YAF
      READ(1,*)STEP
      READ(1,*)FACTR
      READ(1,*)YTOL
      WRITE(11,*)' TAUL     EAI      EA       CM          RATIO'
      WRITE(10,1)'YAF=',YAF,'TLF=',TLF,'TGF=',TGF,'K=',CK
      WRITE(9,1)'YAF=',YAF,'TLF=',TLF,'TGF=',TGF,'K=',CK
      WRITE(9,*)'TAUL   UPR   HTPR    HJPR'
      WRITE(8,1)'YAF=',YAF,'TLF=',TLF,'TGF=',TGF,'K=',CK
      WRITE(8,*)' TAUL    T     XG      XL    EA   YB0 '
    1 FORMAT(A,F7.5,1X,A,F6.2,A,F6.2,A,F7.5)
      NSOL1=1
      NSOL2=1
      NSOL3=1
      NSOL4=1
      NSOL5=1
      NSOL6=1
      NSOL7=1
      READ(2,*)FG
      TAUG=VL/FG
      VSG=FG/(((22./7.)/4.)*DT*DT)
      IF(VSG.GT.5.)THEN
      WRITE(6,*)'CHANGE THE VALUE OF FG'
      GO TO 101
      ENDIF
   10 READ(3,*)TAUL
      FL=VL/(TAUL*60)
      PRINT3,TAUL,FL
    3 FORMAT(/' TAUL(MIN) =',F10.4,'     FL =',F8.4,
     S     /2X,'*********')
      IF (TAUL .EQ. 1001.) GO TO 101
      IWRITE=IWRITE+1
      ITEMP=0
      ICOUNT2=0
      TLB=297.0
   20 CONTINUE
      HA=R2*TGF/H0
      TF=TLF
      TC=(TCI+TCO)/2.
      D=.66E-7*TLB*EXP(1172*((1./273)-(1./TLB)))
      CPL=4.25+0.234*TLB
      CPCL2=8.28+5.6E-4*TLB
```

```
      CPHCL=6.7+8.4*1E-4*TLB
      CPG=YAF*CPCL2+(1.-YAF)*CPHCL
      MUL=1.3*EXP(-1172.*((1./273.)-(1./TLB)))/100.
      MUC=1./(2.148*((TC-273.-8.435)+((8078.4+((TC-273.-8.435)**2))**.5
     ))-120.)
      TBR=TBL/TRL
      TR=TLB/TRL
      TRR=293./TRL
      A3L=0.1207*(1.+(TBR*LOG(PCL)/(1.-TBR)))-0.281
      SIGL=A3L*(PCL**.6667)*(TRL**.333)*((1.-TR)**(11./9.))
      LAMDAL=(2.64E-3/(AMWL**.5))*((3.+20.*((1.-TR)**.667))/
     S(3.+20.*((1.-TBR)**.667)))
      IF(TR.GE. .2 .AND. TR .LE. .8)THEN
      VR0=.33593-.33953*TR+1.51941*TR*TR-2.02512*(TR**3.)+1.11422
     S*(TR**4)
      GAMAL0=.29607-.09045*TR-.04842*TR*TR
      VRR=.33593-.33953*TRR+1.51941*TRR*TRR-2.02512*(TRR**3.)+1.11422
     S*(TRR**4)
      GAMALR=.29607-.09045*TRR-.04842*TRR*TRR
      ELSEIF(TR.GT. .8 .AND. TR.LT. 1.)THEN
      VR0=1.+1.3*((1.-TR)**.5)*(LOG(1.-TR)/2.303)-0.50879*(1.-TR)
     S-.91534*((1.-TR)**2.)
      GAMAL0=.29607-.09045*TR-.04842*TR*TR
      VRR=1.0+1.3*((1.-TRR)**.5)*(LOG(1.-TRR)/2.303)-0.50879*(1.-TRR)
     S-.91534*((1.-TRR)**2.)
      GAMALR=.29607-.09045*TRR-.04842*TRR*TRR
      ENDIF
      VMOLAL=VRL*VR0*(1.-(OMEGA*GAMAL0))/(VRR*(1.-(OMEGA*GAMALR)))
      IF(ITEMP.EQ.0)THEN
      RAOLF=1./VMOLAL
      RAOL=RAOLF
      ELSE
      RAOL=1./VMOLAL
      ENDIF
      RAOG=PTOT/(R2*TLB)
      DN=.4266
      DLAMD=9400.
      DETHV=DLAMD*(((TRL-TLB)/(TRL-TBL))**DN)
C     WRITE(6,*)'DETHV=',DETHV
C     WRITE(6,*)'LIQUID DENSITY=',RAOL
C     WRITE(6,*)'SIGL=',SIGL
C     WRITE(6,*)'LAMDAL=',LAMDAL
      DAI=DAIT1*((TLB/273.)**1.81)
      PI=(1.-YAF)*PTOT
C
C READ STIRRER SPEED
C
      IF(ICOUNT1.EQ.0)THEN
```

```
      READ(4,*)N
C     WRITE(6,*)'N=',N
      ICOUNT1=ICOUNT1+1
      ENDIF
      CALL POWER(RAOL,RAOGF,N,DI,DT,MUL,MUG,G,IND,PO,PG,PGA,PGT,
           FG,VSG,VO,AMWL,AMWG,TGF,TLB,W,GBL,IGEOMET,VL,DO,NF)
      IF(IND.EQ.1)THEN
      WRITE(6,*) 'PROGRAM INTERUPTED BECAUSE IND=1'
      WRITE(6,*) 'INCREASE STIRRER SPEED'
      GO TO 101
      ENDIF
      CALL HYDEM(CKL,CKG,MUL,VT,DB,SIGL,RAOL,RAOG,G,PGT,VL,EPSG,VSG,
     $AV,D,DAI,R,TGF,RG,AMWL,VR,VG,YAF,DI,DT,N,FG,PTOT,PI,TLB,PG,AMWG,
     $CKGRT,IGEOMET)
      IF(IWRITE.EQ.1)THEN
      IF(RG.NE.0) THEN
      WRITE(10,*)'TAUL   CKL    CKG     AV    EPSG    DB    HT'
      ELSE
      WRITE(10,*)'BECAUSE GAS IS PURE CKG IS VERY HIGH'
      WRITE(10,*)'AND GAS SIDE RESISTANCE IS ZERO'
      WRITE(10,*)'TAUL  CKL  AV  EPSG  DB  HT'
      ENDIF
      ENDIF
C     WRITE(7,*) 'CKG=',CKG
      SI=CKL*RG/HA
C     WRITE(7,*) 'SI=',SI
      EPSL=1.-EPSG
      VR=VL/EPSL
C     WRITE(6,*)'VR=',VR
      CALL HCOEF(RAOL,RAOG,RAOC,MUL,MUG,MUC,LAMDAL,LAMDAM,
           LAMDAC,SIGL,ITYPE,N,PO,DI,G,DT,VL,HL,SE,QC,TLB,
           TCI,TCO,ALM,BLM,CPL,CPC,VSG,DCP,DCI,DCO,DC,TH,
           TTH,U,AMWL,AMWG,AMWC,LAMDAI,THI,HT,HJ,JTH,SAI,SAO,HCI,
           IGEOMET,PG)
      IF(ITYPE.EQ.1)THEN
      US=U*SAI
      ELSE
      US=U*S
      ENDIF
      UPR=4.184E4*U
      HTPR=4.18E4*HT
      IF(ITYPE.EQ.1)THEN
      HOPR=4.18E4*HJ
      ELSE
      HOPR=4.18E4*HCI
      ENDIF
      WRITE(6,*)'US=',US
      OMEG=(CKL*0.5*DB/D)-1.
```

```
      AGF = RAOGF*YAF
      BLF = RAOLF
      ALFAP = EPSL*CKL/AV/D
      YC = (TC-TF)/TF
      YR = TGF/TF
      DA = CKL*AV*VR*H0/FG
      BETA = US/FG/RAOLF/CPL
      HP = (14.34/60.)*1E-7*PGT/FG/RAOLF/CPL TLF
      SQ = BLF/AGF
      SR = (RAOGF*CPG)/(RAOLF*CPL)
      SV = (DETHV*RAOGF)/(RAOLF*CPL*TF)
    8 FORMAT(//'       E   =',F10.2/'   (- HR)  =',F10.2//)
      B = (DETHS + DETHR)*AGF/RAOLF/CPL/TF
      G1 = E/R/TF
      G2 = DETHS/R/TF
      GARMA = G1/2.-G2
      CK0 = CK*EXP(E/R/TSTAR)
      DAP = (CK0*(DA**2)*D*BLF/((CKL**2)*EXP(2.*GARMA)))**0.5
      ZETAP = CKL*AV*(TAUL*60.)/EPSL
      ALFA = (FG*RAOGF*CPG + FL*RAOLF*CPL)/FG/RAOLF/CPL
      SP = DETHR*FL*AGF/FG/RAOLF/CPL/TF
      Q = FG/FL
      ABT = ALFA + BETA
      BEYC = BETA*YC
      YLOW = (BEYC + HP + (SR*(YR-1.)))/ABT
      YUP = (BEYC + HP + B + SR*YAF + SR*(YR-1.))/(ABT-SR*YAF)
      TUP = TF*(1. + YUP)-273.1
      PRINT2,CK,B,BETA,DAP,SR,SV,YAF
2   FORMAT(/8X,'K @ 50 DEG C = ',F8.5,/8X,'B    = ',F9.6,/8X,'BETA = '
     $      ,F14.6,/8X,'DA  = ',F9.6/,8X,'SR  = ',F9.6/,8X,'SV  = ',F9.6,
     $      /8X,'YAF = ',F9.6/)
14   FORMAT(2X,'  Y(LB) = ',F10.5,8X,'  Y(UB) = ',F10.5/)
      IF(ICOUNT2.EQ.0) THEN
      PRINT7,STEP,YTOL
7   FORMAT(/8X,'STEP SIZE  = ',F9.6,/8X,'Y TOLERANCE = ',F9.6/)
      ENDIF
      PRINT144,TUP,ALFA
144  FORMAT(2X,'  T(UB) = ',F10.5,5X,'  ALFA',F12.8/)
      IF(ICOUNT2.EQ.0)THEN
      BI = 1.
      BL = BLF
      YN = YLOW
      SAL = 0.01
      IF(MODEL.EQ.1 .OR. MODEL.EQ.3 ) THEN
      SYB = 0.0
      ELSE
      SYB = 0.0025
      ENDIF
```

```
      ISIGNAL=0
      ENDIF
C
C FIRST CALL TO TRYAL
C
      IF(MODEL.EQ.1)THEN
      CALL TRYAL1 (EA,SAL,YN,CM,X,SI,IPARA,AI,EI,SYB,HP)
      ELSEIF(MODEL.EQ.2)THEN
      CALL TRYAL2 (EA,SAL,YN,CM,X,SI,IPARA,AI,EI,SYB,CKG,HP)
      ELSEIF(MODEL.EQ.3)THEN
      CALL TRYAL3 (EA,SAL,YN,CM,X,SI,IPARA,AI,EI,SYB,HP,OMEG)
      ENDIF
      IF(ISIGNAL.EQ.1)THEN
      WRITE(6,*)'NEXT VALUE OF TAUL BECAUSE OF -VE BL'
      IF(YN.GT.YUP) THEN
      GO TO 10
      ELSE
      BL=BLF
      YN=YN+STEP
      GO TO 102
      ENDIF
      ELSEIF(ISIGNAL.EQ.2)THEN
      WRITE(6,*)'NEXT VALUE OF TAUL BECAUSE NO CONVERGENCE FOR SAL'
      IF(YN.GT.YUP) THEN
      GO TO 10
      ELSE
      YN=YN+STEP
      GO TO 102
      ENDIF
      ENDIF
      IF(IPARA .EQ. 1) THEN
      WRITE(6,*) 'NO CONVERGENCE FOR EA'
      IF(YN.GT.YUP) THEN
      GO TO 10
      ELSE
      YN=YN+STEP
      GO TO 102
      ENDIF
      ELSEIF(IPARA .EQ. 2) THEN
      WRITE(6,*) 'NO CONVERGENCE FOR YB0'
      IF(YN.GT.YUP) THEN
      GO TO 10
      ELSE
      YN=YN+STEP
      GO TO 102
      ENDIF
      ENDIF
      DENOM=1.+(SI/DA)+(1./(DA*EA*EXP(G2*(1.+YN))))
```

```
      FY=-(1.0/Q + SR*(1.0-YAF*X))*YN+B*DENOM*((1.0-SYB)*(1.0-X)
     $/(1.0-YAF*X))+YAF*(SR+SV*SYB/(1.0-SYB)
     $)*X-SP*SAL-SV*SYB/(1.0-SYB)-BETA*(YN-YC)+SR*(YR-1.0)+HP
   30 Y1=YN+STEP
      IF(Y1.GT.YUP) THEN
      WRITE(6,*) 'NEXT VALUE OF TAUL BECAUSE SEARCH IS COMPLETED'
      GO TO 10
      ENDIF
C
C SECOND CALL TO TRYAL
C
      IF(MODEL.EQ.1)THEN
      CALL TRYAL1 (EA,SAL,Y1,CM,X,SI,IPARA,AI,EI,SYB,HP)
      ELSEIF(MODEL.EQ.2)THEN
      CALL TRYAL2 (EA,SAL,Y1,CM,X,SI,IPARA,AI,EI,SYB,CKG,HP)
      ELSEIF(MODEL.EQ.3)THEN
      CALL TRYAL3 (EA,SAL,Y1,CM,X,SI,IPARA,AI,EI,SYB,HP,OMEG)
      ENDIF
      IF(ISIGNAL.EQ.1)THEN
      WRITE(6,*)'NEXT VALUE OF TAUL BECAUSE OF -VE BL'
      IF(Y1.GT.YUP) THEN
      GO TO 10
      ELSE
      BL=BLF
      YN=Y1
      GO TO 102
      ENDIF
      ELSEIF(ISIGNAL.EQ.2)THEN
      WRITE(6,*)'NEXT VALUE OF TAUL BECAUSE NO CONVERGENCE FOR SAL'
      IF(Y1.GT.YUP) THEN
      GO TO 10
      ELSE
      YN=Y1
      GO TO 102
      ENDIF
      ENDIF
      IF(IPARA .EQ. 1) THEN
      WRITE(6,*) 'NO CONVERGENCE FOR EA'
      IF(Y1.GT.YUP) THEN
      GO TO 10
      ELSE
      YN=Y1
      GO TO 102
      ENDIF
      ELSEIF(IPARA .EQ. 2) THEN
      WRITE(6,*) 'NO CONVERGENCE FOR YB0'
      IF(Y1.GT.YUP) THEN
      GO TO 10
```

```
      ELSE
      YN = Y1
      GO TO 102
      ENDIF
      ENDIF
      DENOM1 = 1./((SI/DA)+(1./(DA*EA*EXP(G2*(1.+Y1)))))
      FY1 = -(1.0/Q + SR*(1.0-YAF*X))*Y1+B*DENOM1*((1.0-SYB)*(1.0-X)
     S/(1.0-YAF*X))+YAF*(SR+SV*SYB/(1.0-SYB)
     S)*X-SP*SAL-SV*SYB/(1.0-SYB)-BETA*(Y1-YC)+SR*(YR-1.0)+HP
      IF(FY*FY1.LT.0.) GO TO 50
   40 FY = FY1
      YN = Y1
      GO TO 30
   50 YL = YN
      YU = Y1
      FYU = FY1
   60 YS = (YL+YU)/2.
C
C THIRD CALL TO TRYAL
C
      IF(MODEL.EQ.1)THEN
      CALL TRYAL1 (EA,SAL,YS,CM,X,SI,IPARA,AI,EI,SYB,HP)
      ELSEIF(MODEL.EQ.2)THEN
      CALL TRYAL2 (EA,SAL,YS,CM,X,SI,IPARA,AI,EI,SYB,CKG,HP)
      ELSEIF(MODEL.EQ.3)THEN
      CALL TRYAL3 (EA,SAL,YS,CM,X,SI,IPARA,AI,EI,SYB,HP,OMEG)
      ENDIF
      IF(ISIGNAL.EQ.1)THEN
      WRITE(6,*)'NEXT VALUE OF TAUL BECAUSE OF -VE BL'
      IF(YS.GT.YUP) THEN
      GO TO 10
      ELSE
      BL = BLF
      YN = YS
      GO TO 102
      ENDIF
      ELSEIF(ISIGNAL.EQ.2)THEN
      WRITE(6,*)'NEXT VALUE OF TAUL BECAUSE NO CONVERGENCE FOR SAL'
      IF(YS.GT.YUP) THEN
      GO TO 10
      ELSE
      YN = YS
      GO TO 102
      ENDIF
      ENDIF
      IF(IPARA .EQ. 1) THEN
      WRITE(6,*) 'NO CONVERGENCE FOR EA'
      IF(YS.GT.YUP) THEN
```

```
      GO TO 10
      ELSE
      YN=YS
      GO TO 102
      ENDIF
      ELSEIF(IPARA .EQ. 2) THEN
      WRITE(6,*) 'NO CONVERGENCE FOR YB0'
      IF(YS.GT.YUP) THEN
      GO TO 10
      ELSE
      YN=YS
      GO TO 102
      ENDIF
      ENDIF
      IF(ABS(YU-YL).LT.YTOL) THEN
      GO TO 80
      ENDIF
      DENOMS=1./((SI/DA)+(1./(DA*EA*EXP(G2/(1.+YS)))))
      FYS=-(1.0/Q + SR*(1.0-YAF*X))*YS+B*DENOMS*((1.0-SYB)*(1.0-X)
     S/(1.0-YAF*X))+YAF*(SR+SV*SYB/(1.0-SYB)
     S)*X-SP*SAL-SV*SYB/(1.0-SYB)-BETA*(YS-YC)+SR*(YR-1.)+HP
      IF(FYU*FYS.GT.0.) GO TO 70
      YL=YS
      GO TO 60
70    YU=YS
      FYU=FYS
      GO TO 60
80    T=TF*(1.+YS)-273.
      IF(ABS(T+273.-TLB) .GT. 2.)THEN
      TLB=T+273.
      ITEMP=ITEMP+1
      ICOUNT1=ICOUNT1+1
      IF(ITEMP .GT. 10 ) THEN
      WRITE(6,*)'NEXT VALUE OF TAUL BECAUSE'
      WRITE(6,*)'NO CONERGENCE FOR TEMPERATURE AT TAUL =',TAUL
      IF(YS .GT. YUP) THEN
      GO TO 10
      ELSE
      GO TO 102
      ENDIF
      ENDIF
      ISIGNAL=0
      YN=YN-FACTR*STEP
      GO TO 20
      ELSE
      ENDIF
      ICOUNT2=ICOUNT2+1
      WRITE(6,*)'ICOUNT2=',ICOUNT2
```

```
 RYB=SYB/(1.0-SYB)
 XG=(ABT*YS-SP*SAL-BEYC-HP-SR*(YR-1.)+SV*RYB)/(B+SR*YAF*(1.0+YS)
$+SV*YAF*RYB)
 XL=1.0-BL/BLF
 SALP=SAL/SQ
 AL=SALP*BLF
 RATIO=AL/AI
 EAI=EA/(1.-RATIO)
 WRITE(6,*)'SAL=',SAL
 WRITE(6,*)'SYB',SYB
 WRITE(6,*)'EA=',EA
 WRITE(7,*)ERR1,ERR2,ERR3
 WRITE(6,4)T,XG,XL,SALP,CM,EA,BI,SYB
 WRITE(11,88)TAUL,EAI,EA,CM,RATIO
 IF(RG.NE.0) THEN
 WRITE(10,5)TAUL,CKL,CKG,AV,EPSG,DB,HT
 ELSE
 WRITE(10,6)TAUL,CKL,AV,EPSG,DB,HT
 ENDIF
 WRITE(9,86)TAUL,UPR,HTPR,HOPR
 WRITE(8,87)TAUL,T,XG,XL,EA,SYB
 IF(ICOUNT2.EQ.1)THEN
 SOL1(NSOL1,1)=TAUL
 SOL1(NSOL1,2)=T
 SOL1(NSOL1,3)=XG
 SOL1(NSOL1,4)=XL
 SOL1(NSOL1,5)=EA
 SOL1(NSOL1,6)=SYB
 SOL1(NSOL1,7)=EPSG
 SOL1(NSOL1,8)=AV
 SOL1(NSOL1,9)=DB*10.
 SOL1(NSOL1,10)=HT*4.184E4
 SOL1(NSOL1,11)=EAI
 SOL1(NSOL1,12)=CM
 SOL1(NSOL1,13)=RATIO
 SOL1(NSOL1,14)=CKL
 SOL1(NSOL1,15)=CKGRT
 SOL1(NSOL1,16)=U*4.184E4
 SOL1(NSOL1,17)=PG*1E-1/VL
 SOL1(NSOL1,18)=NF
 SOL1(NSOL1,19)=PGT*1E-1/VL
 NSOL1=NSOL1+1
 ELSEIF(ICOUNT2.EQ.2)THEN
 SOL2(NSOL2,1)=TAUL
 SOL2(NSOL2,2)=T
 SOL2(NSOL2,3)=XG
 SOL2(NSOL2,4)=XL
 SOL2(NSOL2,5)=EA
```

```
SOL2(NSOL2,6)=SYB
SOL2(NSOL2,7)=EPSG
SOL2(NSOL2,8)=AV
SOL2(NSOL2,9)=DB*10.
SOL2(NSOL2,10)=HT*4.184E4
SOL2(NSOL2,11)=EAI
SOL2(NSOL2,12)=CM
SOL2(NSOL2,13)=RATIO
SOL2(NSOL2,14)=CKL
SOL2(NSOL2,15)=CKGRT
SOL2(NSOL2,16)=U*4.184E4
SOL2(NSOL2,17)=PG*1E-1/VL
SOL2(NSOL2,18)=NF
SOL2(NSOL2,19)=PGT*1E-1/VL
NSOL2=NSOL2+1
ELSEIF(ICOUNT2.EQ.3)THEN
SOL3(NSOL3,1)=TAUL
SOL3(NSOL3,2)=T
SOL3(NSOL3,3)=XG
SOL3(NSOL3,4)=XL
SOL3(NSOL3,5)=EA
SOL3(NSOL3,6)=SYB
SOL3(NSOL3,7)=EPSG
SOL3(NSOL3,8)=AV
SOL3(NSOL3,9)=DB*10.
SOL3(NSOL3,10)=HT*4.184E4
SOL3(NSOL3,11)=EAI
SOL3(NSOL3,12)=CM
SOL3(NSOL3,13)=RATIO
SOL3(NSOL3,14)=CKL
SOL3(NSOL3,15)=CKGRT
SOL3(NSOL3,16)=U*4.184E4
SOL3(NSOL3,17)=PG*1E-1/VL
SOL3(NSOL3,18)=NF
SOL3(NSOL3,19)=PGT*1E-1/VL
NSOL3=NSOL3+1
ELSEIF(ICOUNT2.EQ.4)THEN
SOL4(NSOL4,1)=TAUL
SOL4(NSOL4,2)=T
SOL4(NSOL4,3)=XG
SOL4(NSOL4,4)=XL
SOL4(NSOL4,5)=EA
SOL4(NSOL4,6)=SYB
SOL4(NSOL4,7)=EPSG
SOL4(NSOL4,8)=AV
SOL4(NSOL4,9)=DB*10.
SOL4(NSOL4,10)=HT*4.184E4
SOL4(NSOL4,11)=EAI
```

```
SOL4(NSOL4,12)=CM
SOL4(NSOL4,13)=RATIO
SOL4(NSOL4,14)=CKL
SOL4(NSOL4,15)=CKGRT
SOL4(NSOL4,16)=U*4.184E4
SOL4(NSOL4,17)=PG*1E-1/VL
SOL4(NSOL4,18)=NF
SOL4(NSOL4,19)=PGT*1E-1/VL
NSOL4=NSOL4+1
ELSEIF(ICOUNT2.EQ.5)THEN
SOL5(NSOL5,1)=TAUL
SOL5(NSOL5,2)=T
SOL5(NSOL5,3)=XG
SOL5(NSOL5,4)=XL
SOL5(NSOL5,5)=EA
SOL5(NSOL5,6)=SYB
SOL5(NSOL5,7)=EPSG
SOL5(NSOL5,8)=AV
SOL5(NSOL5,9)=DB*10.
SOL5(NSOL5,10)=HT*4.184E4
SOL5(NSOL5,11)=EAI
SOL5(NSOL5,12)=CM
SOL5(NSOL5,13)=RATIO
SOL5(NSOL5,14)=CKL
SOL5(NSOL5,15)=CKGRT
SOL5(NSOL5,16)=U*4.184E4
SOL5(NSOL5,17)=PG*1E-1/VL
SOL5(NSOL5,18)=NF
SOL5(NSOL5,19)=PGT*1E-1/VL
NSOL5=NSOL5+1
ELSEIF(ICOUNT2.EQ.6)THEN
SOL6(NSOL6,1)=TAUL
SOL6(NSOL6,2)=T
SOL6(NSOL6,3)=XG
SOL6(NSOL6,4)=XL
SOL6(NSOL6,5)=EA
SOL6(NSOL6,6)=SYB
SOL6(NSOL6,7)=EPSG
SOL6(NSOL6,8)=AV
SOL6(NSOL6,9)=DB*10.
SOL6(NSOL6,10)=HT*4.184E4
SOL6(NSOL6,11)=EAI
SOL6(NSOL6,12)=CM
SOL6(NSOL6,13)=RATIO
SOL6(NSOL6,14)=CKL
SOL6(NSOL6,15)=CKGRT
SOL6(NSOL6,16)=U*4.184E4
SOL6(NSOL6,17)=PG*1E-1/VL
```

```
      SOL6(NSOL6,18)=NF
      SOL6(NSOL6,19)=PGT*1E-1/VL
      NSOL6=NSOL6+1
      ELSEIF(ICOUNT2.EQ.7)THEN
      SOL7(NSOL7,1)=TAUL
      SOL7(NSOL7,2)=T
      SOL7(NSOL7,3)=XG
      SOL7(NSOL7,4)=XL
      SOL7(NSOL7,5)=EA
      SOL7(NSOL7,6)=SYB
      SOL7(NSOL7,7)=EPSG
      SOL7(NSOL7,8)=AV
      SOL7(NSOL7,9)=DB*10.
      SOL7(NSOL7,10)=HT*4.184E4
      SOL7(NSOL7,11)=EAI
      SOL7(NSOL7,12)=CM
      SOL7(NSOL7,13)=RATIO
      SOL7(NSOL7,14)=CKL
      SOL7(NSOL7,15)=CKGRT
      SOL7(NSOL7,16)=U*4.184E4
      SOL7(NSOL7,17)=PG*1E-1/VL
      SOL7(NSOL7,18)=NF
      SOL7(NSOL7,19)=PGT*1E-1/VL
      NSOL7=NSOL7+1
      ENDIF
    4 FORMAT(/8X,'T(C) =',F7.2,6X,'XG  =',F7.4/,
     $      8X,'XL =',F9.6,8X,'SAL(L) =',F8.5,8X,'M =',F8.4,
     $      8X,'EA=',F8.4/,8X,'BI=',F8.6,8X,'YB0 =',F8.4/)
    5 FORMAT(F7.2,1X,F5.3,1X,F8.6,1X,F5.3,1X,F5.3,1X,F5.3,1X,F6.4)
    6 FORMAT(F7.2,1X,F5.3,1X,F5.3,1X,F5.3,1X,F5.3,1X,F6.4)
   86 FORMAT(F7.2,1X,F7.3,1X,F7.3,1X,F9.3)
   87 FORMAT(F7.2,1X,F7.3,1X,F7.3,1X,F9.6,1X,F5.3,1X,F7.5)
   88 FORMAT(F7.2,1X,F7.3,1X,F5.3,1X,F8.5,1X,F5.3)
  102 GO TO 40
  101 DO 991 I=0,NSOL1-1
      IF(I.EQ.0) THEN
C     WRITE(17,*) 'TAUL  T'
C     WRITE(18,*) 'TAUL  XG'
      WRITE(19,*) 'TAUL  XL'
      WRITE(20,*) 'TAUL  EA'
      WRITE(21,*) 'TAUL  SYB'
      WRITE(22,*) 'TAUL  EPSG'
      WRITE(23,*) 'TAUL  AV'
      WRITE(24,*) 'TAUL  DB'
      WRITE(25,*) 'TAUL  HT'
      WRITE(26,*) 'TAUL  EAI'
      WRITE(27,*) 'TAUL  CM'
      WRITE(28,*) 'TAUL  RATIO'
```

```
      WRITE(29,*) 'TAUL  CKL '
      WRITE(30,*) 'TAUL  CKG '
      WRITE(31,*) 'TAUL  U '
      WRITE(32,*) 'TAUL  PG/VL'
      WRITE(33,*) 'TAUL  NF'
      WRITE(34,*) 'TAUL  PGT/VL'
      ELSE
      WRITE(17,89) SOL1(I,1),SOL1(I,2)
      WRITE(18,89) SOL1(I,1),SOL1(I,3)
      WRITE(19,89) SOL1(I,1),SOL1(I,4)
      WRITE(20,89) SOL1(I,1),SOL1(I,5)
      WRITE(21,89) SOL1(I,1),SOL1(I,6)
      WRITE(22,89) SOL1(I,1),SOL1(I,7)
      WRITE(23,89) SOL1(I,1),SOL1(I,8)
      WRITE(24,89) SOL1(I,1),SOL1(I,9)
      WRITE(25,89) SOL1(I,1),SOL1(I,10)
      WRITE(26,89) SOL1(I,1),SOL1(I,11)
      WRITE(27,89) SOL1(I,1),SOL1(I,12)
      WRITE(28,89) SOL1(I,1),SOL1(I,13)
      WRITE(29,89) SOL1(I,1),SOL1(I,14)
      WRITE(30,89) SOL1(I,1),SOL1(I,15)
      WRITE(31,89) SOL1(I,1),SOL1(I,16)
      WRITE(32,89) SOL1(I,1),SOL1(I,17)
      WRITE(33,89) SOL1(I,1),SOL1(I,18)
      WRITE(34,89) SOL1(I,1),SOL1(I,19)
      ENDIF
991   CONTINUE
      DO 992 I=1,NSOL2-1
      WRITE(17,89) SOL2(I,1),SOL2(I,2)
      WRITE(18,89) SOL2(I,1),SOL2(I,3)
      WRITE(19,89) SOL2(I,1),SOL2(I,4)
      WRITE(20,89) SOL2(I,1),SOL2(I,5)
      WRITE(21,89) SOL2(I,1),SOL2(I,6)
      WRITE(22,89) SOL2(I,1),SOL2(I,7)
      WRITE(23,89) SOL2(I,1),SOL2(I,8)
      WRITE(24,89) SOL2(I,1),SOL2(I,9)
      WRITE(25,89) SOL2(I,1),SOL2(I,10)
      WRITE(26,89) SOL2(I,1),SOL2(I,11)
      WRITE(27,89) SOL2(I,1),SOL2(I,12)
      WRITE(28,89) SOL2(I,1),SOL2(I,13)
      WRITE(29,89) SOL2(I,1),SOL2(I,14)
      WRITE(30,89) SOL2(I,1),SOL2(I,15)
      WRITE(31,89) SOL2(I,1),SOL2(I,16)
      WRITE(32,89) SOL2(I,1),SOL2(I,17)
      WRITE(33,89) SOL2(I,1),SOL2(I,18)
      WRITE(34,89) SOL2(I,1),SOL2(I,19)
992   CONTINUE
      DO 993 I=1,NSOL3-1
```

```
      WRITE(17,89) SOL3(I,1),SOL3(I,2)
      WRITE(18,89) SOL3(I,1),SOL3(I,3)
      WRITE(19,89) SOL3(I,1),SOL3(I,4)
      WRITE(20,89) SOL3(I,1),SOL3(I,5)
      WRITE(21,89) SOL3(I,1),SOL3(I,6)
      WRITE(22,89) SOL3(I,1),SOL3(I,7)
      WRITE(23,89) SOL3(I,1),SOL3(I,8)
      WRITE(24,89) SOL3(I,1),SOL3(I,9)
      WRITE(25,89) SOL3(I,1),SOL3(I,10)
      WRITE(26,89) SOL3(I,1),SOL3(I,11)
      WRITE(27,89) SOL3(I,1),SOL3(I,12)
      WRITE(28,89) SOL3(I,1),SOL3(I,13)
      WRITE(29,89) SOL3(I,1),SOL3(I,14)
      WRITE(30,89) SOL3(I,1),SOL3(I,15)
      WRITE(31,89) SOL3(I,1),SOL3(I,16)
      WRITE(32,89) SOL3(I,1),SOL3(I,17)
      WRITE(33,89) SOL3(I,1),SOL3(I,18)
      WRITE(34,89) SOL3(I,1),SOL3(I,19)
993   CONTINUE
   89 FORMAT(F7.2,1X,F14.9)
      END
C
C TRYAL1 =  NON-VOLATILE LIQUID CASE ( SLAB GEOMETRY )
C
      SUBROUTINE TRYAL1 (EA,SAL,Y,CM,X,SI,IPARA,AI,EI,SYB,HP)
      COMMON /DATA/CK0,H0,G1,G2,ABT,BEYC,B,SP,AGF,BLF,Q,SQ,D,CKL,
     $           ALFAP,ZETAP,BL,BI,ISIGNAL,YAF,SR,YR,FG,RAOLF,RAOGF,
     $           VR,PTOT,AV,SV,TF,ERR1,ERR2,ERR3
      IPARA=0
      CK=CK0*EXP(-G1/(1.0+Y))
      ITER1=0
      ITER2=0
      EAS=1.0
   10 X=(ABT*Y+SP*SAL-BEYC-HP-SR*(YR-1.)+SV*(SYB/(1.-SYB)))/
     $(B+SR*YAF*(1.+Y)+YAF*SV*(SYB/(1.-SYB)))
      DENOM=1./(SI*EAS*EXP(G2/(1.0+Y))+1.0)
      AI=H0*AGF*(1.0-X)*(1.-SYB)*DENOM*EXP(G2/(1.0+Y))/(1.- YAF*X)
      BL=AGF*(SQ+SAL-Q*X)
      IF(BL .LT. 0)GO TO 60
      EI=1.+BL/AI
      CM=SQRT(CK*D*BL)/CKL
      CMALZE=CM**2*(ALFAP-1.0)+1./ZETAP
      CALL BIROOT(BI,EI,CMALZE,CM)
      CMBI=CM*SQRT(BI)
      IF(CMBI .GT.1.E2) GO TO 30
      ALNUM=AI/AGF*CMBI/(CMBI*COSH(CMBI)+CMALZE*SINH(CMBI))
      IF(ALNUM .LT.0) ALNUM=0
      IF(ABS(SAL-ALNUM).LT.1.E-3) GO TO 20
```

```
      SAL=ALNUM
      ITER1=ITER1+1
      IF(ITER1 .GE. 30) GO TO 40
      GO TO 10
   20 SAL=ALNUM
      EA=CMBI*(CMALZE+CMBI*TANH(CMBI))/(CMALZE*TANH(CMBI)+CMBI)
      IF(ABS(EA-EAS).GT.1E-3)THEN
      EAS=EA
      ITER1=0
      ITER2=ITER2+1
      IF(ITER2 .GT. 40)THEN
      IPARA=1
      GO TO 70
      ENDIF
      GO TO 10
      ENDIF
      RETURN
   30 EA=CMBI
      IF(ABS(EA-EAS).GT.1E-3)THEN
      EAS=EA
      ITER1=0
      ITER2=ITER2+1
      IF(ITER2 .GT. 40)THEN
      IPARA=1
      GO TO 70
      ENDIF
      GO TO 10
      ENDIF
      SAL=0.0
      RETURN
   40 PRINT1,ITER1
    1 FORMAT(/' NO CONVERGENCE FOR SOL IN',I3,' ITERATIONS'/)
      ISIGNAL=2
      RETURN
   60 ISIGNAL=1
   70 RETURN
      END
C
C TRYAL2 = VOLATILE LIQUID CASE ( SLAB GEOMETRY )
C
      SUBROUTINE TRYAL2 (EA,SAL,Y,CM,X,SI,IPARA,AI,EI,SYB,CKG,HP)
      COMMON /DATA CK0,H0,G1,G2,ABT,BEYC,B,SP,AGF,BLF,Q,SQ,D,CKL,
     $           ALFAP,ZETAP,BL,BI,ISIGNAL,YAF,SR,YR,FG,RAOLF,RAOGF,
     $           VR,PTOT,AV,SV,TF,ERR1,ERR2,ERR3
      C1=6.95367
      C2=1501.268
      C3=194.480
      IPARA=0
```

```
      CK = CK0*EXP(-G1/(1.0+Y))
      ITER1 = 0
      ITER2 = 0
      ITER3 = 0
      EAS = 0.1
   10 X = (ABT*Y + SP*SAL-BEYC-HP-SR*(YR-1.) + SV*(SYB/(1.-SYB)))/
     $(B + SR*YAF*(1. + Y) + YAF*SV*(SYB/(1.-SYB)))
      DENOM = 1./(SI*EAS*EXP(G2/(1.0+Y)) + 1.0)
      AI = H0*AGF*(1.0-X)*(1.-SYB)*DENOM*EXP(G2/(1.0+Y))/(1.- YAF*X)
      ALOAI = SAL*AGF/AI
      BL = AGF*(SQ + SAL-Q*X)
      IF(BL .LT. 0) THEN
      GO TO 60
      ENDIF
      RQ = BL/AI
      EI = 1. - RQ
      PB0 = 10.**(C1-C2/(TF*(1.0+Y)-273.1 + C3))/760.
      CM = SQRT(CK*D*BL)/CKL
      CM1 = CM**2*(ALFAP-1.0) + 1./ZETAP
      IF(YAF.LT.1) THEN
      GAMP1 = CKG*PB0/(RAOLF*CKL)
      GAMP2 = FG*RAOGF*(1.0-YAF*X)/(1.0-SYB)
      GAMP3 = PTOT*VR*AV*CKG
      GAMP4 = GAMP3/GAMP2
      GAMP5 = 1./(1. + GAMP4)
      GAMP = GAMP1*GAMP5
      ELSE
      GAMP1 = PB0*FG*RAOGF*(1.0-YAF*X)/(1.0-SYB)
      GAMP2 = PTOT*CKL*AV*VR*RAOLF
      GAMP = GAMP1/GAMP2
      ENDIF
      APRIM = (1./RQ)-((1. + (1/RQ)-BI)/EAS) + (ALOAI/(EAS*RQ))
      ALAMD = CM*(BI-(APRIM/3.))
      ALOAI1 = ALAMD*COSH(ALAMD)/TANH(ALAMD)
      ALOAI2 = ALAMD*SINH(ALAMD)
      ALOAI3 = CM1 + (ALAMD/TANH(ALAMD))
      ALOAI = (ALOAI1-ALOAI2)/ALOAI3
      BI = (EI-EAS-ALOAI)/((1. + GAMP)*(EI-1.))
      CSYB = PB0*BL*BI/(RAOLF*PTOT)
      IF(CSYB.GT.1.) CSYB = 0.025
      ALNUM = AI*ALOAI/AGF
      EA = ((ALAMD*ALAMD) + (CM1*ALAMD/TANH(ALAMD)))/
     $((ALAMD/TANH(ALAMD)) + CM1)
      ERR1 = ABS(EA-EAS)
      IF(ERR1.GT.1E-2)THEN
      EAS = EA
      ITER1 = ITER1 + 1
      IF(ITER1 .GT. 90)THEN
```

```
      IPARA=1
      GO TO 70
      ENDIF
      GO TO 10
      ENDIF
      ERR2=ABS(SYB-CSYB)
      IF(ERR2.GT.1E-2)THEN
      ITER1=0
      ITER2=ITER2+1
      IF(ITER1.GT.100)THEN
      IPARA=2
      GO TO 70
      ENDIF
      SYB=CSYB
      GO TO 10
      ENDIF
      SYB=CSYB
      ERR3=ABS(SAL-ALNUM)
      IF(ERR3.LT.1.E-2) GO TO 20
      SAL=ALNUM
      ITER1=0
      ITER2=0
      ITER3=ITER3+1
      IF(ITER2 .GE. 90) GO TO 40
      GO TO 10
   20 SAL=ALNUM
      RETURN
   40 PRINT1,ITER3
    1 FORMAT(/' NO CONVERGENCE FOR SOL IN',I3,' ITERATIONS'/)
      ISIGNAL=2
      RETURN
   60 ISIGNAL=1
   70 RETURN
      END
C
C TRYAL3 =  NON-VOLATILE LIQUID CASE ( SPHERICAL GEOMETRY )
C
      SUBROUTINE TRYAL3 (EA,SAL,Y,CM,X,SI,IPARA,AI,EI,SYB,HP,OMEG)
      COMMON /DATA/CK0,H0,G1,G2,ABT,BEYC,B,SP,AGF,BLF,Q,SQ,D,CKL,
     $          ALFAP,ZETAP,BL,BI,ISIGNAL,YAF,SR,YR,FG,RAOLF,RAOGF,
     $          VR,PTOT,AV,SV,TF,ERR1,ERR2,ERR3
      IPARA=0
      ALFAPP=ALFAP*(OMEG/(1.+OMEG))
      ZETAPP=ZETAP*((1.+OMEG)/OMEG)
      CK=CK0*EXP(-G1/(1.0+Y))
      ITER1=0
      ITER2=0
      EAS=1.0
```

```
10 X=(ABT*Y+SP*SAL-BEYC-HP-SR*(YR-1.)+SV*(SYB/(1.-SYB)))/
  S(B+SR*YAF*(1.+Y)+YAF*SV*(SYB/(1.-SYB)))
   DENOM=1./(SI*EAS*EXP(G2/(1.0+Y))+1.0)
   AI=H0*AGF*(1.0-X)*(1.-SYB)*DENOM*EXP(G2/(1.0+Y))/(1.-YAF*X)
   BL=AGF*(SQ+SAL-Q*X)
   IF(BL .LT. 0)GO TO 60
   EI=1.+BL/AI
   CM=SQRT(CK*D*BL)/CKL
   CMP=CM*((1.+OMEG)/OMEG)
   CMALZE=(CM**2)*(ALFAPP-((1./(3*OMEG*OMEG))+
  S(1./OMEG)+1.0))+(1./ZETAPP)
   CALL BROOT(BI,EI,CMALZE,CM,OMEG)
   CMBI=CMP*SQRT(BI)
   IF(CMBI.GT.1.E2) GO TO 30
   ALNUM=(AI/AGF)*(OMEG*CMBI/(CMBI*(OMEG+1.)*COSH(CMBI)+
  S((CMALZE*(OMEG+1.))-1.)*SINH(CMBI)))
   IF(ALNUM .LT.0) ALNUM=0
   IF(ABS(SAL-ALNUM).LT.1.E-3) GO TO 20
   SAL=ALNUM
   ITER1=ITER1+1
   IF(ITER1 .GE. 30) GO TO 40
   GO TO 10
20 SAL=ALNUM
   EA=((OMEG*CMBI/(1.+OMEG))*(((CMALZE*(OMEG+1.))-1.)+
  SCMBI*(1.+OMEG)*TANH(CMBI))/(((CMALZE*(1.+OMEG))-1.)
  S*TANH(CMBI)+(CMBI*(1.+OMEG))))+(1./(1.+OMEG))
   IF(ABS(EA-EAS).GT.1E-3)THEN
   EAS=EA
   ITER1=0
   ITER2=ITER2+1
   IF(ITER2 .GT. 40)THEN
   IPARA=1
   GO TO 70
   ENDIF
   GO TO 10
   ENDIF
   RETURN
30 EA=(CMBI+(1./OMEG))*(OMEG/(OMEG+1.))
   IF(ABS(EA-EAS).GT.1E-3)THEN
   EAS=EA
   ITER1=0
   ITER2=ITER2+1
   IF(ITER2 .GT. 40)THEN
   IPARA=1
   GO TO 70
   ENDIF
   GO TO 10
   ENDIF
```

```
      SAL=0.0
      RETURN
   40 PRINT1,ITER1
    1 FORMAT(/' NO CONVERGENCE FOR SOL IN',I3,' ITERATIONS'/)
      ISIGNAL=2
      RETURN
   60 ISIGNAL=1
   70 RETURN
      END
C
C SUBROUTINE BIROOT IS USED FOR SUBROUTINE TRYAL1
C
      SUBROUTINE BIROOT(BI,EI,CMALZE,CM)
      FB(BI,CMBI)=BI-1./(EI-1.)*(EI-CMBI*(CMALZE+CMBI*TANH(CMBI))
     $          /(CMALZE*TANH(CMBI)+CMBI)-CMBI/(CMBI*COSH(CMBI)
     $          +CMALZE*SINH(CMBI)))
      ICNTL=0
      BIN=1.0
      CMBI=CM*SQRT(BIN)
      FM=FB(BIN,CMBI)
  10  BI1=BIN-0.001
      IF(BI1.LT.0) GO TO 60
  15  CMBI1=CM*SQRT(BI1)
      FM1=FB(BI1,CMBI1)
      IF(FM*FM1.LT.0) GO TO 20
      FM=FM1
      BIN=BI1
      GO TO 10
  20  BIU=BIN
      BIL=BI1
      FU=FM
  30  BIS=(BIL+BIU)/2.
C
C  CHECK CONVERGENCE BI
C
      IF(ABS(BIU-BIL).LT.1.E-4) GO TO 50
      CMBIS=CM*SQRT(BIS)
      FMS=FB(BIS,CMBIS)
      IF(FU*FMS.GT.0) GO TO 40
      BIL=BIS
      GO TO 30
  40  BIU=BIS
      FU=FMS
      GO TO 30
  50  BI=BIS
      RETURN
  60  ICNTL=ICNTL+1
      IF(ICNTL..GT.1) GO TO 70
```

```
      BI1 = 1.E-8
      GO TO 15
   70 RETURN
      END
C
C SUBROUTINE BROOT IS USED FOR SUBROUTINE TRYLA3
C
      SUBROUTINE BROOT(BI,EI,CMALZE,CM,OMEG)
      FB(BI,CMBI) = BI-((1.-(EI-1))*(EI-
     $      (((OMEG*CMBI/(1.+OMEG))*(((CMALZE*(OMEG+1.))-1.)+
     $      CMBI*(1.+OMEG)*TANH(CMBI))/(((CMALZE*(1.+OMEG))-1.)*
     $      TANH(CMBI)+(CMBI*(1.+OMEG))))+(1./(1.+OMEG)))-
     $      (OMEG*CMBI-(CMBI*(OMEG+1.)*COSH(CMBI)+
     $      ((CMALZE*(OMEG+1.))-1.)*SINH(CMBI)))))
      ICNTL = 0
      BIN = 1.0
      CMP = CM*((1.+OMEG)/OMEG)
      CMBI = CMP*SQRT(BIN)
      FM = FB(BIN,CMBI)
   10 BI1 = BIN-0.001
      IF(BI1.LT.0) GO TO 60
   15 CMBI1 = CMP*SQRT(BI1)
      FM1 = FB(BI1,CMBI1)
      IF(FM*FM1.LT.0) GO TO 20
      FM = FM1
      BIN = BI1
      GO TO 10
   20 BIU = BIN
      BIL = BI1
      FU = FM
   30 BIS = (BIL+BIU)/2.
C
C  CHECK CONVERGENCE BI
C
      IF(ABS(BIU-BIL).LT.1.E-4) GO TO 50
      CMBIS = CMP*SQRT(BIS)
      FMS = FB(BIS,CMBIS)
      IF(FU*FMS.GT.0) GO TO 40
      BIL = BIS
      GO TO 30
   40 BIU = BIS
      FU = FMS
      GO TO 30
   50 BI = BIS
      RETURN
   60 ICNTL = ICNTL+1
      IF(ICNTL.GT.1) GO TO 70
      BI1 = 1.E-8
```

```
      GO TO 15
   70 RETURN
      END
C
C SUBROUTINE GEOMET1
C
      SUBROUTINE GEOMET1(HL,VL,TH,DI,SH,GBL,W,BLM,DM,ALM,DCP,DCI,
     DCO,DC,S,DT,MUG,SE,RAOGF,AMWG,ITYPE,TTH,VO,THI,JTH,SAI,SAO,
     RAOC,AMWC,QC,DO)
      REAL MUG
C
C 1. VESSEL DIMENSION
C
      HL = DT
      VL = (22./(7.*4.))*DT*DT*HL
      TH = 0.8
      NB = 4
      BW = DT/10.
      OS = BW/6.
C INSULATION THICKNESS
      THI = 1.0
C
C 2. IMPELLER DIMENSION
C
      DI = DT/3.
      SH = DI
      GBL = DI/4.
      W = DI/5.
      NB = 6
      NI = 1
C
C 3. SPARGER DIMENSION
C
      DSP = 0.875*DI
      DO = 1.50/10.
      NO = 5.
      VO = 5000.0
      REO = DO*VO*RAOGF*AMWG/MUG
      WRITE(6,*)'VO = ',VO,'ORIFICE REYNOLD  = ',REO
      SE = 0.062*DT
C
C 4. JACKET DIMENSION
C
      BLM = 0.75
      JTH = 0.5
      DM = DT + 2.*TH
      DJO = DM + (2.*BLM)
      ALM = .98*DT
```

```
      DCP=0.5
C
C 5. DIMENSIONS OF COOLING COIL
C
      DCI=0.5
      DCO=0.7
      DC=0.8*DT
      HCC=0.79*DT
      CPITCH=1.7
      TTH=.1
      IF(ITYPE .EQ. 1)THEN
      SAI=(22./7.)*DT*ALM
      SAO=(22./7)*(DM+ 2.*BLM+2.*JTH+2.*THH)*ALM
C     WRITE(6,*)'SAI=',SAI,'SAO=',SAO
      ELSE
      PI=22./7.
      S=PI*DCO*HCC*(1./CPITCH)*((PI*PI*DC*DC)+(1./(CPITCH**2)))**0.5)
C     WRITE(6,*)'S=',S
      ENDIF
      AMUC=1.E-2
      ROWC=RAOC*AMWC
      IF(ITYPE.EQ.1) THEN
      DEQ=DJO-DM
      AX=(22./7.)*((DJO**2)-(DM**2)) 4.
      REC=10000.
      QC=AX*AMUC*REC/(DEQ*ROWC)
C     WRITE(6,*)'QC=',QC
      ELSE
      REC=10000.
      AX=(22./7.)*(DCI**2)/4
      QC=AX*AMUC*REC/(DCI*ROWC)
C     WRITE(6,*)'QC=',QC
      ENDIF
      RETURN
      END
C
C SUBROUTINE GEOMET2
C
      SUBROUTINE GEOMET2(HL,VL,TH,DI,SH,GBL,W,BLM,DM,ALM,DCP,DCI,
     DCO,DC,S,DT,MUG,SE,RAOGF,AMWG,ITYPE,TTH,VO,THH,JTH,SAI,SAO,
     RAOC,AMWC,QC,DO)
      REAL MUG
C
C 1. VESSEL DIMENSION
C
      HL=DT
      VL=(22./(7.*4.))*DT*DT*HL
      TH=0.8
```

```
      NB=4
      BW=DT/10.
      OS=BW/6.
C INSULATION THICKNESS
      THI=1.0
C
C 2. IMPELLER DIMENSION
C
      DI=DT/3.
      SH=DI
      GBL=DI/4.
      W=DI/5.
      NB=6
      NI=1
C
C 3. SPARGER DIMENSION
C
      DSP=0.875*DI
      DO=3.18/10.
      NO=20.
      VO=5000.0
      REO=DO*VO*RAOGF*AMWG/MUG
      WRITE(6,*)'VO=',VO,'ORIFICE REYNOLD  =',REO
      SE=0.062*DT
C
C 4. JACKET DIMENSION
C
      BLM=1.25
      JTH=0.8
      DM=DT+2.*TH
      DJO=DM+(2.*BLM)
      ALM=0.98*DT
      DCP=0.7
C
C 5. DIMENSIONS OF COOLING COIL
C
      DCI=1.7
      DCO=1.9
      DC=0.8*DT
      HCC=0.79*DT
      CPITCH=3.4
      TTH=.1
      IF(ITYPE .EQ. 1)THEN
      SAI=(22./7.)*DT*ALM
C     SAO=(22./7)*(DM+ 2.*BLM+2.*JTH+2.*THI)*ALM
      SAO=(22./7)*(DM)*ALM
C     WRITE(6,*)'SAI=',SAI,'SAO=',SAO
      ELSE
```

```
      PI = 22./7.
      S = PI*DCO*HCC*(1./CPITCH)*(((PI*PI*DC*DC) - (1./(CPITCH**2)))**0.5)
C     WRITE(6,*)'S = ',S
      ENDIF
      AMUC = 1.E-2
      ROWC = RAOC*AMWC
      IF(ITYPE.EQ.1) THEN
      DEQ = DJO-DM
      REC = 10000.
      AX = (22./7.)*((DJO**2)-(DM**2))/4.
      QC = AX*AMUC*REC/(DEQ*ROWC)
C     WRITE(6,*)'QC = ',QC
      ELSE
      REC = 10000.
      AX = (22./7.)*(DCI**2)/4
      QC = AX*AMUC*REC/(DCI*ROWC)
C     WRITE(6,*)'QC = ',QC
      ENDIF
      RETURN
      END
C
C SUBROUTINE GEOMET3
C
      SUBROUTINE GEOMET3(HL,VL,TH,DI,SH,GBL,W,BLM,DM,ALM,DCP,DCI,
     DCO,DC,S,DT,MUG,SE,RAOGF,AMWG,ITYPE,TTH,VO,THI,JTH,SAI,SAO,
     RAOC,AMWC,QC,DO)
      REAL MUG
C
C 1. VESSEL DIMENSION
C
      HL = DT
      VL = (22./(7.*4.))*DT*DT*HL
      TH = 1.0
      NB = 4
      BW = DT/10.
      OS = BW/6.
C INSULATION THICKNESS
      THI = 1.0
C
C 2. IMPELLER DIMENSION
C
      DI = DT/3.
      SH = DI
      GBL = DI/4.
      W = DI/5.
      NB = 6
      NI = 1
C
```

```
C 3. SPARGER DIMENSION
C
      DSP = 0.875*DI
      DO = 3.18/10.
      NO = 50.
      VO = 5000.0
      REO = DO*VO*RAOGF*AMWG/MUG
      WRITE(6,*)'VO = ',VO,'ORIFICE REYNOLD  = ',REO
      SE = 0.062*DT
C
C 4. JACKET DIMENSION
C
      BLM = 2.5
      JTH = 0.8
      DM = DT + 2.*TH
      DJO = DM + (2.*BLM)
      ALM = 0.98*DT
      DCP = 1.3
C
C 5. DIMENSIONS OF COOLING COIL
C
      DCI = 2.8
      DCO = 3.0
      DC = 0.8*DT
      HCC = 0.79*DT
      CPITCH = 4.5
      TTH = .1
      IF(ITYPE .EQ. 1)THEN
      SAI = (22./7.)*DT*ALM
C     SAO = (22./7)*(DM +  2.*BLM + 2.*JTH + 2.*THI)*ALM
      SAO = (22./7)*DM*ALM
C     WRITE(6,*)'SAI = ',SAI,'SAO = ',SAO
      ELSE
      PI = 22./7.
      S = PI*DCO*HCC*(1./CPITCH)*(((PI*PI*DC*DC) + (1./(CPITCH**2)))**0.5)
C     WRITE(6,*)'S = ',S
      ENDIF
      AMUC = 1.E-2
      ROWC = RAOC*AMWC
C     WRITE(6,*)'ROWC = ',ROWC
      IF(ITYPE.EQ.1) THEN
      DEQ = DJO-DM
      REC = 10000.
      AX = (22./7.)*((DJO**2)-(DM**2))/4.
      QC = AX*AMUC*REC/(DEQ*ROWC)
C     WRITE(6,*)'QC = ',QC
      ELSE
      REC = 10000.
```

```
      AX=(22./7.)*(DCI**2) 4
      QC=AX*AMUC*REC (DCI*ROWC)
C     WRITE(6,*)'QC=',QC
      ENDIF
      RETURN
      END
C
C SUBROUTINE GEOMET4  DT=1.2 M
C
      SUBROUTINE GEOMET4(HL,VL,TH,DI,SH,GBL,W,BLM,DM,ALM,DCP,DCI,
     DCO,DC,S,DT,MUG,SE,RAOGF,AMWG,ITYPE,TTH,VO,THI,JTH,SAI,SAO,
     RAOC,AMWC,QC,DO)
      REAL MUG
C
C 1. VESSEL DIMENSION
C
      HL=DT
      VL=(22./(7.*4.))*DT*DT*HL
      TH=1.5
      NB=4
      BW=DT/10.
      OS=BW/6.
C INSULATION THICKNESS
      THI=1.0
C
C 2. IMPELLER DIMENSION
C
      DI=DT/3.
      SH=DI
      GBL=DI/4.
      W=DI/5.
      NB=6
      NI=1
C
C 3. SPARGER DIMENSION
C
      DSP=0.875*DI
      DO=3.18/10.
      NO=100.0
      VO=5000.0
      REO=DO*VO*RAOGF*AMWG/MUG
      WRITE(6,*)'VO=',VO,'ORIFICE REYNOLD   =  ',REO
      SE=0.062*DT
C
C 4. JACKET DIMENSION
C
      BLM=5.0
      JTH=1.0
```

```
      DM = DT + 2.*TH
      DJO = DM + (2.*BLM)
      ALM = 0.98*DT
      DCP = 2.6
C
C 5. DIMENSIONS OF COOLING COIL
C
      DCI = 4.13
      DCO = 4.76
      DC = 0.8*DT
      HCC = 0.79*DT
      CPITCH = 6.1
      TTH = .32
      IF(ITYPE .EQ. 1)THEN
      SAI = (22./7.)*DT*ALM
C     SAO = (22./7)*(DM + 2.*BLM + 2.*JTH + 2.*THI)*ALM
      SAO = (22./7)*DM*ALM
C     WRITE(6,*)'SAI = ',SAI,'SAO = ',SAO
      ELSE
      PI = 22./7.
      S = PI*DCO*HCC*(1./CPITCH)*(((PI*PI*DC*DC) + (1./(CPITCH**2)))**0.5)
C     WRITE(6,*)'S = ',S
      ENDIF
      AMUC = 1.E-2
      ROWC = RAOC*AMWC
      IF(ITYPE.EQ.1) THEN
      DEQ = DJO-DM
      REC = 10000.
      AX = (22./7.)*((DJO**2)-(DM**2))/4.
      QC = AX*AMUC*REC/(DEQ*ROWC)
C     WRITE(6,*)'QC = ',QC
      ELSE
      REC = 10000.
      AX = (22./7.)*(DCI**2)/4
      QC = AX*AMUC*REC/(DCI*ROWC)
C     WRITE(6,*)'QC = ',QC
      ENDIF
      RETURN
      END
C
C SUBROUTINE POWER
C
      SUBROUTINE POWER(RAOL,RAOGF,N,DI,DT,MUL,MUG,G,IND,PO,PG,PGA,PGT,
     1     FG,VSG,VO,AMWL,AMWG,TGF,TLB,W,GBL,IGEOMET,VL,DO,NF)
      REAL N,MUL,MUG,NF
      IND = 0
      ROL = RAOL*AMWL
      QG = FG
```

```
C
C 1. AGITATOR POWER REQUIREMENT
C
      PN=120.*GBL*W*(DI-GBL)/(DI**3)
      PO=PN*ROL*(N**3)*(DI**5)
C     WRITE(7,*)'PO=',PO
      NF=0.322*((G*QG/(DI**4))**(1./3.))*((DT/DI)**1.167)
      REI=ROL*N*DI*DI/MUL
      FR=N*N*DI/G
      FRF=NF*NF*DI/G
      AN=QG/(N*(DI**3))
      ANTT=3.8E-3*((REI*REI/FR)**0.07)*((DT/DI)**0.5)
      ANF=30.*((DI/DT)**3.5)*(FRF)
C     WRITE(7,*)'PN=',PN,'NF=',NF
C     WRITE(7,*)'AN=',AN,'ANF=',ANF
C     WRITE(7,*)'ANTT=',ANTT
      AAA=1.-(17.*ANTT*(FR**.35))
      BBB=0.27+(0.022/FR)
      IF(AN .GT. 0 .AND. AN .LT. ANTT ) THEN
      PG=PO*(1-(16.7*AN*(FR**0.35)))
      ELSEIF(AN .GE. ANTT .AND. AN .LT. 0.1 ) THEN
      PG=PO*(BBB-(0.1*(AAA-BBB)/(ANTT-0.1))+((AAA-BBB)*AN/(ANTT-.1)))
      ELSEIF(AN .GT. 0.1 .AND. AN .LT. ANF) THEN
      PG=PO*(0.27+(0.022/FR))
      ELSE
      IND=1
      GO TO 1
      ENDIF
C     WRITE(7,*)'PG=',PG
C
C 2. SPARGER POWER REQUIREMENT
C
      R1=8.314E7
      IF(IGEOMET .EQ. 1 ) THEN
      PIN=1.05
      ELSE
      PIN=1.2
      ENDIF
      P=1.0
      ROGF=RAOGF*AMWG*(PIN/P)
      PGA=QG*ROGF*((0.06*VO*VO/2.)+((R1*TGF/AMWG)*LOG(PIN/P)))
      PGT=PG+(C1*PGA)
C     WRITE(7,*)'PGT=',PGT
C     WRITE(7,*)'PG/PO=',PG/PO
    1 RETURN
      END
C
C SUBROUTINE HYDEM
```

```
C
      SUBROUTINE HYDEM(CKL,CKG,MUL,VT,DB,SIGL,RAOL,RAOG,G,PGT,VL,EPSG,
     VSG,AV,DAB,DAI,R,TGF,RG,AMWL,VR,VG,YAF,DI,DT,N,FG,PTOT,PI,TLB,
     PG,AMWG,CKGRT,IGEOMET)
      REAL MUL,N
      ROL=RAOL*AMWL
      ROG=RAOL*AMWG
      DB=0.04
   10 FNH=G*(DB**2.67)*(ROL-ROG)*(ROL**.667)/((MUL**1.33)*(SIGL**.33))
      VT=0.75*((MUL**.33)*(SIGL**.33)/((DB**.667)*(ROL**.667)))*
     S((LOG(FNH)/2.303)**2.)
      EPSG1=0.005
      EPSG2=0.90
      CAN=(SIGL**0.6)/((ROL**0.2)*((PGT/VL)**0.4))
   20 F1=EPSG1-(((VSG/(VSG+VT))**0.5)*((EPSG1**.5)+(.0216/CAN)))
      F2=EPSG2-(((VSG/(VSG+VT))**0.5)*((EPSG2**.5)+(.0216/CAN)))
      EPSGN=EPSG2-(F2*((EPSG2-EPSG1)/(F2-F1)))
      IF(ABS(F2-F1).LT.1E-4)THEN
      EPSG=EPSGN
      DBC=(4.15*CAN*(EPSG**0.5))+0.09
      IF(ABS(DBC-DB).GT.1E-4)THEN
      DB=DBC
      GO TO 10
      ELSE
      AV=(1.44*CAN)*((VSG/(VSG+VT))**.5)
      ENDIF
      ELSE
      EPSG1=EPSG2
      EPSG2=EPSGN
      GO TO 20
      ENDIF
      AV=(1.44*CAN)*((VSG/(VSG+VT))**.5)
      VN=VT*(DB**.667)*(ROL**.667)/((MUL**.33)*(SIGL**.33))
      IF(IGEOMET.LE.2) THEN
      CKL=.592*((PG/(ROL*VL))**.25)*((MUL/ROL)**.25)*((DAB*ROL/MUL)**.5)
C     WRITE(7,*)'KL(PRASHAR)=',CKL
      ELSE
      CKL=((PG/(ROL*VL))**.25)*((MUL/ROL)**.25)*((DAB*ROL/MUL)**.667)
C     WRITE(7,*)'KL(BARONA)=',CKL
      ENDIF
      IF(YAF.EQ.1.0)THEN
      RG=0.0
      ELSE
      R2=82.05
      CKG=6.58*(DAI/DB)*(PTOT/PI)/(R2*TLB)
      CKGRT=CKG*R2*TLB
      RG=1./CKG
      ENDIF
```

```
      RETURN
      END
C
C SUBROUTINE HCOEF
C
      SUBROUTINE HCOEF(RAOL,RAOG,RAOC,MUL,MUG,MUC,LAMDAL,LAMDAM,
     1     LAMDAC,SIGL,ITYPE,N,PO,DI,G,DT,VL,HL,SE,QC,T,
     2     TCI,TCO,ALM,BLM,CPL,CPC,VSG,DCP,DCI,DCO,DC,TH,
     3     TTH,U,AMWL,AMWG,AMWC,LAMDAI,THI,HT,HJ,JTH,SAI,SAO,HCI,
     4     IGEOMET,PG)
      REAL MUL,MUG,MUC,MUCW,LAMDAL,LAMDAM,NE,MULW,N,LAMDAC,LAMDA
C
C SELECT THE MODE OF HEAT EXCHANGE
C WHEN ITYPE=1 JACKET
C WHEN ITYPE=2 INTERNAL COIL
C
C     WRITE(6,*)'N=',N
      ROL=RAOL*AMWL
      ROG=RAOG*AMWG
      ROC=RAOC*AMWC
      IF(ITYPE.EQ.2)GO TO 30
C
C CALCULATE DIMENSIONLESS PARAMETERS FOR VESSEL SIDE COEFFICIENT
C
      NE=PO/(ROL*(N**3)*(DI**5))
c     NE=PG/(ROL*(N**3)*(DI**5))
      GA=(ROL**2)*G*(DT**3)/(MUL**2)
      FRN=DI*(N**2)/G
      REN=ROL*N*DI*DI/MUL
      REG=ROL*VSG*DT/MUL
      PRL=MUL*CPL/(AMWL*LAMDAL)
C
C ASSUME VESSEL WALL TEMPERATURE (TW) AND CALCULATE LIQUID VISCOSITY
C AT TW
C
      TW=T-5
   10 MULW=1.3*EXP(-1172*((1./273)-(1./TW)))/100.
      VISCL=MUL/MULW
C
C CALCULATE VESSEL SIDE HEAT TRANSFER COEFFICIENT(HT)
C
      HT1=0.2*(DT/DI)*((DT**3)/VL)*NE*(REN**3)
      HT2=GA*REG*(1.-(2*(DI/DT)*(DI/(HL-SE))*(NE**0.5)*FRN))
      HT3=(HT1+HT2)**0.25
      HT=(LAMDAL/DT)*0.1*HT3*(PRL**0.4)*(VISCL**0.23)
C
C CALCULATE DIMENSIONLESS PARAMETERS FOR JACKET SIDE HEAT TRANSFER
C COEFFICIENT.
```

```
C
  20  VCIN=(4.*7.*QC)/(22.*DCP*DCP)
      AX=ALM*BLM
      VCX=QC/AX
      TCB=(TCI+TCO)/2.
      DLNROWT=303.E-6
      VCA=(G*ALM*(DLNROWT)*(TCO-TCI) 2.)**0.5
      VC=((VCX*VCIN)**0.5)+VCA
      DG=((8./3.)**0.5)*BLM
      REC=VC*DG*ROC/MUC
      IF(REC .LT. 9000.) THEN
      QC=QC+2.
      GO TO 20
      ELSEIF(REC .GT. 25000) THEN
      QC=QC-20.
      GO TO 20
      ENDIF
      PRC=CPC*MUC/(AMWC*LAMDAC)
C
C CALCULATE MUCW AT VESSEL WALL TEMPERATURE (TW)
C
      MUCW=1./(2.148*((TW-273.-8.435)+((8078.4+((TW-273.-8.435)**2))
     **.5))-120.)
      VISCW=MUC/MUCW
C
C CALCULATE JACKET SIDE HEAT TRANSFER COEFFICIENT (HJ)
C
      HJ1=0.03*(REC**0.75)*PRC
      HJ2=1.+(1.74*(PRC-1.)/(REC**0.125))
      SNUJ=HJ1/HJ2
      HJ=(LAMDAC/DG)*(HJ1/HJ2)*(VISCW**0.14)
C
C CHECK VESSEL WALL TEMPERATURE(TWC)
C
      TWC=TCB-((TCB-T)/(1+(HJ/HT)))
      IF(ABS(TWC-TW).GT.0.1) THEN
      TW=TWC
      GO TO 10
      ENDIF
C
C CALCULATE OVERALL HEAT TRANSFER COEFFICIENT (U)
C
      FT=36.84
      FJ=14.73
      IF(IGEOMET .EQ. 1) THEN
      RT=(1./HT)+FT+(SAI*THI/(SAO*LAMDAM))+FJ+(SAI/(SAO*HJ))+
     (SAI*JTHI/(SAO*LAMDAM))+(SAI*THI/(SAO*LAMDAI))
      ELSE
```

```
      RT=(1./HT)+FT+(SAI*TH/(SAO*LAMDAM))+FJ+(SAI/(SAO*HJ))
      ENDIF
      U=1./RT
      RETURN
C
C CALCULATION OF HEAT TRANSFER COEFFICIENT FOR INTERNAL COIL
C

C
C CALCULATE DIMENSIONLESS PARAMETERS FOR VESSEL SIDE COEFFICIENT
C
 30   RES=(DI*ROL/MUL)*((DI*N)+(4.*VSG))
      PRL=CPL*MUL/(AMWL*LAMDAL)
      FRN=N*N*DI/G
C
C ASSUME VESSEL WALL TEMPERATURE (TW) AND CALCULATE LIQUID VISCOSITY
C AT TW
C
      TW=T-5
 40   MULW=1.3*EXP(-1172.*((1./273.)-(1./TW)))/100.
      VISC=MUL/MULW
C
C CALCULATE VESSEL SIDE HEAT TRANSFER COEFFICIENT
C
      HT=(.87*LAMDAL/DT)*(RES**.64)*(PRL**.33)*(VISC**0.14)*(FRN**(-.1))
C
C CALCULATE DIMENSIONLESS PARAMETER FOR FOR COIL SIDE HEAT TRANSFER
C COEFFICIENT.
C
 50   VC=4.*7.*QC/(22.*DCI*DCI)
      REC=DCI*VC*ROC/MUC
      PRC=CPC*MUC/(AMWC*LAMDAC)
      TCB=(TCI+TCO)/2.
      IF(REC .LT. 15000)THEN
      QC=QC+2.
      GO TO 50
      ENDIF
C
C CALCULATE MUCW AT VESSEL WALL TEMPERATURE (TW)
C
      MUCW=1./(2.148*((TW-273.-8.435)+((8078.4+((TW-273.-8.435)**2))
     **.5))-120.)
      VISCW=MUC/MUCW
C
C CALCULATE COIL SIDE HEAT TRANSFER COEFFICIENT (HCI)
C
      HCI=(.027*LAMDAC/DCI)*(REC**.8)*(PRC**.33)*(VISCW**.14)*
     (1.+(3.5*DCI/DC))
```

```
C
C CHECK VESSEL WALL TEMPERATURE(TWC)
C
      TWC = TCB-((TCB-T)/(1+(HCI/HT)))
      IF(ABS(TWC-TW).GT.0.1) THEN
      TW = TWC
      GO TO 40
      ENDIF
C
C CALCULATE OVERALL HEAT TRANSFER COEFFICIENT (U)
C
      FT = 22.00
      FC = 19.00
      DCM = (DCO-DCI)/LOG(DCO/DCI)
      RT = (1./HT)+FT+(TTH*DCO/(LAMDAM*DCM))+FC+(1./HCI)*(DCO/DCI)
      U = 1./RT
      RETURN
      END
```

APPENDIX B2

COMPUTER CODE FOR SOLVING FILM THEORY MODEL EQUATIONS

```
C-------------------------------------------------------------------------
C
C COMPUTER CODE NAME : GLRXN
C
C WRITTEN BY                : AQIL JAMAL
C
C
C THIS CODE SOLVES  EQUATIONS  (4.10)  AND  (4.11)
C USING  FINITE  DIFFERENCE  METHOD  COMBINED  WITH
C QUASI-LINEARIZATION  TECHNIQUE AND CALCULATES THE
C REACTION  FACTOR. THE CODE ALSO CALCULATES REACTION
C FACTOR USING APPROXIMATE ANALYTICAL EXPRESSION GIVEN
C BY EQUATIONS (4.17) TO (4.19).
C
C-------------------------------------------------------------------------
C
C-----------------------------------------------------------------
C                   MAIN PROGRAM
C-----------------------------------------------------------------
C
      COMMON AM,EI,OMEGA
      DIMENSION U(999),V(999),W(999),X(999)
      DIMENSION FO(0:1000),F(0:1000),DIFF(999)
      DIMENSION B1(11),AM1(10),AM2(10),AM3(10),AM4(10),AM5(10)
      DIMENSION AM6(10),E(10)
C
C DATA SECTION
C
      DATA  B1(1)/250./,B1(2)/10./,B1(3)/5./,B1(4)/2.5/,B1(5)/1./
      DATA  B1(6)/0.5 ,B1(7)/.25/,B1(8)/.15/,B1(9)/.1/,B1(10)/.05/
      DATA  B1(11)/.025/,E(1)/2./,E(2)/5./,E(3)/10./,E(4)/50./
      DATA  E(5)/100./,E(6)/200./
      DATA  AM1(1)/0.01/,AM1(2)/1.25/,AM1(3)/1.5/,AM1(4)/1.5/,AM1(5)/2./
      DATA  AM2(1)/1./,AM2(2)/2./,AM2(3)/3./,AM2(4)/4./,AM2(5)/5.5/
```

```
      DATA  AM3(1)/1./,AM3(2)/3./,AM3(3)/6./,AM3(4)/10./,AM3(5)/11./
      DATA  AM4(1)/1./,AM4(2)/10./,AM4(3)/20./,AM4(4)/40./,AM4(5)/60./
      DATA  AM5(1)/1./,AM5(2)/20./,AM5(3)/50./,AM5(4)/80./,AM5(5)/150./
      DATA  AM6(1)/1./,AM6(2)/20./,AM6(3)/80./,AM6(4)/150./,AM6(5)/200./
      DATA  AM6(6)/300./,AM6(7)/500./,AM6(8)/1000./
      WRITE(6,*)'-----------------------------------------------------'
      WRITE(6,*)'-------------------* THE RESULT *--------------------'
      WRITE(6,*)'-----------------------------------------------------'
      ERROR=1.E-5
      MITER=200
      EI=2.0
      S0=0.0
      SF=1.0
      DELS=0.005
C     N=(SF-S0)/DELS
      N=200
      AV=3.0
      CKL=0.04
      DA=6E-5
      TAUL=10.*60.
      EPSL=.85
C
C MAIN COMPUTATION STARTS FROM HERE
C
      DO 10 M1=1,11
      OMEGA= B1(M1)
      WRITE(6,12)OMEGA
      DO 9 M=1,4
      EI=E(M)
      WRITE(6,11)EI
      IF(M.GE.1.AND.M.LE.5 )THEN
      MCOUNT=5
      ELSE
      MCOUNT=8
      ENDIF
      DO 8 M2=1,MCOUNT
      IF(M.EQ.1)THEN
      AM=AM1(M2)
      ELSEIF(M.EQ.2)THEN
      AM=AM2(M2)
      ELSEIF(M.EQ.3)THEN
      AM=AM3(M2)
      ELSEIF(M.EQ.4)THEN
      AM=AM4(M2)
      ELSEIF(M.EQ.5)THEN
      AM=AM5(M2)
      ELSEIF(M.EQ.6)THEN
      AM=AM6(M2)
```

```
      ENDIF
      ITER=1
      ALFA=EPSL*CKL*OMEGA/(AV*DA*(1.+OMEGA))
      ZETA=EPSL*OMEGA/(CKL*AV*TAUL*(1.+OMEGA))
      WRITE(8,*)'OMEGA=',OMEGA
      WRITE(8,*)'ZETA=',ZETA
      WRITE(8,*)'ALFA=',ALFA
      AMM=AM*(1.+OMEGA)/OMEGA
      PM1=ZETA+(AM*AM*(ALFA-((1./(3*OMEGA*OMEGA))+(1./OMEGA)+1.)))
      F(0)=1.0
      DO 1 I = 1,N-1
      FO(I)=0.125
      EA=1.0
    1 CONTINUE
    2 CONTINUE
      FO(N)=FO(N-1)/(1.+(PM1*DELS))
      F(N)=FO(N)
C     WRITE(6,*)' EA= ', EA
      CALL COEF(N,U,V,W,X,AMM,EI,DELS,OMEGA,FO,EA,PM1)
      CALL TRIDAG(N,U,V,W,X,F)
      DO 5 I= 1,N-1
      DIFF(I)=ABS(FO(I)-F(I))
      IF(DIFF(I) .GT. ERROR) THEN
      DO 3 J=1,N-1
      FO(J)=F(J)
    3 CONTINUE
      ITER=ITER+1
      EA=-((F(1)-F(0))/DELS)*(OMEGA/(1.+OMEGA))
      IF(ITER .GT.MITER)THEN
      WRITE(6,*)'NO CONVERGENCE'
      GO TO 6
      ENDIF
      GO TO 2
      ELSE
      DO 4 K=0,N,5
C     WRITE(7,*)'EI=',EI,'AM=',AM
C     WRITE(7,*)K*DELS,F(K)
    4 CONTINUE
C
C
      CALL ANALYT(EA,AMM,EI,OMEGA,ERROR,EAP,NO,PM1)
      GO TO 6
      ENDIF
    5 CONTINUE
    6 IF(NO .EQ.1)THEN
      WRITE(6,7)AM,EA
      GO TO 8
      ELSE
```

```
      PDIFF=ABS(EA-EAP)*100./EA
      WRITE(6,7)AM,EA,EAP,PDIFF
      ENDIF
    7 FORMAT(2X,4(2X,F8.3))
    8 CONTINUE
    9 CONTINUE
   10 CONTINUE
   11 FORMAT(' EI    = ', 2X,F8.3)
   12 FORMAT(' OMEGA = ', 2X,F8.3)
      STOP
      END
C-----------------------------------------------------------------------
C                  ** SUBROUTINE COEF **
C  THIS SUBROUTINE DEVELOP THE COEFFICIENT MATRIX FOR THE
C  SUBROUTINE TRIDAG
C-----------------------------------------------------------------------
C
      SUBROUTINE COEF(N,U,V,W,X,AMM,EI,DELS,OMEGA,FO,EA,PM1)
      DIMENSION U(999),V(999),W(999),X(999),FO(0:1000)
      DO 1 I=1,N-1
      AA=(EI-1.)*((REAL(I)*DELS)+OMEGA)
      BB=EA*OMEGA*((REAL(I)*DELS)-1.)
      P1=2./(DELS*DELS)
      P2=2./((REAL(I)*DELS*DELS)+(OMEGA*DELS))
      P3=AMM*AMM*(2*FO(I)-FO(N))/(EI-1.)
      P4=AMM*AMM*(1.+(BB/AA))
      U(I)= 1.0/(DELS*DELS)
      W(I)= (1./(DELS*DELS))+P2
      IF(I.EQ.N-1)THEN
      V(I)=(-P1-P2-P3-P4)+(W(I)/(1.+(DELS*PM1)))
      ELSE
      V(I)=-P1-P2-P3-P4
      ENDIF
      IF(I.EQ.1)THEN
      X(I)=-(AMM*AMM*FO(I)*FO(I)/(EI-1.))-U(1)
      ELSE
      X(I)=-AMM*AMM*FO(I)*FO(I)/(EI-1.)
      ENDIF
    1 CONTINUE
      RETURN
      END
C-----------------------------------------------------------------------
C                  ** SUBROUTINE TRIDAG **
C THIS SUBROUTINE SOLVES THE TRIDIAGONAL MATRIX, Generated
C FROM FINITE DIFFERENCE, METHOD USING THOMAS ALGORITHM
C-----------------------------------------------------------------------
C
      SUBROUTINE TRIDAG(N,A,B,C,E,F)
```

```
      DIMENSION A(999),B(999),C(999),E(999),F(0:999)
      DO 4 K = 1,N-2
      XMULT = A(K + 1)/B(K)
      B(K + 1) = B(K + 1)-XMULT*C(K)
      E(K + 1) = E(K + 1)-XMULT*E(K)
    4 CONTINUE
      F(N-1) = E(N-1)/B(N-1)
      DO 5 K = N-2,1,-1
      F(K) = (E(K)-(C(K)*F(K + 1)))/B(K)
    5 CONTINUE
      RETURN
      END

C-----------------------------------------------------------------------
C                  ** SUBROUTINE ANALYT **
C THIS SUBROUTINE SOLVES EQ.(4.23) FOR EA USING HALF INTERVAL METHOD
C-----------------------------------------------------------------------
      SUBROUTINE ANALYT(EAA,AMM,EI,OMEGA,ERROR,EAP,NO,PM1)
      FG(GI,AMGI) = GI-(1./(EI-1.))*(EI-((OMEGA*AMGI/(1. + OMEGA))*(CONST +
     $          AMGI*(1. + OMEGA)*TANH(AMGI))/(AMGI*(1. + OMEGA) + CONST*
     $          TANH(AMGI)) + (1./(1. + OMEGA))) -(OMEGA*AMGI/
     $          (AMGI*(1. + OMEGA)*COSH(AMGI) + CONST*SINH(AMGI))))
      CONST = PM1*(1. + OMEGA)-1.
      NO = 0
      ICOUNT = 0
      GIN = 1.0
      AMGI = AMM*SQRT(GIN)
      FM = FG(GIN,AMGI)
   10 GI1 = GIN-0.01
      IF(GI1.LT.0) GO TO 60
   15 AMGI1 = AMM*SQRT(GI1)
      FM1 = FG(GI1,AMGI1)
      IF(FM*FM1.LT.0) GO TO 20
      FM = FM1
      GIN = GI1
      GO TO 10
   20 GIU = GIN
      GIL = GI1
      FU = FM
   30 GIS = (GIL + GIU)/2.
C
C  CHECK CONVERGENCE GI
C
      IF(ABS(GIU-GIL).LT.ERROR) GO TO 50
      AMGIS = AMM*SQRT(GIS)
      FMS = FG(GIS,AMGIS)
      IF(FU*FMS.GT.0) GO TO 40
      GIL = GIS
```

```
      GO TO 30
40    GIU = GIS
      FU = FMS
      GO TO 30
50    GI = GIS
      SGI = SQRT(GI)
      ANUM = (AMM*SGI*TANH(AMM*SGI)*(1. + OMEGA)) + (PM1*(1. + OMEGA)-1.)
      DENUM = (AMM*SGI*(1. + OMEGA)) + (PM1*(1. + OMEGA)-1.)*TANH(AMM*SGI)
      EAP = ((OMEGA*AMM*SGI/(1. + OMEGA))*(ANUM/DENUM)) + (1./(1. + OMEGA))
      FL = OMEGA*AMM*SGI/(COSH(AMM*SGI)*DENUM)
      WRITE(7,*)EAP,FL
      RETURN
60    GI1 = 1.E-8
      ICOUNT = ICOUNT + 1
      IF(ICOUNT.GT.100)THEN
      NO = 1
      GO TO 70
      ENDIF
      GO TO 15
70    RETURN
      END
```